

Washington University in St. Louis
Washington University Open Scholarship

All Theses and Dissertations (ETDs)

Spring 4-25-2013

Molecular Design and Photophysical Characterization of Synthetic Bacteriochlorins for Solar Energy Conversion and Photodynamic Therapy

Eunkyung Yang

Washington University in St. Louis

Follow this and additional works at: <https://openscholarship.wustl.edu/etd>



Part of the [Chemistry Commons](#)

Recommended Citation

Yang, Eunkyung, "Molecular Design and Photophysical Characterization of Synthetic Bacteriochlorins for Solar Energy Conversion and Photodynamic Therapy" (2013). *All Theses and Dissertations (ETDs)*. 1074.

<https://openscholarship.wustl.edu/etd/1074>

This Dissertation is brought to you for free and open access by Washington University Open Scholarship. It has been accepted for inclusion in All Theses and Dissertations (ETDs) by an authorized administrator of Washington University Open Scholarship. For more information, please contact digital@wumail.wustl.edu.

WASHINGTON UNIVERSITY IN ST. LOUIS

Department of Chemistry

Dissertation Examination Committee:

Dewey Holten, Chair

Mikhail Y. Berezin

Robert Blankenship

Richard A. Loomis

Liviu Mirica

Yan Mei Wang

Molecular Design and Photophysical Characterization of Synthetic Bacteriochlorins for Solar
Energy Conversion and Photodynamic Therapy

by

Eunkyung Yang

A dissertation presented to the
Graduate School of Arts and Sciences
of Washington University in
partial fulfillment of the
requirements for the degree
of Doctor of Philosophy

May 2013

St. Louis, Missouri

Table of Contents

List of Figures	vii
List of Tables	x
List of Charts	xii
Acknowledgements	xiv
Abstract	xv

Section 1: Introduction

Chapter 1: Background, Overview and Methods

Background on the study of bacteriochlorins	2
Electronic and photophysical characteristics of porphyrins	3
Electronic and photophysical characteristics of bacteriochlorins	7
Rate constants for excited-state process in monomeric bacteriochlorins	10
Rate constants for quenching of the excited-state	11
Photodynamic therapy	12
Experimental methods	15
Overview of the thesis	18
Collaborations	20
References	22

Section 2: Molecular design and photophysical characterization of synthetic bacteriochlorins

Chapter 2: De Novo Synthesis and Photophysical Characterization of Annulated

Bacteriochlorins. Mimicking and Extending the Properties of Bacteriochlorophylls

Abstract	25
Introduction.....	26
Experimental methods	28
Results and Discussion	29
References.....	42

Chapter 3: Photophysical Properties and Electronic Structure of Stable, Tunable

Synthetic Bacteriochlorins: Extending the Features of Native Photosynthetic Pigments

Abstract	48
Introduction.....	49
Experimental methods	55
Results.....	56
Discussion.....	66
References	89

Chapter 4: Synthesis and Photophysical Characterization of Stable Indium

Bacteriochlorins

Abstract.....	95
Introduction.....	96
Experimental methods	100
Results and Discussion	102
References	118

Chapter 5: Synthesis and Photophysical Properties of Metallobacteriochlorins

Abstract	124
Introduction	125
Experimental methods	128
Results.....	130
Conclusion and outlook	145
References.....	148

Chapter 6: Photophysical Properties and Electronic Structure of Bacteriochlorin– Chalcones with Extended Near-Infrared Absorption

Abstract	155
Introduction	156
Experimental methods	160
Results	163
Discussion	189
Overview.....	189
References.....	204

Section 3: Study of Synthetic Bacteriochlorins as Photosensitizer for Photodynamic

Therapy

Chapter 7: In Vitro Photodynamic Therapy and Quantitative Structure-Activity

Relationship Studies with Stable Synthetic Near-Infrared-Absorbing Bacteriochlorin

Photosensitizers

Abstract.....	212
Introduction.....	213
Experimental methods	216
Results	216
Discussion.....	222
References.....	223

Chapter 8: Stable Synthetic Bacteriochlorins Overcome the Resistance of Melanoma to Photodynamic Therapy

Abstract.....	228
Introduction.....	229
Experimental methods	232
Results.....	232
Discussion.....	238
References.....	240
Supplementary materials.....	245

Chapter 9: Stable Synthetic Bacteriochlorins for Photodynamic Therapy: Role of Dicyano Peripheral Groups, Central Metal Substitution (2H, Zn, Pd), and Cremophor EL Delivery

Abstract.....	250
Introduction.....	251
Experimental methods	254

Results.....	254
Discussion.....	262
References.....	264

Chapter 10: Stable Synthetic Cationic Bacteriochlorins as Selective Antimicrobial

Photosensitizers

Abstract.....	267
Introduction.....	268
Experimental methods	271
Results	272
Discussion.....	282
References.....	287

Chapter 11: Molecular Electronic Tuning of Photosensitizers to Enhance Photodynamic

Therapy: Synthetic Dicyanobacteriochlorins as a Case Study

Abstract.....	293
Introduction	294
Experimental methods	299
Results and Discussion	302
References.....	335

List of Figures

Chapter 1

Figure 1. Naturally occurring tetrapyrrole chromophores.	2
Figure 2. Basic porphyrin skeleton	3
Figure 3. Absorption spectra of FbTPP and ZnTPP	4
Figure 4. The highest energy occupied orbitals	6
Figure 5. Structure and absorption spectrum	8
Figure 6. Schematic energy level diagram	9
Figure 7. Jablonski energy level diagram	10
Figure 8. Modified Jablonski diagram to show mechanism	13

Chapter 2

Figure 1. Absorption (— solid lines) and emission	31
Figure 2. Orbital energies, energy gaps, singlet excited-state lifetime	34

Chapter 3

Figure 1. Absorption (— solid lines) and emission	58
Figure 2. Integrated intensity ratio of the Q _y and B absorption	65
Figure 3. Singlet excited-state lifetime (τ_S)	71
Figure 4. Molecular orbital energies (A) and energy gaps	79
Figure 5. Frontier molecular orbital energies (A)	80
Figure 6. Transition-dipole-moment directions	87
Figure 7. Energy (and wavelength) of the Q _x (0,0) absorption	88

Chapter 4

Figure 1. Spectra in toluene at room temperature.....	105
---	-----

Figure 2. LUMO – HOMO energy gap	115
Chapter 5	
Figure 1. Summary of metalation of synthetic bacteriochlorins.....	131
Figure 2. ORTEP drawing of (A) free base bacteriochlorin	132
Figure 3. Comparison of core structural	134
Figure 4. Absorption spectra in toluene	135
Figure 5. Absorption spectra in toluene	135
Figure 6. The effect of the number	143
Chapter 6	
Figure 1. Absorption spectra of representative	158
Figure 2. Absorption spectra in toluene	168
Figure 3. Qy absorption (A) and fluorescence (B)	169
Figure 4. Transient absorption difference spectra.....	176
Figure 5. Characteristics	180
Figure 6. Characteristics	182
Figure 7. Characteristics	184
Figure 8. Characteristics	186
Figure 9. HOMO – LUMO energy gap	198
Chapter 7	
Figure 1. (A) Octanol-water partition coefficients. Calculated LogP (cLogP)	219
Chapter 8	
Figure 1. Molecular structures	233
Figure 2. (A) <i>In vitro</i> PDT effectiveness	237

Supplementary Figure 1. TEM micrographs	245
Supplementary Figure 2. Visible absorption spectra	246
Chapter 9	
Figure 1. Absorption spectra of the four bacteriochlorins.....	258
Figure 2. Relative effectiveness	259
Figure 3. Effect of incubation time	260
Chapter 10	
Figure 1. Bacteriochlorin photosensitizer	269
Figure 2. Absorption spectra of bacteriochlorins.....	272
Figure 3. Survival fraction against photosensitizer	273
Figure 4. Survival fraction against photosensitizer.....	274
Figure 5. Survival fraction against photosensitizer.....	276
Figure 6. Two color confocal fluorescence micrographs.....	277
Figure 7. Survival fraction against photosensitizer.....	279
Chapter 11	
Figure 1. Absorption spectra.....	307
Figure 2. Emission spectrum	311
Figure 3. Photobleaching studies	314
Figure 4. Photostability of bacteriochlorins.....	316
Figure 5. Photobleaching studies	318
Figure 6. Photobleaching studies	319
Figure 7. Electron densities	331
Figure 8. Electronic properties	332

List of Tables

Chapter 2

Table 1. Photophysical Properties of Bacteriochlorin Compounds. <i>a</i>	33
Table 2. Molecular-orbital energies	36

Chapter 3

Table 1. Structures of Bacteriochlorins	53
Table 2. Structures of Bacteriochlorins, Bacteriochlorinimides,	54
Table 3. Spectral Characteristics of Bacteriochlorins	60
Table 4. Photophysical Properties of Bacteriochlorins	68
Table 5. Molecular Orbital Energies and Energy Gaps for Bacteriochlorins.....	72
Table 6. Molecular-orbital Energies	77

Chapter 4

Table 1. Spectral Characteristics of Indium.....	106
Table 2. Photophysical and Molecular Orbital Properties	110
Table 3. Molecular-Orbital Characteristics	114

Chapter 5

Table 1. Spectral Properties of Bacteriochlorins.	136
Table 2. Photophysical, Redox,	141

Chapter 6

Table 1. Spectral properties of bacteriochlorins	171
Table 2. Photophysical properties of bacteriochlorins.....	175
Table 3. Molecular-orbital energies of bacteriochlorins.....	188

Chapter 7

Table 1. Chemical structures of bacteriochlorins215

Table 2. Properties of Bacteriochlorins218

Chapter 8

Table S1. Photophysical Properties247

Chapter 9

Table 1. PDT activity and photostability of the bacteriochlorins.257

Chapter 10

Table 1. Chemical and photophysical properties of bacteriochlorins.....280

Chapter 11

Table 1. PDT activity, photostability306

Table 2. Absorption and fluorescence308

Table 3. Spectral, state-energy, redox,.....324

List of Charts

Chapter 2

Chart 1. (A) Naturally occurring bacteriochlorophylls.....	27
Chart 2. Structures of MeOBOP, HBC-I, and MeOBC-I	29
Chart 3. Benchmark bacteriochlorins.	29
Chart 4. Fictive bacteriochlorin for which DFT	35

Chapter 3

Chart 1. Naturally occurring bacteriochlorophylls (top).....	49
--	----

Chapter 4

Chart 1.....	97
Chart 2.....	102
Chart 3.....	102
Chart 4.....	103

Chapter 6

Chart 1. Representative bacteriochlorins studied.....	157
Chart 2. Bacteriochlorin–chalcones prepared	165
Chart 3. Push-pull chalcone architecture	191
Chart 4. Benchmark extended chalcones	192

Chapter 11

Chart 1. Representative native bacteriochlorin	296
Chart 2. Representative synthetic bacteriochlorins	297
Chart 3. Imidazole-substituted	298
Chart 4. Synthetic bacteriochlorins	298

Chart 5. Two sets of305

Acknowledgements

I cannot find words to express my gratitude to my committee chair Professor Dewey Holten for his valuable guidance, patience, kindness, and encouragement throughout my graduate school career. I have been extremely lucky to have a supervisor who cared so much about my work. Without his guidance and persistent help my graduate career would not have been possible.

I am also indebted to the members of my dissertation committee Professors Loomis, Blankenship, Mirica, Berezin, and Wang. They have generously given their time and expertise to better my work. I thank them for their contribution and their good-natured support.

I would like to thank current and former members of Holten group. Dr. Christine Kirmaier provided experimental assistance and was willing to listen and offer valuable feedback. My colleagues, Joey Springer, Michelle Harris and Kaitlyn Faries have all extended their support in a very special way and I gained a lot from them through their personal and scholarly interaction, their suggestion at various points of my research program. I am also grateful to Dr. Darek Niedzwiedzki in PARC ultrafast facility for his help with TA experiments.

I consider it an honor to work with the groups of Professor Lindsey at North Carolina State University for providing me with numerous samples of bacteriochlorins, Professor David Bocian at the University of California, Riverside for offering DFT calculations, and Professor Michael R. Hamblin at Harvard medical school for performing photodynamic therapy activities. I am pleased to have been part of such a fruitful collaboration.

I wish to thank my family and friends for their faith in me. I especially thank my parents for their material and spiritual support and encouragements in all aspects of my life.

ABSTRACT OF THE DISSERTATION

Molecular Design and Photophysical Characterization of Synthetic Bacteriochlorins for Solar Energy Conversion and Photodynamic Therapy

By

Eunkyung Yang

Doctor of Philosophy in Chemistry

Washington University in St. Louis, 2013

Professor Dewey Holten, Chairperson.

The design, photophysical characteristics and some potential applications of synthetic bacteriochlorins are discussed. Bacteriochlorins (e.g., bacteriochlorophylls) are tetrapyrrole macrocycles with two reduced pyrrole rings, whereas chlorins (e.g., chlorophylls) and porphyrins (e.g., hemes) have one and zero reduced pyrrole rings. Molecular design characteristics are revealed by understanding the effects of substituent types and patterns and the central metal ion on the photophysical properties and electronic structure. These effects are elucidated via studies of the optical absorption and emission spectra and excited-state decay pathways, and analysis of the molecular-orbital characteristics within the four-orbital model. The studies also encompass analysis of the properties of bacteriochlorins as photosensitizers for photodynamic therapy (PDT). The factors studied and correlated include photostability, redox potentials, photophysical properties, electrochemical and molecular-orbital characteristics, reactive-oxygen-species production, photosensitizer cellular uptake and distribution. Collectively, the studies address the design of synthetic bacteriochlorins for solar-energy conversion and photomedicine.

Section 1. Introduction

Chapter 1

Background, Methods, and Overview

Background on the study of bacteriochlorins

Tetrapyrrole macrocycles play important roles that serve nature in various ways. They are the active sites of numerous proteins whose functions range from oxygen transport and storage to electron transfer to energy conversion. Such molecules include the heme group of hemoglobin, the chlorophylls of plants and cyanobacteria and the bacteriochlorophylls of photosynthetic bacteria. In addition, they have proven to be efficient sensitizers and catalysts in a number of chemical and photochemical systems.¹ Tetrapyrrole molecules can be divided to three major classes. The classes are porphyrin, chlorin and bacteriochlorin, which have zero, one or two reduced pyrrole rings, respectively (Figure 1).

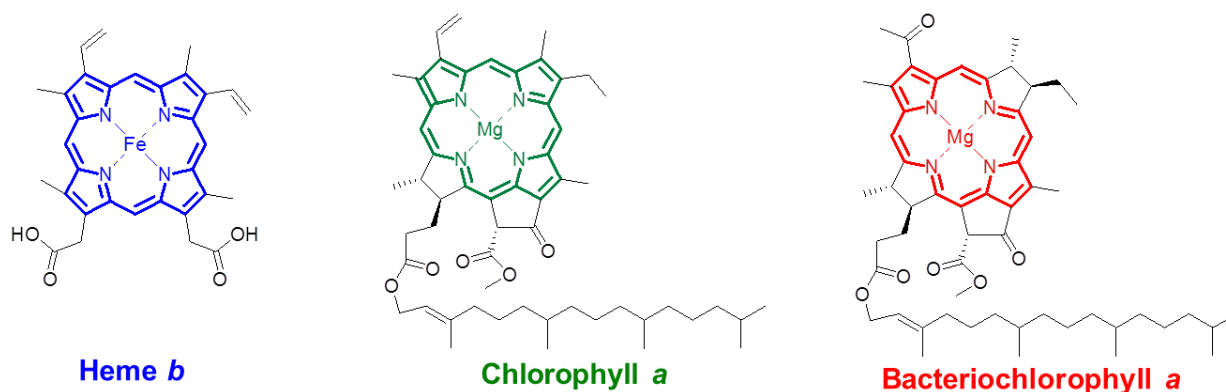


Figure 1. Naturally occurring tetrapyrrole chromophores.

All three chromophore classes are characterized by strong absorption in the near-ultraviolet region but weak absorption in the green-orange region; chlorins also afford moderately strong absorption in the red region whereas bacteriochlorins afford intense absorption in the near-infrared (NIR) region, the latter of comparable strength to the near-ultraviolet features. The strong NIR absorption characteristics of bacteriochlorins have been applied to diverse systems such as artificial photosynthetic light-harvesting, optical imaging,

photodynamic therapy of soft tissue, and fluorescent markers in clinical diagnostics. As such, investigations of fundamental properties of bacteriochlorins are needed to elucidate the design principles that relate molecular composition, photophysical properties and electronic structure to allow a wide range of photochemical applications.

Electronic and photophysical characteristics of porphyrins

A basic porphyrin consists of four pyrrole rings linked by methylene bridges as shown in Figure 2. The electronic structure of a porphyrin is an inner 16-membered ring with 18π electrons. When protons are bound to two of the central nitrogen atoms the molecule is called a free base (Fb) porphyrin. When the two protons are replaced by one of among various metal ions, it is called as metalloporphyrin.

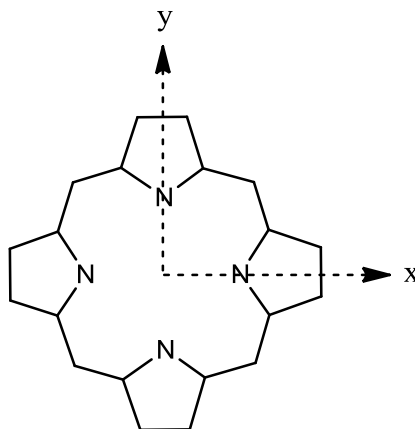


Figure 2. Basic porphyrin skeleton.²

Figure 3 shows the absorption spectra of two different porphyrins, in this case tetraphenylporphyrins (TPP). The major features are referred to as the Soret or B band around 400 nm in the near-UV region, and the Q bands around 500-700 nm in the visible region. The features denoted Q(0,0), Q(1,0), Q(2,0) refer to the excitation of no, one or two vibrational

quanta accompanying the electronic transition. Metalloporphyrins have D_{4h} symmetry and as such, the absorption transitions have E_u symmetry. E_u symmetry consists of two equivalent dipole transitions in the x- and y- directions (Figure 2); the B and Q bands of a typical metalloporphyrin are shown in Figure 3B.

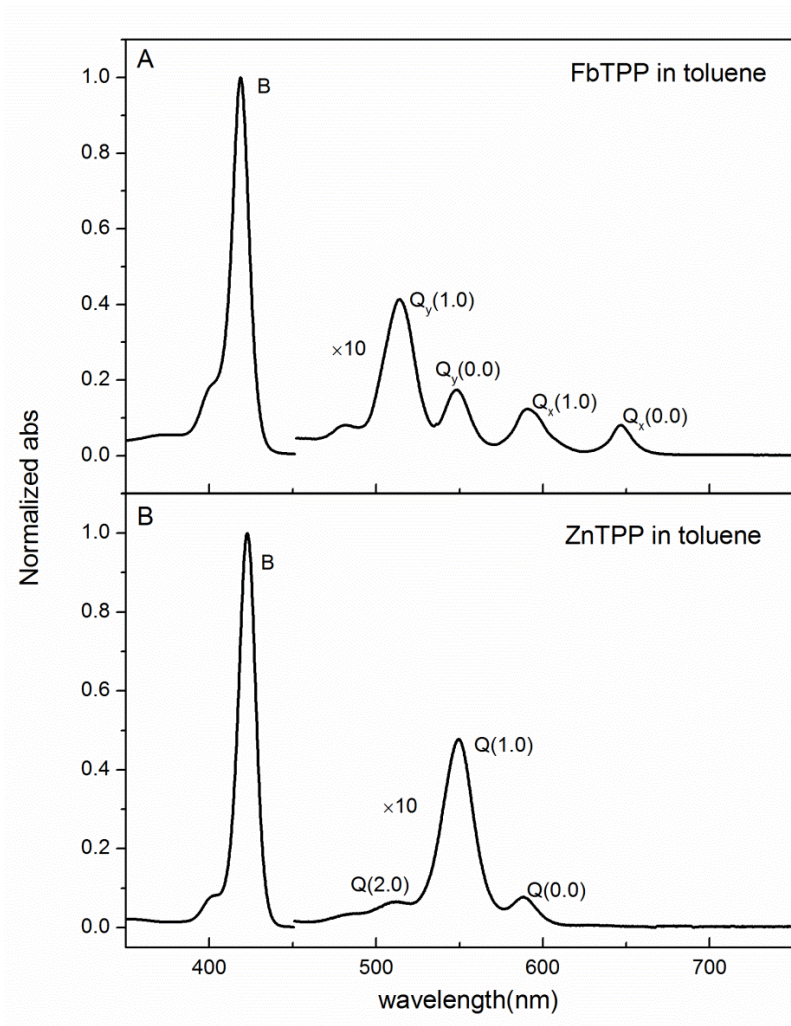


Figure 3. Absorption spectra of FbTPP and ZnTPP

In the free base porphyrin, the D_{4h} symmetry of metalloporphyrin is changed to D_{2h} symmetry because of the presence of the two central protons. Because the x and y axes of E_u symmetry are no longer equivalent, the B band is split into the B_x and the B_y bands and the Q

band is split into the Q_x and the Q_y bands. These features are labeled as Q_x , Q_y , B_x and B_y for individual components of the transition pairs (Figure 3A). As in the case of metalloporphyrins, each (0,0) origin transition is usually accompanied by a (1,0) vibronic transition. Thus in Figure 3A the four Q bands are indicated as $Q_x(0,0)$, $Q_x(1,0)$, $Q_y(0,0)$ and $Q_y(1,0)$ in the visible region.^{2,3}

These spectral and electronic characteristics of porphyrins can be interpreted by Gouterman's four-orbital model shown in Figure 4. Because the visible bands are ascribed to the $\pi-\pi^*$ transition, the π orbitals of metalloporphyrin have a_{1u} , a_{2u} , e_g , b_{1u} , and b_{2u} symmetry. According to the Hückel calculations, the two highest occupied molecular orbitals, $a_{1u}(\pi^*)$ and $a_{2u}(\pi^*)$, and the lowest empty (and degenerate) molecular orbitals, $e_{gx}(\pi)$ and $e_{gy}(\pi)$, are obtained and assigned (Figure 4). The $a_{1u}(\pi)$ and $a_{2u}(\pi)$ orbitals are close in energy (they are often called "accidentally" degenerate), and their energy ordering depends on the substituents (or metallation state). For many porphyrins (such as metallotetraphenylporphyrins) the $a_{1u}(\pi)$ orbital is lower in energy than the $a_{2u}(\pi)$ orbital. Therefore, early models (before the four-orbital model) would assign the ($a_{1u} \rightarrow e_g$) one-electron promotion to the Q band and the ($a_{2u} \rightarrow e_g$) one-electron promotion to the B band. However, this simplified assignment does not account for the fact that the intensity of the Q band is much (about 30-fold) lower than the B band intensity. Gouterman addressed this discrepancy by proposing that because the top filled orbitals, $a_{1u}(\pi)$ and $a_{2u}(\pi)$, are nearly degenerate, and the two lowest unoccupied orbitals, $e_{gx}(\pi)$ and $e_{gy}(\pi)$, are rigorously degenerate (in D_{4h} metalloporphyrins) the electronic transitions and optical spectra of porphyrins are described as a linear combination of ($a_{1u} \rightarrow e_g$) and ($a_{2u} \rightarrow e_g$) one-electron promotions (orbital configurations), as given by Eq(1).^{2,3}

$$\begin{aligned}
 B_x^0 &= [(b_1 \rightarrow c_2) \mp (b_2 \rightarrow c_1)]/\sqrt{2} \\
 Q_x^0 &= [(b_1 \rightarrow c_1) \pm (b_2 \rightarrow c_2)]/\sqrt{2} \\
 B_y^0 &= [(b_1 \rightarrow c_1) \pm (b_2 \rightarrow c_2)]/\sqrt{2} \\
 Q_y^0 &= [(b_1 \rightarrow c_2) \mp (b_2 \rightarrow c_1)]/\sqrt{2}
 \end{aligned}
 \tag{1}$$

Here, Q^0 and B^0 respectively denote the Q and B states of an arbitrary porphyrin assuming exactly 50:50 mixtures of the one-electron promotions, as would occur if the a_{1u} and a_{2u} are degenerate and e_{gx} and e_{gy} are degenerate.

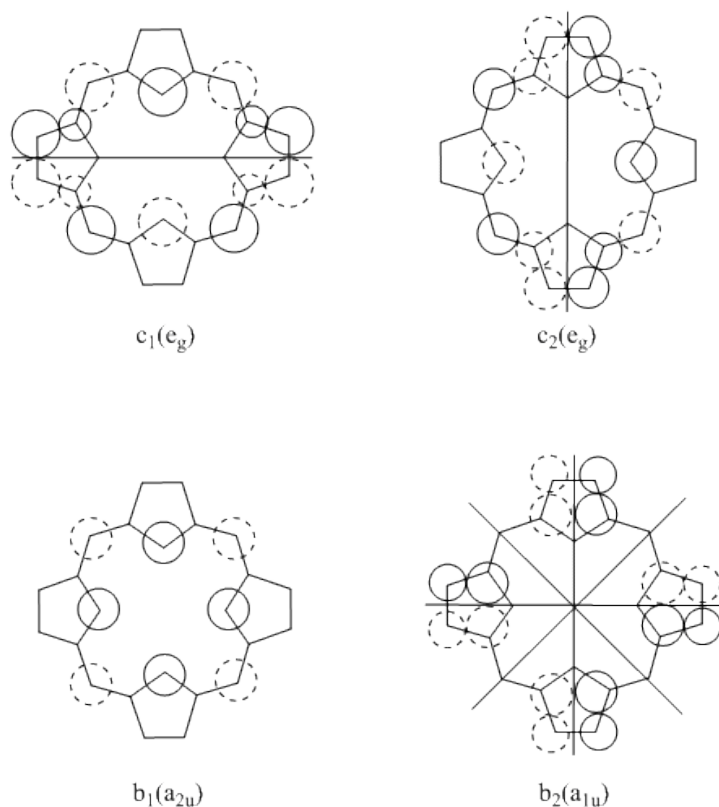


Figure 4. The highest energy occupied orbitals and the two lowest energy unoccupied orbitals of the Gouterman four-orbital model. The orbital coefficients are proportional to the size of the circles. Solid or dashed circles indicate sign. Symmetry nodes are indicated by solid lines.²

Electronic and photophysical characteristics of bacteriochlorins

Bacteriochlorin has a tetrapyrrole macrocycle structure with two reduced pyrrole rings. The absorption spectrum of a typical bacteriochlorin is shown in Figure 5. The B bands, especially the B_y band, is hypsochromically shifted from those of porphyrin, and the Q_y band, the lowest energy transition, shows a large bathochromic shift. This result can be understood in terms of the energies of the HOMO and LUMO configurations in Figure 6. In progressing from porphyrin to chlorin to bacteriochlorin, the energies of the filled $a_{1u}(\pi)$ and empty $e_{gy}(\pi^*)$ orbitals are raised in energy as a result of the reduction of two pyrrole rings. On the other hand, the energies of the filled $a_{2u}(\pi)$ and empty $e_{gx}(\pi^*)$ orbitals do not change nearly as much (Figure 6). Therefore, the energy of the lowest one-electron promotion (configuration), $a_{1u}(\pi) \rightarrow e_{gx}(\pi^*)$ or HOMO \rightarrow LUMO, decreases in the following order: porphyrin > chlorin > bacteriochlorin. As such, following the description in Eq. 1, in this series this configuration makes an increasing contribution to the nature of the Q_y state and optical transition, and a decreasing contribution to the B_y state and optical transition. Modern density functional theory calculations suggest that the $a_{1u}(\pi) \rightarrow e_{gx}(\pi^*)$ makes about a 50% contribution to Q_y for porphyrins and about 90% for bacteriochlorins, in agreement with the simple four-orbital model. The intensity of the lowest transition energy increases in the same order because the cancellation of the transition dipole moments associated with $a_{1u}(\pi) \rightarrow e_{gx}(\pi^*)$ and $a_{2u}(\pi) \rightarrow e_{gy}(\pi^*)$ associated with the high symmetry of porphyrins is dramatically lowered for bacteriochlorin. In addition, the redox properties are affected because the increase in the energy of HOMO gives a greater ease of oxidization along the series porphyrin < chlorin < bacteriochlorin.⁴ According to Figure 6, the reduction potential (associated with the LUMO) does not change nearly as much, also in agreement with observation.⁴

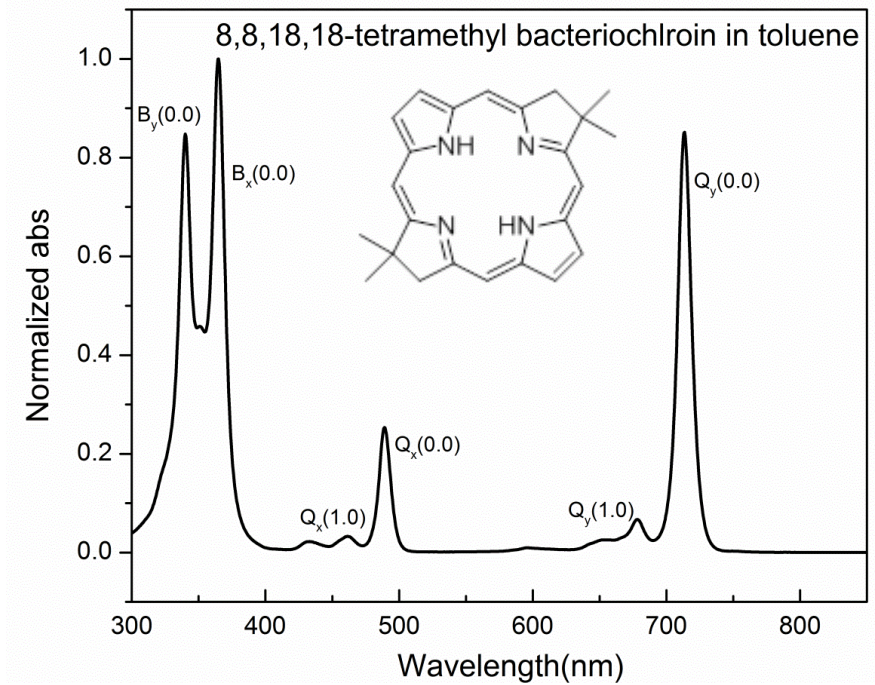


Figure 5. Structure and absorption spectrum of 8,8,18,18 –tetramethyl bacteriochlorin in toluene

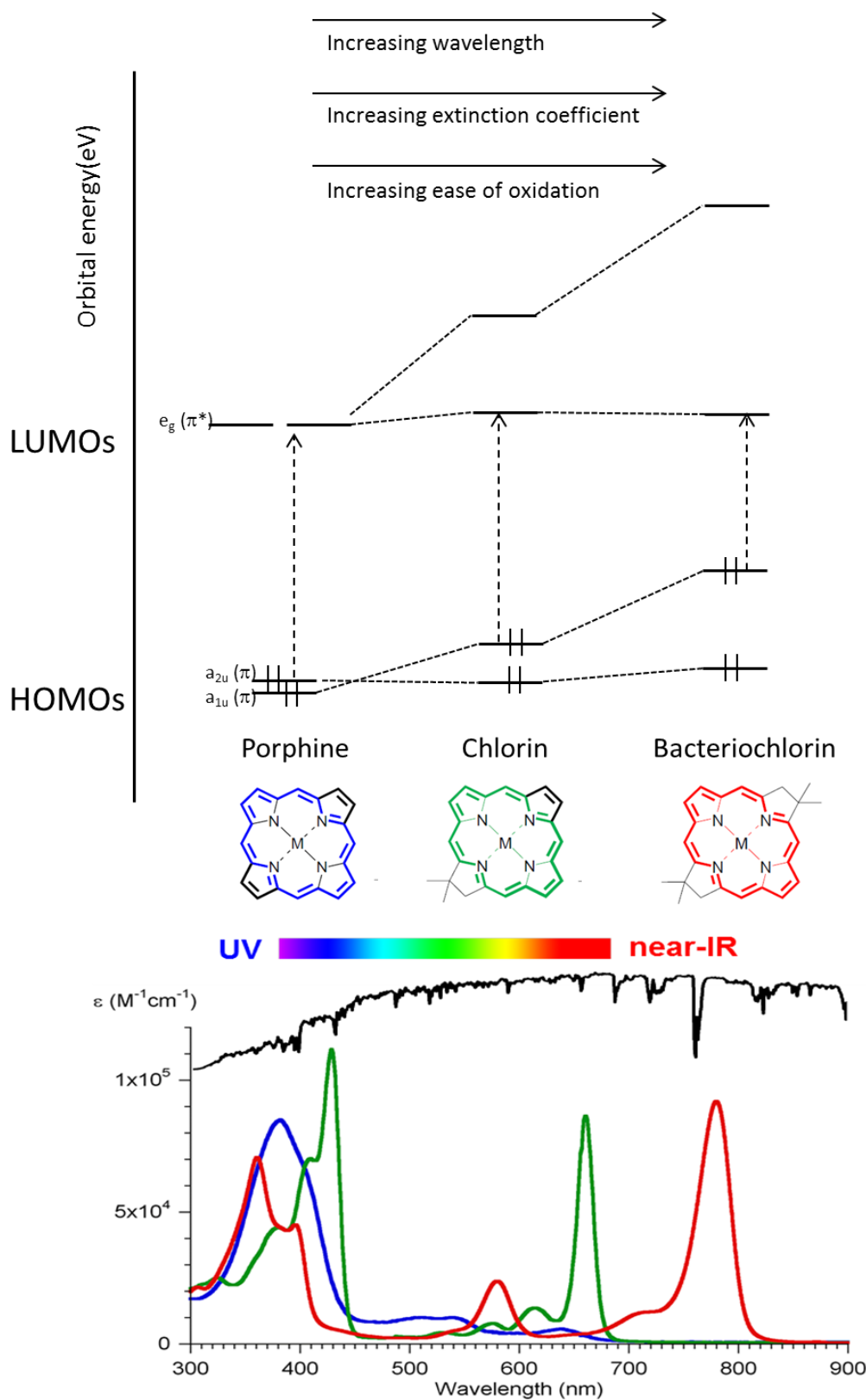


Figure 6. Schematic energy level diagram for highest occupied orbitals and lowest unoccupied orbitals of porphyrin, chlorin and bacteriochlorin (zinc complexes).⁴

Rate constants for excited-state processes in monomeric bacteriochlorins

The photophysical processes in bacteriochlorins, like most chromophores, can be understood using the Jablonski diagram shown in Figure 7.

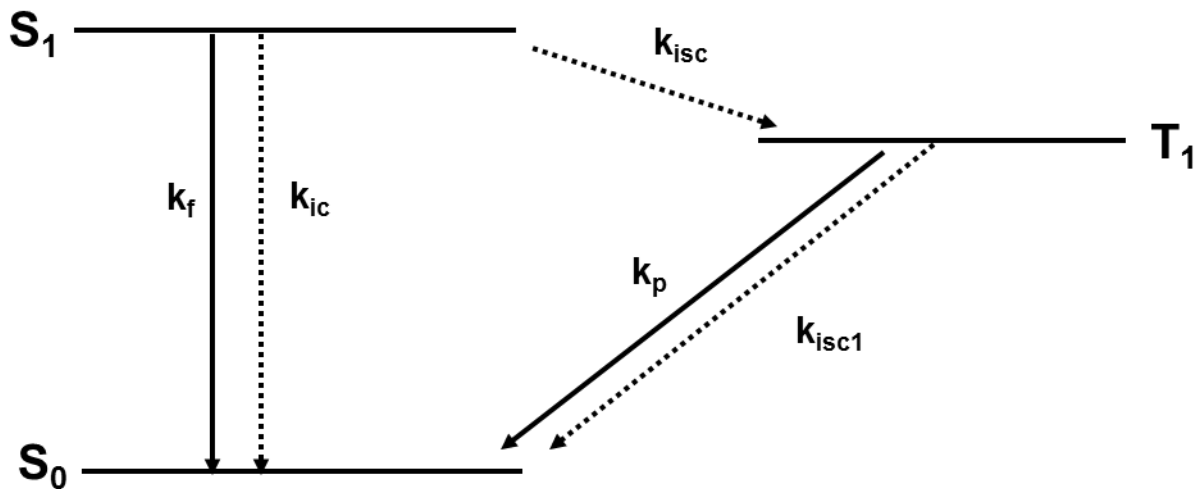


Figure 7. Jablonski energy level diagram

The observables (measured in the research described in this thesis) are lifetime (τ_S) and yield (Φ_f) of fluorescence of the lowest singlet excited state (S_1) and the yield (Φ_{isc}) of intersystem crossing to the lowest triplet excited state (T_1), often called the triplet yield (Φ_T). These observables are connected to the rate constants of the three decay processes of the S_1 excited state (e.g., the Q_y excited state of bacteriochlorins), namely $S_1 \rightarrow S_0$ spontaneous fluorescence (k_f), $S_1 \rightarrow S_0$ internal conversion (k_{ic}), and $S_1 \rightarrow T_1$ intersystem crossing (k_{isc}), via Eqs. (2) to (4).

$$\tau_S = (k_f + k_{ic} + k_{isc})^{-1} \quad (2)$$

$$\Phi_f = k_f / (k_f + k_{ic} + k_{isc}) \quad (3)$$

$$\Phi_{isc} = k_{isc} / (k_f + k_{ic} + k_{isc}) \quad (4)$$

The internal conversion yield can be calculated from Eq. (5).

$$\Phi_{ic} = 1 - \Phi_f - \Phi_{isc} \quad (5)$$

The radiative, intersystem-crossing, and internal-conversion rate constants can be calculated from the above quantities via Eq. (6), where $i = f, isc$ or ic .

$$k_i = \Phi_i / \tau_S \quad (6)$$

The Φ_{ic} , k_{ic} , k_f , and k_{isc} values are obtained using Eqs. 2-6, along with the measured values of τ_S , Φ_f , Φ_{isc} for the bacteriochlorins.

The triplet lifetime is given by Eq. 7, where k_p is the rate constant for phosphorescence emission and k_{isc1} is the rate constant for $T_1 \rightarrow S_0$ intersystem crossing

$$\tau_T = (k_p + k_{isc1}) \quad (7)$$

Rate constants for quenching of the excited state

The lifetime of the S_1 excited state and the fluorescence yield in the presence of a quencher (q) are given by Eqs. (8) and (9).

$$\tau_S^q = (k_f + k_{ic} + k_{isc} + k_q)^{-1} \quad (8)$$

$$\Phi_f^q = k_f / (k_f + k_{ic} + k_{isc} + k_q) \quad (9)$$

If the quencher is covalently attached to the bacteriochlorin, k_q is a first order process such as charge (electron or hole) transfer or energy transfer. If the quencher is not attached to the bacteriochlorin and has high concentration, then k_q reflects a pseudo first-order process and is given by Eq. 10, where k_{diff} is the second order rate constant for diffusion (units $M^{-1}sec^{-1}$) and $[Q]$ is the molar concentration of the quencher.

$$k_q = k_{\text{diff}} [Q] \quad (10)$$

In this diffusive process, such as is caused by quenching by molecular oxygen, the quenching rate constant is connected to the fluorescence yield and singlet excited state lifetime via the Stern-Volmer equation, indicated in Figure 11.

$$\Phi_f^0 / \Phi_f^q = \tau_s^0 / \tau_s^q = 1 + k_q \tau_0 [Q] \quad (11)$$

Similarly, quenching of the triplet excited state, and reduction in the lifetime (τ_T) of that state, by diffusible molecular oxygen can occur, via energy transfer or charge-transfer mechanisms.

Photodynamic therapy

Overview

Photodynamic therapy (PDT) is a phototherapy treatment in which living tissues are damaged or destroyed by using visible or NIR light in the presence of a photoactivatable dye and oxygen. Figure 8 shows the general mechanisms of PDT. An excited photosensitizer absorbing visible or NIR light generates a reactive oxygen species by transferring energy or electrons to ground state oxygen, and the reactive oxygen species in turn can damage living tissues.^{5,6}

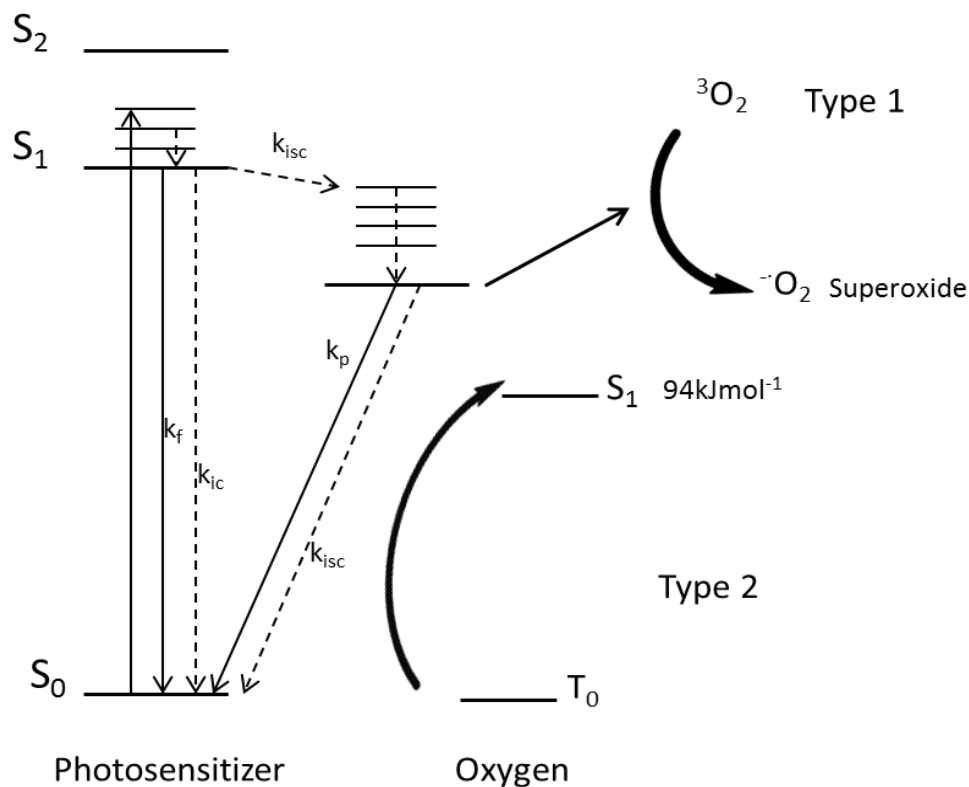


Figure 8. Modified Jablonski diagram to show mechanism of photodynamic therapy via Type 1 and Type 2 mechanisms.⁵

Photosensitizing agents

A photosensitizer is a critical element in the PDT process because following photon absorption, the photosensitizer provides the energy required to generate the reactive oxygen species. Therefore, a photosensitizer must satisfy several important requirements to be suitable for use. It should have absorption in the visible or NIR region because in this region penetrates more deeply into tissue and is less harmful than UV light. In addition, the photosensitizer's triplet-state energy should be higher than 94 kJ mol⁻¹, which corresponds to the singlet oxygen energy (1274 nm). It finally should have a highly efficient yield of intersystem crossing. Many types of photosensitizers have explored. For tetrapyrroles, three general classes that have been

examined include: porphyrin (Photofrin, BPD-MA), chlorophyll-based photosensitizers (chlorin, bacteriochlorin, purpurins) and dyes (phtalocyanine, naphthalocyanine).⁷ Bacteriochlorins are particularly attractive because of they absorb light in the NIR region where absorption by endogenous species (such as blood) is minimal. They also have favorable and tunable photophysical properties and chemical characteristics that can affect photostability and deliverability to the target site.

Reactive oxygen species

It is generally thought that two basic types of reactive oxygen species are produced: superoxide radical anion produced by direct electron transfer from agents or substrates through sensitizers and singlet oxygen produced by energy transfer. The production of these two general types of reactive oxygen species is respectively referred to as Types 1 and 2 processes, as shown in Figure 8. In the Type 1 photoreaction, a photosensitizer generates superoxide radical anions directly via by electron exchange with an organic substrate to produced reduced photosensitizer. This reduced agent reacts with ground state oxygen to generate a superoxide anion (Eq. 13). Another possible reaction is that an excited photosensitizer directly reacts with oxygen to generate superoxide radical anion by transferring electrons (Eq. 14).^{6,8}



In the Type 2 photoreaction, the excited triplet-state energy of a photosensitizer is transferred to ground state oxygen to produce reactive singlet oxygen (Eq. 15).⁸



There is considerable debate concerning which type of reaction is the most effective. Traditionally the Type 2 process has been reported to be dominant during PDT. A great deal of recent work suggests that the Type 1 process can be particularly effective, and a number of reactive oxygen species including superoxide, hydroxyl radicals, and other entities have been discussed. The PDT action depends on many other factors such as the photophysical properties of the photosensitizer, localization, aggregation, and solvent (including pH). As such, the mechanism of action may differ depending on such variables. In the later chapters, these factors are investigated by the use of synthetic bacteriochlorins, a suitable candidate as a photosensitizer.⁶

Experimental methods

The following methods were generally employed in the studies described in this thesis. Specific conditions are described as appropriate in the individual chapters.

Static ground state absorption measurements

Static ground state absorption spectra were obtained using a Shimadzu UV-1800 UV-VIS spectrophotometer. The spectra were scanned with 2-nm intervals in the range of 300-900 nm. The spectra were acquired using either 1 cm or 2 mm glass or quartz cuvettes and were corrected against a solvent blank.

Static fluorescence measurements

Static fluorescence measurements were performed on a Spex Fluorolog Tau2 spectrofluorometer. Excitation light provided by a 450W Xenon lamp passed through a single

grating monochromator (500 nm blaze, 1200 grooves/mm, 3.7 nm/mm) to the sample. The fluorescence signal was detected by a Hamamatsu R928 photomultiplier tube operating in photon counting mode and corrected for the detection-system spectral response. Most samples were contained in a 1 cm glass or quartz cuvette and studied at room temperature. Samples were typically prepared with absorption <0.2 in the Q_y band region to minimize the inner filter effect and were Ar-purged for 30 min. FbTPP ($\Phi_f = 0.07$ nondegassed toluene)⁹ and 8,8,18,18-tetramethylbacteriochlorin ($\Phi_f = 0.14$ Ar-purged toluene)¹⁰ were used as reference samples for the fluorescence yields.

Singlet-excited state lifetimes

The lifetime of the singlet excited state of bacteriochlorins was generally measured by a time-correlated single photon counting (TCSPC) instrument that employed Soret excitation flashes derived from a nitrogen pumped dye laser (PTI LaserStrobe) and a Gaussian instrument response function of 0.6 ns. The sample preparation procedure was the same as used for the static state measurements. The singlet excited-state lifetime ($\tau_s < 1$ ns) was also measured by transient absorption spectroscopy, using the transient absorption (TA) system described below in the section on measurement of intersystem crossing yields.

Triplet lifetimes

The triplet lifetime was obtained using a nanosecond to second time-resolved absorption spectrometer system. The excitation light was provided by either a 532 nm Q-switched Nd:YAG laser (YG400, Quantel) or a dye laser pumped by the Nd:YAG laser in the Q band with 5 ns pulses. The probe light was provided by a filtered 100W CW quartz tungsten halogen lamp

(Spectra-physics). The probe light passed through the excited sample and monochromator (Jarrell-Ash Monospec27) to arrive at the detection system. The signal was typically detected by an R928 PMT followed by a current to voltage amplifier and recorded on an oscilloscope (Tektronix). The overall instrument response of the detection system was adjustable depending on the set up, but typically was set to ~100 ns to ~1 μ s. Samples were prepared in tetrahydrofuran (THF) or 2Me-THF and Ar-purged for 30–60 min in a 1 cm glass cuvette.

Yields of intersystem crossing

The Φ_{isc} value for each compound was obtained using a TA technique in which the extent of bleaching of the ground-state $Q_x(1,0)$ band due to the lowest singlet excited state was measured immediately following a 130 fs flash in the $Q_y(0,0)$ band and compared with bleaching due to formation of the lowest triplet excited state at the asymptote of the singlet excited-state decay. TA measurement was performed at the PARC ultrafast laser facility (with the assistance of Dr. Dariusz Niedzwiedki). The TA system consists of a kilohertz femtosecond amplified Ti:sapphire laser (MaiTai oscillator and Empower pumped amplifier; Spectra-physics), and optical parametric amplifier (TOPAS; Light Conversion) and transition absorption system (Helios, Ultrafast Systems). Most bacteriochlorin samples were measured using excitation pulses 0.5 μ J per pulse in the Soret or Q_y bands regions (NUV to NIR) focused to a size of about 1 mm at the sample. The samples were prepared in a 2 mm glass cell with an absorbance of 0.4–0.5 in the Q_y band region and were Ar-purged for 30 min. Samples were stirred with a small magnetic stir bar during the measurements.

Photobleaching studies

The excitation light obtained from a 300W xenon lamp (Model R300-3 lamp and PS300-1 power supply; ILC Technologies, Sunnyvale, CA) passed through a 70 cm path cell containing deionized water followed by the monochromator with 10 nm bandpass to arrive at a sample. The sample was exposed to continuous illumination during the fixed time as calculated from the light intensity using an optometer (Model S471, United Detector Technologies, San Diego, CA). Samples in organic solvents were Ar-purged for at least 30 min. Samples in polar solvents such as micelles in deionized water and DMSO were subject to a repeated freeze-pump-thaw cycles on a high vacuum system to remove oxygen. During illumination, the samples were stirred using a magnetic bar at the bottom of the cuvette to avoid light exposure to only one side of the sample.

Phosphorescence spectra

Phosphorescence spectra were obtained using a QuantaMaster™40 spectrofluorometer attached to an InGaSA NIR detection system (Photon Technology International). The samples were prepared in 2MeTHF or THF and Ar-purged for 2h.

Overview of the thesis

The overall goal of this research is to (1) understand the electronic structure and the photophysical properties of synthetic bacteriochlorins and to elucidate design principles for tuning the spectra and photophysical characteristics for applications in solar-conversion systems, optical imaging, and PDT (as described in Chapters 2–6), and to (2) analyze various parameters of photodynamic action with synthetic bacteriochlorins as a new photosensitizer for PDT (as described in Chapters 7-11). All eleven chapters have been published in the scientific literature

and contain some results from collaborative work. The details of the collaborative studies are described below. This thesis focuses on the photophysical properties of the bacteriochlorins, their electronic structure as revealed by analysis of the optical and redox properties using molecular orbital characteristics, and how these fundamental properties may impact utilization in solar conversion and photomedical studies.

Chapter 2 describes the route and photophysical properties of synthetic bacteriochlorins, bearing a germinal dimethyl group in each pyrroline ring with extension to include a bacterio-13-oxophorbine and bacteriochlorin-13,15 dicarboximides. This study shows that the absorption of these bacteriochlorins can be tuned in the NIR spectral region out to 818 nm, which extends the spectral coverage beyond that obtained previously with synthetic bacteriochlorins lacking a fifth ring.

Chapter 3 analyzes the spectroscopic and photophysical properties of 33 synthetic bacteriochlorins by fluorescence quantum yields, singlet-excited lifetimes, intersystem crossing yields, triplet lifetimes and density functional theory (DFT) calculations. According to this analysis, design principles are presented for tuning the spectral and photophysical characteristics for various photochemical applications.

Chapter 4 and 5 describe the synthesis and characterization of bacteriochlorins containing magnesium, indium, zinc, palladium and copper. An approach is described to reduce the difficulty of the metallation of tetrapyrrole macrocycles by increasing the number of electron-withdrawing groups. In addition, comparison of the photophysical characteristics of free base and metallochlorins is presented. The yield of the intersystem crossing of

metallobacteriochlorins is determined to be higher than that of free base bacteriochlorins by the heavy metal enhancement of the spin-orbit coupling.

Chapter 6 focuses on the study of bacteriochlorins that contain various chalcone (3-phenyl-oxo-1-enyl) substituents at the 3,13-positions. The discussion includes the spectral, and photophysical properties (Φ_f , τ_s , Φ_T , τ_T , k_f , k_{ic} , k_{isc}) and analysis of the spectral properties using the four-orbital model and molecular-orbital characteristics provided by density functional theory (DFT) calculations. Bacteriochlorins with chalcone substituents extend the NIR absorption range of the Q_y band, and in some of the molecules have excited state charge-transfer (CT) characteristics.

Chapter 7, 8, 9, and 10 discuss effectiveness of PDT with stable synthetic bacteriochlorins against malignant melanoma cancer cells, and HeLa Cells, and for antimicrobial treatment. The results of PDT killing survival fractions, localization, reactive oxygen type detection, cell uptake, photostability, and photophysical properties of various synthetic bacteriochlorins used as photosensitizers are presented.

Chapter 11 analyzes these results to determine significant factors that influence the PDT activity. These results are interpreted using the reactive oxygen mechanism that is described in terms of excited-state redox potentials and photophysical properties. Collectively this analysis suggests important parameters that should be considered in developing next-generation photosensitizers, especially those based on bacteriochlorins, which appear quite promising.

Collaborations

All synthetic bacteriochlorins were synthesized in the laboratory of Dr. Jonathan Lindsey at the North Carolina State University. The DFT calculations to obtain molecular orbital characteristics, and the ground-state redox potential measurements were performed in the laboratory of Dr. David Bocian at the University of California, Riverside. The PDT activity studies such as the *in vitro* PDT experiments, *in vivo* fluorescence imaging, photosensitizer uptake, localization, and reactive oxygen species detection were performed in the laboratory of Dr. Michael R. Hamblin at the Harvard Medical School (Chapters 7-11).

In this dissertation, I collaborated with these researchers and the coworkers in their laboratories via my studies of the photophysical properties (including absorption, fluorescence and phosphorescence spectra, excited-state lifetimes, yields and rate constants of the excited-state decay pathways), four-orbital analyses of the optical spectra, photostability studies of bacteriochlorins for PDT, and analysis and correlation of these properties. These studies provide a broad fundamental understanding of the photophysical properties and electronic structure of bacteriochlorins that is relevant to their roles in natural photosynthesis, artificial systems for solar energy conversion, and potential use in photomedicine.

References

- (1) K. Kalyanasundaram, Photochemistry of Polypyridine and Porphyrin Complex, 1992, Academic Press in San Diego.
- (2) Gouterman, M. Study of the Effects of Substitution on Absorption Spectra of Porphyrin. *Journal of Chemical Physics*, Vol 30, No 5, 1139-1161
- (3) Gouterman, M. The Porphyrins, Vol 3; Dolphin D., Ed; Academic Press: New York. 1978 P 1-165
- (4) Chang, C.K; Hanson, L.K; Richardson, P.F; Young, R; Fajer, J. π Cation radicals of ferrous and free base isobacteriochlorins: Models for siroheme and sirohydrochlorin, *proc.Natl.Acad.Sci USA* 1981, Vol 78, No 5, pp 2652-2656
- (5) Bonnett, R. Chemical Aspects of Photodynamic Therapy. Gordon and Breach Science Publisher: Amsterdam, the Netherlands, 2000
- (6) Dougherty, T.J; Gomer C.J; Henderson B.W; Jori. G; Kessel, D; Korbelik, M; Moan, Johan; Peng, Q., Photodynamic Therapy, *Journal of the National Cancer Institute*, 1998, Vol. 90, No. 12, June 17
- (7) Macdonald, I.J; Dougherty, T.J, Basic principles of photodynamic therapy. *Journal of porphyrins and phthalocyanines*, 2001;5;405-129
- (8) Huang, Z. A review of progress in clinical photodynamic therapy. *Technology in cancer research and treatment*. 2005, Vol 4, No.3 June.
- (9) Seybold, P. G.; Gouterman, M. *J. Mol. Spectrosc.* 1969, 31, 1–13.
- (10) Yang, EK; Kirmaier, C; Krayner, M; Taniguchi, M; Kim, HJ; Diers, J.R; Bocian, D.F; Lindsey J.S; Holten, D. Photophysical Properties and Electronic Structure of Stable, Tunable Synthetic Bacteriochlorins: Extending the Features of Native Photosynthetic Pigments. *J. Phys. Chem. B.* 2011, 115, 10801–10816

Section 2

Molecular design and photophysical characterization of synthetic bacteriochlorins

Collaborations

All synthetic bacteriochlorins were synthesized in the laboratory of Dr. Jonathan Lindsey at the North Carolina State University. The DFT calculations to obtain molecular orbital characteristics, and the redox potential measurements were performed in the laboratory of Dr. David Bocian at the University of California, Riverside. I collaborated with these researchers and the coworkers in their laboratories via my studies of the photophysical properties (including absorption, fluorescence and phosphorescence spectra, excited-state lifetimes, yields and rate constants of the excited-state decay pathways), four-orbital analyses of the optical spectra, and analysis and correlation of these properties.

Chapter 2

De Novo Synthesis and Photophysical Characterization of Annulated Bacteriochlorins. Mimicking and Extending the Properties of Bacteriochlorophylls

Krayer, M; Yang, EK; Diers, J.R; Bocian, D.F; Holten,D; Lindsey, J.S. De Novo Synthesis and Photophysical Characterization of Annulated Bacteriochlorins. Mimicking and Extending the Properties of Bacteriochlorophylls. *New J. Chem.* 2011, 35, 587–601. DOI: 10.1039/c0nj00771d-
Reproduced by permission of The Royal Society of Chemistry (RSC) on behalf of the Centre National de la Recherche Scientifique (CNRS) and the RSC

Abstract

Bacteriochlorophylls contain the bacteriochlorin chromophore and a fifth, five-membered oxopentano ring that encompasses positions 13–15 known as the “isocyclic” ring E. Such bacterio-13¹-oxophorbines have heretofore only been available in the naturally occurring compounds, and analogues bearing six-membered rings have only been available by derivatization of bacteriochlorophylls. A de novo route to synthetic bacteriochlorins, which bear a geminal dimethyl group in each pyrroline ring, has been extended to gain access to a bacterio-13¹-oxophorbine and bacteriochlorin-13,15-dicarboximides. The route relies on acid-catalyzed condensation of a dihydrodipyrin–acetal to form the bacteriochlorin, which then is subjected to regioselective 15-bromination. Pd-mediated cyclization of the 15-bromobacteriochlorin bearing a 13-acetyl group (intramolecular β -arylation) or 13-ethoxycarbonyl group (carbamylation and intramolecular imidation) gives the bacterio-13¹-oxophorbine or bacteriochlorin-13,15-dicarboximide, respectively. The resulting macrocycles exhibit absorption in the near-infrared spectral region (733–818 nm), which extends the spectral coverage beyond that obtained previously with synthetic bacteriochlorins that lack a fifth ring. The macrocycles also exhibit excited singlet-state lifetimes (1.9–4.6 ns) comparable to or longer than those of natural photosynthetic pigments. Density functional theory calculations predict that the red-shifted absorption is primarily due to lowering of the energy of the lowest unoccupied molecular orbital. The new route complements existing semisynthetic routes and should enable fundamental spectroscopic studies and diverse photochemical applications.

Introduction

Bacteriochlorins absorb strongly in the near-infrared spectral region¹ and hence are attractive candidates for a wide variety of photochemical studies, including artificial photosynthesis,²⁻⁹ photodynamic therapy (PDT),¹⁰⁻²³ optical imaging,²⁴⁻²⁶ and perhaps flow cytometry.^{24,27} Naturally occurring bacteriochlorophylls *a*, *b*, and *g* contain the bacteriochlorin chromophore and provide the basis for light-harvesting processes and electron-transfer reactions in bacterial photosynthesis (Chart 1, panel A).²⁸ Bacteriochlorophylls also possess a five-membered ring (ring E) that encompasses the 13- and 15-positions; the ring contains a 13¹-oxo moiety and a 13²-methoxycarbonyl substituent. Synthetic manipulation of bacteriochlorophylls has afforded a number of derivatives including (i) bacteriopyropheophorbides, which lack the 13²-methoxycarbonyl substituent, the phytyl-like chain, and the central magnesium^{2-4,29,30}, and (ii) bacteriopurpurinimides (hereafter referred to as bacteriochlorin-imides), which bear a six-membered imide ring (Chart 1, panel B).^{6,12,16,17,31-37}

The presence of the imide ring in bacteriochlorin-imides provides a number of attractions including (1) a hyperchromic and bathochromic shift of the long-wavelength absorption band; (2) the ability to introduce diverse groups at the nitrogen of the imide ring;³⁸ and (3) increased stability of the macrocycle toward routine handling due to the presence of the second carbonyl group at the 15-position. So far, bacteriochlorins bearing the five membered oxopentano or six-membered imide ring have only been available from the natural compounds or upon semisynthesis therefrom, respectively, although synthetic porphyrins and chlorins with a wide variety of annulated rings have been prepared.^{39,40} Two significant problems in the preparation of derivatives of bacteriochlorophylls include limited stability^{36,41,42} and poor synthetic malleability owing to the presence of a nearly full complement of substituents about the

perimeter of the macrocycle.^{13,18} The synthesis of bacteriochlorins by reduction or addition of porphyrins or chlorins is appropriate for a number of applications but generally suffers from a lack of regiocontrol.⁴³

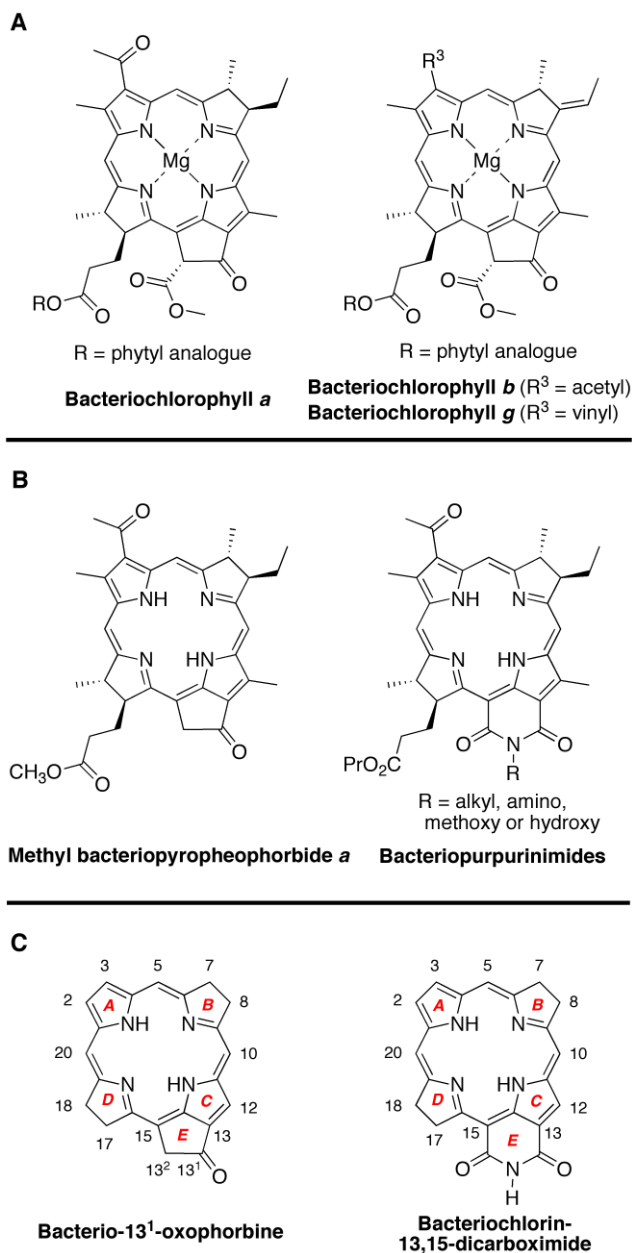


Chart 1. (A) Naturally occurring bacteriochlorophylls. (B) Derivatives of naturally occurring bacteriochlorophylls. (C) Nomenclature of the core macrocycles.

Over the past decade we have been developing a de novo synthesis of bacteriochlorins.⁴⁴⁻
⁴⁶ The route affords bacteriochlorins wherein each pyrroline ring contains a geminal dimethyl group rather than the *trans*-dialkyl and *exo*-ethylidene moieties of the naturally occurring bacteriochlorophylls. The geminal dimethyl group has the attractive feature of stabilizing the macrocycle toward adventitious dehydrogenation. Synthetic bacteriochlorins bearing diverse substituents at specific sites in the pyrrolic units have been prepared, and selected derivatization processes of the bacteriochlorins have been examined (including regioselective bromination); however, no annulated rings have yet been introduced.⁴⁴⁻⁵¹ Here we extend the de novo route to create stable, tailorable analogues of the fundamental bacterio-13¹-oxophorbine and bacteriochlorin-13,15-dicarboximide macrocyclic skeletons (Chart 1, panel C).⁵² The synthesis and spectroscopic analysis of such synthetic macrocycles is essential for understanding the structural features that underpin the characteristic spectral properties of the naturally occurring bacteriochlorophylls.

Experimental methods

Synthesis and DFT calculation

Experimental methods are described in detail in elsewhere.^A

Photophysical measurements

Static absorption and fluorescence measurements were performed as described previously.^{69,70} Argon-purged solutions of the samples in toluene with an absorbance of ≤ 0.10 at the excitation wavelength were used for the fluorescence spectral, quantum yield, and lifetime measurements. Fluorescence lifetimes were obtained using a phase modulation technique and Soret-band excitation⁷⁰ or via decay measurements using Soret-region excitation pulses obtained

from a nitrogen-pumped dye laser and time-correlated-single-photon-counting detection. Emission measurements employed 2-4 nm excitation- and detection-monochromator bandwidths and 0.2 nm data intervals. Emission spectra were corrected for detection-system spectral response. Fluorescence quantum yields were determined relative to free base tetraphenylporphyrin ($\Phi_f = 0.090$),⁷¹ chlorophyll *a* in benzene ($\Phi_f = 0.325$)⁷² or chlorophyll *a* in toluene (which was found here to have the same value as in benzene).

Results and Discussion

Synthesis and characterization

The synthesis and structure characterization shown in chart 2 and 3 of all the compounds investigated in this study are described in detail in elsewhere.^A

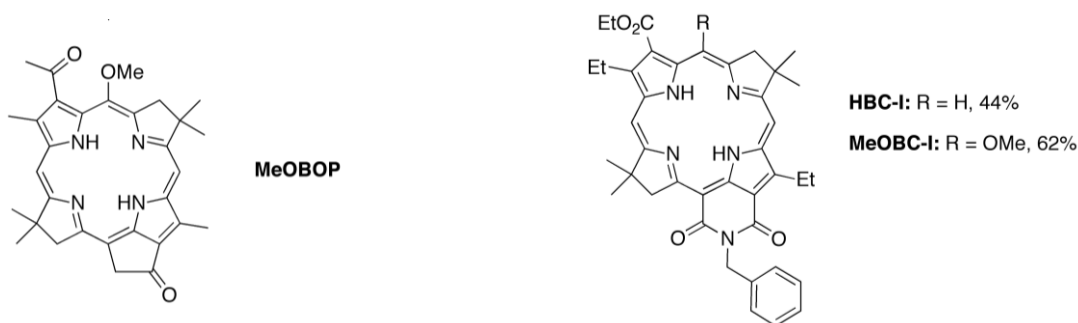


Chart 2. Structures of MeOBOP, HBC-I, and MeOBC-I^A

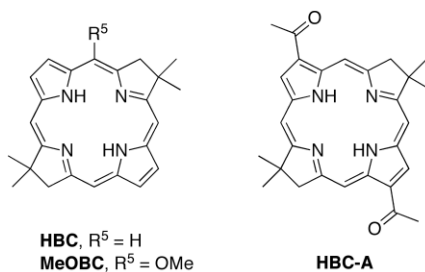


Chart 3. Benchmark bacteriochlorins.⁴⁵

Absorption spectra

The annulated bacteriochlorins prepared herein exhibit characteristic bacteriochlorin absorption spectra,¹ with near-ultraviolet (Soret or B) bands, a long-wavelength feature, the $Q_y(0,0)$ band, in the near-infrared region of comparable peak intensity, and the weaker Q_x bands in the intervening region (500–600 nm). The position of the long wavelength absorption band of a photochemically active species is of central importance, defining not only the spectral region where absorption occurs but also the energy of the lowest singlet excited-state, which dominates key photophysical properties. These properties include fluorescence and, for the native bacteriochlorophylls, the energy- and electron-transfer reactions of photosynthesis.

Prior studies with synthetic bacteriochlorins have shown that the position of the $Q_y(0,0)$ band could be tuned from 707 nm to 792 nm (typically measured in toluene).^{44-46,51} The synthetic bacterio-13¹-oxophorbine **MeOBOP** (733 nm) absorbs in this range, to be compared with that of methyl bacteriopyropheophorbide *a* (754 nm in CH₂Cl₂).²⁹ Bacteriopheophytin *a* (**BPh-a**), which differs from methyl bacteriopyropheophorbide *a* owing to the presence of a 13²-methoxycarbonyl group and a long alkyl ester chain, also absorbs at 750–760 nm in hydrocarbon solvents.^{64,65} The bacteriochlorin–imides **MeOBC-I** (793 nm) and **HBC-I** (818 nm) exhibit $Q_y(0,0)$ bands that extend further into the near infrared. The $Q_y(0,0)$ band of bacteriochlorin–imides derived from bacteriochlorophyll *a* occurs in the same spectral range (800–830 nm).^{32,33,36}

The spectra of **MeOBOP**, **MeOBC-I** and **HBC-I** in toluene are shown in Figure 1. The $Q_y(0,0)$ positions are listed in Table 1 along with those of a number of bacteriochlorin benchmarks that lack the annulated ring E. Reference molecules for **MeOBOP** include a set of 3,13-diacetylbacteriochlorins: **MeOBC-MeA** (743 nm), **MeOBC-A** (740 nm), **HBC-MeA** (766

nm) and **HBC-A** (768 nm). The first three of these 3,13-diacetyl bacteriochlorins were prepared here whereas **HBC-A** was synthesized previously.⁴⁵ Comparison among the four 3,13-diacetyl bacteriochlorins shows that (1) the 5-methoxy group results in an average 25-nm hypsochromic shift in the $Q_y(0,0)$ position, and (2) the 2,12-dimethyl groups have little (≤ 3 nm) effect on the $Q_y(0,0)$ position. The first point, regarding the 5-methoxy group, is also made upon comparison of the $Q_y(0,0)$ positions of bacteriochlorins **MeOBC-EtEs** (739 nm) and **HBC-EtEs** (761 nm).⁴⁶ The latter two compounds serve as benchmarks for the two bacteriochlorin-imides (**MeOBC-I** and **HBC-I**): the benchmarks contain the 2,12-diethyl and 3-ester groups but lack the 13,15-dicarboximide moiety. The $Q_y(0,0)$ position for **MeOBC-I** (793 nm) and **HBC-I** (818 nm), like the three pairs of bacteriochlorins noted above, shows a 25-nm hypsochromic shift due to the 5-methoxy group. Interestingly, the impact of the 5-methoxy group is diminished in bacteriochlorins that lack a carbonyl moiety (acetyl, ester, imide) at the 3,13-positions. This point is seen upon comparison of the $Q_y(0,0)$ positions of bacteriochlorins **MeOBC** (709 nm)⁴⁶ and **HBC** (713 nm)⁴⁵ that bear one or no substituents, respectively, other than the geminal dimethyl groups.

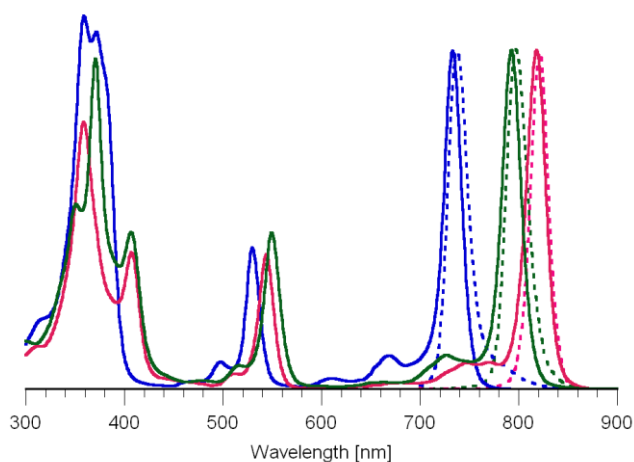


Figure 1. Absorption (— solid lines) and emission (--- dashed lines) spectra (normalized) in toluene at room temperature of **MeOBOP** (blue), **MeOBC-I** (green), and **HBC-I** (magenta)

Fluorescence spectra, quantum yields, and singlet excited-State lifetimes

The fluorescence spectra of **MeOBOP**, **MeOBC-I** and **HBC-I** in toluene are shown in Figure 1 (dotted lines). Each fluorescence spectrum is dominated by the $Q_y(0,0)$ band, which lies ~5 nm to longer wavelength than the corresponding $Q_y(0,0)$ absorption feature. The same is generally true for the benchmark bacteriochlorins listed in Table 1; exceptions include **HBC-EtEs** and **MeOBC-EtEs**, which show larger (~15 nm) Stokes shifts, suggesting greater changes in structure or solvent interactions upon photoexcitation.

The bathochromic shift of the $Q_y(0,0)$ band of **MeOBOP**, **MeOBC-I** and **HBC-I** (733 nm, 793 nm, 818 nm) is accompanied by a decrease in the fluorescence yield (0.19, 0.052, 0.036) and shortening of the singlet excited-state lifetime (4.6 ns, 2.2 ns, 1.9 ns). The same is true of the benchmark bacteriochlorins. These data are plotted in Figures 2C and D and listed in Table 1. For comparison, the average singlet excited-state lifetime of bacteriopheophytin *a* is 2.0–2.7 ns and has a $Q_y(0,0)$ band at 750–760 nm in organic solvents (Table 1).^{64,65} Thus, the two synthetic bacteriochlorin–imides absorb at significantly longer wavelengths (by ~40 and ~70 nm) than the natural pigment and yet have comparable excited-state lifetime.

Frontier molecular orbitals and electronic properties

The energies and electron-density distributions of the frontier molecular orbitals (MOs) of the bacterio-13¹-oxophorbine, bacteriochlorin–imides, and benchmark compounds were obtained from density functional theory (DFT) calculations. Such methods were also applied to the fictive bacteriochlorin **MeOBC-MeAMe**¹⁵ (Chart 4), which differs from the benchmark compound **MeOBC-MeA** in the addition of a 15-methyl substituent. Examination of **MeOBC-MeAMe**¹⁵ provides deeper insight into the origin of the effects caused by the formation of the

fifth ring. The four frontier molecular orbitals and energy levels for nine compounds are shown in Table 2.

Table 1. Photophysical Properties of Bacteriochlorin Compounds.^a

Compound	Cmpd code for Fig. 2	λ_{Q_y} abs (nm)	λ_{Q_y} em (nm)	I_{Q_y}/I_B ^b	Φ_f ^c	τ_s (ns) ^d	HOMO – LUMO (eV) ^e	HOMO-1 – LUMO+1 (eV) ^f
<i>Targets:</i>								
HBC-I	<i>a</i>	818	823	1.3	0.036	1.9	1.92	4.01
MeOBC-I	<i>b</i>	793	798	1.0	0.052	2.2	2.02	3.92
MeOBOP	<i>h</i>	733	739	0.93	0.19	4.6	2.18	3.86
<i>Benchmarks:</i>								
HBC	<i>i</i>	713	716	0.85	0.17	4.0	2.26	4.06
HBC-A	<i>c</i>	768	771	1.2	0.11	2.9	2.05	3.95
HBC-MeA		766					2.02	3.94
HBC-EtEs	<i>d</i>	761	775	0.94	0.14	3.3	2.10	3.98
MeOBC	<i>j</i>	709	711	0.87	0.25	5.0	2.28	3.98
MeOBC-A	<i>f</i>	740	747	0.96	0.14	3.8	2.14	3.88
MeOBC-MeA	<i>e</i>	743	749	0.95	0.13	3.4	2.14	3.87
MeOBC-EtEs	<i>g</i>	739	749	1.1	0.17	4.3	2.16	3.91
BPh-a^g		758	768	0.69	0.10	2.7	2.03 ^h	3.89 ^h
<i>Fictive:</i>								
MeOBC-MeAMe¹⁵							2.17	3.80

^aIn toluene at room temperature unless noted otherwise. ^bRatio of the peak intensities of the $Q_y(0,0)$ and B bands. ^cFluorescence quantum yield (error $\pm 7\%$). ^dLifetime of the lowest singlet excited state measured using fluorescence techniques (error $\pm 7\%$). Values for several of the benchmark compounds were reported in ref. 45. ^eEnergy gap between the LUMO and HOMO orbitals. ^fEnergy gap between the LUMO+1 and HOMO-1 orbitals. ^gValues are in toluene. The values in ethanol are $\lambda_{abs} = 750$ nm, $\lambda_{em} = 768$ nm, $I_{Q_y}/I_B = 0.39$, $\Phi_f = 0.081$, and $\tau_s = 2.3$ ns. A value of $\tau_s = 2.0$ ns in acetone/methanol 7:3 was found in ref 65. ^hDFT calculations were performed with the truncated phytol tail $-\text{CH}_2\text{CH}=\text{C}(\text{CH}_3)(\text{CH}_2\text{CH}_3)$.

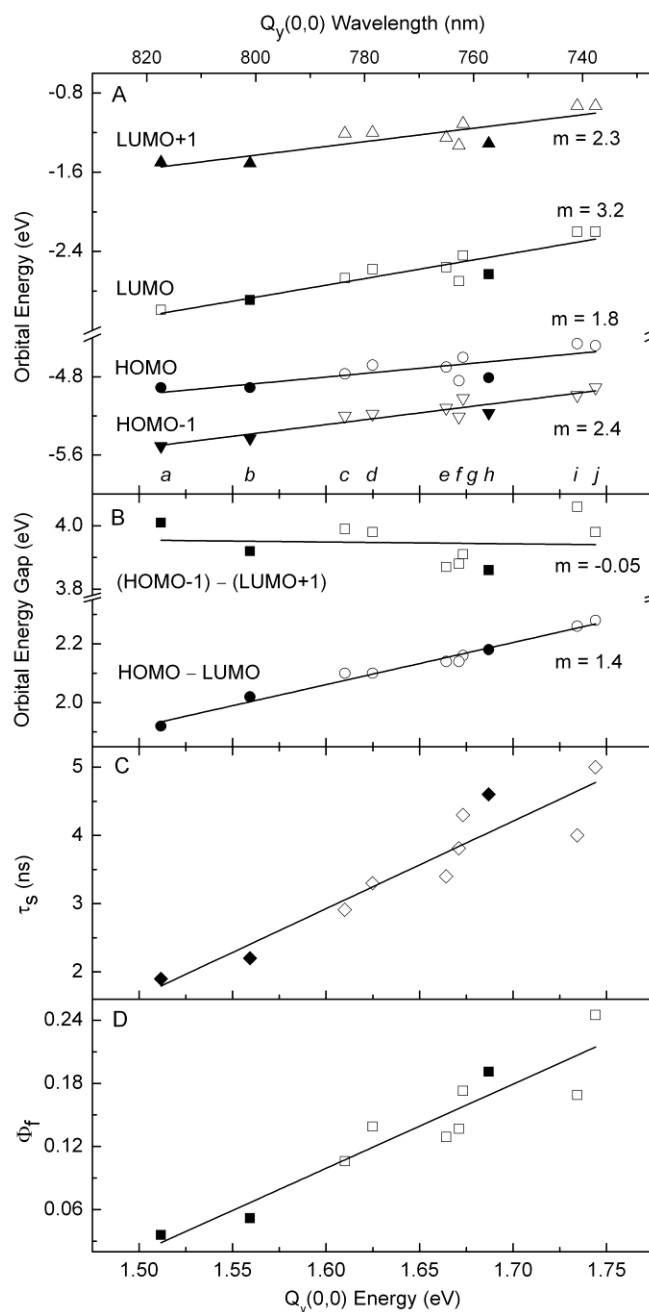


Figure 2. Orbital energies, energy gaps, singlet excited-state lifetime, and fluorescence yield as a function of the $Q_y(0,0)$ energy (bottom axis) and wavelength (top axis). For each plot, the solid symbols are for the three target compounds, **MeOBOP**, **MeOBC-I** and **HBC-I**, and the open symbols are for the benchmark bacteriochlorins. The letter code (*a-j*) at the bottom of panel A gives the left-to-right order of the data points for each plot in the figure and identifies the compounds as listed in the first two columns of Table 1.

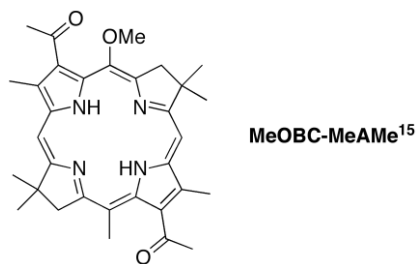
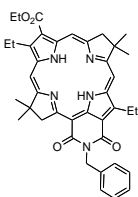
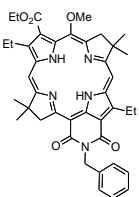
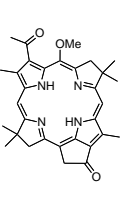
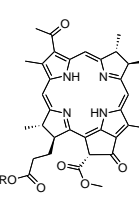
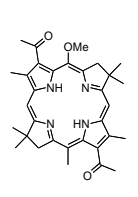
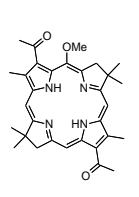
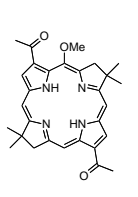
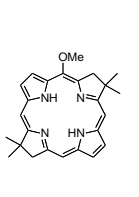
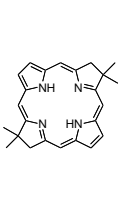
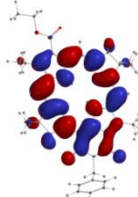
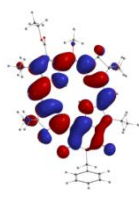
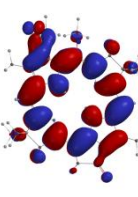
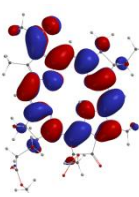
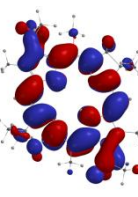
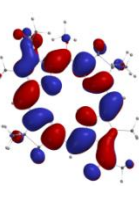
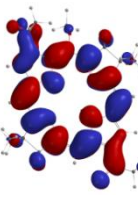
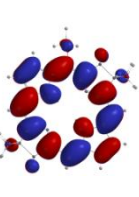
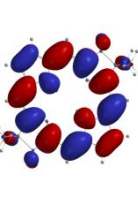
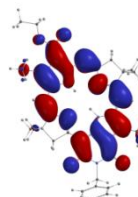
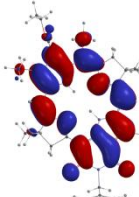
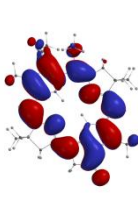
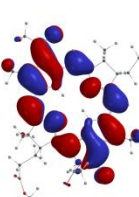
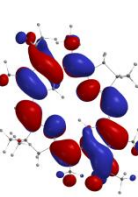
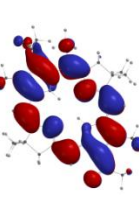
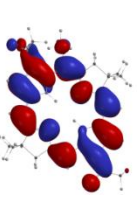
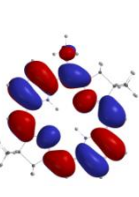
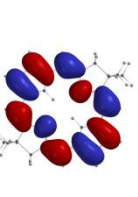
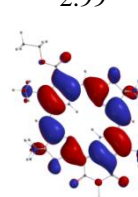
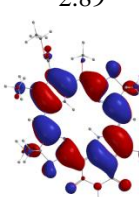
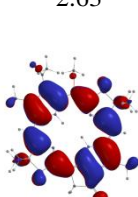
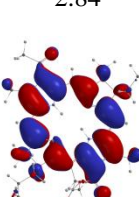
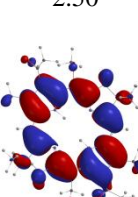
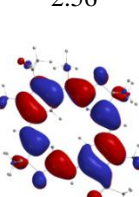
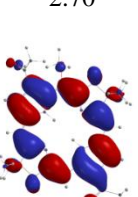
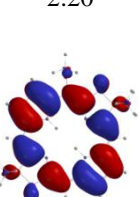
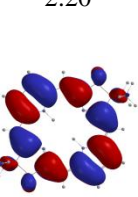
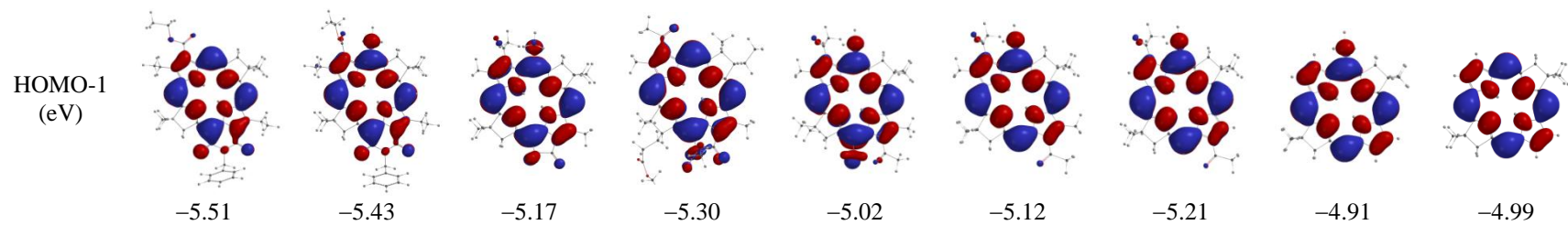


Chart 4. Fictive bacteriochlorin for which DFT calculations were performed.

The key results of the DFT calculations for **MeOBOP**, **MeOBC-I**, **HBC-I** and representative benchmark synthetic and fictive compounds are summarized in Figure 2. This figure shows the characteristics of the four frontier orbitals: the highest occupied molecular orbital (HOMO), the lowest unoccupied molecular orbital (LUMO), the HOMO-1, and LUMO+1. The energies of these MOs are plotted as a function of the $Q_y(0,0)$ absorption-band energy/wavelength in Figure 2A, and analogous plots for the HOMO – LUMO energy gap and HOMO-1 – LUMO+1 energy gap are shown in Figure 2B. In each of these plots, the data for the key target compounds (**MeOBOP**, **MeOBC-I** and **HBC-I**) are given by closed symbols and those for the benchmark bacteriochlorins by open symbols. The values for the HOMO – LUMO and HOMO-1 – LUMO+1 energy gaps for the various compounds are listed in Table 1. These two energy gaps are relevant to the spectral analysis given below.

Table 2. Molecular-orbital energies and electron-density distributions of bacteriochlorin compounds.

	HBC-I	MeOBC-I	MeOBOP	BPh-a ^a	MeOBC-MeAm ¹⁵	MeOBC-MeA	MeOBC-A	MeOBC	HBC
Structure									
LUMO+1 (eV)	 -1.50	 -1.51	 -1.31	 -1.41	 -1.22	 -1.25	 -1.33	 -0.93	 -0.93
LUMO (eV)	 -2.99	 -2.89	 -2.63	 -2.84	 -2.50	 -2.56	 -2.70	 -2.20	 -2.20
HOMO (eV)	 -4.91	 -4.91	 -4.81	 -4.87	 -4.67	 -4.70	 -4.84	 -4.48	 -4.46



^aFor **BPh-a**, calculations were performed with a truncated phtyl tail [-CH₂-CH=C(CH₃)(CH₂CH₃)], which is omitted in the display here.

The salient points from the DFT calculations and the relationship to the observed spectral properties are as follows:

(1) The slopes of the trend lines given in Figure 2A show that the LUMO ($m = 3.2$) is more strongly connected with the wavelength/energy of the $Q_y(0,0)$ absorption band than are the HOMO ($m = 1.8$), LUMO+1 ($m = 2.3$) and HOMO-1 ($m = 2.4$). These differences can be traced to the generally greater electron density in the LUMO at the substituent sites (Table 2). The most important sites in this regard are the 3,13-positions of the carbonyl substituents (acetyl, ester, imide) of **MeOBOP**, **MeOBC-I**, **HBC-I** and the benchmark bacteriochlorins. These sites (and the 2,12-positions) are on the molecular y -axis, which is the axis on which the Q_y optical transition is polarized.

(2) In Gouterman's four-orbital model,^{66,67} the position of the $Q_y(0,0)$ absorption band depends on the average value of the HOMO – LUMO energy gap and the HOMO-1 – LUMO+1 energy gap. Because of the trends in the individual molecular orbitals described above and shown in Figure 2A, there is a much greater variation in the HOMO – LUMO energy gap versus the HOMO-1 – LUMO+1 energy gap for **MeOBOP**, **MeOBC-I**, **HBC-I** and the benchmark bacteriochlorins (Table 1). The consequence is a much greater magnitude of the slope of the trend line for the HOMO – LUMO energy gap ($m = 1.4$) versus the HOMO-1 – LUMO+1 energy gap ($m = -0.05$) plotted against the $Q_y(0,0)$ wavelength/energy (Figure 2B). Consequently, the wavelength/position of the $Q_y(0,0)$ band is dominated by the HOMO – LUMO energy gap for the bacterio-13¹-oxophorbine, bacteriochlorin–imides, and bacteriochlorins described here. In turn, following the findings given in point (1), the spectral position is dictated much more strongly by the dependence of the LUMO than the HOMO on the macrocycle-substituent pattern for these molecules.

(3) The DFT calculations reproduce the effect of the 5-methoxy group on the position of the $Q_y(0,0)$ wavelength/energy. This can be seen by comparing the value for the $Q_y(0,0)$ wavelength and the HOMO – LUMO energy gap for the following pairs of 3,13-carbonyl-containing (acetyl, ester, imide) compounds (Table 1): **MeOBC-I** (793 nm, 2.02 eV) versus **HBC-I** (818 nm, 1.92 eV); **MeOBC-EtEs** (739 nm, 2.16 eV) versus **HBC-EtEs** (761 nm, 2.10 eV); **MeOBC-MeA** (743 nm, 2.14 eV) versus **HBC-MeA** (766 nm, 2.02 eV); and **MeOBC-A** (740 nm, 2.14 eV) versus **HBC-A** (768 nm, 2.05 eV). For these pairs of compounds (with versus without the 5-methoxy group), the average bathochromic shift is 24 nm and the average shift in the HOMO – LUMO gap to lower energy is 0.09 eV. By comparison, the values for **MeOBC** (709 nm, 2.28 eV) versus **HBC** (713 nm, 2.26 eV) reveal a much smaller spectral shift of 4 nm and a corresponding smaller molecular-orbital energy-gap shift of 0.02 eV. Obviously there is interplay between the electron-donating ability of the 5-methoxy group and the sensitivity of the 3,13-positions to the presence of auxochromes such as carbonyl moieties.

(4) The DFT calculations of the benchmark compounds reproduce the finding that the 2,12-dimethyl groups of bacterio-13¹-oxophorbine **MeOBOP**, and in analogy the 2-ethyl group of **MeOBC-I** and **HBC-I**, have little effect. This result is shown by the $Q_y(0,0)$ wavelength and the HOMO – LUMO energy gap for the following pairs of compounds: **HBC-A** (768 nm, 2.05 eV) versus **HBC-MeA** (766 nm, 2.02 eV); and **MeOBC-A** (740 nm, 2.14 eV) versus **MeOBC-MeA** (743 nm, 2.14 eV). In both cases the presence of the 2,12-dimethyl groups results in ≤ 3 nm spectral shift and a ≤ 0.03 eV shift in the molecular-orbital energy gap. Collectively, these results suggest that the alkyl groups at the 2- or 12-positions of **MeOBOP**, **MeOBC-I** and **HBC-I**, and by implication the native photosynthetic pigments such as **BPh-a** (Table 2), play an insignificant role in determining the spectral properties of these molecules.

(5) The data and analysis given above (Table 1 and Figures 1 and 2) provide insights into which substituents are most responsible for the spectral characteristics of **MeOBOP** versus that of the benchmark bacteriochlorin **MeOBC**. The $Q_y(0,0)$ position and HOMO – LUMO gap for **MeOBC** (709 nm, 2.28 eV) are strongly affected upon the addition of the 3,13-diacetyl groups (**MeOBC-A**: 740 nm, 2.14 eV), with little further effect upon addition of the 2,12-dimethyl groups (**MeOBC-MeA**: 743 nm, 2.14 eV). The final step to obtain **MeOBOP** (733 nm, 2.18 eV) is closure to form the five-membered ring. The latter can be thought of as first, placement of a substituent at the 15-methyl group, and second, ring closure accompanied by structural/electronic effects such as ring strain and shift toward planarity. To gain insights into the effect of the 15-substituent, DFT calculations were carried out on the fictive bacteriochlorin **MeOBC-MeAMe**¹⁵, wherein a methyl group is placed at the 15-position (Tables 1 and 2). The HOMO – LUMO energy gap (2.17 eV) for this fictive compound is between those for **MeOBC-MeA** (2.14 eV) and **MeOBOP** (2.18 eV), consistent with a modest effect of substitution at the 15-position. Given the small (0.03–0.04 eV) energy shifts involved, however, the effects of 15-substitution versus ring closure (once the 13-acetyl group is in place) are of uncertain relative magnitude in dictating the ultimate spectral properties of the bacterio-13¹-oxophorbine chromophores.

Outlook

Bacteriochlorophylls are Nature's pigments for absorption of sunlight in the near-infrared region. The ability to utilize such compounds in diverse artificial systems – such as artificial photosynthesis, clinical diagnostics, and photomedicine – depends on versatile synthetic methods that afford stable macrocycles and that enable the spectral properties to be tuned at will. The designs we have chosen employ a geminal dimethyl group in each pyrroline ring to ensure

stability toward adventitious dehydrogenation. The resulting synthetic bacteriochlorins thus differ slightly in structure from the natural pigments, yet are more robust toward routine handling and synthetic manipulation. Here we have explored the ability to install an exocyclic ring, either the five-membered “ring E” as occurs in all bacteriochlorophylls, or the six-membered imide ring characteristic of derivatives of bacteriochlorophylls commonly known as bacteriopurpurinimides.

Of the de novo synthesized bacteriochlorins that we have prepared to date, **MeOBC**⁴⁶ and **HBC**⁴⁵ are at the shorter wavelength end of the range of Q_y(0,0) absorption positions while the two bacteriochlorin–imides **MeOBC-I** and **HBC-I** are at the longer extreme. A naturally occurring bacteriochlorin (wherein each pyrroline ring bears a geminal dialkyl unit and an oxo group) known as tolyporphin A absorbs at 678 nm.⁶⁸ The ability to tune the absorption band almost at will from ~680–820 nm bodes well for the use of synthetic bacteriochlorins, bacterio-13¹-oxophorbines, and bacteriochlorin-13,15-dicarboximides in diverse photochemical applications. The pursuit of such applications will be facilitated by the fluorescence yields (0.036–0.19), singlet excited-state lifetimes (1.9–4.6 ns), and photostability of the bacterio-13¹-oxophorbine and bacteriochlorin-13,15-dicarboximides prepared herein, as well as the obvious sites for synthetic elaboration provided by the keto and *N*-imide groups of the annulated ring E.

Acknowledgment

This work was supported by grants from the Division of Chemical Sciences, Geosciences and Biosciences Division, Office of Basic Energy Sciences of the U.S. Department of Energy to D.F.B. (DE-FG02-05ER15660), D.H. (DE-FG02-05ER15661) and J.S.L. (DE-FG02-96ER14632). Mass spectra were obtained at the Mass Spectrometry Laboratory for Biotechnology at North Carolina State University. Partial funding for the facility was obtained from the North Carolina Biotechnology Center and the National Science Foundation. The link can be found in the publication reference (A).

References

- (A) Kraymer, M; Yang, EK; Diers, J.R; Bocian, D.F; Holten, D; Lindsey, J.S. De Novo Synthesis and Photophysical Characterization of Annulate Bacteriochlorins. Mimicking and Extending the Properties of Bacteriochlorophylls. *New J. Chem.* **2011**, 35, 587-601
- (1) M. Kobayashi, M. Akiyama, H. Kano and H. Kise, in *Chlorophylls and Bacteriochlorophylls: Biochemistry, Biophysics, Functions and Applications*, ed. B. Grimm, R. J. Porra, W. Rüdiger and H. Scheer, Springer, Dordrecht, The Netherlands, 2006, vol. 25, ch. 6, pp. 79–94.
- (2) M. Wasielewski and W. A. Svec, *J. Org. Chem.*, 1980, **45**, 1969–1974.
- (3) A. Osuka, S. Marumo, Y. Wada, I. Yamazaki, T. Yamazaki, Y. Shirakawa and Y. Nishimura, *Bull. Chem. Soc. Jpn.*, 1995, **68**, 2909–2915.
- (4) T. Miyatake, H. Tamiaki, A. R. Holzwarth and K. Schaffner, *Photochem. Photobiol.*, 1999, **69**, 448–456.
- (5) H. Mössler, M. Wittenberg, D. Niethammer, R. K. Mudrassagam, H. Kurreck and M. Huber, *Magn. Reson. Chem.*, 2000, **38**, 67–84.
- (6) M. A. Grin, I. S. Lonin, S. V. Fedyunin, A. G. Tsiprovskiy, A. A. Strizhakov, A. A. Tsygankov, A. A. Krasnovsky and A. F. Mironov, *Mendeleev Commun.*, 2007, **17**, 209–211.
- (7) C. Muthiah, M. Taniguchi, H.-J. Kim, I. Schmidt, H. L. Kee, D. Holten, D. F. Bocian and J. S. Lindsey, *Photochem. Photobiol.*, 2007, **83**, 1513–1528.
- (8) J. R. Stromberg, A. Marton, H. L. Kee, C. Kirmaier, J. R. Diers, C. Muthiah, M. Taniguchi, J. S. Lindsey, D. F. Bocian, G. J. Meyer and D. Holten, *J. Phys. Chem. C*, 2007, **111**, 15464–15478.
- (9) C. Muthiah, H. L. Kee, J. R. Diers, D. Fan, M. Ptaszek, D. F. Bocian, D. Holten and J. S. Lindsey, *Photochem. Photobiol.*, 2008, **84**, 786–801.
- (10) J. J. Schuitmaker, J. A. van Best, J. L. van Delft, T. M. A. R. Dubbelman, J. A. Oosterhuis and D. de Wolff-Rouendaal, *Invest. Ophthalmol. Vis. Sci.*, 1990, **31**, 1444–1450.
- (11) J. P. Rovers, M. L. de Jode, H. Rezzoug and M. F. Grahn, *Photochem. Photobiol.*, 2000, **72**, 358–364.
- (12) Y. Chen, A. Graham, W. Potter, J. Morgan, L. Vaughan, D. A. Bellnier, B. W. Henderson, A. Oseroff, T. J. Dougherty and R. K. Pandey, *J. Med. Chem.*, 2002, **45**, 255–258.
- (13) Y. Chen, G. Li and R. K. Pandey, *Curr. Org. Chem.*, 2004, **8**, 1105–1134.
- (14) F. H. van Duijnhoven, J. P. Rovers, K. Engelmann, Z. Krajina, S. F. Purkiss, F. A. Zoetmulder, T. J. Vogl and O. T. Terpstra, *Ann. Surg. Oncol.*, 2005, **12**, 808–816.

- (15) A. S. Brandis, Y. Salomon and A. Scherz, in *Chlorophylls and Bacteriochlorophylls: Biochemistry, Biophysics, Functions and Applications*, ed. B. Grimm, R. J. Porra, W. Rüdiger and H. Scheer, Springer, Dordrecht, The Netherlands, 2006, vol. 25, ch. 33, pp. 485–494.
- (16) A. L. Gryshuk, Y. Chen, W. Potter, T. Ohulchansky, A. Oseroff and R. K. Pandey, *J. Med. Chem.*, 2006, **49**, 1874–1881.
- (17) S. Fukuzumi, K. Ohkubo, X. Zheng, Y. Chen, R. K. Pandey, R. Zhan and K. M. Kadish, *J. Phys. Chem. B*, 2008, **112**, 2738–2746.
- (18) M. A. Grin, A. F. Mironov and A. A. Shtil, *Anti-Cancer Agents Med. Chem.*, 2008, **8**, 683–697.
- (19) M. M. Pereira, C. J. P. Monteiro, A. V. C. Somões, S. M. A. Pinto, L. G. Arnaut, G. F. F. Sá, E. F. F. Silva, L. B. Rocha, S. Simões and S. J. Formosinho, *J. Porphyrins Phthalocyanines*, 2009, **13**, 567–573.
- (20) E. F. F. Silva, C. Serpa, J. M. Dabrowski, C. J. P. Monteiro, S. J. Formosinho, G. Stochel, K. Urbanska, S. Simões, M. M. Pereira and L. G. Arnaut, *Chem. Eur. J.*, 2010, **16**, 9273–9286.
- (21) P. Mroz, Y.-Y. Huang, A. Szokalska, T. Zhiyentayev, S. Janjua, A.-P. Nifli, M. E. Sherwood, C.; Ruzié, K. E. Borbas, D. Fan, M. Krayner, T. Balasubramanian, E. Yang, H. L. Kee, C. Kirmaier, J. R. Diers, D. F. Bocian, D. Holten, J. S. Lindsey and M. R. Hamblin, *FASEB J.*, 2010, **24**, 3160–3170.
- (22) Y.-Y. Huang, P. Mroz, T. Zhiyentayev, T. Balasubramanian, C. Ruzié, M. Krayner, D. Fan, K. E. Borbas, E. Yang, H. L. Kee, C. Kirmaier, J. R. Diers, D. F. Bocian, D. Holten, J. S. Lindsey and M. R. Hamblin, *J. Med. Chem.*, 2010, **53**, 4018–4027.
- (23) L. Huang, Y.-Y. Huang, P. Mroz, G. P. Tegos, T. Zhiyentayev, S. K. Sharma, Z. Lu, T. Balasubramanian, M. Krayner, C. Ruzié, E. Yang, H. L. Kee, C. Kirmaier, J. R. Diers, D. F. Bocian, D. Holten, J. S. Lindsey and M. R. Hamblin, *Antimicrob. Agents Chemother.*, 2010, **54**, 3834–3841.
- (24) J. M. Sutton, O. J. Clarke, N. Fernandez and R. W. Boyle, *Bioconjugate Chem.*, 2002, **13**, 249–263.
- (25) H. L. Kee, R. Nothdurft, C. Muthiah, J. R. Diers, D. Fan, M. Ptaszek, D. F. Bocian, J. S. Lindsey, J. P. Culver and D. Holten, *Photochem. Photobiol.*, 2008, **84**, 1061–1072.
- (26) H. L. Kee, J. R. Diers, M. Ptaszek, C. Muthiah, D. Fan, J. S. Lindsey, D. F. Bocian and D. Holten, *Photochem. Photobiol.*, 2009, **85**, 909–920.
- (27) (a) S. C. De Rosa, J. M. Brenchley and M. Roederer, *Nature Med.*, 2003, **9**, 112–117. (b) S. P. Perfetto, P. K. Chattopadhyay and M. Roederer, *Nature Rev. Immunol.*, 2004, **4**, 648–655. (c) P. K. Chattopadhyay, D. A. Price, T. F. Harper, M. R. Betts, J. Yu, E. Gostick, S. P. Perfetto, P. Goepfert, R. A. Koup, S. C. De Rosa, M. P. Bruchez and M. Roederer, *Nature Med.*, 2006, **12**, 972–977.

- (28) Scheer, H. in *Chlorophylls and Bacteriochlorophylls: Biochemistry, Biophysics, Functions and Applications*, ed. B. Grimm, R. J. Porra, W. Rüdiger and H. Scheer, Springer, Dordrecht, The Netherlands, 2006, vol. 25, ch. 1, pp. 1–26.
- (29) H. Tamiaki, M. Kouraba, K. Takeda, S.-I. Kondo and R. Tanikaga, *Tetrahedron:Asymm.*, 1998, **9**, 2101–2111.
- (30) S.-I. Sasaki and H. J. Tamiaki, *Org. Chem.*, 2006, **71**, 2648–2654.
- (31) A. N. Kozyrev, G. Zheng, C. Zhu, T. J. Dougherty, K. M. Smith and R. K. Pandey, *Tetrahedron Lett.*, 1996, **37**, 6431–6434.
- (32) A. F. Mironov, M. A. Grin and A. G. Tsyprovskiy, *J. Porphyrins Phthalocyanines*, 2002, **6**, 358–361.
- (33) A. F. Mironov, M. A. Grin, A. G. Tsiprovskiy, V. V. Kachala, T. A. Karmakova, A. D. Plyutinskaya and R. I. Yakubovskaya, *J. Porphyrins Phthalocyanines*, 2003, **7**, 725–730.
- (34) A. F. Mironov, M. A. Grin, A. G. Tsiprovskii, A. V. Segenevich, D. V. Dzardanov, K. V. Golovin, A. A. Tsygnkov and Y. K. Shim, *Russ. J. Bioorg. Chem.*, 2003, **29**, 190–197.
- (35) A. F. Mironov, M. A. Grin, A. G. Tsiprovskii, R. A. Titeev, E. A. Nizhnik and I. S. Lonin, *Mendeleev Commun.*, 2004, **14**, 204–207.
- (36) A. N. Kozyrev, Y. Chen, L. N. Goswami, W. A. Tabaczynski and R. K. Pandey, *J. Org. Chem.*, 2006, **71**, 1949–1960.
- (37) L. N. Goswami, Y. Chen, J. Missert, G. Li, A. Pallenberg and R. K. Pandey, *Heterocycles*, 2007, **71**, 1929–1949.
- (38) M. A. Grin, I. S. Lonin, A. A. Lakhina, E. S. Ol'shanskaya, A. I. Makaraov, Y. L. Sebyakin, L. Y. Guryeva, P. V. Toukach, A. S. Kononikhin, V. A. Kuzmin and A. F. Mironov, *J. Porphyrins Phthalocyanines*, 2009, **13**, 336–345.
- (39) S. Fox and R. W. Boyle, *Tetrahedron*, 2006, **62**, 10039–10054.
- (40) (a) T. D. Lash, *J. Porphyrins Phthalocyanines*, 2001, **5**, 267–288. (b) B. E. Smith and T. D. Lash, *Tetrahedron*, 2010, **66**, 4413–4422.
- (41) Y. Vakrat-Haglili, L. Weiner, V. Brumfeld, A. Brandis, Y. Salomon, B. McIlroy, B. C. Wilson, A. Pawlak, M. Rozanowska, T. Sarna and A. Scherz, *J. Am. Chem. Soc.*, 2005, **127**, 6487–6497.
- (42) L. Limantara, P. Koehler, B. Wilhelm, R. J. Porra and H. Scheer, *Photochem. Photobiol.*, 2006, **82**, 770–780.
- (43) M. Galezowski and D. T. Gryko, *Curr. Org. Chem.*, 2007, **11**, 1310–1338.
- (44) H.-J. Kim and J. S. Lindsey, *J. Org. Chem.*, 2005, **70**, 5475–5486.

- (45) M. Taniguchi, D. L. Cramer, A. D. Bhise, H. L. Kee, D. F. Bocian, D. Holten and J. S. Lindsey, *New J. Chem.*, 2008, **32**, 947–958.
- (46) M. Kraye, M. Ptaszek, H.-J. Kim, K. R. Meneely, D. Fan, K. Secor and J. S. Lindsey, *J. Org. Chem.*, 2010, **75**, 1016–1039.
- (47) D. Fan, M. Taniguchi and J. S. Lindsey, *J. Org. Chem.*, 2007, **72**, 5350–5357.
- (48) K. E. Borbas, C. Ruzié and J. S. Lindsey, *Org. Lett.*, 2008, **10**, 1931–1934.
- (49) C. Ruzié, M. Kraye, T. Balasubramanian and J. S. Lindsey, *J. Org. Chem.*, 2008, **73**, 5806–5820.
- (50) M. Kraye, T. Balasubramanian, C. Ruzié, M. Ptaszek, D. L. Cramer, M. Taniguchi and J. S. Lindsey, *J. Porphyrins Phthalocyanines*, 2009, **13**, 1098–1110.
- (51) C. Ruzié, M. Kraye and J. S. Lindsey, *Org. Lett.*, 2009, **11**, 1761–1764.
- (52) Nomenclature of bacteriochlorin macrocycles is not fully settled.^a We here introduce the terminology bacterio-13¹-oxophorbine for the annulated bacteriochlorin by analogy with the accepted nomenclature for the corresponding 13¹-oxophorbine skeleton of chlorophylls. (a) G. P. Moss, *Pure Appl. Chem.*, 1987, **59**, 779–832.
- (53) J. K. Laha, C. Muthiah, M. Taniguchi and J. S. Lindsey, *J. Org. Chem.*, 2006, **71**, 7049–7052.
- (54) M. Ptaszek, D. Lahaye, M. Kraye, C. Muthiah and J. S. Lindsey, *J. Org. Chem.*, 2010, **75**, 1659–1673.
- (55) (a) H. Muratake and M. Natsume, *Tetrahedron Lett.*, 1997, **38**, 7581–7582. (b) H. Muratake, M. Natsume and H. Nakai, *Tetrahedron*, 2004, **60**, 11783–11803.
- (56) R. K. Pandey, N. Jagerovic, J. M. Ryan, T. J. Dougherty and K. M. Smith, *Tetrahedron*, 1996, **52**, 5349.
- (57) (a) F. Bellamy, P. Martz and J. Streith, *Heterocycles*, 1975, **3**, 395–400. (b) F. Bellamy and J. Streith, *J. Chem. Res.-S.*, 1979, 18–19.
- (58) M. Kosugi, T. Sumiya, Y. Obara, M. Suzuki, H. Sano and T. Migita, *Bull. Chem. Soc. Jpn.*, 1987, **60**, 767–768.
- (59) O. Mass, M. Taniguchi, M. Ptaszek, J. W. Springer, K. M. Faries, J. R. Diers, D. F. Bocian, D. Holten and J. S. Lindsey, *New J. Chem.*, 2011, **35**, DOI: 10.1039/c0nj00652a.
- (60) J. Helaja, A. Y. Tauber, Y. Abel, N. V. Tkachenko, H. Lemmetyinen, I. Kilpeläinen and P. H. Hynninen, *J. Chem. Soc., Perkin Trans. I*, 1999, 2403–2408.
- (61) M. Kunieda and H. Tamiaki, *J. Org. Chem.*, 2005, **70**, 820–828.
- (62) (a) H. Tamiaki, M. Amakawa, Y. Shimono, R. Tanikaga, A. R. Holzwarth and K. Schaffner, *Photochem. Photobiol.*, 1996, **63**, 92–99. (b) H. Tamiaki, S. Yagai and T.

- Miyatake, *Bioorg. Med. Chem.*, 1998, **6**, 2171–2178. (c) H. Tamiaki, M. Amakawa, A. R. Holzwarth and K. Schaffner, *Photosynth. Res.*, 2002, **71**, 59–67. (d) H. Morishita and H. Tamiaki, *Tetrahedron*, 2005, **61**, 6097–6107. (e) H. Tamiaki, H. Kitamoto, T. Watanabe and R. Shibata, *Photochem. Photobiol.*, 2005, **81**, 170–176. (f) R. Shibata, T. Mizoguchi, T. Inazu and H. Tamiaki, *Photochem. Photobiol. Sci.*, 2007, **6**, 749–757. (g) S. Sasaki, K. Mizutani, M. Kunieda and H. Tamiaki, *Tetrahedron Lett.*, 2008, **49**, 4113–4115. (h) H. Morishita and H. Tamiaki, *Spectrochim. Acta A*, 2009, **72**, 274–279.
- (63) M. Kunieda and H. Tamiaki, *Eur. J. Org. Chem.*, 2006, 2352–2361.
- (64) J. H. C. Smith and A. Benitez, in *Modern Methods of Plant Analysis*, ed. K. Paech and M. V. Tracey, Springer-Verlag, Berlin, 1955, vol. IV, pp. 142–196.
- (65) D. Holten, M. Gouterman, W. W. Parson, M. W. Windsor and M. G. Rockley, *Photochem. Photobiol.*, 1976, **23**, 415–423.
- (66) M. Gouterman, in *The Porphyrins*, ed. D. Dolphin, Academic Press, New York, 1978, vol. 3, pp. 1–165.
- (67) M. Gouterman, *J. Mol. Spectroscopy*, 1961, **6**, 138–163.
- (68) W. Wang and Y. Kishi, *Org. Lett.*, 1999, **1**, 1129–1132.
- (69) F. Li, S. Gentemann, W. A. Kalsbeck, J. Seth, J. S. Lindsey, D. Holten and D. F. Bocian, *J. Mater. Chem.*, 1997, **7**, 1245–1262.
- (70) H. L. Kee, C. Kirmaier, L. Yu, P. Thamyongkit, W. J. Youngblood, M. E. Calder, L. Ramos, B. C. Noll, D. F. Bocian, W. R. Scheidt, R. R. Birge, J. S. Lindsey and D. Holten, *J. Phys. Chem. B*, 2005, **109**, 20433–20443.
- (71) A. T. Gradyushko, A. N. Sevchenko, K. N. Solovyov and M. P. Tsvirko, *Photochem. Photobiol.*, 1970, **11**, 387–400.
- (72) G. Weber and F. W. J. Teale, *Trans. Faraday Soc.*, 1957, **53**, 646–655.
- (73) Except for molecular mechanics and semi-empirical models, the calculation methods used in Spartan have been documented in Y. Shao, L. F. Molnar, Y. Jung, J. Kussmann, C. Ochsenfeld, S. T. Brown, A. T. B. Gilbert, L. V. Slipchenko, S. V. Levchenko, D. P. O'Neill, R. A. DiStasio Jr., R. C. Lochan, T. Wang, G. J. O. Beran, N. A. Besley, J. M. Herbert, C. Y. Lin, T. Van Voorhis, S. H. Chien, A. Sodt, R. P. Steele, V. A. Rassolov, P. E. Maslen, P. P. Korambath, R. D. Adamson, B. Austin, J. Baker, E. F. C. Byrd, H. Dachsel, R. J. Doerksen, A. Dreuw, B. D. Dunietz, A. D. Dutoi, T. R. Furlani, S. R. Gwaltney, A. Heyden, S. Hirata, C.-P. Hsu, G. Kedziora, R. Z. Khalliulin, P. Klunzinger, A. M. Lee, M. S. Lee, W.-Z. Liang, I. Lotan, N. Nair, B. Peters, E. I. Proynov, P. A. Pieniazek, Y. M. Rhee, J. Ritchie, E. Rosta, C. D. Sherrill, A. C. Simmonett, J. E. Subotnik, H. L. Woodcock III, W. Zhang, A. T. Bell, A. K. Chakraborty, D. M. Chipman, F. J. Keil, A. Warshel, W. J. Hehre, H. F. Schaefer III, J. Kong, A. I. Krylov, P. M. W. Gill and M. Head-Gordon, *Phys. Chem. Chem. Phys.*, 2006, **8**, 3172–3191.

Chapter 3

Photophysical Properties and Electronic Structure of Stable, Tunable Synthetic Bacteriochlorins: Extending the Features of Native Photosynthetic Pigment

Reproduced with permission from Yang, EK; Kirmaier, C; Krayner, M; Taniguchi, M; Kim, HJ; Diers, J.R; Bocian, D.F; Lindsey J.S; Holten, D. Photophysical Properties and Electronic Structure of Stable, Tunable Synthetic Bacteriochlorins: Extending the Features of Native Photosynthetic Pigments. *J. Phys. Chem. B.* 2011, *115*, 10801–10816. Doi:10.1021/jp205258s. Copyright 2011 American Chemical Society.

Abstract

Bacteriochlorins, which are tetrapyrrole macrocycles with two reduced pyrrole rings, are Nature's near-infrared (NIR) absorbers (700 – 900 nm). The strong absorption in the NIR region renders bacteriochlorins excellent candidates for a variety of applications including solar light harvesting, flow cytometry, molecular imaging, and photodynamic therapy. Regardless, natural bacteriochlorins are inherently unstable due to oxidative conversion to the chlorin (one reduced pyrrole ring) or the porphyrin. The natural pigments are also only modestly amenable to synthetic manipulation, owing to a near full complement of substituents on the macrocycle. Recently, new synthetic methodology has afforded access to stable synthetic bacteriochlorins wherein a wide variety of substituents can be appended to the macrocycle at preselected locations. Herein, the spectroscopic and photophysical properties of 33 synthetic bacteriochlorins are investigated. The NIR absorption bands of the chromophores range from ~700 to ~820 nm; the lifetimes of the lowest excited singlet state range from ~2 to ~6 ns; the fluorescence quantum yields range from ~0.05 to ~0.25; the average yield of the lowest triplet excited state is ~0.5. The spectroscopic/photophysical studies of the bacteriochlorins are accompanied by density functional theory (DFT) calculations that probe the characteristics of the frontier molecular orbitals. The DFT calculations indicate that the impact of substituents on the spectral properties of the molecules derives primarily from effects on the lowest unoccupied molecular orbital. Collectively, the studies show how the palette of synthetic bacteriochlorins extends the properties of the native photosynthetic pigments (bacteriochlorophylls). The studies have also elucidated design principles for tunability of spectral and photophysical characteristics as required for a wide variety of photochemical applications.

Introduction

The centrality of chlorophylls in plant photosynthesis is well appreciated and has led to numerous studies of the spectroscopic and photophysical properties of chlorophylls and their synthetic analogues. Less studied but equally important are the bacteriochlorophylls, which underpin bacterial photosynthesis. Bacteriochlorophylls are tetrahydroporphyrins wherein two reduced pyrrole rings are located at opposite sides of the macrocycle, to be compared with the single reduced ring of chlorophylls (which are dihydroporphyrins). The structures of bacteriochlorophylls *a*, *b*, and *g* are shown in Chart 1 (bacteriochlorophylls *c-f* contain the dihydroporphyrin chromophore and hence are misnamed). The increased saturation of the macrocycle leads to strong absorption in the near-infrared (NIR) spectral region: bacteriochlorophylls *a*, *b*, and *g* (in dioxane) absorb at 772, 794, and 762 nm, respectively, to be compared with absorption at 662 and 644 nm for chlorophylls *a* and *b*.¹

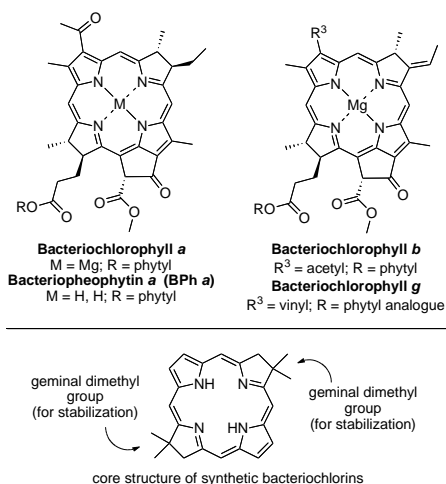


Chart 1. Naturally occurring bacteriochlorophylls (top) and synthetic bacteriochlorins (bottom)

Two major impediments to studies of bacteriochlorophylls have entailed (i) instability of the naturally occurring macrocycles (including susceptibility toward adventitious

dehydrogenation thereby forming the corresponding chlorin),² and (ii) a nearly full complement of substituents about the perimeter of the macrocycles, thereby limiting semisynthetic transformations.^{3,4} Synthetic bacteriochlorins in principle offer an attractive alternative to the bacteriochlorins derived semisynthetically from bacteriochlorophylls. Traditional methods for the synthesis of bacteriochlorins involve subjecting a chlorin or porphyrin to hydrogenation or addition (e.g., vicinal dihydroxylation).⁵ While operationally simple, both methods can yield regioisomers depending on the substituents about the perimeter of the macrocycle, and the former method leaves the bacteriochlorin susceptible toward aerobic dehydrogenation.

The limited bacteriochlorin architectures available have precluded addressing a number of fundamental questions concerning the relation between molecular structure and photophysical features. Chief among the structural questions include the effects of substituents arrayed about the perimeter of the macrocycle (including the presence of the isocyclic ring and variants thereof) on the spectra and photophysical properties. Because bacteriochlorophylls are Nature's NIR absorbers par excellence, a related question concerns the extent to which synthetic manipulations can shift the long-wavelength absorption band deeper into the NIR while retaining a singlet excited-state lifetime of sufficient duration for viable photochemical reactions. The position of the long-wavelength absorption band is important not only with regards to light-harvesting but also in establishing an upper limit on the energy level of the first singlet excited state. Finally, it warrants emphasis that photosynthetic phenomena stem from large numbers of pigments working in concert. In that regard, synthetic multichromophore arrays have been widely used to good effect to delineate molecular factors that affect electron-transfer and energy-transfer phenomena. Such arrays have largely employed porphyrins and to lesser extent chlorins despite the absence of NIR absorption for both types of chromophores.⁶ Very few synthetic arrays have

incorporated bacteriochlorins.⁷ Indeed, the studies to date of bacteriochlorins tend to encompass the bacteriochlorophylls either as monomers or as part of natural protein assemblies.⁸ Thus, a large body of important studies concerning bacteriochlorins has remained unaddressed.

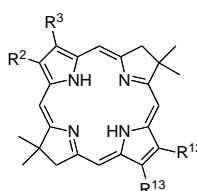
In addition to fundamental studies, bacteriochlorins are of interest for a number of applications wherein capture of NIR light is of paramount importance. Exemplary applications include (i) bioinspired solar energy conversion, given the abundance of solar radiation in the NIR region;⁹ (ii) polychromatic flow cytometry, given the dearth of spectroscopically distinct fluorescent markers in the virtually unexplored NIR region, thereby complementing the numerous markers for the visible spectral region;^{10,11} and (iii) molecular imaging¹¹⁻¹⁹ and photodynamic therapy (PDT),^{3,4,12,19-26} given the deep penetration in soft tissue afforded by NIR light. Porphyrins annulated with conjugated rings have recently been found to shift the long-wavelength absorption band into the NIR,^{27,28} but in one case that has been studied, the excited-state lifetime was dramatically shortened (to ~13 ps).²⁸ Maintaining a singlet excited-state lifetime of reasonable magnitude (≥ 1 ns) is important for achieving a number of efficient photochemical processes such as energy transfer and electron transfer.

To gain access to stable bacteriochlorins and retain the synthetic versatility required to address fundamental questions and diverse applications, we have been working to develop a *de novo* synthesis that affords bacteriochlorins equipped with a geminal dimethyl group in both reduced rings. The geminal dimethyl group blocks adventitious dehydrogenation and thereby affords a stable tetrahydroporphyrin chromophore. The core structure of the synthetic bacteriochlorins is shown in Chart 1. Synthetic manipulations have provided access to bacteriochlorins bearing diverse substituents at the 2,3,12,13 positions. One such class of bacteriochlorins also contains a methoxy group at the 5-position (termed “MeOBC” series)

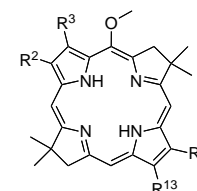
whereas a second class lacks the 5-methoxy substituent (termed “HBC” series). Table 1 shows 10 members of the former class and 17 members of the latter class. Further synthetic transformations have provided access to six bacteriochlorins wherein the 15-substituent is altered, affording three distinct classes as shown in Table 2. The classes include the “15-substituted” series and two series wherein a fifth ring has been annulated to the macrocycle. The rings include the five-membered isocyclic ring characteristic of naturally occurring bacteriochlorophylls (i.e., a bacterio-13¹-oxophorbine) and a six-membered imide ring (bacteriochlorin-13,15-dicarboximide) for which there are no natural counterparts. The imide motif has been accessed in (bacterio)chlorophyll chemistry (by base-mediated treatment of the natural macrocycles) as a means of achieving a more stable construct with bathochromically shifted absorption.

Herein, we first describe the spectral properties of the 33 synthetic bacteriochlorins shown in Tables 1 and 2. The syntheses of all compounds except one (see Supporting Information) have been reported.²⁹⁻³⁶ The compounds exhibit a range of long-wavelength absorption that spans 709–818 nm. We report measurements of the singlet excited-state lifetime, triplet excited-state lifetime, and quantum yields of all three decay processes of the singlet excited state (fluorescence, intersystem crossing, and internal conversion), from which the rate constants for these fundamental processes are derived. Density functional theoretical calculations have been carried out to assess the energy and composition of the four frontier molecular orbitals. Finally, we draw insights concerning the relation between diverse substituents in various patterns, observed spectral and photophysical properties, and molecular orbital characteristics. Taken together, the studies provide a foundation for the rational design of bacteriochlorin-containing molecular architectures that capture NIR light.

Table 1. Structures of Bacteriochlorins with Substituents at the 2,3,12,13-Positions.

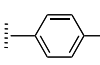


HBC series

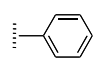


MeOBC series

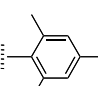
	Ref	R ²	R ¹²	R ³	R ¹³
<i>HBC series</i>					
HBC-H	32	H	H	H	H
HBC-Swt ^{2,12}	33	Swt	Swt	H	H
HBC-M ^{3,13}	31	H	H	M	M
HBC-Re ^{3,13}	34	H	H	Re	Re
HBC-F ³	34	H	H	F	H
HBC-T ^{2,12}	29	T	T	H	H
HBC-P ^{3,13}	32	H	H	P	P
HBC-C ^{3,13}	34	H	H	C	C
HBC-CN ^{3,13}	34	H	H	CN	CN
HBC-V ^{3,13}	32	H	H	V	V
HBC-MEs ^{3,13}	34	H	H	MEs	MEs
HBC-Me ^{2,12} EEs ^{3,13}	35	Me	Me	EEs	EEs
HBC-Et ^{2,12} EEs ^{3,13}	35	Et	Et	EEs	EEs
HBC-PE ^{3,13}	32	H	H	PE	PE
HBC-T ^{2,12} EEs ^{3,13}	See SI	T	T	EEs	EEs
HBC-A ^{3,13}	32	H	H	A	A
HBC-F ^{3,13}	32	H	H	F	F
<i>MeOBC series</i>					
MeOBC-H	35	H	H	H	H
MeOBC-T ^{2,12}	29	T	T	H	H
MeOBC-Py ^{3,13}	35	H	H	Py	Py
MeOBC-EEs ^{3,13}	35	H	H	EEs	EEs
MeOBC-	35	Me	Me	EEs	EEs
MeOBC-	35	Et	Et	EEs	EEs
MeOBC-A ^{3,13}	36	H	H	A	A
MeOBC-Me ^{2,12} A ^{3,13}	36	Me	Me	A	A
MeOBC-	35	An	An	EEs	EEs
MeOBC-EEs ^{2,3,12,13}	35	EEs	EEs	EEs	EEs



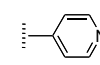
p-tolyl
(T)



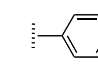
phenyl
(P)



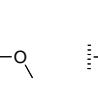
mesityl
(M)



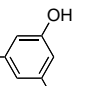
4-pyridyl
(Py)



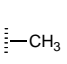
4-methoxyphenyl
(An)




3,5-dihydroxyphenyl
(Re)



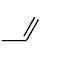
1,5-dimethoxypent-3-yl
(Swt)



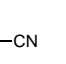
methyl
(Me)



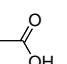
ethyl
(Et)



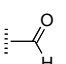
vinyl
(V)



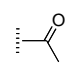
cyano
(CN)



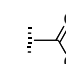
carboxyl
(C)




formyl
(F)



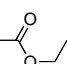
acetyl
(A)



methyl ester
(MEs)

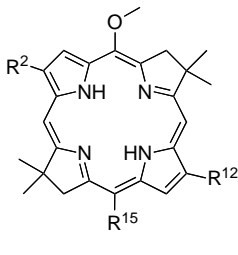
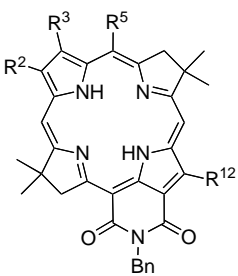
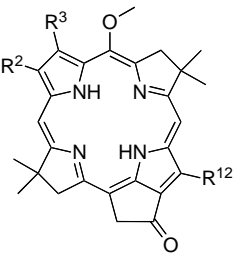
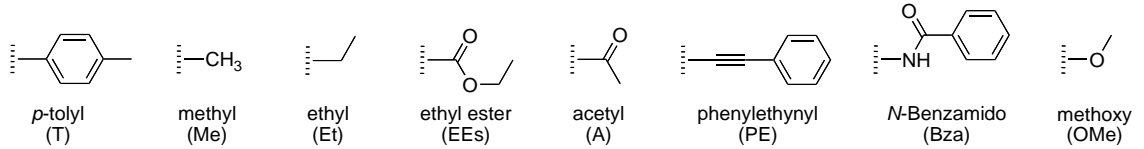


ethyl ester
(EEs)



phenylethynyl
(PE)

Table 2. Structures of Bacteriochlorins, Bacteriochlorinimides, and Bacteriooxophorbine.

							
		15-substituted series	Bacteriochlorinimides	Bacteriooxophorbine			
	Ref.	R ²	R ¹²	R ³	R ¹³	R ⁵	R ¹⁵
<i>15-substituted series</i>							
MeOBC-OMe¹⁵	35	H	H	H	H	OMe	OMe
MeOBC-T^{2,12}Bza¹⁵	30	T	T	H	H	OMe	Bza
MeOBC-T^{2,12}PE¹⁵	30	T	T	H	H	OMe	PE
<i>Bacteriooxophorbine</i>							
MeOBOP	36	Me	Me	A	–	OMe	–
<i>Bacteriochlorinimides</i>							
MeOBC-I	36	Et	Et	EEs	–	OMe	–
HBC-I	36	Et	Et	EEs	–	H	–
							

Experimental methods

Photophysical measurements

Static and time-resolved photophysical measurements were performed as described previously.³⁷ Measurement of the fluorescence (Φ_f) and triplet-excited-state (Φ_{isc}) quantum yields and singlet (τ_S) and triplet (τ_T) lifetimes utilized, unless noted otherwise, dilute (μM) Ar-purged toluene solutions at room temperature. Samples for Φ_f measurements had an absorbance <0.12 at the excitation wavelength. The Φ_f values were generally determined with respect to two standards and the results averaged. The standards (deoxygenated solutions) were (1) free base *meso*-tetraphenylporphyrin (**FbTPP**) in nondegassed toluene, for which $\Phi_f = 0.070$ was established with respect to the zinc chelate **ZnTPP** in nondegassed toluene ($\Phi_f = 0.030$),³⁸ consistent with prior results on **FbTPP**,³⁹ and (2) 8,8,18,18-tetramethylbacteriochlorin³² in Ar-purged toluene, for which $\Phi_f = 0.14$ was established with respect to **FbTPP** and chlorophyll *a* (**Chl a**) in deoxygenated benzene⁴⁰ ($\Phi_f = 0.325$).

The τ_S value for each bacteriochlorin was first probed using a time-correlated single photon counting (TCSPC) instrument that employed Soret excitation flashes derived from a nitrogen-pumped dye laser (PTI LaserStrobe) and a Gaussian instrument response function of 0.6 ns. The values were in good agreement with those obtained for select compounds using a fluorescence modulation technique (Spex Tau2).⁴¹

The Φ_{isc} values were obtained using a transient-absorption technique in which the extent of bleaching of the ground-state Q(1,0) band due to the lowest singlet excited state was measured immediately following a 130 fs flash in the $Q_y(0,0)$ band and compared with that due to the

lowest triplet excited state at the asymptote of the singlet excited-state decay.³⁷ The bleaching signals are referenced to a relatively featureless Q_x-region transient absorption that is generally not substantially different for the S₁ and S₀ excited states of the free base bacteriochlorins.

Density Functional Theory calculations

DFT calculations were performed with Spartan '08 for Windows version 1.2.0 in parallel mode⁴² on a PC equipped with an Intel i7-975 cpu, 24 GB ram, and three 300 GB, 10k rpm hard drives. The hybrid B3LYP functional and the LACVP basis set were employed. The equilibrium geometries were fully optimized using the default parameters of the Spartan '08 program.

Results

Absorption spectra

Electronic ground-state absorption spectra of representative bacteriochlorins are shown in Figure 1. The absorption spectrum of each bacteriochlorin contains four main features with maxima in the following spectral ranges: B_y(0,0) (340–371 nm), B_x(0,0) (357–408 nm), Q_x(0,0) (489–550 nm), and Q_y(0,0) (707–818 nm). For each of these four origin bands, a weaker (1,0) vibronic satellite feature can be seen roughly 1300 cm⁻¹ to higher energy. [Note that the B_x and B_y bands may each have contributions from x- and y-polarized transitions, and for some bacteriochlorins are substantially spectrally overlapped.] The Q_y(0,0) bands have a full width at half maximum (FWHM) in the range 11–25 nm. The absorption characteristics of all the synthetic bacteriochlorins along with those of the natural photosynthetic pigment bacteriopheophytin *a* (**BPh a**) are listed in Table 3.

The $Q_y(0,0)$ band is of interest because it represents absorption of light to produce the lowest singlet excited state, which is key to much of the photophysical behavior. The two bacteriochlorinimides have $Q_y(0,0)$ bands at the longer wavelength (lower energy) end of the range: **HBC-I** (818 nm) and **MeOBC-I** (793 nm). The two analogues that have no substituents at the β -pyrrole positions absorb near the shorter wavelength end of the range: **HBC-H** (713 nm) and **MeOBC-H** (709 nm). Other analogues, such as those bearing 3,13-diacetyl groups, absorb at intermediate wavelengths: **HBC-A**^{3,13} (768 nm) and **MeOBC-A**^{3,13} (740 nm). These pairs of compounds also illustrate the effect of the 5-OMe group to modestly shift the $Q_y(0,0)$ band hypsochromically compared to analogues bearing a 5-hydrogen substituent (Table 3).

Because of uncertainties associated with determination of molecular absorption (extinction) coefficients (e.g., weighing small amounts of material), it has been common in the literature on photosynthetic pigments (chlorophylls and bacteriochlorophylls) to examine how changes in molecular characteristics affect the intensity of the $Q_y(0,0)$ band relative to the Soret (B_y , B_x) maximum.⁴³ This peak-intensity ratio (I_{Q_y}/I_B) is listed in Table 3. It deserves mention that where molar absorption coefficients have been measured (e.g., **MeOBC-T**^{2,12} or **HBC-T**^{2,12}, $\epsilon_{Q_y} = 120,000$ or $130,000 \text{ M}^{-1}\text{cm}^{-1}$, respectively),²⁹ the magnitude is fully in line with those reported for naturally occurring bacteriochlorophylls.^{1,8} Because of variations in absorption bandwidths and in spectral overlap, trends in the oscillator strengths of the transitions are more faithfully gauged using integrated band intensities. For this purpose, Table 3 also includes the integrated intensity of the Q_y manifold [$Q_y(0,0) + Q_y(1,0)$ bands] relative to the integrated intensity of the entire B manifold [$B_y(0,0) + B_y(1,0) + B_x(0,0) + B_x(1,0)$ bands]. The table also lists analogous intensity ratios for the $Q_x(0,0)$ band relative to the $Q_x(1,0)$ band, which normally

has a relatively constant extinction coefficient for a series of related tetrapyrroles (because its intensity is derived from vibronic borrowing with the B_x transition).

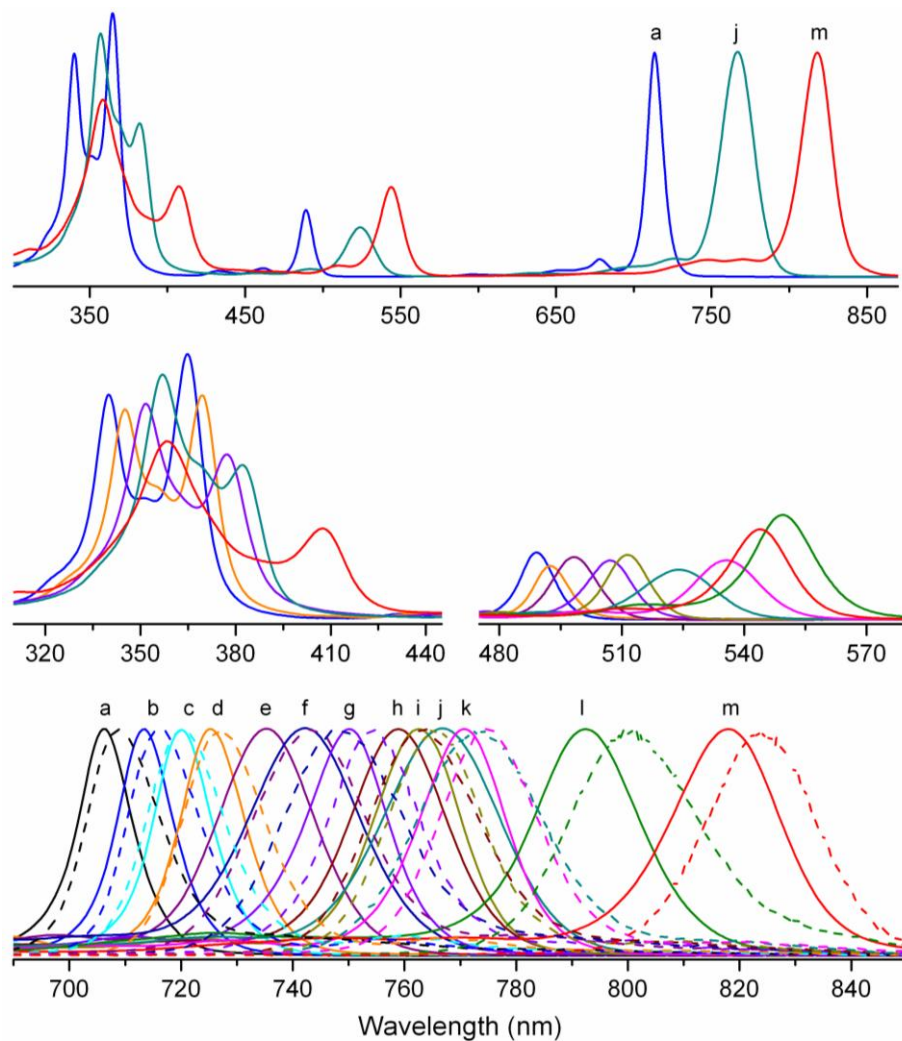


Figure 1. Absorption (— solid lines) and emission (--- dashed lines) spectra in toluene at room temperature of bacteriochlorins (normalized at the $Q_y(0,0)$ absorption bands); (top left) entire spectra, (middle left) magnification of the Soret (B_x and B_y) region, (middle right) magnification of the Q_x region, and (bottom) magnification of the Q_y region. The labels in the bottom and top panels and the colors in all panels are as follows: **MeOBC-OMe**¹⁵ (a, black), **HBC-H** (b, blue), **HBC-Swt**^{2,12} (c, cyan), **HBC-M**^{3,13} (d, orange), **HBC-P**^{3,13} (e, purple), **MeOBC-Me**^{2,12}**A**^{3,13} (f, royal), **HBC-V**^{3,13} (g, violet), **MeOBC-EEs**^{2,3,12,13} (h, wine), **HBC-PE**^{3,13} (i, dark yellow), **HBC-T**^{2,12}**EEs**^{3,13} (j, dark cyan), **HBC-F**^{3,13} (k, magenta), **MeOBC-I** (l, olive), and **HBC-I** (m, red).

Figure 2A plots the Q_y/B integrated intensity ratio versus the $Q_y(0,0)$ energy (and wavelength). With the exception of the bacteriochlorinimides (**HBC-I** and **MeOBC-I**), there is a good linear relationship between these two quantities for all the synthetic bacteriochlorins (and natural photosynthetic pigment **BPh *a***). The greatest effect of the 5-OMe group on the intensity of the $Q_y(0,0)$ band occurs for bacteriochlorins containing a 3,13-carbonyl (acetyl, ester, imide) moiety, including a 30% increase for **MeOBC-I** versus **HBC-I**. These results are analyzed below in terms of the connection between the spectral properties and molecular-orbital (MO) characteristics.

Table 3. Spectral Characteristics of Bacteriochlorins^a

Compound	$B_y(0,0)$ _b abs (nm)	$B_x(0,0)$ _b abs (nm)	$Q_x(0,0)$ abs (nm)	$Q_y(0,0)$ _c abs (nm)	$Q_y(0,0)$ ^d abs FWHM (nm)	$Q_y(0,0)$ ^e em (nm)	$Q_y(0,0)$ ^d em FWHM (nm)	ΔQ_y ^g abs-em (cm ⁻¹)	$I_{Q_y}/$ I_B ^h	$I_{Q_x(0,0)}/$ $I_{Q_x(1,0)}$ ⁱ	$\Sigma Q_y/\Sigma B$ ^j
<i>HBC Series</i>											
HBC-H	340	365	489	713	12	716	16	59	0.85	7.86	0.111
HBC-Swt ^{2,12}	344	364	492	720	13	722	17	38	1.00	6.09	0.122
HBC-M ^{3,13}	345	370	493	725	14	727	18	38	0.99	5.81	0.134
HBC-Re ^{3,13}	346	368	496	731	14	737	23	111	0.71	3.46	0.133
HBC-F ³	352	359	513	733	22	739	23	111	0.91	4.74	0.157
HBC-T ^{2,12}	351	374	499	736	20	742	23	110	1.00	6.11	0.143
HBC-P ^{3,13}	351	373	498	736	20	742	26	110	0.98	6.41	0.146
HBC-C ^{3,13 k}	344	371	506	734	19	737	20	55	0.76	5.48	0.135
HBC-CN ^{3,13}	347	372	515	748	14	752	17	71	1.33	10.2	0.156
HBC-V ^{3,13}	352	377	507	750	21	754	20	71	0.94	6.82	0.171
HBC-MEs ^{3,13}	352	377	523	754	17	757	19	53	1.06	7.83	0.165
HBC-Me ^{2,12} EEs ^{3,13}	354	384	520	760	19	764	20	69	0.97	8.20	0.186
HBC-Et ^{2,12} EEs ^{3,13}	354	383	521	761	20	764	21	52	0.94	8.32	0.165
HBC-PE ^{3,13}	363	380	511	763	18	766	20	51	1.72	8.60	0.173
HBC-T ^{2,12} EEs ^{3,13}	349	357	548	767	25	773	29	101	0.92	6.06	0.179
HBC-A ^{3,13}	360	389	533	768	19	771	20	51	1.19	5.84	0.194
HBC-F ^{3,13}	363	393	536	771	22	775	21	67	0.80	7.29	0.204
<i>MeOBC Series</i>											
MeOBC-H	345	367	501	709	11	711	18	40	0.87	8.07	0.112

MeOBC-T^{2,12}	356	373	511	731	20	736	23	93	0.89	5.86	0.144
MeOBC-Py^{3,13}	364	364	515	734	22	741	21	129	0.89	5.33	0.138
MeOBC-EEs^{3,13}	355	375	525	735	20	740	24	92	1.01	6.10	0.142
MeOBC-Me^{2,12}EEs^{3,13}	357	380	520	738	18	741	21	55	0.96	6.48	0.129
MeOBC-Et^{2,12}EEs^{3,13}	357	379	521	739	18	749	21	37	1.10	6.50	0.149
MeOBC-A^{3,13}	363	363	529	740	23	748	27	145	0.96	3.68	0.151
MeOBC-Me^{2,12}A^{3,13}	363	363	523	743	24	749	26	108	0.95	3.36	0.166
MeOBC-An^{2,12}EEs^{3,13}	360	376	527	749	23	755	26	106	1.09	5.99	0.164
MeOBC-EEs^{2,3,12,13}	361	368	550	759	20	763	23	69	1.21	4.63	0.182
<i>15-substituted series</i>											
MeOBC-OMe¹⁵	359	368	511	707	12	713	16	119	0.54	7.856	0.087
MeOBC-T^{2,12}Bza¹⁵	358	378	519	736	20	741	23	92	0.87	6.26	0.142
MeOBC-T^{2,12}PE¹⁵	387	387	551	754	22	759	24	87	0.95	3.92	0.145
<i>Bacteriooxophorbine</i>											
MeOBOP	359	376	530	733	19	739	26	111	0.93	4.89	0.138
<i>Bacteriochlorinimides</i>											
MeOBC-I	371	407	550	793	22	798	26	79	1.02	7.25	0.142
HBC-I	358	408	544	818	24	823	24	74	1.28	8.40	0.185
<i>Standard</i>											
BPh a	362	389	532	758	31	768	27	172	0.69	4.17	0.153

^aObtained in toluene at room temperature unless noted otherwise. ^bThe two Soret features are labeled B_x(0,0) and B_y(0,0) but the bands may be of mixed parentage. ^cPosition (nm) of the Q_y(0,0) absorption band. ^dFWHM (in nm) of the Q_y(0,0) absorption band. ^ePosition (nm) of the Q_y(0,0) fluorescence emission band. ^fFWHM (in nm) of the Q_y(0,0) fluorescence band. ^gDifference in energy (cm⁻¹) between the peak positions of the Q_y(0,0) absorption and fluorescence bands. ^hRatio of the peak intensities of the Q_y(0,0) band to the Soret (B) maximum, which could be either B_x(0,0) or B_y(0,0). ⁱRatio of the peak intensities of the Q_x(0,0) and Q_x(1,0) bands. ^jRatio of the integrated intensities of the Q_y manifold [Q_y(0,0), Q_y(1,0)] to the Soret manifold [B_y(0,0), B_y(1,0), B_x(0,0), B_x(1,0)], for spectra plotted in cm⁻¹. ^kSpectra measured in methanol.

Fluorescence spectra

The fluorescence emission spectra of representative bacteriochlorins in toluene are shown in Figure 1 (dashed lines). The fluorescence spectrum of each bacteriochlorin is dominated by the $Q_y(0,0)$ band, which is positioned on the average 6 nm to longer wavelength (80 cm^{-1} to lower energy) than the $Q_y(0,0)$ absorption maximum (Table 3). This rather small “Stokes” shift indicates little change in bacteriochlorin structure or solvent interactions upon photoexcitation. The $Q_y(0,0)$ fluorescence bands have a FWHM in the range 16–29 nm.

Fluorescence quantum yields and singlet excited-state lifetimes

The fluorescence quantum yields (Φ_f) of the bacteriochlorins are in the range 0.04–0.25 with an average value of 0.15. The singlet excited-state lifetimes (τ_s) are in the range 1.9–6.2 ns with an average value of 3.8 ns. These values and other photophysical parameters are collected in Table 4.

Close examination of the Table 4 reveals two trends: (i) The Φ_f and τ_s values modestly decrease as the $Q_y(0,0)$ absorption band shifts to longer wavelength (lower singlet excited-state energy). These trends are shown for representative bacteriochlorins in Figure 3. (ii) The average Φ_f and τ_s value for the bacteriochlorins containing a 5-OMe substituent (“MeOBC series”) (0.18, 4.3 ns) are modestly larger than those of the analogues bearing a 5-H substituent (“HBC series”) (0.13, 3.6 ns). The same is true for the respective bacteriochlorinimides (Table 4). These trends are illustrated by comparison of the λ_{Q_y} , Φ_f , and τ_s values for six representative compounds (and three 5-OMe versus 5-H pairs) in order of increasing $Q_y(0,0)$ wavelength (decreasing excited-state energy): **MeOBC-H** (709 nm, 0.25, 5.0 ns) > **HBC-H** (713 nm, 0.13, 4.0 ns) > **MeOBC-A**^{3,13} (740 nm, 0.14, 3.8 ns) > **HBC-A**^{3,13} (768 nm, 0.11, 2.9 ns) > **MeOBC-I** (793 nm, 0.05, 2.2

ns) > **HBC-I** (818 nm, 0.04, 1.9 ns). Similarly, the average Φ_f and τ_S values for the bacteriochlorins containing a 5-OMe substituent plus a 15-substituent (“15-substituted series”) (0.19, 5.4 ns) are modestly larger than those containing only a 5-OMe group (MeOBC series) (0.18, 4.3 ns). Selected members of these sets allow comparison of λ_{Qy} , Φ_f , and τ_S values for bacteriochlorins containing 5,15-OMe, 5-OMe, and no OMe group: **MeOBC-OMe**¹⁵ (707 nm, 0.16, 6.2 ns) > **MeOBC-H** (709 nm, 0.25, 5.0 ns) > **HBC-H** (713 nm, 0.13, 4.0 ns). For comparison, typical (solvent dependent) values for the native photosynthetic pigment **BPh a** are 750 nm, 0.10 and 2.7 ns (Table 4).⁴⁴

Yields and lifetimes of the triplet excited state

The quantum yield of intersystem crossing from the lowest singlet excited state to the lowest triplet excited state (Φ_{isc}), commonly referred to as the triplet yield, is in the range 0.24 to 0.80. All but four of the 33 bacteriochlorins have triplet yields in the range 0.40 to 0.65 despite a substantial variation in the nature and pattern of substituents. Furthermore, the average value and standard deviation is 0.5 ± 0.1 for both the HBC series (17 compounds) and MeOBC series (10 compounds). These Φ_{isc} values of the synthetic bacteriochlorins are in general comparable to the value of 0.57 for **BPh a** (Table 4). On the other hand, the lifetimes of the lowest triplet excited state (τ_T) for the synthetic bacteriochlorins (35–233 μ s) are generally significantly longer than those (16–30 μ s) for **BPh a** in several solvents (Table 4).⁴⁴

Excited-state decay pathways and rate constants

The observables τ_S , Φ_f , and Φ_{isc} (Table 4) for decay of the lowest-energy singlet excited state (S_1) are connected to the rate constants for $S_1 \rightarrow S_0$ spontaneous fluorescence (k_f), $S_1 \rightarrow S_0$ internal conversion (k_{ic}), and $S_1 \rightarrow T_1$ intersystem crossing (k_{isc}) via Eqs. (1) to (3).

$$\tau_S = (k_f + k_{ic} + k_{isc})^{-1} \quad (1)$$

$$\Phi_f = k_f / (k_f + k_{ic} + k_{isc}) \quad (2)$$

$$\Phi_{isc} = k_{isc} / (k_f + k_{ic} + k_{isc}) \quad (3)$$

The internal conversion yield can be calculated from Eq. (4).

$$\Phi_{ic} = 1 - \Phi_f - \Phi_{isc} \quad (4)$$

The radiative, intersystem-crossing, and internal-conversion rate constants can be calculated from the above quantities via Eq. (5), where $i = f, isc$ or ic .

$$k_i = \Phi_i / \tau_S \quad (5)$$

The F_{ic} , k_f , k_{isc} , and k_{ic} values obtained using Eqs. 3-5, along with the measured values of τ_S , Φ_f , Φ_{isc} for the bacteriochlorins are given in Table 4.

The $S_1 \rightarrow S_0$ radiative rate constants are in the range $(18 \text{ ns})^{-1}$ to $(48 \text{ ns})^{-1}$. The rate constant for $S_1 \rightarrow S_0$ internal conversion are the range $(4 \text{ ns})^{-1}$ to $(27 \text{ ns})^{-1}$ and increases weakly with decreasing S_1 excited-state energy (based on the $Q_y(0,0)$ position), which is consistent with the energy-gap law for nonradiative decay.⁴⁵ The rate constant for $S_1 \rightarrow T_1$ intersystem crossing is in the range $(3 \text{ ns})^{-1}$ to $(18 \text{ ns})^{-1}$. The average values of k_f , k_{isc} , and k_{ic} for the HBC series are comparable to those for the MeOBC series.

Molecular orbital characteristics

To gain insights into the trends in the spectral and photophysical properties of the bacteriochlorins as a function of molecular characteristics, DFT calculations were performed.⁴²

These calculations provide the energies and electron-density distributions of the frontier MOs. The principal orbitals of interest are the highest occupied molecular orbital (HOMO), the lowest unoccupied molecular orbital (LUMO), and the HOMO-1 and LUMO+1. The energies of these orbitals and various energy gaps relevant to the photophysical properties are given in Table 5. Table 6 shows electron density plots of the MOs for representative bacteriochlorins.

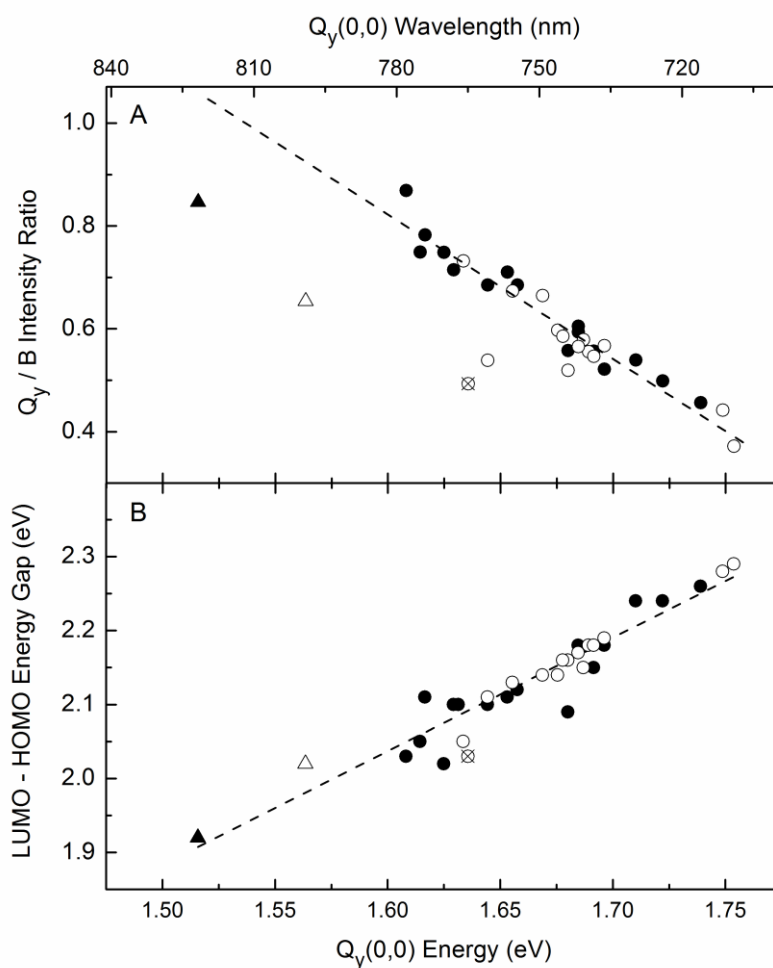


Figure 2. Integrated intensity ratio of the Q_y and B absorption manifolds versus (A) the $Q_y(0,0)$ absorption energy (and wavelength) and (B) the LUMO – HOMO energy gap. For both panels, the symbols designate the compounds as follows: 5-H bacteriochlorins (closed circles), 5-OMe bacteriochlorins and bacteriooxophorbine (open circles), bacteriochlorinimides **HBC-I** (closed triangle) and **MeOBC-I** (open triangle), and photosynthetic pigment **BPh a** (open circle containing an “x”). The dashed line in each panel is the fit of the data for the synthetic bacteriochlorins and in (A) does not include the two bacteriochlorinimides.

The energies of the four frontier MOs are plotted as a function of the $Q_y(0,0)$ absorption-band wavelength/energy in Figure 4A, and analogous plots for the LUMO – HOMO energy gap and LUMO+1 – HOMO-1 energy gap are shown in Figure 4B. In each of these plots, the data for bacteriochlorins containing 5-H and 5-OMe substituents are given by closed and open symbols, respectively. The data for the photosynthetic pigment **BPh a** are given by the open symbol containing an “x”. The HOMO – LUMO versus $Q_y(0,0)$ energy plot is reproduced in Figure 2B for direct comparison with the spectral data in Figure 2A (and the data for the two bacteriochlorinimides indicated by triangles). In analogy to Figure 4 for the $Q_y(0,0)$ band, the energies of the four frontier MOs are plotted as a function of the $Q_x(0,0)$ absorption-band wavelength/energy in Figure 5A, and analogous plots for the LUMO+1 – HOMO energy gap and LUMO – HOMO-1 energy gap are shown in Figure 5B. The relationships depicted in these various plots are discussed as part of the spectral analysis given below.

Discussion

The elucidation of the relationships between structural/MO characteristics and spectral/photophysical properties provides a foundation for the design of bacteriochlorins and extended analogues with desired properties for diverse applications. The variations in the MO characteristics reflect the nature and positions of the peripheral substituents on the bacteriochlorin. Access to diverse substituted bacteriochlorins is now under synthetic control. The MO characteristics in turn influence the photophysical properties (excited-state lifetimes, and yields and rate constants of excited-state decay routes). The subsections below discuss the

observed spectral and photophysical properties of the bacteriochlorins and the correlation of these properties with the calculated MO characteristics of the molecules.

General characteristics of the $Q_y(0,0)$ absorption band

The $Q_y(0,0)$ transition is of particular interest because it corresponds to absorption of light to produce the lowest singlet excited state, which dominates much of the photophysical behavior. For applications, such behavior includes fluorescence (molecular imaging and flow cytometry) and energy/electron transfer (solar-energy conversion). Thus, understanding the impact of molecular factors that can be manipulated via synthesis is of great value toward the design of bacteriochlorins and related macrocycles with tunable properties.

The bacteriochlorins described herein span a large range of NIR positions of the $Q_y(0,0)$ absorption band (Figure 1 and Table 3), primarily due to the effects of 2,3,12,13-substituents (Tables 1 and 2). These positions are on the molecular y-axis, which is the axis along which the Q_y optical transition is polarized. This fact is illustrated by the results of time-dependent DFT calculations for representative bacteriochlorins shown in Figure 6. These calculations show that the transition-dipole-moment direction for absorption to the lowest singlet excited state (the Q_y state) essentially bisects the pyrrole rings (which contain the 2,3,12,13-positions). The $Q_y(0,0)$ band varies from 818 nm for imide **HBC-I** to 707 nm for **MeOBC-MeO**¹⁵. Analogues bearing a variety of 2,3,12,13 substituents, and with hydrogen or methoxy at the 5-position, provide coverage in relatively fine increments across the 700–800 nm spectral region (Figure 1).

Table 4. Photophysical Properties of Bacteriochlorins^a

Compound	$Q_y(0,0)^b$ energy (cm^{-1})	τ_s^c (ns)	Φ_f^d	Φ_{isc}^e	Φ_{ic}^f	$(k_f)^{-1g}$ (ns)	$(k_{isc})^{-1h}$ (ns)	$(k_{ic})^{-1i}$ (ns)	τ_T^j (μs)
<i>HBC Series</i>									
HBC-H	13996	4.0	0.14	0.62	0.24	29	6.5	17	169
HBC-Swt ^{2,12}	13870	3.6	0.11	0.40	0.49	33	9.0	7	190
HBC-M ^{3,13}	13774	3.5	0.15	0.65	0.20	23	5.4	18	233
HBC-Re ^{3,13}	13624	3.0	0.08	0.56	0.36	38	5.4	8.3	198
HBC-F ³	13615	3.4	0.12	0.80	0.08	28	4.2	42	66
HBC-T ^{2,12}	13532	3.3	0.18	0.55	0.27	18	6.0	12	163
HBC-P ^{3,13}	13532	3.3	0.13	0.68	0.19	25	4.9	17	118
HBC-C ^{3,13} ^k	13596	3.7	0.09	0.41	0.50	41	9.0	7	70
HBC-CN ^{3,13}	13333	4.1	0.15	0.43	0.42	27	9.5	9.8	84
HBC-V ^{3,13}	13298	3.3	0.17	0.55	0.28	19	6.0	12	108
HBC-MEs ^{3,13}	13236	3.9	0.14	0.40	0.46	28	9.8	9	76
HBC-Me ^{2,12} EEs ^{3,13}	13123	3.0	0.13	0.52	0.35	23	5.8	9	64
HBC-Et ^{2,12} EEs ^{3,13}	13115	3.3	0.14	0.55	0.31	24	6.0	11	110
HBC-PE ^{3,13}	13080	3.3	0.15	0.63	0.22	22	5.2	15	95
HBC-T ^{2,12} EEs ^{3,13}	12987	3.4	0.13	0.40	0.47	26	8.5	7	92
HBC-A ^{3,13}	12996	2.9	0.11	0.49	0.40	26	5.9	7	55
HBC-F ^{3,13}	12937	2.9	0.11	0.52	0.37	26	5.6	7	60
<i>MeOBC Series</i>									
MeOBC-H	14085	5.0	0.25	0.55	0.20	20	9.1	25	107
MeOBC-T ^{2,12}	13633	4.5	0.20	0.42	0.38	23	10.7	12	107

MeOBC-Py ^{3,13 k}	13560	4.0	0.13	0.51	0.36	31	7.8	11	96
MeOBC-EES ^{3,13}	13559	4.8	0.19	0.52	0.29	25	9.2	17	51
MeOBC-Me ^{2,12 EES} ^{3,13}	13523	4.4	0.17	0.53	0.30	26	8.3	15	85
MeOBC-Et ^{2,12 EES} ^{3,13}	13514	4.3	0.17	0.63	0.20	25	6.8	22	83
MeOBC-A ^{3,13 k}	13441	3.8	0.14	0.48	0.38	27	7.9	10	38
MeOBC-Me ^{2,12 A} ^{3,13 k}	13405	3.4	0.13	0.48	0.39	26	7.1	9	78
MeOBC-An ^{2,12 EES} ^{3,13}	13298	4.1	0.22	0.43	0.35	19	9.5	12	83
MeOBC-EES ^{2,312,13}	13141	4.3	0.16	0.24	0.60	27	17.9	7	46
<i>15-substituted series</i>									
MeOBC-OMe ¹⁵	14124	6.2	0.16	0.71	0.13	39	8.7	48	103
MeOBC-T ^{2,12 Bza} ¹⁵	13541	4.6	0.20	0.54	0.26	23	8.5	18	111
MeOBC-T ^{2,12 PE} ^{15 k}	13219	5.3	0.19	0.62	0.19	28	8.5	28	96
<i>Bacteriooxophorbine</i>									
MeOBOP	13587	4.6	0.19	0.31	0.50	24	15	9	36
<i>Bacteriochlorinimides</i>									
MeOBC-I	12571	2.2	0.05	0.76	0.19	44	2.9	12	72
HBC-I	12188	1.9	0.04	0.51	0.45	48	3.7	4.2	85
<i>Standard</i>									
BPh a ^l	13107	2.7	0.10	0.57	0.33	27	4.7	8	25

^aMeasured in toluene at room temperature unless noted otherwise. ^bAverage energy of the Q_y(0,0) absorption and emission bands (Table 3). ^cLifetime of the lowest singlet excited state measured using fluorescence techniques ($\pm 7\%$). ^dFluorescence quantum yield ($\pm 5\%$). ^eIntersystem crossing (triplet) yield (± 0.09). ^fInternal conversion yield calculated via Eq. (4). ^gInverse of the radiative (fluorescence) rate constant obtained via Eq. (5). ^hInverse of the intersystem crossing rate constant obtained via Eq. (5). ⁱInverse of the internal conversion rate constant obtained via Eq. (5). ^jLifetime of the lowest triplet excited state in Ar-purged 2-methyltetrahydrofuran measured via transient absorption spectroscopy ($\pm 10\%$). ^kProperties except Φ_{isc} measured in methanol. ^lValues in toluene. The values in ethanol are $\Phi_f = 0.081$, and $\tau_s = 2.3$ ns, $\tau_T = 30$ μ s. The values from ref 44 in acetone/methanol (7:3) are $\tau_s = 2.0$ ns, $\tau_S = 16$ μ s, and $\Phi_{isc} = 0.57$ (average of 0.54 and 0.60 from two methods).

Although there is significant tunability in the position of the $Q_y(0,0)$ absorption band (and in the analogous $Q_y(0,0)$ fluorescence band), the band retains its rather narrow bandwidth more or less independent of wavelength. The typical FWHM is 15 nm (Table 3). Such narrow absorption bandwidths are important for selective excitation in multi-color applications in optical molecular imaging or flow cytometry. The analogous narrow fluorescence bandwidths are similarly useful for selective detection in multi-chromophore imaging and cytometry protocols. For example, we have utilized these narrow bandwidths to illustrate the favorable properties of bacteriochlorins (in chlorin–bacteriochlorin dyads) versus common commercial dyes for optical molecular imaging^{15,16} including in mouse models.⁴⁶

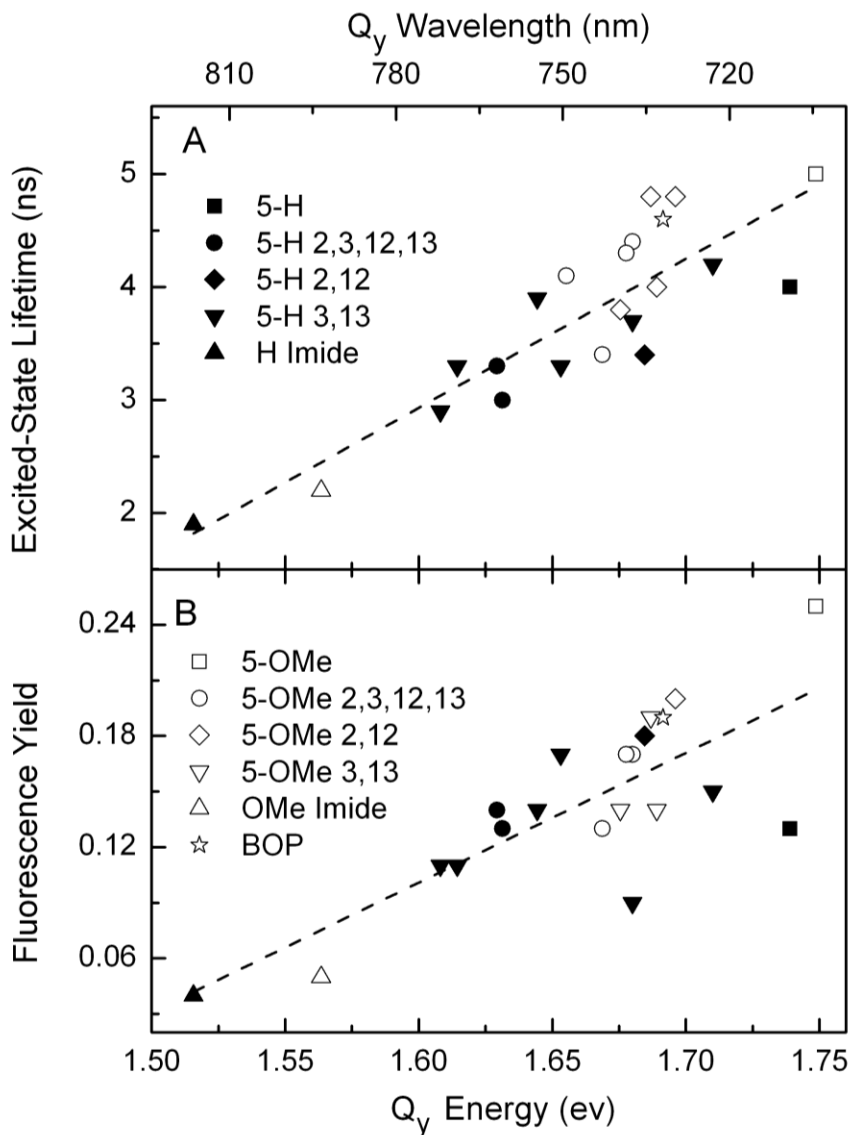


Figure 3. Singlet excited-state lifetime (τ_s) and fluorescence yield (Φ_f) versus the $Q_y(0,0)$ absorption energy (and wavelength) for representative bacteriochlorins, the bacteriochlorinimides, and **MeOBOP** (BOP). The closed symbols designate compounds containing a 5-H substituent and the open symbols compounds containing a 5-OMe group. The open and closed symbols represent the same compounds in both panels, but the legends for one type (5-H vs 5-OMe) are shown in only one panel due to space limitations. The trend lines represent fits to all of the data shown in each panel.

Table 5. Molecular Orbital Energies and Energy Gaps for Bacteriochlorins.

Compound	HOMO-1 (eV)	HOMO (eV)	LUMO (eV)	LUMO+1 (eV)	LUMO - HOMO (eV)	LUMO+1 - HOMO-1 (eV)	LUMO - HOMO-1 (eV)	LUMO+1 - HOMO (eV)
<i>HBC series</i>								
HBC-H	-4.99	-4.46	-2.20	-0.93	2.26	4.06	2.79	3.53
HBC-Swt ^{2,12}	-4.92	-4.36	-2.12	-0.89	2.24	4.03	2.8	3.47
HBC-M ^{3,13}	-4.98	-4.43	-2.19	-0.95	2.24	4.03	2.79	3.48
HBC-Re ^{3,13}	-5.01	-4.46	-2.28	-1.01	2.18	4.00	2.73	3.45
HBC-F ³	-5.21	-4.73	-2.58	-1.26	2.15	3.95	2.63	3.47
HBC-T ^{2,12}	-4.95	-4.40	-2.22	-0.96	2.18	3.99	2.73	3.44
HBC-P ^{3,13}	-5.00	-4.45	-2.28	-1.00	2.17	4.00	2.72	3.45
HBC-C ^{3,13}	-5.28	-4.86	-2.77	-1.30	2.09	3.98	2.51	3.56
HBC-CN ^{3,13}	-5.68	-5.22	-3.10	-1.65	2.12	4.03	2.58	3.57
HBC-V ^{3,13}	-5.03	-4.48	-2.37	-1.04	2.11	3.99	2.66	3.44
HBC-MES ^{3,13}	-5.20	-4.77	-2.67	-1.21	2.10	3.99	2.53	3.56
HBC-Me ^{2,12} EEs ^{3,13}	-5.17	-4.67	-2.57	-1.19	2.1	3.98	2.6	3.48
HBC-Et ^{2,12} EEs ^{3,13}	-5.18	-4.68	-2.58	-1.20	2.10	3.98	2.60	3.48
HBC-PE ^{3,13}	-5.11	-4.53	-2.51	-1.17	2.02	3.94	2.60	3.36
HBC-T ^{2,12} EEs ^{3,13}	-5.27	-4.75	-2.64	-1.30	2.11	3.97	2.63	3.45
HBC-A ^{3,13}	-5.26	-4.83	-2.78	-1.31	2.05	3.95	2.48	3.52
HBC-F ^{3,13}	-5.41	-4.97	-2.94	-1.49	2.03	3.92	2.47	3.48
<i>MeOBC series</i>								
MeOBC-H	-4.91	-4.48	-2.20	-0.93	2.28	3.98	2.71	3.55
MeOBC-T ^{2,12}	-4.88	-4.42	-2.23	-0.96	2.19	3.92	2.65	3.46

MeOBC-Py^{3,13}	-5.21	-4.78	-2.60	-1.31	2.18	3.90	2.61	3.47
MeOBC-EEs^{3,13}	-5.09	-4.75	-2.60	-1.21	2.15	3.88	2.49	3.54
MeOBC-Me^{2,12}EEs^{3,13}	-5.02	-4.61	-2.45	-1.12	2.16	3.90	2.57	3.49
MeOBC-Et^{2,12}EEs^{3,13}	-5.02	-4.60	-2.44	-1.11	2.16	3.91	2.58	3.49
MeOBC-A^{3,13}	-5.21	-4.84	-2.70	-1.33	2.14	3.88	2.51	3.51
MeOBC-Me^{2,12}A^{3,13}	-5.12	-4.70	-2.56	-1.25	2.14	3.87	2.56	3.45
MeOBC-An^{2,12}EEs^{3,13}	-4.96	-4.56	-2.43	-1.08	2.13	3.88	2.53	3.48
MeOBC-EEs^{2,3,12,13}	-5.32	-5.00	-2.95	-1.53	2.05	3.79	2.37	3.47
<i>15-substituted series</i>								
MeOBC-OMe¹⁵	-4.84	-4.50	-2.21	-0.94	2.29	3.90	2.63	3.56
MeOBC-T^{2,12}Bza¹⁵	-4.89	-4.47	-2.30	-1.01	2.17	3.88	2.59	3.46
MeOBC-T^{2,12}PE¹⁵	-4.78	-4.51	-2.40	-1.18	2.11	3.60	2.38	3.33
<i>Bacteriooxophorbine</i>								
MeOBOP	-5.17	-4.81	-2.63	-1.31	2.18	3.86	2.54	3.5
<i>Bacteriochlorinimides</i>								
MeOBC-I	-5.43	-4.91	-2.89	-1.51	2.02	3.92	2.54	3.4
HBC-I	-5.51	-4.91	-2.99	-1.50	1.92	4.01	2.52	3.41
<i>Standard</i>								
BPh a	-5.30	-4.87	-2.84	-1.41	2.03	3.89	2.46	3.46

Factors affecting the wavelength/energy of the $Q_y(0,0)$ absorption band

The one-electron configuration resulting from light-induced promotion of an electron from the HOMO to the LUMO normally makes a significant contribution to the electronic characteristics of the lowest singlet excited state (S_1) of most molecules. According to Gouterman's four-orbital model,⁴⁷ this configuration as well as that derived from electron promotion from the HOMO-1 to LUMO+1, define the wavefunction for the S_1 excited-state and thus, key characteristics (wavelength and intensity) of the $Q_y(0,0)$ absorption band of tetrapyrrole chromophores (including porphyrins, chlorins, and bacteriochlorins). We have previously applied this model to a series of about two dozen zinc chlorins.⁴⁸⁻⁵⁰

In Gouterman's description, the HOMO \rightarrow LUMO and HOMO-1 \rightarrow LUMO+1 one-electron configurations make roughly equal contributions to the S_1 wavefunction for porphyrins, with a proportionately greater contribution of HOMO \rightarrow LUMO configurations along the following series: porphyrin < chlorin < bacteriochlorin.⁴⁷ Indeed, time-dependent DFT calculations show that S_1 excited state of bacteriochlorins is comprised of roughly 75% HOMO \rightarrow LUMO, with most of the remainder due to HOMO-1 \rightarrow LUMO+1. These contributions can be seen from the following examples: **HBC-H** (71%, 27%); **MeOBC-H** (71%, 28%); **MeOBOP** (73%, 25%); **HBC-I** (78%, 18%); **MeOBC-I** (76%, 20%); **MeOBC-A**^{3,13} (72%, 24%). These results are in keeping with those obtained from prior DFT⁵¹ and *ab initio*⁵² calculations.

The experimental results and MO calculations presented here are fully consistent with a dominant contribution of the HOMO \rightarrow LUMO configuration for the bacteriochlorins, and give insights into the underlying molecular origin. The slopes of the trend lines given in Figure 4A show that the LUMO ($m = 3.8$) is more strongly connected with the wavelength/energy of the

$Q_y(0,0)$ absorption band than the HOMO ($m = 2.3$), LUMO+1 ($m = 2.9$) and HOMO-1 ($m = 2.8$). The slopes for the latter two orbitals are about equal. The result is a much greater magnitude of the slope of the trend line for the LUMO – HOMO energy gap ($m = 1.5$) versus the LUMO+1 – HOMO-1 energy gap ($m = 0.09$) plotted against the $Q_y(0,0)$ wavelength/energy (Figure 4B). Consequently, the wavelength/position of the $Q_y(0,0)$ band is dominated by the LUMO – HOMO energy gap.

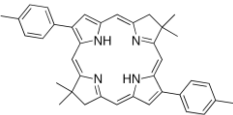
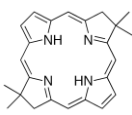
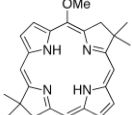
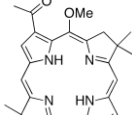
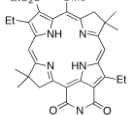
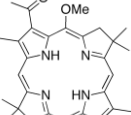
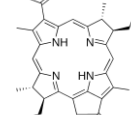
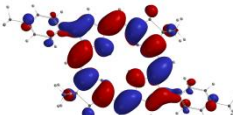
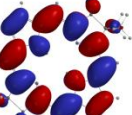
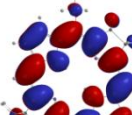
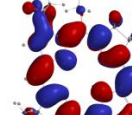
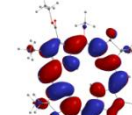
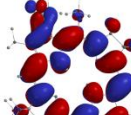
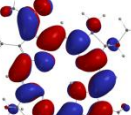
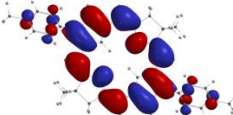
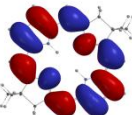
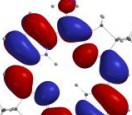
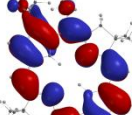
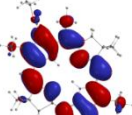
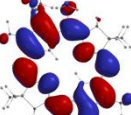
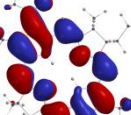
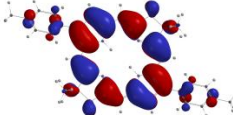
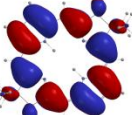
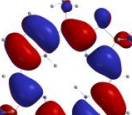
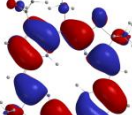
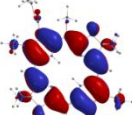
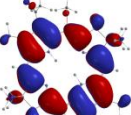
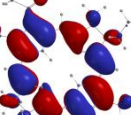
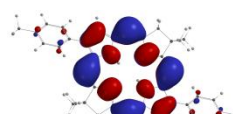
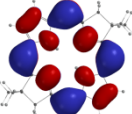
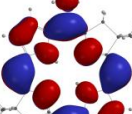
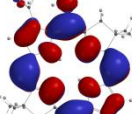
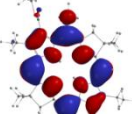
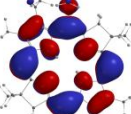
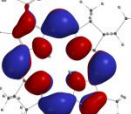
The greater dependence of the $Q_y(0,0)$ wavelength/energy on the LUMO (rather than the HOMO) can be traced to the generally greater electron-density in the LUMO at the 2,3,12,13-positions, which are the locations of most of the substituents in the bacteriochlorins studied here (Tables 1, 2 and 6). [Note that for porphyrins the HOMO is an analogue of the HOMO-1 orbital of the bacteriochlorins and thus the substituent effect on the LUMO – HOMO energy gap derives more from both orbitals rather than primarily from the LUMO.] For the molecules depicted in Table 6, these are the positions of the 2,12-*p*-tolyl groups of **HBC-T** and of the 3,13-carbonyl substituents (acetyl, ester, imide) of **MeOBC-A**^{3,13}, **MeOBC-I** and **MeOBOP**. As noted above, the 2,3,12,13-positions are on the molecular *y*-axis, which is the axis on which the Q_y optical transition is polarized.

Effect of a 5-Methoxy group on the position of the $Q_y(0,0)$ band

The 5-OMe group causes a hypsochromic shift in the $Q_y(0,0)$ band. The shift in the (i) Q_y wavelength, (ii) Q_y energy, and (iii) LUMO – HOMO energy gap upon replacing 5-H with 5-OMe for six pairs of bacteriochlorins are as follows (Tables 3 and 5): **MeOBC-I** vs **HBC-I** (–25 nm, 0.05 eV, 0.10 eV); **MeOBCEtEs** vs **HBC-EtEs** (–22 nm, 0.05 eV, 0.06 eV); **MeOBCMeEs** vs **HBC-MeEs** (–22 nm, 0.05 eV, 0.06 eV); **MeOBC-A**^{3,13} vs **HBC-A**^{3,13} (–28 nm, 0.06 eV,

0.09 eV); **MeOBC-T^{2,12}** vs **HBC-T^{2,12}** (−5 nm, 0.01 eV, 0.01 eV); **MeOBC-H** vs **HBC-H** (−4 nm, 0.02 eV, 0.01 eV). The calculated shift in the MO energy gap parallels the observed shift in Q_y(0,0) energy. There is a greater shift in both quantities for compounds containing 3,13-carbonyl moieties (acetyl, ester, imide) compared to 3,13-H, even with 2,12-di-*p*-tolyl groups present. Furthermore, with no 2,3,12,13-substituents, the incorporation of a second mesomethoxy group in **MeOBC-OMe¹⁵** (707 nm) gives a modest incremental hypsochromic shift of the Q_y(0,0) wavelength compared to one in **MeOBC-H** (709 nm), versus none in **HBC-H** (713 nm).

Table 6. Molecular-orbital Energies and Electron-density Distributions of Bacteriochlorins

	HBC-T ^{2,12}	HBC-H	MeOBC-H	MeOBC-A ^{3,13}	MeOBC-I	MeOBOP	BPh <i>a</i> ^a
Structure							
LUMO+1 (eV)	 -0.96	 -0.93	 -0.93	 -1.33	 -1.51	 -1.31	 -1.41
LUMO (eV)	 -2.22	 -2.20	 -2.20	 -2.70	 -2.89	 -2.63	 -2.84
HOMO (eV)	 -4.40	 -4.46	 -4.48	 -4.84	 -4.91	 -4.81	 -4.87
HOMO-1 (eV)	 -4.95	 -4.99	 -4.91	 -5.21	 -5.43	 -5.17	 -5.3

^aCalculations for **BPh a** were performed with a truncated phytol tail [-CH₂-CH=C(CH₃)(CH₂CH₃)], which is omitted in the display here

Close examination of the frontier MOs of the above-noted six pairs of compounds containing 5-OMe versus 5-H reveals an average effect on the orbital energies ($E_{5\text{-OMe}} - E_{5\text{-H}}$) in the following order: HOMO (+0.01 eV) < LUMO+1 (+0.02 eV) < LUMO (+0.07 eV) < HOMO-1 (+0.10 eV). This ordering is consistent with the relative electron densities of the four frontier MOs at the 5-position (Table 6). These average orbital-energy values in turn give rise to average effects on the orbital-energy-gaps ($\Delta E_{5\text{-OMe}} - \Delta E_{5\text{-H}}$) that are positive for the HOMO \rightarrow LUMO configuration (+0.06 eV) and negative for the HOMO-1 \rightarrow LUMO+1 (-0.08 eV). Given that the HOMO \rightarrow LUMO configuration dominates the properties of the $Q_y(0,0)$ band, these considerations correctly predict the hypsochromic shift (i.e., to higher energy) in the position of the band upon replacement of 5-H with 5-OMe. In turn, because the 5-OMe group does not strongly affect the HOMO energy, the spectral effect on the $Q_y(0,0)$ band derives primarily from the impact on the LUMO. Similar arguments should apply to bacteriochlorins with and without a 15-methoxy group and various 2,3,12,13 substituents because of the similar electron densities for each frontier MO at the 5- and 15-positions.

The effect of the 5-OMe group to reduce electron density in the bacteriochlorin π -system in the S_1 excited state is exacerbated by an increased contribution of the HOMO-1 \rightarrow LUMO+1 configuration in the S_1 wavefunction within the four-orbital model. The LUMO+1 – HOMO-1 energy gap is reduced, and becomes closer to the LUMO – HOMO energy gap (thereby increasing mixing of the two configurations), when a 5-OMe group is present (Table 5). This result derives primarily from the destabilizing effect of the 5-OMe group on the HOMO-1 orbital, which places considerable electron density at the 5 position, and then onto the OMe group itself (Table 6).

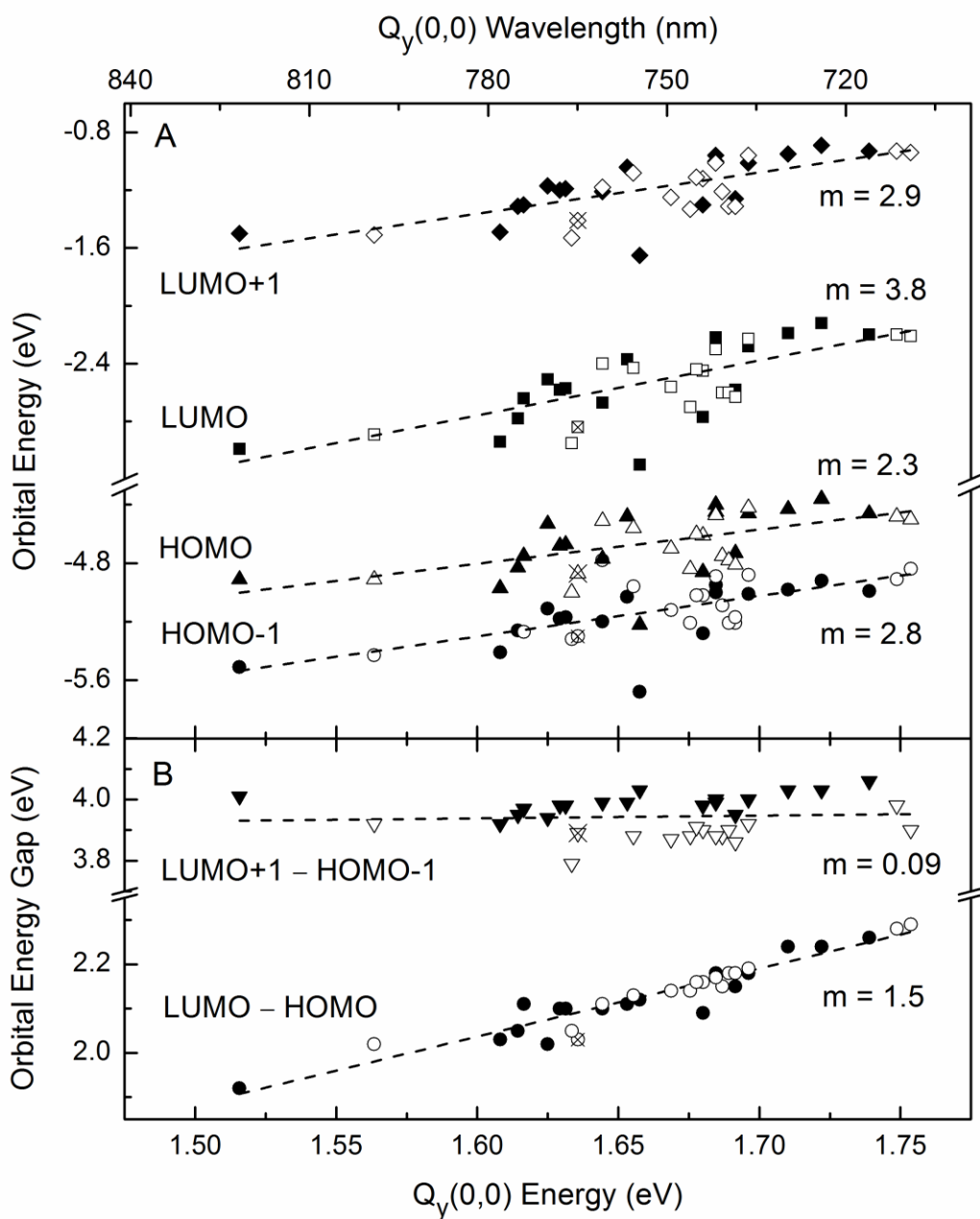


Figure 4. Molecular orbital energies (A) and energy gaps corresponding to the two y-polarized one-electron configurations (B) versus $Q_y(0,0)$ absorption energy (and wavelength). For each plot, the symbols designate the compounds as follows: 5-H bacteriochlorins and bacteriochlorinimide **HBC-I** (closed symbols); 5-OMe bacteriochlorins, bacteriochlorinimide **MeOBC-I** and bacteriooxophorbine **MeOBOP** (open symbols); **BPh a** (open circle containing an “x”). The slopes (m) of the trendlines are shown.

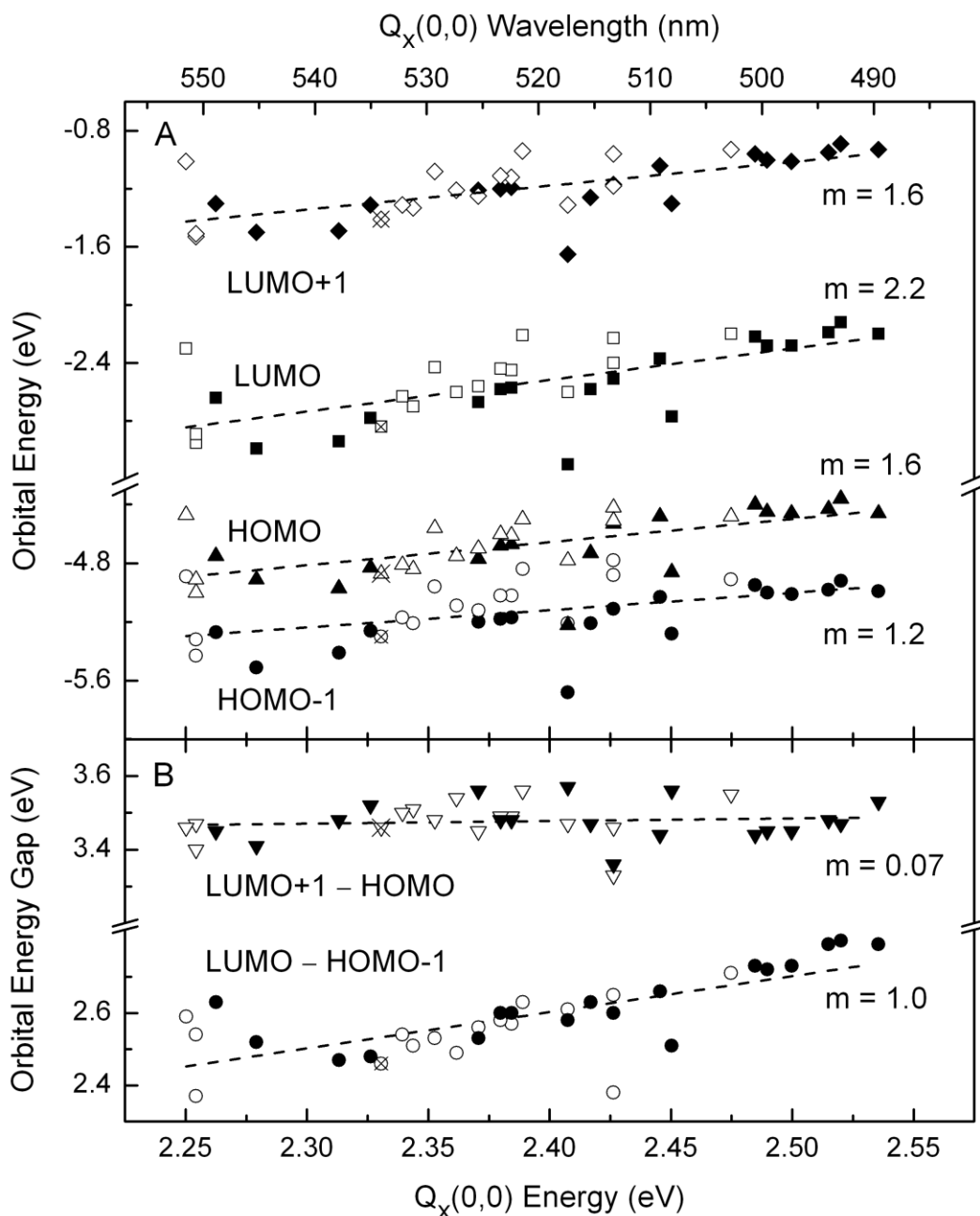


Figure 5. Frontier molecular orbital energies (A) and energy gaps corresponding to the two x-polarized one-electron configurations (B) versus $Q_y(0,0)$ absorption energy (and wavelength). For each plot, the symbols designate the compounds as follows: 5-H bacteriochlorins and bacteriochlorinimide **HBC-I** (closed symbols); 5-OMe bacteriochlorins, bacteriochlorinimide **MeOBC-I** and bacteriooxophorbine **MeOBOP** (open symbols); **BPh a** (open circle containing an “x”). The slopes (m) of the trend lines are shown.

The hypsochromic shift imparted by the 5-OMe group thus provides a design feature, along with placement of groups at the 2,3,12,13-positions, to obtain a palette of NIR absorbing bacteriochlorins with finely spaced bands. The 5-OMe group also allows modest control of excited-state lifetimes and fluorescence yields. This group also is quite useful for synthetic purposes in affording regioselective 15-bromination³⁰ and thereby enabling access to bacteriochlorinimides and a bacteriooxophorbine.³⁶

Intensity of the $Q_y(0,0)$ absorption band

Figure 2A shows that the $Q_y(0,0)$ band increases in relative intensity with a shift to longer wavelength (lower energy). In the four-orbital description, the Q_y -band intensity is related to the difference in energy of the LUMO – HOMO and LUMO+1 – HOMO-1 energy gaps.⁴⁷ As can be seen from Figure 4B, the LUMO – HOMO energy gap changes substantially with $Q_y(0,0)$ wavelength/energy whereas the LUMO+1 – HOMO-1 energy gap does not. Thus, the intensity of the $Q_y(0,0)$ band is expected to track the LUMO – HOMO energy gap, as is observed (Figure 2B). Because the LUMO – HOMO energy gap also tracks the $Q_y(0,0)$ wavelength/energy (Figure 4B), the positive correlation of $Q_y(0,0)$ energy/wavelength and intensity can be understood (Figure 2A). In turn, because the variation in LUMO – HOMO energy gap is associated substantially with the LUMO (Figure 4A), bacteriochlorin substituents that preferentially alter the LUMO versus HOMO energy (*e.g.*, at the 2,3,12,13-positions) will change the intensity (like the wavelength) of the $Q_y(0,0)$ band in a predictable manner.

The position of the $Q_x(0,0)$ absorption band

The $Q_x(0,0)$ band reflects absorption to the second singlet excited state, which occurs in the blue-green spectral region (Figure 1 and Table 3). The analysis of substituent effects on the $Q_x(0,0)$ band closely parallels that given above concerning the $Q_y(0,0)$ band. The key findings

are as follows: (i) The LUMO energy shows a much greater connection with $Q_x(0,0)$ energy/wavelength than the other frontier MOs (Figure 5A). (ii) Of the two electronic configurations that contribute to the Q_x wavefunction within the four-orbital model, the LUMO – HOMO-1 energy gap correlates with the $Q_x(0,0)$ energy/wavelength while the LUMO+1 – HOMO energy gap is essentially invariant (Figure 5B). (iii) It follows that the dependence of the LUMO on 2,3,12,13-substituents dominates the variation in the position of the $Q_x(0,0)$ band for the bacteriochlorins studied here, which again is derived from the generally greater electron-density in the LUMO at these positions (Tables 1, 2 and 6). (iv) Similarly, because the intensity of the $Q_x(0,0)$ band, as reflected in the $Q_x(0,0)/Q_x(1,0)$ intensity ratio in Table 3, is expected to track the difference in the LUMO – HOMO-1 and LUMO+1 – HOMO energy gaps, the $Q_x(0,0)$ intensity primarily tracks the LUMO – HOMO-1 gap and thus the LUMO energy. (v) The conclusion in (iii) along with the above-noted dominance of the LUMO in the substituent-dependence of the $Q_y(0,0)$ band implies a correlation between the energy/wavelength of the two bands, as is observed (Figure 7). (vi) The offset parallel trend lines for bacteriochlorins containing 5-H substituents, 5-OMe groups, and 5,15-OMe (or 5-OMe plus the oxophorbine) (Figure 6) are related to the different (often reversed) effects of these substituents on the two bands (Table 3). For example, of the six pairs of bacteriochlorins that have a 5-OMe versus 5-H substituent, the greatest 5-OMe effect on the $Q_x(0,0)$ band is found for the -H, -T^{2,12} compounds (a 12 nm bathochromic shift), whereas the greatest effect on the $Q_y(0,0)$ band is found for the carbonyl-containing (-A^{3,13}, -MeEs, -EtEs, imide) analogues (24–28 nm bathochromic shift). These differences are related to the electron densities in the MOs involved in the respective transitions.

Yields and Rate Constants of the excited-state decay pathways

For all the (free base) bacteriochlorins under study, the average yields of fluorescence, intersystem crossing, and internal conversion are $\Phi_f = 0.15$, $\Phi_{isc} = 0.52$, and $\Phi_{ic} = 0.33$. The associated average rate constants are $k_f = (27 \text{ ns})^{-1}$, $k_{isc} = (8 \text{ ns})^{-1}$, and $k_{ic} = (12 \text{ ns})^{-1}$, which are in concert with the average singlet excited-state lifetime of $\tau_S = 3.8 \text{ ns}$. For comparison, typical values obtained from the photophysical data for free base *meso*-tetraphenylporphyrin are $\Phi_f = 0.10$, $\Phi_{isc} = 0.70$, $\Phi_{ic} = 0.20$, and $\tau_S = 13 \text{ ns}$.^{39,53-56} Using Eq 5, these values give corresponding rate constants of $k_f = (130 \text{ ns})^{-1}$, $k_{isc} = (19 \text{ ns})^{-1}$, and $k_{ic} = (65 \text{ ns})^{-1}$. The roughly 5-fold greater rate constant for $S_1 \rightarrow S_0$ (spontaneous) fluorescence (k_f) for bacteriochlorins versus porphyrins is paralleled by stronger (stimulated) $S_0 \rightarrow S_1$ absorption, namely the integrated intensity of the Q_y absorption manifold [$Q_y(0,0)$, $Q_y(1,0)$, etc]; these two quantities are connected by the respective Einstein coefficients.

Although the average yield for $S_1 \rightarrow T_1$ intersystem crossing for the bacteriochlorins is about 30% lower for bacteriochlorins versus porphyrins (0.5 versus 0.7), the average rate constant for the process is about two-fold greater [(8 ns)⁻¹ versus (19 ns)⁻¹]. Thus, spin-orbit coupling is actually enhanced in the bacteriochlorins versus porphyrins. Furthermore, the typical values of $\Phi_{isc} \sim 0.5$ for free base bacteriochlorins, along with triplet excited-state lifetimes of tens of microseconds to over one hundred microseconds (in the absence of O_2), is ample to support efficient sensitization in PDT,²⁰⁻²² a process that is initiated via the triplet excited state. A key factor for the efficacy of the bacteriochlorins as PDT sensitizers is that their appropriate photophysical properties are coupled with (i) absorption in the NIR region, for which penetration into animal tissues is greater than for shorter wavelength (UV-Vis) or longer wavelength (infrared) radiation and (ii) the synthetic amenability to allow tailoring of the chromophores for cell uptake and delivery to diverse target sites.²⁰⁻²²

Turning to the third decay process of the S_1 excited state, there is a five-fold enhanced average rate constant for $S_1 \rightarrow S_0$ internal conversion for bacteriochlorins versus the typical free base porphyrin [(12 ns)⁻¹ versus (65 ns)⁻¹]. There is also a modest, yet less dramatic general increase in k_{ic} with decreasing S_1 [i.e., $Q_y(0,0)$] energy among the bacteriochlorins themselves (Table 4). These trends are expected on the basis of the energy-gap law for nonradiative decay.⁴⁵ In particular, the rate constant for internal conversion is expected to increase exponentially as the $S_1 - S_0$ energy gap decreases, via the typical energy-gap dependence of a Franck-Condon factor. Nonetheless, the average yield of the internal conversion process increases only from about 0.2 for free base porphyrins to 0.3 for the free base bacteriochlorins. Furthermore, the enhancement of this nonradiative decay process occurs to such a modest degree that average bacteriochlorin singlet excited-state lifetime of ~4 ns is still quite long, and more than sufficient to drive efficient energy/charge-transfer processes in solar-energy and other applications. Relatively long S_1 lifetimes are retained even for the longest wavelength-absorbing bacteriochlorins studied here, namely the bacteriochlorinimides **MeOBC-I** ($\lambda_{Q_y(0,0)} = 793$ nm; $\tau_S = 2.2$ ns) and **HBC-I** ($\lambda_{Q_y(0,0)} = 818$ nm; $\tau_S = 1.9$ ns). These synthetic bacteriochlorins absorb at longer wavelength than the native photosynthetic free base bacteriochlorin **BPh a** (by ~40 and ~70 nm, respectively) yet have comparable excited-state lifetimes. Such characteristics bode well for the use of tunable synthetic bacteriochlorins to extend the properties available in the native photosynthetic pigments for diverse applications.

Outlook

The studies reported herein delineate the spectral and photophysical properties of about three dozen synthetic bacteriochlorins and elucidate the origin of the variations in these properties as a function of substituent type and position on the macrocycle. The palette of

synthetic bacteriochlorins represents a significant extension of the properties of the native photosynthetic pigments (bacteriochlorophylls). Understanding the design principles for tuning the spectral and photophysical characteristics establishes a path forward for utilizing the synthetic bacteriochlorins in a wide variety of photochemical applications. A result that deserves emphasis is that the wavelength tunability (achieved by introduction of diverse β -pyrrole substituents) stems largely from interaction of the auxochromes with the LUMO of the bacteriochlorin. The interaction of the auxochromes with the LUMO is also expected to alter the reduction potential with little effect on the oxidation potential of the bacteriochlorin. The lowest singlet excited-state lifetimes (from ~2 to ~6 ns) augur well for a wide variety of photochemical applications.

The types of applications that might be envisioned for the synthetic bacteriochlorins include the following:

(1) Effective molecular imaging requires bright fluorophores in the NIR spectral region with avoidance of spectral overlap and light scattering. Brightness stems from the product of illumination intensity, absorption intensity, and fluorescence quantum yield; spectral overlap and light scattering are mitigated with sharp absorption/emission bands and relatively long excited-state lifetimes. The choice of NIR-active compound ultimately depends on a large number of factors including the aforementioned photophysical features as well as synthetic accessibility, solubility, toxicity, and amenability toward alteration of the molecular design. A malleable molecular design is essential, for example, to accommodate incorporation of diverse targeting agents. Versatility in molecular design depends in turn on the robustness of the synthetic plan and intrinsic features of the molecular architecture. While the diversity of NIR imaging applications undoubtedly requires diverse chromophores,^{19,20} the intrinsic photophysical features

delineated herein and the molecular tailoring achieved to date (for the related topic of PDT)²⁰⁻²² together indicate the synthetic bacteriochlorins appear well suited for such applications.

(2) Enhanced sorting capabilities of cellular components require molecular tags with absorption that extends beyond the visible region. The strong and relatively narrow (as well as tunable) NIR absorption feature of the synthetic bacteriochlorins suggests utility as individually addressable dye markers in flow cytometry.

(3) Enhanced capabilities for PDT applications require high triplet excited-state (intersystem crossing) yields. The synthetic bacteriochlorins exhibit this capability, in addition to the amenability toward synthetic tailoring for cell uptake and delivery to diverse target sites.

(4) Efficient solar energy conversion requires the capability to capture NIR light because a significant fraction of the solar spectrum falls to the red of 600 nm. Bacteriochlorophyll *a* and its metal free analogue BPh *a* typically absorb near 780 nm and 750 nm, respectively, as *monomers* in organic solvents yet exhibit longer wavelength absorption (e.g., 800, 850, 870 nm) in many native photosynthetic antenna systems owing to interactions between bacteriochlorophylls in oligomeric assemblies.¹ The synthetic free base bacteriochlorins reported herein extend the accessible spectral range as *monomers* to encompass ~700 to ~820 nm. The fine tuning of the wavelength maximum of the lowest energy absorption band across a significant portion of the NIR spectral region should enable enhanced collection of solar radiation, and the design of energy-cascade systems wherein excitons are delivered in a controlled manner to a designated site. The wavelength tunability demonstrated here combined with the rich synthetic chemistry affords versatile building blocks for biomimetic construction of multi-pigment architectures in artificial photosynthesis, and should facilitate the rational design

of a wide variety of photochemical systems that function upon illumination in the NIR spectral region.

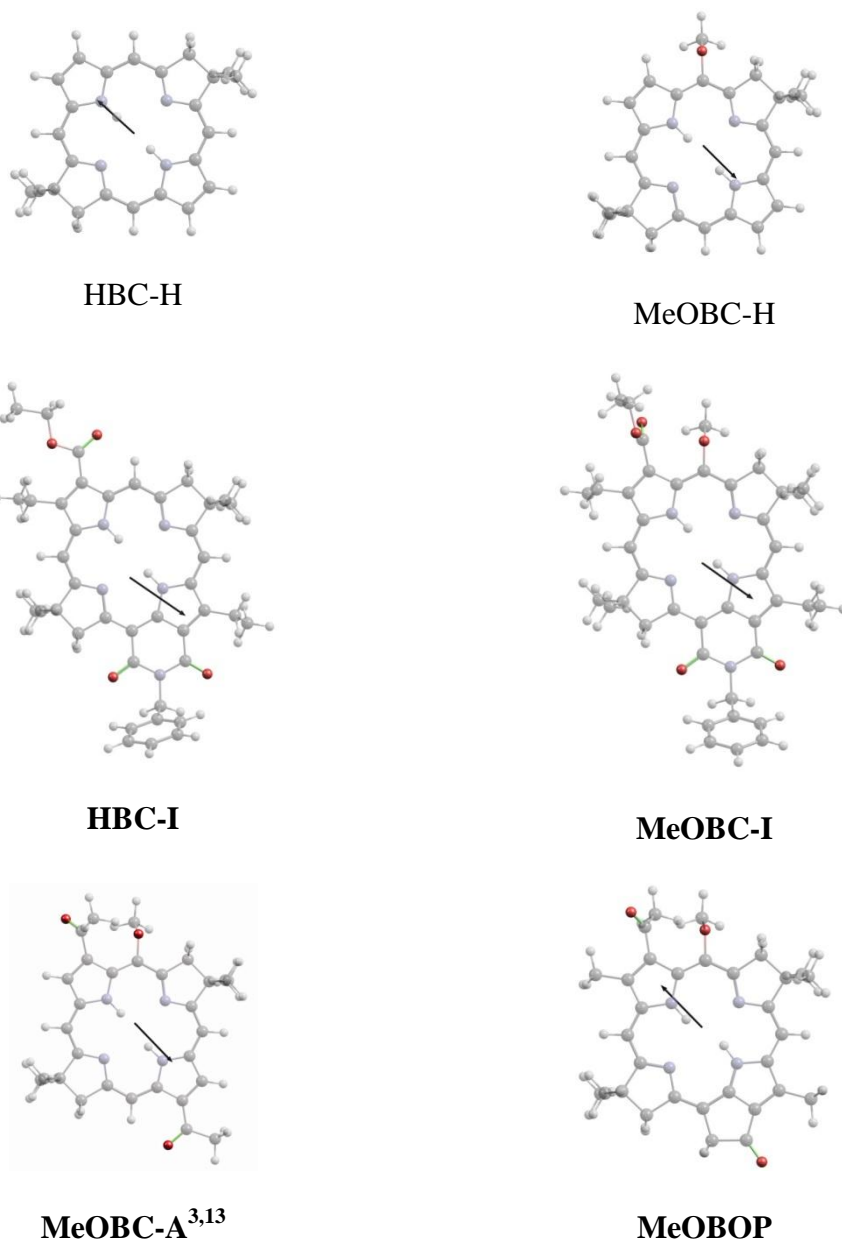


Figure 6. Transition-dipole-moment directions from time-dependent DFT calculations

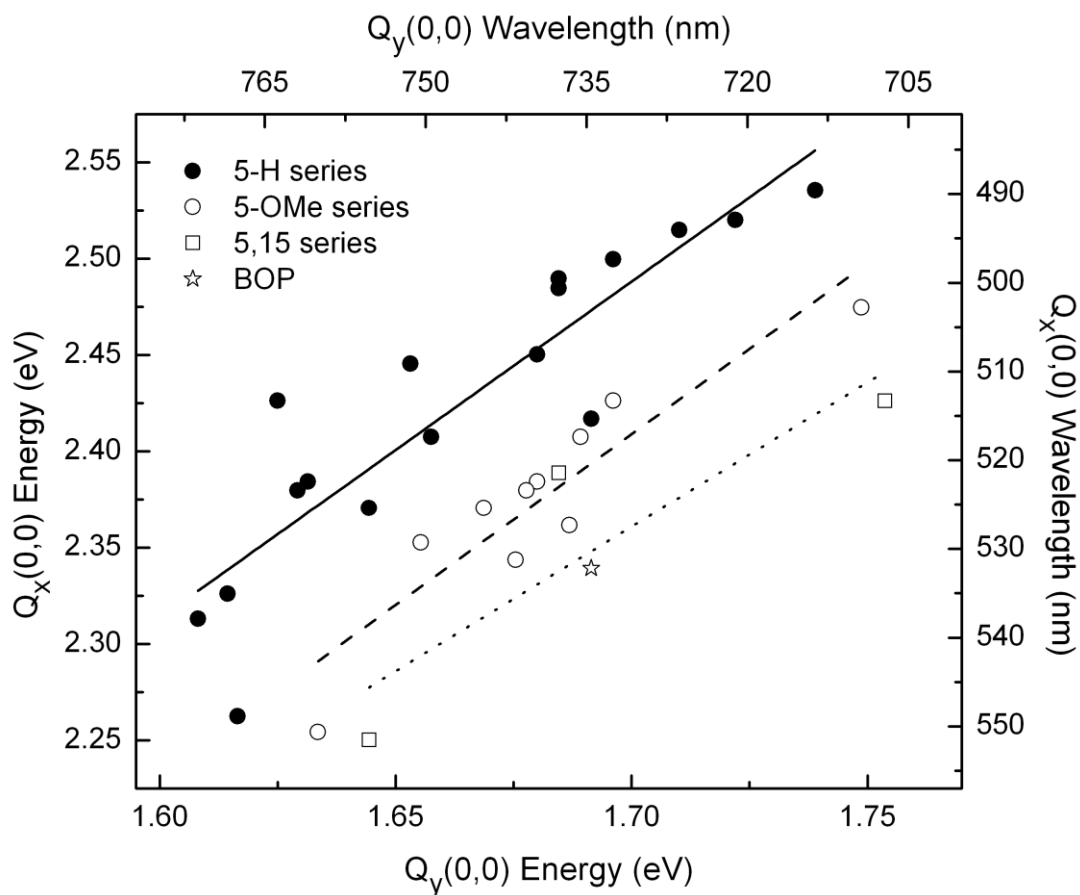


Figure 7. Energy (and wavelength) of the $Q_x(0,0)$ absorption band versus the energy (and wavelength) of the $Q_y(0,0)$ absorption band. The symbols designate the compounds as follows: 5-H bacteriochlorins (closed circles), 5-OMe bacteriochlorins (open circles), bacteriochlorins containing 5-OMe plus a 15-substituent (open squares), and bacteriooxophorbine **MeOBOP** (open star). The trend lines are fits to the data sets as follows: 5-H bacteriochlorins (solid), 5-OMe bacteriochlorins (dashed), 5,15-bacteriochlorins plus bacteriooxophorbine (dotted).

Acknowledgment This work was supported by grants from the Division of Chemical Sciences, Geosciences, and Biosciences, Office of Basic Energy Sciences of the U.S. Department of Energy to D.F.B. (DE-FG02-05ER15660), D.H. (DE-FG02-05ER15661) and J.S.L. (DE-FG02-96ER14632). We thank the following individuals for contributing bacteriochlorins for photophysical analysis: Dr. Thiagarajan Balasubramanian, Dr. Eszter K. Borbas, Mr. Chih-Yuan Chen, Mr. David Cramer, Dr. Dazhong Fan, Dr. Brian E. McDowell, Dr. Marcin Ptaszek, and Dr. Christian Ruzié. We thank Dr. Hooi Ling Kee for photophysical measurements of several bacteriochlorins.

Supporting Information Available: Synthesis procedures and characterization data for bacteriochlorin **HBC-T^{2,12}EEs^{3,13}** and the link are given in Ref A.

References

- (A) Yang, E.K.; Kirmaier, C.; Krayner, M.; Taniguchi, M.; Kim, H.J.; Diers, J.R.; Bocian, D.F.; Lindsey J.S.; Holten, D. Photophysical Properties and Electronic Structure of Stable, Tunable Synthetic Bacteriochlorins: Extending the Features of Native Photosynthetic Pigments. *J. Phys. Chem. B.* 2011, *115*, 10801–10816
- (1) Scheer, H. In *Chlorophylls and Bacteriochlorophylls. Biochemistry, Biophysics, Functions and Applications*; Grimm, B.; Porra, R. J.; Rüdiger, W.; Scheer, H., Eds., Advances in Photosynthesis and Respiration, 2006, Vol. 25; Springer, Dordrecht, The Netherlands, pp 1–26.
- (2) (a) Ashur, I.; Goldschmidt, R.; Pinkas, I.; Salomon, Y.; Szewczyk, G.; Sarna, T.; Scherz, A. *J. Phys. Chem. A* **2009**, *113*, 8027–8037. (b) Kozyrev, A. N.; Chen, Y.; Goswami, L. N.; Tabaczynski, W. A.; Pandey, R. K. *J. Org. Chem.* **2006**, *71*, 1949–1960. (c) Limantara, L.; Koehler, P.; Wilhelm, B.; Porra, R. J.; Scheer, H. *Photochem. Photobiol.* **2006**, *82*, 770–780. (d) Vakrat-Haglili, Y.; Weiner, L.; Brumfeld, V.; Brandis, A.; Salomon, Y.; McIlroy, B.; Wilson, B. C.; Pawlak, A.; Rozanowska, M.; Sarna, T.; Scherz, A. *J. Am. Chem. Soc.* **2005**, *127*, 6487–6497. (e) Fiedor, J.; Fiedor, L.; Kammhuber, N.; Scherz, A.; Scheer, H. *Photochem. Photobiol.* **2002**, *76*, 145–152.
- (3) Grin, M. A.; Mironov, A. F.; Shtil, A. A. *Anti-Cancer Agents Med. Chem.* **2008**, *8*, 683–697.
- (4) Chen, Y.; Li, G.; Pandey, R. K. *Curr. Org. Chem.* **2004**, *8*, 1105–1134.
- (5) Galezowski, M.; Gryko, D. T. *Curr. Org. Chem.* **2007**, *11*, 1310–1338.
- (6) (a) Aratani, N.; Osuka, A. In *Handbook of Porphyrin Science*; Kadish, K. M., Smith, K. M., Guillard, R., Eds.; World Scientific Publishing Co.: Singapore, Vol. 1, 2010, pp 1–132. (b) Maretina, I. A. *Russ. J. Gen. Chem.* **2009**, *79*, 1544–1581. (c) Flamigni, L. *J. Photochem. Photobiol. C: Photochem. Rev.* **2007**, *8*, 191–210. (d) Iengo, E.; Scandola, F.; Alessio, E. *Struct. Bond.* **2006**, *121*, 105–143. (e) Harvey, P. D. In *The Porphyrin Handbook*; Kadish, K. M., Smith, K. M., Guillard, R., Eds.; Academic Press: San Diego, CA, 2003; Vol. 18, pp 63–250. (f) Holten, D.; Bocian, D. F.; Lindsey, J. S. *Acc. Chem.*

- Res.* **2002**, *35*, 57–69. (g) Gust, D.; Moore, T. A. In *The Porphyrin Handbook*; Kadish, K. M., Smith, K. M., Guillard, R., Eds.; Academic Press: San Diego, CA, 2000; Vol. 8, pp 153–190. (h) Gribkova, S. E.; Evstigneeva, R. P.; Luzgina, V. N. *Russ. Chem. Rev.* **1993**, *62*, 963–979. (i) Wasielewski, M. R. *Chem. Rev.* **1992**, *92*, 435–461. (j) Wasielewski, M. R. In *Chlorophylls*; Scheer, H. Ed.; CRC Press, Boca Raton, FL, USA, 1991, pp 269–286.
- (7) Lindsey, J. S.; Mass, O.; Chen, C.-Y. *New J. Chem.* **2011**, *35*, 511–516.
- (8) Kobayashi, M.; Akiyama, M.; Kano, H.; Kise, H. In *Chlorophylls and Bacteriochlorophylls: Biochemistry, Biophysics, Functions and Applications*; Grimm, B.; Porra, R. J.; Rüdiger, W.; Scheer, H., Eds.; Springer: Dordrecht, The Netherlands, 2006, pp 79–94.
- (9) Stromberg, J. R.; Marton, A.; Kee, H. L.; Kirmaier, C.; Diers, J. R.; Muthiah, C.; Taniguchi, M.; Lindsey, J. S.; Bocian, D. F.; Meyer, G. J.; Holten, D. *J. Phys. Chem. C* **2007**, *111*, 15464–15478.
- (10) (a) Chattopadhyay, P. K.; Hogerkorp, C.-M.; Roederer, M. *Immunol.* **2008**, *125*, 441–449. (b) Shapiro, H. M. in *Flow Cytometry for Biotechnology*; Sklar, L. A., Ed.; Oxford University Press: NY, 2005, pp 15–39.
- (11) Sutton, J. M.; Clarke, O. J.; Fernandez, N.; Boyle, R. W. *Bioconjugate Chem.* **2002**, *13*, 249–263.
- (12) Ethirajan, M.; Chen, Y.; Joshi, P.; Pandey, R. K. *Chem. Soc. Rev.* **2011**, *40*, 340–362.
- (13) Singh, S.; Aggarwal, A.; Thompson, S.; Tomé, J. P. C.; Zhu, X.; Samaroo, D.; Vinodu, M.; Gao, R.; Drain, C. M. *Bioconjugate Chem.* **2010**, *21*, 2136–2146.
- (14) Cao, W.; Ng, K. K.; Corbin, I.; Zhang, Z.; Ding, L.; Chen, J.; Zheng, G. *Bioconjugate Chem.* **2009**, *20*, 2023–2031.
- (15) Kee, H. L.; Diers, J. R.; Ptaszek, M.; Muthiah, C.; Fan, D.; Lindsey, J. S.; Bocian, D. F.; Holten, D. *Photochem. Photobiol.* **2009**, *85*, 909–920.
- (16) Kee, H. L.; Nothdurft, R.; Muthiah, C.; Diers, J. R.; Fan, D.; Ptaszek, M.; Bocian, D. F.; Lindsey, J. S.; Culver, J. P.; Holten, D. *Photochem. Photobiol.* **2008**, *84*, 1061–1072.
- (17) Akers, W.; Lesage, F.; Holten, D.; Achilefu, S. *Mol. Imag.* **2007**, *6*, 237–246.
- (18) Frangioni, J. V. *Curr. Opin. Chem. Biol.* **2003**, *7*, 626–634.
- (19) Licha, K. *Top. Curr. Chem.* **2002**, *222*, 1–29.
- (20) Mroz, P.; Huang, Y.-Y.; Szokalska, A.; Zhiyentayev, T.; Janjua, S.; Nifli, A.-P.; Sherwood, M. E.; Ruzié, C.; Borbas, K. E.; Fan, D.; Krayner, M.; Balasubramanian, T.;

- Yang, E.; Kee, H. L.; Kirmaier, C.; Diers, J. R.; Bocian, D. F.; Holten, D.; Lindsey, J. S.; Hamblin, M. R. *FASEB J.* **2010**, *24*, 3160–3170.
- (21) Huang, Y.-Y.; Mroz, P.; Zhiyentayev, T.; Sharma, S. K.; Balasubramanian, T.; Ruzié, C.; Krayner, M.; Fan, D.; Borbas, K. E.; Yang, E.; Kee, H. L.; Kirmaier, C.; Diers, J. R.; Bocian, D. F.; Holten, D.; Lindsey, J. S.; Hamblin, M. R. *J. Med. Chem.* **2010**, *53*, 4018–4027.
- (22) Huang, L.; Huang, Y.-Y.; Mroz, P.; Tegos, G. P.; Zhiyentayev, T.; Sharma, S. K.; Lu, Z.; Balasubramanian, T.; Krayner, M.; Ruzié, C.; Yang, E.; Kee, H. L.; Kirmaier, C.; Diers, J. R.; Bocian, D. F.; Holten, D.; Lindsey, J. S.; Hamblin, M. R. *Antimicrob. Agents Chemother.* **2010**, *54*, 3834–3841.
- (23) O'Connor, A. E.; Gallagher, W. M.; Byrne, A. T. *Photochem. Photobiol.* **2009**, *85*, 1053–1074.
- (24) Brandis, A. S.; Salomon, Y.; Scherz, A. In *Chlorophylls and Bacteriochlorophylls: Biochemistry, Biophysics, Functions and Applications*; Grimm, B.; Porra, R. J.; Rüdiger, W.; Scheer, H.; Eds.; Springer: Dordrecht, The Netherlands, 2006; pp 485–494.
- (25) Nyman, E. S.; Hynninen, P. H. *J. Photochem. Photobiol. B: Biol.* **2004**, *73*, 1–28.
- (26) Bonnett, R. *Chemical Aspects of Photodynamic Therapy*; Gordon and Breach Science Publishers: Amsterdam, 2000.
- (27) Davis, N. K. S.; Thompson, A. L.; Anderson, H. L. *J. Am. Chem. Soc.* **2011**, *133*, 30–31.
- (28) Ikeda, S.; Toganoh, M.; Easwaramoorthi, S.; Lim, J. M.; Kim, D.; Furuta, H. *J. Org. Chem.* **2010**, *75*, 8637–8649.
- (29) Kim, H.-J.; Lindsey, J. S. *J. Org. Chem.* **2005**, *70*, 5475–5486.
- (30) Fan, D.; Taniguchi, M.; Lindsey, J. S. *J. Org. Chem.* **2007**, *72*, 5350–5357.
- (31) McDowell, B. E. Ph.D. thesis, North Carolina State University, 2007.
- (32) Taniguchi, M.; Cramer, D. L.; Bhise, A. D.; Kee, H. L.; Bocian, D. F.; Holten, D.; Lindsey, J. S. *New J. Chem.* **2008**, *32*, 947–958.
- (33) Borbas, K. E.; Ruzié, C.; Lindsey, J. S. *Org. Lett.* **2008**, *10*, 1931–1934.
- (34) Ruzié, C.; Krayner, M.; Balasubramanian, T.; Lindsey, J. S. *J. Org. Chem.* **2008**, *73*, 5806–5820.
- (35) Krayner, M.; Ptaszek, M.; Kim, H.-J.; Meneely, K. R.; Fan, D.; Secor, K.; Lindsey, J. S. *J. Org. Chem.* **2010**, *75*, 1016–1039.

- (36) Krayer, M.; Yang, E.; Diers, J. R.; Bocian, D. F.; Holten, D.; Lindsey, J. S. *New J. Chem.* **2011**, *35*, 587–601.
- (37) Kee, H. L.; Bhaumik, J.; Diers, J. R.; Mroz, P.; Hamblin, M. R.; Bocian, D. F.; Lindsey, J. S.; Holten, D. *J. Photochem. Photobiol. A: Chem.* **2008**, *200*, 346–355.
- (38) Seybold, P. G.; Gouterman, M. *J. Mol. Spectrosc.* **1969**, *31*, 1–13.
- (39) Gradyushko, A. T.; Sevchenko, A. N.; Solovyov, K. N.; Tsvirko, M. P. *Photochem. Photobiol.* **1970**, *11*, 387–400.
- (40) Weber, G.; Teale, F. W. J. *Trans. Faraday Soc.* **1957**, *53*, 646–655.
- (41) Kee, H. L.; Kirmaier, C.; Yu, L.; Thamyongkit, P.; Youngblood, W. J.; Calder, M. E.; Ramos, L.; Noll, B. C.; Bocian, D. F.; Scheidt, W. R.; Birge, R. R.; Lindsey, J. S.; Holten, D. *J. Phys. Chem. B* **2005**, *109*, 20433–20443.
- (42) Except for molecular mechanics and semi-empirical models, the calculation methods used in Spartan have been documented in: Shao, Y.; Molnar, L. F.; Jung, Y.; Kussmann, J.; Ochsenfeld, C.; Brown, S. T.; Gilbert, A. T. B.; Slipchenko, L. V.; Levchenko, S. V.; O'Neill, D. P.; DiStasio, R. A., Jr.; Lochan, R. C.; Wang, T.; Beran, G. J. O.; Besley, N. A.; Herbert, J. M.; Lin, C. Y.; Van Voorhis, T.; Chien, S. H.; Sodt, A.; Steele, R. P.; Rassolov, V. A.; Maslen, P. E.; Korambath, P. P.; Adamson, R. D.; Austin, B.; Baker, J.; Byrd, E. F. C.; Dachsel, H.; Doerksen, R. J.; Dreuw, A.; Dunietz, B. D.; Dutoi, A. D.; Furlani, T. R.; Gwaltney, S. R.; Heyden, A.; Hirata, S.; Hsu, C.-P.; Kedziora, G.; Khalliulin, R. Z.; Klunzinger, P.; Lee, A. M.; Lee, M. S.; Liang, W.-Z.; Lotan, I.; Nair, N.; Peters, B.; Proynov, E. I.; Pieniazek, P. A.; Rhee, Y. M.; Ritchie, J.; Rosta, E.; Sherrill, C. D.; Simmonett, A. C.; Subotnik, J. E.; Woodcock, H. L., III; Zhang, W.; Bell, A. T.; Chakraborty, A. K.; Chipman, D. M.; Keil, F. J.; Warshel, A.; Hehre, W. J.; Schaefer, H. F., III; Kong, J.; Krylov, A. I.; Gill, P. M. W.; Head-Gordon, M. *Phys. Chem. Chem. Phys.* **2006**, *8*, 3172–3191.
- (43) Smith, J. H. C.; Benitez, A. In *Modern Methods of Plant Analysis*; Paech, K.; Tracey, M. V., Eds.; Springer-Verlag: Berlin, 1955, Vol. IV, pp 142–196.
- (44) Holten, D.; Gouterman, M.; Parson, W. W.; Windsor, M. W.; Rockley, M. G. *Photochem. Photobiol.* **1976**, *23*, 415–423.
- (45) Birks, J. B. *Photophysics of Aromatic Molecules*, Wiley-Interscience: London, 1970, pp 140–192.
- (46) Ptaszek, M.; Kee, H. L.; Muthiah, C.; Nothdurft, R.; Akers, W.; Achilefu, S.; Culver, J. P.; Holten, D. *Proc. SPIE* **2010**, *7576*, 75760E1–11.

- (47) (a) Gouterman, M. in *The Porphyrins*, Vol. 3, Dolphin, D. Ed., Academic Press: New York, 1978, pp 1–165. (b) Gouterman, M. *J. Mol. Spectroscopy* **1961**, *6*, 138–163. (c) Gouterman, M. *J. Chem. Phys.* **1959**, *30*, 1139–1161.
- (48) Kee, H. L.; Kirmaier, C.; Tang, Q.; Diers, J. R.; Muthiah, C.; Taniguchi, M.; Laha, J. K.; Ptaszek, M.; Lindsey, J. S.; Bocian, D. F.; Holten, D. *Photochem. Photobiol.* **2007**, *83*, 1110–1124.
- (49) Kee, H. L.; Kirmaier, C.; Tang, Q.; Diers, J. R.; Muthiah, C.; Taniguchi, M.; Laha, J. K.; Ptaszek, M.; Lindsey, J. S.; Bocian, D. F.; Holten, D. *Photochem. Photobiol.* **2007**, *83*, 1125–1143.
- (50) Mass, O.; Ptaszek, M.; Taniguchi, M.; Diers, J. R.; Kee, H. L.; Bocian, D. F.; Holten, D.; Lindsey, J. S. *J. Org. Chem.* **2009**, *74*, 5276–5289.
- (51) (a) Linnanto, J.; Korppi-Tommola, J. *Phys. Chem. Chem. Phys.* **2006**, *8*, 663–687. (b) Petit, L.; Quartarolo, A.; Adamo, C.; Russo, N. *J. Phys. Chem. B* **2006**, *110*, 2398–2404.
- (52) (a) Petke, J. D.; Maggiora, G. M.; Shipman, L. L.; Christoffersen, R. E. *Photochem. Photobiol.* **1980**, *32*, 399–414. (b) Weiss, C. Jr. *J. Mol. Spectroscopy* **1972**, *44*, 37–80.
- (53) Yang, S. I.; Seth, J.; Strachan, J.-P.; Gentemann, S.; Kim, D.; Holten, D.; Lindsey, J. S.; Bocian, D. F. *J. Porphyrins Phthalocyanines* **1999**, *3*, 117–147.
- (54) Kikuchi, K.; Kurabayashi, Y.; Kokubun, H.; Kaizu, Y.; Kobayashi, H. *J. Photochem. Photobiol. A: Chem.* **1988**, *45*, 261–263.
- (55) Kajii, Y.; Obi, K.; Tanaka, I.; Tobita, S. *Chem. Phys. Lett.* **1984**, *111*, 347–349.
- (56) Bonnett, R.; McGarvey, D. J.; Harriman, A.; Land, E. J.; Truscott, T. G.; Winfield, U.-J. *Photochem. Photobiol.* **1988**, *48*, 271–276.

Chapter 4

Synthesis and Photophysical Characterization of Stable Indium Bacteriochlorins

Reproduced in part with permission from Krayner, M; Yang, EK; Kim, HJ ; Kee, H.L; Deans, R.M.; Sluder, C.E.; Diers, J.R. Kirmaier, C; Bocian, D.F.; Holten, D., and Lindsey, J. S. Synthesis and Photophysical Characterization of Stable Indium Bacteriochlorins. *Inorg. Chem.* 2011, 50, 4607–4618. Doi:10.1021/ic200325d. Copyright 2011 American Chemical Society.

Abstract

Bacteriochlorins have wide potential in photochemistry due to their strong absorption of near-infrared light, yet metallobacteriochlorins traditionally have been accessed with difficulty. Established acid-catalysis conditions [$\text{BF}_3 \cdot \text{OEt}_2$ in CH_3CN or $\text{TMSOTf}/2,6\text{-di-}i\text{-tert-butylpyridine}$ in CH_2Cl_2] for the self-condensation of dihydrodipyrin-acetals (bearing a geminal dimethyl group in the pyrroline ring) afford stable free base bacteriochlorins. Here, InBr_3 in CH_3CN at room temperature was found to give directly the corresponding indium bacteriochlorin. Application of the new acid catalysis conditions has afforded four indium bacteriochlorins bearing aryl, alkyl/ester, or no substituents at the β -pyrrolic positions. The indium bacteriochlorins exhibit (i) a long-wavelength absorption band in the 741–782 nm range, which is shifted bathochromically by 23–31 nm versus the analogous free base species, (ii) fluorescence quantum yields (0.011–0.026) and average singlet lifetime (270 ps), which are diminished by an order of magnitude versus that (0.13–0.25; 4.0 ns) for the free base analogues, and (iii) higher average yield (0.9 versus 0.5) yet shorter average lifetime (30 vs 105 μs) of the lowest triplet excited state compared to the free base compounds. The differences in the excited-state properties of the indium chelates versus free base bacteriochlorins derive primarily from a 30-fold greater rate constant for $S_1 \rightarrow T_1$ intersystem crossing, which stems from the heavy-atom effect on spin-orbit coupling. The trends in optical properties of the indium bacteriochlorins versus free base analogues, and the effects of 5-OMe versus 5-H substituents, correlate well with frontier molecular-orbital energies and energy gaps derived from density functional theory calculations. Collectively the synthesis, photophysical properties, and electronic characteristics of the indium bacteriochlorins and free base analogues reported herein should aid in the further design of such chromophores for diverse applications.

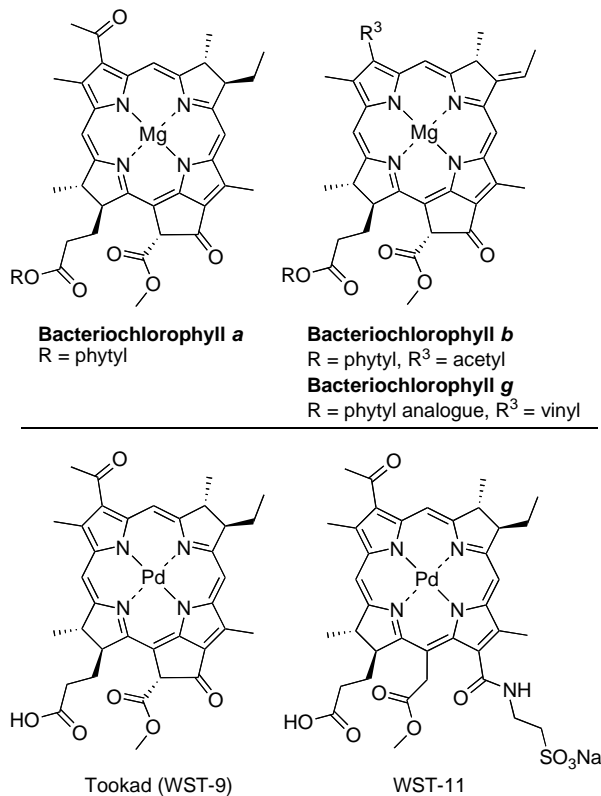
Introduction

Bacteriochlorins are an important class of tetrapyrrolic macrocycles owing to their strong near-infrared absorption band.^{1,2} This feature makes these pigments attractive candidates for a wide variety of applications, including photodynamic therapy (PDT),³⁻¹² optical imaging,^{3,13-19} flow cytometry,^{19,20} and artificial photosynthesis.²¹⁻²³ Naturally occurring bacteriochlorins such as bacteriochlorophylls (Chart 1) provide the basis for bacterial photosynthesis.¹ Palladium-containing bacteriochlorins such as WST-9^{24,25} and WST-11,²⁶ which are derived from bacteriochlorophyll *a* (Chart 1), are particularly interesting for a number of reasons when compared to their free base analogues. First, palladium bacteriochlorins readily undergo intersystem crossing to give higher yields of the triplet excited state. Second, metallobacteriochlorins in general have a bathochromically shifted long-wavelength absorption band.² Near-infrared light absorption and high triplet excited-state yields are valuable for effective photosensitization in PDT. However, the repertoire of metallobacteriochlorins prepared to date is quite limited relative to that of metalloporphyrins and metallochlorins. The dearth stems from limitations in access to and stability of the bacteriochlorin macrocycles, which serve as tetradentate ligands to the metal, as well as limitations in approaches for metalation.

The primary source of bacteriochlorins has stemmed from semisynthesis beginning with the bacterial photosynthetic pigment bacteriochlorophyll *a*.^{8,11} Two significant problems with derivatives of the bacteriochlorophylls include limited stability^{25,27} and poor synthetic malleability owing to the presence of a nearly full complement of substituents about the perimeter of the macrocycle.^{8,11} Nonetheless, macrocycles derived from bacteriochlorophylls have been metalated with a number of divalent metals (Mn^{2+} , Co^{2+} , Ni^{2+} , Cu^{2+} , Zn^{2+} , Pd^{2+} , and Cd^{2+}).² The methods for preparing such metallobacteriochlorins include conversion of the free

base macrocycle to a Cd^{2+} chelate followed by transmetalation,²⁸ magnesiumation of the free base macrocycle with a hindered Grignard reagent,²⁹ or, for selected derivatives, direct treatment with a metal salt.³⁰ The photodynamics of such divalent metallobacteriochlorins have been examined.³¹ On the other hand, fewer metals (Ni^{2+} , Cu^{2+} , Zn^{2+}) have been inserted into wholly synthetic bacteriochlorins. The set of these ligands is also very limited and includes *meso*-tetraaryl bacteriochlorins,³²⁻³⁵ 1,5-dihydroxy-1,5-dimethyloctaethylbacteriochlorin,³⁶ and 3,13-dicyano-8,8,18,18-tetramethylbacteriochlorin.³⁷ The scarcity of synthetic metallobacteriochlorins reflects the dual problems of preparing and metalating the bacteriochlorin ligand.

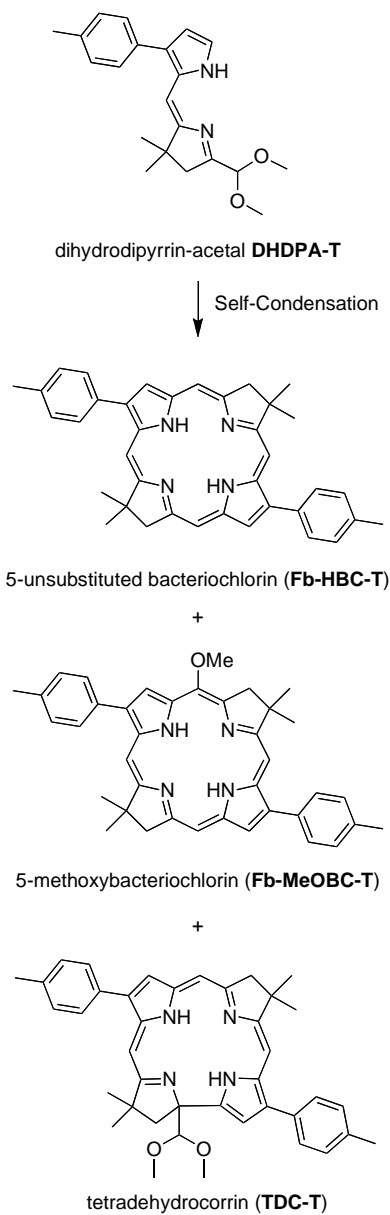
Chart 1.



Recently, we developed a concise route to stable bacteriochlorins that entails self-condensation of a dihydrodipyrin-acetal (Scheme 1).³⁸ Investigation of a wide variety of Lewis acids for the self-condensation revealed two acid conditions that give free base bacteriochlorin formation: $\text{BF}_3 \cdot \text{OEt}_2$ in CH_3CN and $\text{TMSOTf}/2,6\text{-di-}t\text{-butylpyridine}$ (2,6-DTBP) in CH_2Cl_2 .^{38,39} Use of $\text{BF}_3 \cdot \text{OEt}_2$ in CH_3CN for the *p*-tolyl-substituted dihydrodipyrin-acetal (**DHDPA-T**) results in a mixture of a free base 5-unsubstituted bacteriochlorin (**Fb-HBC-T**), a free base 5-methoxybacteriochlorin (**Fb-MeOBC-T**), and a free base B,D-tetradehydrocorrins (**TDC-T**), with **Fb-HBC-T** being the predominant macrocycle at the optimized conditions.³⁸ Use of $\text{TMSOTf}/2,6\text{-DTBP}$ in CH_2Cl_2 exclusively gives **Fb-MeOBC-T**.^{39,40} Other acids investigated resulted either in lower yields of free base bacteriochlorins, preferential formation of **TDC-T**, or gave no macrocycle. One exception was InCl_3 in CH_3CN , which resulted in an indium bacteriochlorin (**In-MeOBC-T**) along with free base **Fb-MeOBC-T** and **TDC-T**.

To our knowledge, no indium bacteriochlorins have been reported. An indium isobacteriochlorin has been reported by Buchler et al.⁴¹ Indium chlorins derived from natural chlorophylls have been extensively used in photodynamic therapy studies due to their high yield of excited triplet state.⁴² The reported indium chlorins result from metalation of the corresponding free base chlorin. Indium porphyrins have also been used for PDT as well as photophysical applications,⁴³⁻⁴⁵ yet also are derived from the free base analogues (except an indium ABCD-porphyrin, which was synthesized via a bilane⁴⁶). In addition to the expected bathochromic shift of the long-wavelength absorption band and the high yield of triplet state, the presence of a tricationic metal chelate introduces a polar site at the core of the macrocycle, providing a more hydrophilic bacteriochlorin, which may be attractive for a number of photobiological studies.

Scheme 1.



Herein, we report the results of an investigation of InX_3 -mediated catalysis of the conversion of dihydrodipyrin-acetals to the corresponding metallochlorins. The paper is

divided into three parts. Part 1 concerns the identification, optimization and scope of application of the reaction conditions for the in situ formation of indium bacteriochlorins. Part 2 provides a comprehensive study of the spectral (absorption, fluorescence) and photophysical properties of the indium bacteriochlorins. Finally, part 3 correlates the molecular orbital characteristics (energies and electron density distributions) and the photophysical properties of the bacteriochlorin owing to the metalation state (indium versus free base) and substituents at the perimeter of the macrocycle.

Experimental methods

Synthesis and general procedures

Experimental methods are described in detail in elsewhere.^A

Photophysical measurements

Static and time-resolved photophysical measurements were performed as described previously.⁴⁴ Measurement of the fluorescence (Φ_f) and triplet-excited-state (Φ_{isc}) quantum yields and singlet (τ_S) and triplet (τ_T) lifetimes utilized, unless noted otherwise, utilized dilute (μM) Ar-purged toluene solutions at room temperature. Samples for Φ_f measurements had an absorbance <0.12 at the excitation wavelength. The Φ_f values were generally determined with respect to two standards and the results averaged. The standards were (1) free base *meso*-tetraphenylporphyrin (**FbTPP**) in nondegassed toluene, for which $\Phi_f = 0.070$ was established with respect to the zinc chelate **ZnTPP** in nondegassed toluene ($\Phi_f = 0.030$),⁵⁹ consistent with prior results on **FbTPP**,⁶⁰ and (2) 8,8,18,18-tetramethylbacteriochlorin²² in Ar-purged toluene,

for which $\Phi_f = 0.14$ was established with respect to **FbTTP** and chlorophyll *a* (**Chl a**) in deoxygenated benzene⁶¹ or toluene⁶² ($\Phi_f = 0.325$).

The τ_S value for each indium bacteriochlorin was first probed using a time-correlated single photon counting (TCSPC) instrument that employed Soret excitation flashes derived from a nitrogen-pumped dye laser (PTI LaserStrobe) and a Gaussian instrument response function of 0.6 ns. These measurements indicated that the τ_S values were within the instrument response and likely in the range 0.2–0.4 ns. The lifetimes were then determined using ultrafast pump-probe absorption spectroscopy employing 130 fs excitation pulses in the Q_y band and probing from 440–660 nm. Global analysis of the data set yielded the reported values. The τ_S values for the free base bacteriochlorins were determined using the above-mentioned TCSPC apparatus as well as a fluorescence modulation technique (Spex Tau2);⁶³ the results from the two techniques were generally averaged.

The Φ_{isc} values were obtained using a transient-absorption technique in which the extent of bleaching of the ground-state $Q(1,0)$ band due to the lowest singlet excited state was measured immediately following a 130 fs flash in the $Q_x(0,0)$ or $Q_y(0,0)$ bands and compared with that due to the lowest triplet excited state at the asymptote of the singlet excited-state decay.⁴⁴ For the free base bacteriochlorins, the bleaching signals are referenced to a relatively featureless transient absorption, which are not substantially different for the S_1 and S_0 excited states. In the case of the indium chelates, the spectra are more featured and show larger differences between the two states. Thus, Gaussian fitting of the spectra (as well as more routine linear interpolation of the excited-state absorption across the ground-state bleaching region) was utilized to

encompass a reasonable range of spectral shapes; an average value of the triplet yields obtained by these methods is reported for each bacteriochlorin.

Density Functional Theory calculations

DFT calculations were performed with Spartan '08 for Windows version 1.2.0 in parallel mode⁶⁴ on a PC equipped with an Intel i7-975 cpu, 24 GB ram, and three 300 GB, 10 k rpm hard drives. The hybrid B3LYP functional and the LACVP basis set were employed. The equilibrium geometries were fully optimized using the default parameters of the Spartan '08 program.

Results and Discussion

Chart 2

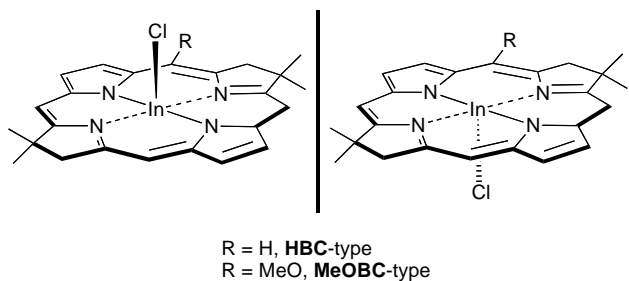


Chart 3

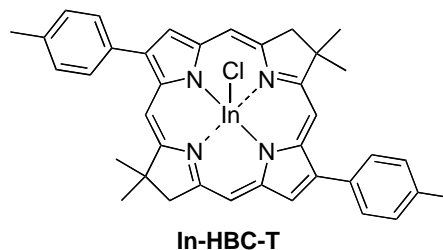
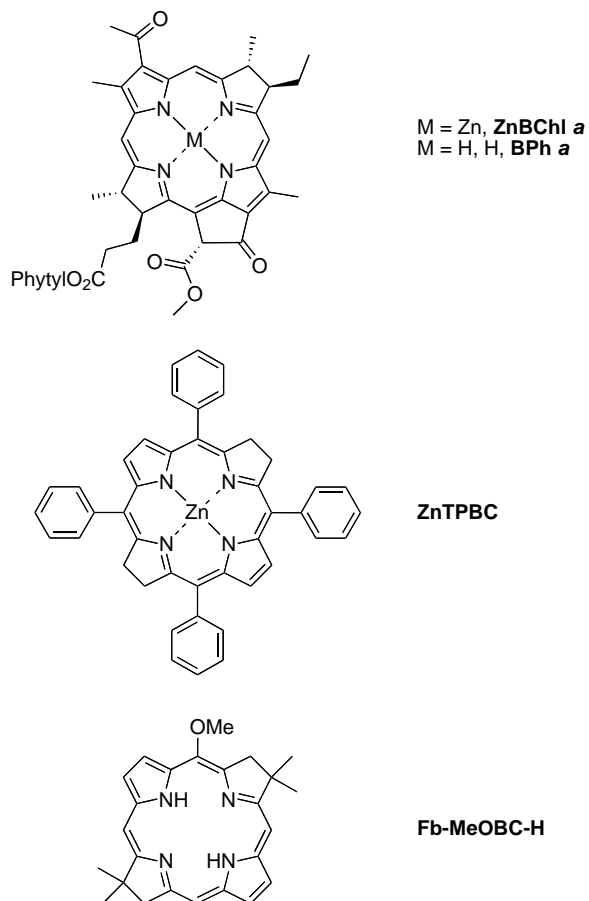


Chart 4



In situ synthesis of indium bacteriochlorins

The synthesis and structure characterization of all the compounds investigated in this study are described in detail in elsewhere.^A The structures of compounds are shown in Chart 2-4.

Spectral and Photophysical

Absorption spectra

The ground state electronic absorption spectra of the four indium bacteriochlorins **In-MeOBC-H**, **In-MeOBC-T**, **In-MeOBC-MeEs**, and **In-HBC-MeEs** in toluene are shown in Figure 1 (solid lines). The spectral data for these four indium bacteriochlorins, and for **In-HBC-**

T (Chart 3; Fan, D.; Lindsey, J. S. unpublished data), are listed in Table 1. For comparison, Table 2 also lists spectral data for the base analogues **Fb-MeOBC-H** (Chart 4); **Fb-MeOBC-T** (Scheme 1); **Fb-MeOBC-MeEs** and **Fb-HBC-MeEs** and **Fb-HBC-T** (Scheme 1).^{38,39} The table also includes spectral data for two literature reference compounds, zinc *meso*-tetraphenylbacteriochlorin (**ZnTPBC**)^{33,35} and zinc bacteriochlorophyll *a* (**ZnBChl a**),²⁸ as well as the two naturally occurring pigments, bacteriochlorophyll *a* (**BChl a**)¹ and bacteriopheophytin *a* (**BPh a**)¹ (Charts 1 and 4).

The absorption spectrum of each bacteriochlorin contains four main features with maxima generally in the following spectral ranges: B_y(0,0) (350–360 nm), B_x(0,0) (365–395 nm), Q_x(0,0) (495–570 nm), and Q_y(0,0) (700–800 nm). Each of these four origin transitions has a weaker (1,0) vibronic satellite feature roughly 1250 cm⁻¹ to higher energy. [Note that the B_x and B_y transitions may have mixed x and y polarization and for some compounds are spectrally overlapped.] The absorption spectrum of **In-MeOBC-T** (355, 388, 553, 760 nm) in toluene is quite similar to that of **ZnTPBC** (350, 385, 540, and 760 nm)³⁵ in CH₂Cl₂, and of **ZnBChl a** (353, 389, 558, and 762 nm)²⁸ in diethyl ether (Table 1).

The Q_y(0,0) transition is of particular interest because it corresponds to absorption of light to produce the lowest singlet excited state, which dominates much of the photophysical behavior. The Q_y(0,0) band for the five indium bacteriochlorins is positioned on the average 27 nm (22–32 nm) to longer wavelength than those for the free base analogues. Similarly, the Q_x(0,0) band for the indium chelates lies on the average 43 nm (39–51 nm) to longer wavelength than those for the free base compounds. The average value of the full-width-at-half-maximum

(FWHM) of the $Q_y(0,0)$ absorption band of the indium bacteriochlorins is 21 nm, which is only slightly greater than the value of 17 nm for the free base analogues.

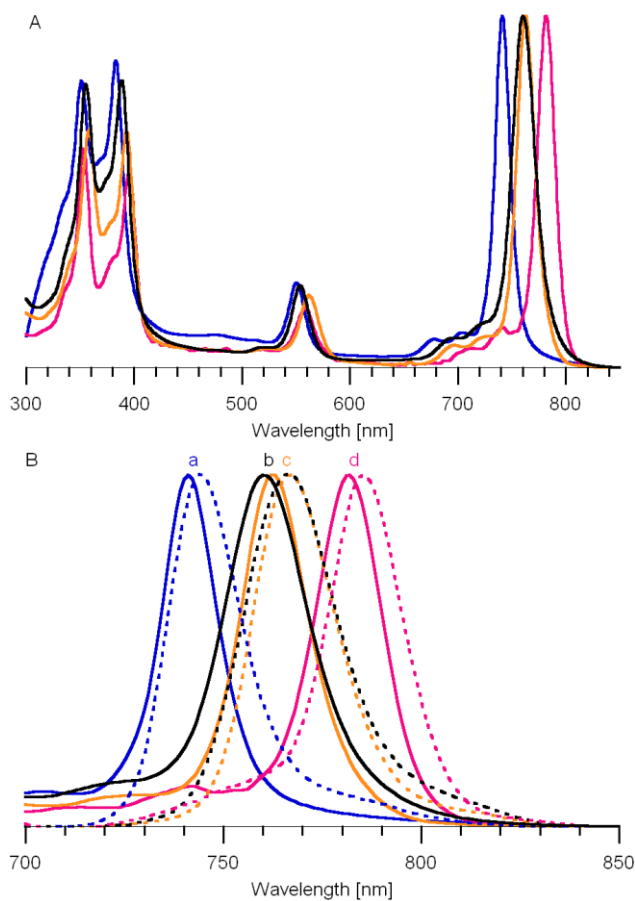


Figure 1. Spectra in toluene at room temperature of indium bacteriochlorins (normalized at the Q_y bands). (A) Absorption spectra. (B) Magnification of Q_y region showing absorption (— solid lines) and emission (--- dashed lines) spectra. The labels and the colors are as follows: **In-MeOBC-H** (a, blue), **In-MeOBC-T** (b, black), **In-MeOBC-MeEs** (c, orange), **In-HBC-MeEs** (d, magenta).

Table 1. Spectral Characteristics of Indium, Free Base, and Reference Bacteriochlorins.^a

Compound	B _y (0,0) ^b abs (nm)	B _x (0,0) ^b abs (nm)	Q _x (0,0) abs (nm)	Q _y (0,0) ^c abs (nm)	Q _y ^d abs FWHM (nm)	Q _y (0,0) ^e em (nm)	Q _y ^f em FWHM (nm)	ΔQ _y ^g abs-em (cm ⁻¹)	I _{Q_y} /I _B ^h	ΣQ _y /ΣB ⁱ
<i>Indium Bacteriochlorins</i>										
In-MeOBC-H	352	384	552	741 [+32]	19	747	24	108	1.1	0.13
In-MeOBC-T	355	388	553	760 [+29]	23	767	30	120	0.91	0.14
In-HBC-T	350	388	539	763 [+27]	23	769	31	102	1.1	0.15
In-MeOBC-	358	393	563	762 [+24]	20	768	27	103	1.6	0.23
In-HBC-MeEs	354	395	559	782 [+22]	21	785	23	49	1.3	0.17
<i>Free Base Bacteriochlorins</i>										
Fb-MeOBC-H	354	367	501	709	11	711	18	40	0.87	0.11
Fb-MeOBC-T	356	380	511	731	20	736	23	93	0.89	0.14
Fb-HBC-T	351	374	499	736	20	742	23	110	1.0	0.14
Fb-MeOBC-	357	398	520	738	18	741	21	217	0.96	0.13
Fb-HBC-MeEs	354	384	520	760	18	764	20	69	0.98	0.19
<i>Reference Bacteriochlorins</i>										
ZnTPBC ^j	350	385	540	760						
ZnBChl a ^k	353	389	558	762						
BChl a ^l	363	396	581	781	32	789	29	130	1.39	0.23
BPh a	362	389	532	758	31	768	27	172	0.69	0.15

^aObtained in toluene at room temperature. ^bThe two Soret features are labeled B_x(0,0) and B_y(0,0) but the bands may be of mixed parentage. ^cPosition (nm) of the Q_y(0,0) absorption band. The value in brackets is the difference in wavelength of the Q_y(0,0) band of the indium bacteriochlorin versus the free base analogue. ^dFull-width-at-half-maximum (FWHM in nm) of the Q_y(0,0) absorption band. ^ePosition (nm) of the Q_y(0,0) fluorescence emission band. ^fFWHM of the Q_y(0,0) fluorescence band. ^gDifference in energy (cm⁻¹) between the peak positions of the Q_y(0,0) absorption and fluorescence bands. ^hRatio of the peak intensities of the Q_y(0,0) band to the Soret (B) maximum, which could be either B_x(0,0) or B_y(0,0). ⁱRatio of the integrated intensities of the Q_y manifold [Q_y(0,0), Q_y(1,0)] to the Soret manifold [B_y(0,0), B_y(1,0), B_x(0,0), B_x(1,0)], for spectra plotted in cm⁻¹. ^jReference 35 in CH₂Cl₂. ^kReference 28 in diethyl ether. ^lIn benzene.

Fluorescence spectra

The fluorescence emission spectra of the four indium bacteriochlorins **In-MeOBC-H**, **In-MeOBC-T**, **In-MeOBC-MeEs**, and **In-HBC-MeEs** in toluene are shown in Figure 1 (dashed lines). The emission spectral characteristics for these four compounds, **In-HBC-T**, the free base analogues, and several synthetic reference and naturally occurring bacteriochlorins are listed in Table 1. The fluorescence spectrum of each bacteriochlorin is dominated by the $Q_y(0,0)$ band. The spectra shown in Figure 1 reveal very weak features ~25 nm to shorter wavelength than the $Q_y(0,0)$ fluorescence band of the indium bacteriochlorins. These weak, higher-energy features are at the positions expected for the free base analogues. Weak emission from the free base is visible even with this material is present in trace amounts because the free base bacteriochlorin has a fluorescence quantum yield roughly an order of magnitude greater than that for the indium chelate (see below).

The $Q_y(0,0)$ fluorescence maximum of the indium bacteriochlorins lies on the average 6 nm to longer wavelength (96 cm^{-1} to lower energy) than the $Q_y(0,0)$ absorption maximum (Table 1). A similar small “Stokes” shift is generally observed for the free base bacteriochlorins (except for **Fb-MeOBC-MeEs**). The average bandwidth (FWHM) of the $Q_y(0,0)$ fluorescence feature of the indium bacteriochlorins is 27 nm, which is about 25% larger than the value of 21 nm observed for the $Q_y(0,0)$ absorption band. The $Q_y(0,0)$ emission feature of the free base analogs is similarly larger than that of the absorption band (21 versus 17 nm).

Fluorescence quantum yields

The fluorescence quantum yields (Φ_f) of the five indium bacteriochlorins are in the range 0.011–0.026 with an average value of 0.018. The Φ_f values for the free base species are in the

range 0.13–0.25 with an average of 0.19. Thus, the fluorescence yields for the indium bacteriochlorins are on the average 10-fold lower than those for the free base analogues (Table 2).

The data can be compared with those of **Bchl a** and **Bph a**.^{50,51}

Singlet excited-state lifetimes

The lifetime of the lowest singlet excited state (τ_S) of each indium bacteriochlorin was determined using ultrafast transient absorption spectroscopy and found to be in the range 210–330 ps with an average value of 270 ps (Table 2). The τ_S values for the free base bacteriochlorins were measured using time-resolved fluorescence spectroscopy and found to be in the range 3.0–5.0 ns with an average value of 4.0 ns (Table 2). Thus, the singlet excited-state lifetimes of the indium bacteriochlorins are about 20-fold shorter than those for the free base analogues.

Triplet excited-state lifetimes

The lifetime of the lowest triplet excited state (τ_T) of each indium and free base bacteriochlorin was measured at room temperature using transient absorption spectroscopy. The τ_T values for the indium bacteriochlorins were found to be in the range 25–44 μ s with an average value of 30 μ s. The triplet excited-state lifetime for each indium chelate is shorter than that for the free base bacteriochlorin, which were found to be in the range 64–163 μ s with an average value of 105 μ s (Table 2).

Triplet excited-state quantum yields

The quantum yield of intersystem crossing from the lowest singlet excited state to the lowest triplet excited state (Φ_{isc}), also known as the triplet yield, was determined using transient

absorption spectroscopy.⁴⁴ The Φ_{isc} values for the indium chelates were found to be 0.9 ± 0.1 . These values are considerably greater than those for the free base analogues, which were found to lie in the range 0.42–0.55 (± 0.08) with an average value of 0.51.

Table 2. Photophysical and Molecular Orbital Properties of Indium, Free Base, and Reference Bacteriochlorins.^a

Compound	Q _y (0,0) ^b energy (eV)	τ _s ^c (ns)	Φ _f ^d	Φ _{isc} ^e	τ _T ^f (μs)	HOMO (eV)	LUMO (eV)	LUMO – HOMO (eV)
<i>Indium Bacteriochlorins</i>								
In-MeOBC-H	1.67	0.33	0.011	0.9	40	-4.62	-2.56	2.06
In-MeOBC-T	1.63	0.26	0.020	0.9	32	-4.54	-2.53	2.01
In-HBC-T	1.62	0.21	0.016	0.9	44	-4.52	-2.52	2.00
In-MeOBC-MeEs	1.63	0.32	0.026	0.9	25	-4.84	-2.85	1.99
In-HBC-MeEs	1.59	0.25	0.015	0.9	30	-4.74	-2.82	1.92
In -BC average	1.63	0.27	0.018	0.9	30	-4.65	-2.66	2.00
<i>Free Base Bacteriochlorins</i>								
Fb-MeOBC-H	1.75	5.0	0.25	0.55	107	-4.48	-2.20	2.28
Fb-MeOBC-T	1.70	4.5	0.20	0.42	107	-4.42	-2.23	2.19
Fb-HBC-T	1.68	3.3	0.18	0.55	163	-4.40	-2.22	2.18
Fb-MeOBC-MeEs	1.68	4.4	0.17	0.53	85	-4.61	-2.45	2.16
Fb-HBC-MeEs	1.69	3.0	0.13	0.52	64	-4.67	-2.57	2.10
Fb-BC average	1.69	4.0	0.19	0.51	105	-4.52	-2.34	2.18
<i>Reference Bacteriochlorins</i>								
BChl a^g	1.59	3.1	0.12	0.33	52	-4.75	-2.86	1.89
BPh a^h	1.64	2.7	0.10	0.54	25	-4.87	-2.84	2.03

^aObtained in toluene at room temperature unless noted otherwise. The molecular orbital energies were obtained from DFT calculations. ^bEnergy of the Q_y(0,0) absorption band (see Table 2). ^cLifetime of the lowest singlet excited state measured via transient absorption spectroscopy for indium bacteriochlorins (±20 ps) and by fluorescence techniques for the free base bacteriochlorins (±5%). ^dFluorescence quantum yield ±15% for the indium bacteriochlorins and ±5% for the free base bacteriochlorins. ^eYield of the lowest triplet excited state measured via transient absorption spectroscopy (±0.1 for indium bacteriochlorins and ±0.08 for the free base bacteriochlorins). ^fLifetime of the lowest triplet excited state measured via transient absorption spectroscopy for compounds in Ar-purged 2-methyltetrahydrofuran (±10%). ^gThe absorption and emission spectral properties, Φ_f, and τ_s were acquired here in benzene and τ_T in pyridine. The value of Φ_T = 0.32 was measured in toluene. Values of 0.44 and 0.41 were measured in acetonitrile and pyridine, respectively. Values of Φ_T = 0.32 and τ_T ~ 60 μs (mixed first and second order decay) have been reported and are the average of values measured in acetonitrile, dimethylsulfoxide and pyridine.⁵⁰ ^hThe values found here in ethanol are Φ_f = 0.081, τ_s = 2.3 ns, and τ_T = 30 μs. The values in acetone/methanol (7:3) are τ_s = 2.0 ns, τ_S = 16 μs, and Φ_{isc} = 0.57 (average of 0.54 and 0.60 from two methods).⁵¹

Excited-state decay pathways and rate constants

The observables τ_S , Φ_f , and Φ_{isc} (Table 2) for decay of the lowest-energy singlet excited state (S_1) are connected to the rate constants for $S_1 \rightarrow S_0$ spontaneous fluorescence (k_f), $S_1 \rightarrow S_0$ internal conversion (k_{ic}), and $S_1 \rightarrow T_1$ intersystem crossing (k_{isc}) via Eqs. (1) to (3).

$$\tau_S = (k_f + k_{ic} + k_{isc})^{-1} \quad (1)$$

$$\Phi_f = k_f / (k_f + k_{ic} + k_{isc}) \quad (2)$$

$$\Phi_{isc} = k_{isc} / (k_f + k_{ic} + k_{isc}) \quad (3)$$

The internal conversion yield can be calculated from Eq. (4).

$$\Phi_{ic} = 1 - \Phi_f - \Phi_{isc} \quad (4)$$

The radiative, intersystem-crossing, and internal-conversion rate constants can be calculated from the above quantities via Eq. (5), where $i = f, isc$ or ic .

$$k_i = \Phi_i / \tau_S \quad (5)$$

The average radiative rate constant of $k_f = (17 \text{ ns})^{-1}$ for the indium bacteriochlorins is slightly greater than that of $(22 \text{ ns})^{-1}$ for the free base analogue, indicating a comparable or slightly higher fluorescence probability. Nevertheless, the average fluorescence yield is about 10-fold smaller for indium versus free base bacteriochlorins (0.018 versus 0.19) because of enhanced rate constants for the two nonradiative processes (internal conversion and intersystem crossing) in the indium chelates, as described below.

The average yields of $S_1 \rightarrow T_1$ intersystem crossing of 0.9 for indium bacteriochlorins and 0.51 ns for the free base analogues, together with the average S_1 lifetimes of 0.27 ns and 4.0 ns, respectively, translate via Eq. 5 into average intersystem-crossing rate constant of $k_{isc} = (0.3 \text{ ns})^{-1}$ for the indium bacteriochlorins being roughly 25-fold greater than that of $(8 \text{ ns})^{-1}$

for the free base analogues. This substantial difference in rates lie well outside the error limits largely associated with the determination of the individual intersystem-crossing yields. The enhancement in k_{isc} for indium versus free base bacteriochlorins almost certainly derives from the effect of the heavy indium ion on spin-orbit coupling, which drives the spin flips underlying the intersystem-crossing process.

The yields of $S_1 \rightarrow S_0$ internal conversion calculated via Eq. 4 for the five indium bacteriochlorins (0.09, 0.08, 0.08, 0.07, 0.09) have an average value of $\Phi_{ic} = 0.08$ that is about 25% of that of $\Phi_{ic} = 0.3$ derived from the individual values for the five free base bacteriochlorins (0.2, 0.4, 0.3, 0.3, 0.4). These average yields give rise to a typical rate constant of $k_{ic} = (3 \text{ ns})^{-1}$ for the indium bacteriochlorins and $(14 \text{ ns})^{-1}$ for the free base analogues. A somewhat greater k_{isc} for indium versus free base bacteriochlorins can be rationalized for two reasons. First, on the basis of the energy-law for nonradiative decay,⁵² k_{ic} is expected to be somewhat greater for the indium versus free base bacteriochlorins because the average energy of the S_1 excited state of the indium bacteriochlorins (13086 cm^{-1} , 1.62 eV) is lower than that for the free base analogues (13543 cm^{-1} , 1.68 eV) (Table 2). Second, greater k_{ic} values for indium versus free base bacteriochlorins also may result from an improved Franck-Condon factor derived from nuclear-coordinate displacements involving the central In^{3+} ion, the apical counterion, and solvent interactions in the S_1 versus S_0 states. Such coordinate displacements should be enhanced because the In^{3+} ion and the apical counterion are displaced toward one side of the bacteriochlorin framework, which itself should be distorted from planarity. Nonplanar macrocycle distortions in tetrapyrrole complexes are thought to open up additional channels for conformational excursions (particularly in the excited state), which enhance internal conversion.⁵³

Correlation of photophysical and molecular orbital characteristics

Molecular orbitals

To gain insights into the trends in the photophysical properties of the bacteriochlorins as a function of molecular characteristics, density functional theory (DFT) calculations were performed. These calculations provide the energies and electron-density distributions of the frontier molecular orbitals. The principal orbitals of interest are the highest occupied molecular orbital (HOMO), the lowest unoccupied molecular orbital (LUMO), and the HOMO-1 and LUMO+1. Table 3 gives electron density plots (and energies) for these four orbitals for two representative indium bacteriochlorins (**In-HBC-T** and **In-MeOBC-T**) and the free base analogues (**Fb-HBC-T** and **Fb-MeOBC-T**).

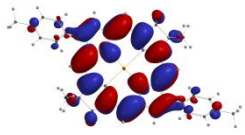
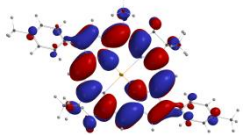
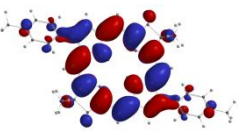
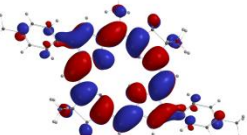
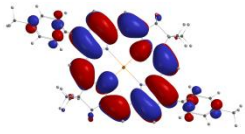
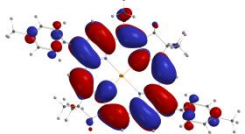
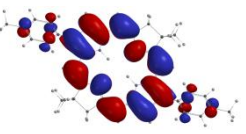
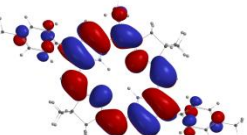
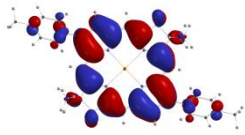
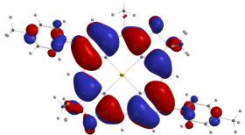
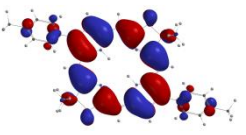
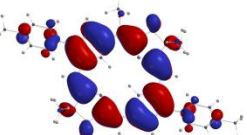
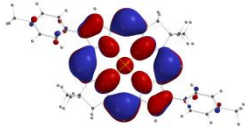
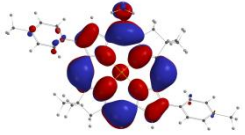
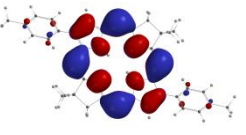
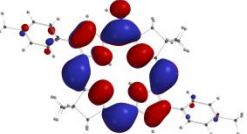
Attention is focused on the HOMO and LUMO, for which the individual energies and energy gap are listed in Table 2. In the following subsections, these orbital characteristics are correlated with (B) the wavelength (energy) of the $Q_y(0,0)$ absorption band of the indium and free base bacteriochlorins, (C) the wavelength (energy) of the $Q_y(0,0)$ absorption band of bacteriochlorins containing a 5-OMe versus 5-H substituent, (D) the effects of a 5-OMe versus 5-H substituent on the various photophysical properties of the bacteriochlorins, and (E) the anticipated redox properties of the molecules.

Absorption spectra of indium versus Free Base bacteriochlorin

The one-electron configuration resulting from light-induced promotion of an electron from the HOMO to the LUMO normally makes a significant contribution to the electronic characteristics of the lowest singlet excited state of most molecules. Thus, for a series of related tetrapyrroles, the LUMO – HOMO energy gap may be expected to reasonably track the energy

of the $S_0 \rightarrow S_1$ electronic transition, namely the $Q_y(0,0)$ band. This behavior is expected for bacteriochlorins because the wavefunction of the S_1 excited state is expected to be comprised of roughly 75% of the HOMO \rightarrow LUMO one-electron configuration, with the remainder due to the HOMO-1 \rightarrow LUMO+1 configuration.⁵⁴⁻⁵⁶ For example, time-dependent DFT calculations on **Fb-MeOBC-H** give percentages of 71% and 28%, respectively.

Table 3. Molecular-Orbital Characteristics of Indium and Free Base Bacteriochlorins.^a

Molecule	In-HBC-T	In-MeOBC-T	Fb-HBC-T	Fb-MeOBC-T
LUMO+1	 -1.07	 -1.07	 -0.96	 -0.96
LUMO	 -2.52	 -2.53	 -2.22	 -2.23
HOMO	 -4.52	 -4.54	 -4.40	 -4.42
HOMO-1	 -5.26	 -5.18	 -4.95	 -4.88

^aObtained from DFT calculations.

Figure 2 plots the LUMO – HOMO energy versus the energy (and wavelength) of the $Q_y(0,0)$ band for the indium bacteriochlorins and free base analogues. Both sets of molecules show good correlations, with similar slopes of the trend lines. It is expected that the trend lines for the indium and free base bacteriochlorins would be displaced along the transition-energy (horizontal) axis because the $Q_y(0,0)$ band for each indium bacteriochlorin is bathochromically shifted from the position for the free base species (Table 1). The displacement between the two sets of data and trend lines along the HOMO – LUMO (vertical) axis can be related to several factors derived from the formation of the indium(III) chelate from the free base analogue. These differential effects include (1) the positions of greater electron density from the metal ion (Table 2) and (2) structural changes in the macrocycle, including a distortion from planarity.

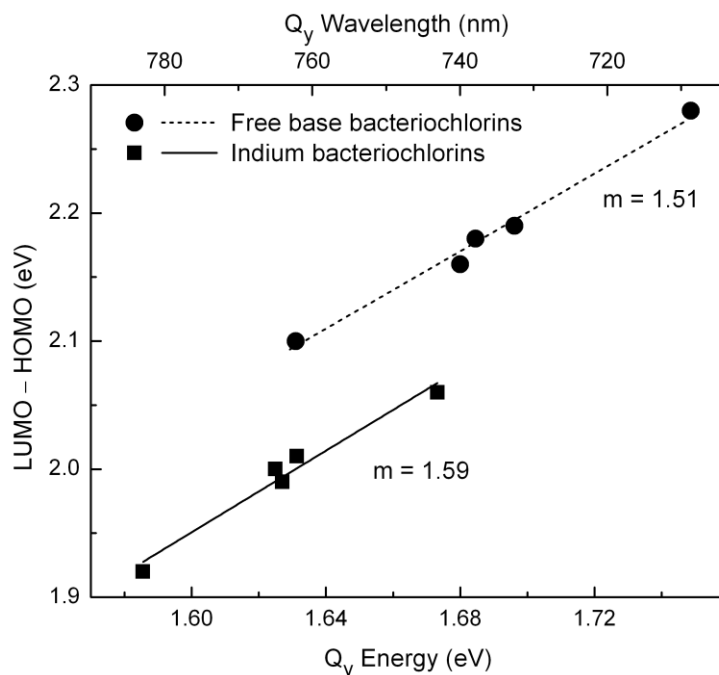


Figure 2. LUMO – HOMO energy gap versus the energy (and wavelength) of the $Q_y(0,0)$ absorption band for indium bacteriochlorins (squares and solid line) and free base bacteriochlorins (circles and dashed line). The slopes (m) of the trend lines are shown.

As noted above, the $Q_y(0,0)$ bands of the indium bacteriochlorins are positioned on the average 27 nm (0.06 eV) to longer wavelength (lower energy) than those of the free base species. The indium bacteriochlorins have an average HOMO energy 0.014 eV more negative than the free base form (-4.65 vs -4.52 eV) and an average LUMO energy 0.032 eV more negative than the free base form (-2.66 vs -2.34 eV) resulting in a smaller LUMO – HOMO energy gap (2.00 vs 2.18 eV). These comparisons show that the smaller LUMO – HOMO gap and thus, the bathochromic shift in the Q_y band, derive from a more substantial metal-derived effect on the LUMO than the HOMO.

Effects of a 5-OMe group on absorption spectra

The MO energies from the DFT calculations also track the effects of the 5-OMe versus 5-H substituent on the electronic spectra of various bacteriochlorins. For each pair of bacteriochlorins, the 5-OMe group results in a shift of the $Q_y(0,0)$ band to higher energy (shorter wavelength). The pairwise comparisons for the 5-MeO versus 5-H bacteriochlorins (Q_y energy shift, LUMO – HOMO energy-gap shift) are as follows: **In-MeOBC-T** versus **In-HBC-T** (0.01 eV, 0.01 eV); **Fb-MeOBC-T** versus **Fb-HBC-T** (0.02 eV, 0.01 eV); **In-MeOBC-MeEs** versus **In-HBC-MeEs** (0.04 eV, 0.07 eV); **Fb-MeOBC-T** versus **Fb-HBC-T** (0.05 eV, 0.06 eV). Thus, the calculations reproduce the small (0.01–0.02 eV; 3–5 nm) effect of the methoxy group for indium and free base bacteriochlorins containing 2,12-di-*p*-tolyl groups, and the larger (0.04–0.05 eV; 10–13 nm) effect of the methoxy group for indium and free base bacteriochlorins containing 2,12-dimethyl and 3,13-diester groups. Close examination of the HOMO and LUMO energies indicates that the greater effect on the -MeEs versus -T complexes is associated with a greater effect of the 5-OMe group on the HOMO than the LUMO for the indium chelates and the opposite effect for the free base compounds. We have previously noted such interplay between

the 5-OMe substituent and the influence of the 2,3,12,13-substituents on the MO energies and spectral characteristics of the bacteriochlorins.⁵⁷

Predictions of redox properties of indium bacteriochlorins

A prior study of two dozen zinc chlorins showed a good correlation between the measured oxidation potential and the HOMO energy, and also between the measured reduction potential and the LUMO energy.⁵⁸ It would be difficult to use those correlations to predict the exact change in redox potentials from the changes in orbital energies, but the trends should be reliable (*i.e.*, whether a given compound in a set will be easier to oxidize or harder to reduce than another). On the basis of such considerations, the data in Table 3 suggest the following. The average HOMO energy of -4.65 eV for the indium bacteriochlorins compared to -4.52 eV for the free base analogues indicates that the indium chelates will be harder to oxidize. Similarly, the average LUMO energy of -2.66 eV for the indium bacteriochlorins versus -2.34 eV for the free base analogues indicates that the indium chelates will be easier to reduce. Such predictions are valuable in potential applications of the bacteriochlorins where redox processes are desired (or to be avoided). For example, the relative redox properties are important in the mechanisms (Type I versus II) for forming reactive oxygen species in photodynamic therapy, as has been shown for free base bacteriochlorins⁴⁻⁶ and for various metalloporphyrin species including indium chelates.^{43,44} Collectively, comparisons and correlations such as those given above between the molecular orbital characteristics, substituent and metal effects, optical properties, and redox potentials facilitates the design of bacteriochlorins for diverse applications.

Acknowledgment

This work was supported by grants from the Division of Chemical Sciences, Geosciences and Biosciences Division, Office of Basic Energy Sciences of the U.S. Department of Energy to D.F.B. (DE-FG02-05ER15660), D.H. (DE-FG02-05ER15661) and J.S.L. (DE-FG02-

96ER14632). RMD and CES were supported by summer fellowships from the JimmyV Cancer Therapeutics Training Program at North Carolina State University. Mass spectra were obtained at the Mass Spectrometry Laboratory for Biotechnology at North Carolina State University. Partial funding for the Facility was obtained from the North Carolina Biotechnology Center and the National Science Foundation.

Supporting Information Available

Investigation of alternative reaction conditions for the formation of indium bacteriochlorins; identification of refined conditions for reaction of a dihydrodipyrin-acetal in the presence of TMSOTf and 2,6-DTBP; and further experimental procedures.^A The link can be found in the publication reference (A).

References

- (A) M. Kraymer, M.; Yang, E. K.; Kim, H. J.; Kee, H. L.; Deans, R. M.; Sluder, C. E.; Diers, J. R.; Kirmaier, C.; Bocian, D. F.; Holten, D., and Lindsey, J. S. *Inorg. Chem.* 2011, 50, 4607–4618
- (1) Scheer, H. In *Chlorophylls and Bacteriochlorophylls. Biochemistry, Biophysics, Functions and Applications*; Grimm, B.; Porra, R. J.; Rüdiger, W.; Scheer, H., Eds., Advances in Photosynthesis and Respiration, 2006, Vol. 25; Springer, Dordrecht, The Netherlands, pp 1–26.
- (2) Kobayashi, M.; Akiyama, M.; Kano, H.; Kise, H. In *Chlorophylls and Bacteriochlorophylls: Biochemistry, Biophysics, Functions and Applications*; Grimm, B.; Porra, R. J.; Rüdiger, W.; Scheer, H., Eds.; Springer: Dordrecht, The Netherlands, 2006, pp 79–94.
- (3) Ethirajan, M.; Chen, Y.; Joshi, P.; Pandey, R. K. *Chem. Soc. Rev.* **2011**, 40, 340–362.
- (4) Mroz, P.; Huang, Y.-Y.; Szokalska, A.; Zhiyentayev, T.; Janjua, S.; Nifli, A.-P.; Sherwood, M. E.; Ruzié, C.; Borbas, K. E.; Fan, D.; Kraymer, M.; Balasubramanian, T.; Yang, E.; Kee, H. L.; Kirmaier, C.; Diers, J. R.; Bocian, D. F.; Holten, D.; Lindsey, J. S.; Hamblin, M. R. *FASEB J.* **2010**, 24, 3160–3170.
- (5) Huang, Y.-Y.; Mroz, P.; Zhiyentayev, T.; Sharma, S. K.; Balasubramanian, T.; Ruzié, C.; Kraymer, M.; Fan, D.; Borbas, K. E.; Yang, E.; Kee, H. L.; Kirmaier, C.; Diers, J. R.; Bocian, D. F.; Holten, D.; Lindsey, J. S.; Hamblin, M. R. *J. Med. Chem.* **2010**, 53, 4018–4027.
- (6) Huang, L.; Huang, Y.-Y.; Mroz, P.; Tegos, G. P.; Zhiyentayev, T.; Sharma, S. K.; Lu, Z.; Balasubramanian, T.; Kraymer, M.; Ruzié, C.; Yang, E.; Kee, H. L.; Kirmaier, C.; Diers, J. R.; Bocian, D. F.; Holten, D.; Lindsey, J. S.; Hamblin, M. R. *Antimicrob. Agents Chemother.* **2010**, 54, 3834–3841.
- (7) O'Connor, A. E.; Gallagher, W. M.; Byrne, A. T. *Photochem. Photobiol.* **2009**, 85, 1053–1074.

- (8) Grin, M. A.; Mironov, A. F.; Shtil, A. A. *Anti-Cancer Agents Med. Chem.* **2008**, *8*, 683–697.
- (9) Brandis, A. S.; Salomon, Y.; Scherz, A. In *Chlorophylls and Bacteriochlorophylls: Biochemistry, Biophysics, Functions and Applications*; Grimm, B.; Porra, R. J.; Rüdiger, W.; Scheer, H.; Eds.; Springer: Dordrecht, The Netherlands, 2006; pp 485–494.
- (10) Nyman, E. S.; Hynninen, P. H. *J. Photochem. Photobiol. B: Biol.* **2004**, *73*, 1–28.
- (11) Chen, Y.; Li, G.; Pandey, R. K. *Curr. Org. Chem.* **2004**, *8*, 1105–1134.
- (12) Bonnett, R. *Chemical Aspects of Photodynamic Therapy*; Gordon and Breach Science Publishers: Amsterdam, 2000.
- (13) Singh, S.; Aggarwal, A.; Thompson, S.; Tomé, J. P. C.; Zhu, X.; Samaroo, D.; Vinodu, M.; Gao, R.; Drain, C. M. *Bioconjugate Chem.* **2010**, *21*, 2136–2146.
- (14) Kee, H. L.; Diers, J. R.; Ptaszek, M.; Muthiah, C.; Fan, D.; Lindsey, J. S.; Bocian, D. F.; Holten, D. *Photochem. Photobiol.* **2009**, *85*, 909–920.
- (15) Kee, H. L.; Nothdurft, R.; Muthiah, C.; Diers, J. R.; Fan, D.; Ptaszek, M.; Bocian, D. F.; Lindsey, J. S.; Culver, J. P.; Holten, D. *Photochem. Photobiol.* **2008**, *84*, 1061–1072.
- (16) Akers, W.; Lesage, F.; Holten, D.; Achilefu, S. *Mol. Imag.* **2007**, *6*, 237–246.
- (17) Frangioni, J. V. *Curr. Opin. Chem. Biol.* **2003**, *7*, 626–634.
- (18) Licha, K. *Top. Curr. Chem.* **2002**, *222*, 1–29.
- (19) Sutton, J. M.; Clarke, O. J.; Fernandez, N.; Boyle, R. W. *Bioconjugate Chem.* **2002**, *13*, 249–263.
- (20) (a) De Rosa, S. C.; Brenchley, J. M.; Roederer, M. *Nature Med.* **2003**, *9*, 112–117. (b) Perfetto, S. P.; Chattopadhyay, P. K.; Roederer, M. *Nat. Rev. Immunol.* **2004**, *4*, 648–655.
- (21) Lindsey, J. S.; Mass, O.; Chen, C.-Y. *New J. Chem.* **2011**, *35*, DOI: 10.1039/c0nj00977f.
- (22) Taniguchi, M.; Cramer, D. L.; Bhise, A. D.; Kee, H. L.; Bocian, D. F.; Holten, D.; Lindsey, J. S. *New J. Chem.* **2008**, *32*, 947–958.
- (23) Stromberg, J. R.; Marton, A.; Kee, H. L.; Kirmaier, C.; Diers, J. R.; Muthiah, C.; Taniguchi, M.; Lindsey, J. S.; Bocian, D. F.; Meyer, G. J.; Holten, D. *J. Phys. Chem. C* **2007**, *111*, 15464–15478.
- (24) (a) Weersink, R. A.; Forbes, J.; Bisland, S.; Trachtenberg, J.; Elhilali, M.; Brún, P. H.; Wilson, B. C. *Photochem. Photobiol.* **2005**, *81*, 106–113. (b) Koudinova, N. V.; Pinthus, J. H.; Brandis, A.; Brenner, O.; Bendel, P.; Ramon, J.; Eshhar, Z.; Scherz, A.; Salomon, Y. *Int. J. Cancer* **2003**, *104*, 782–789. (c) Chen, Q.; Huang, Z.; Luck, D.; Beckers, J.; Brun, P.-H.; Wilson, B. C.; Scherz, A.; Salomon, Y.; Hetzel, F. W. *Photochem. Photobiol.* **2002**, *76*, 438–445.
- (25) Vakrat-Haglili, Y.; Weiner, L.; Brumfeld, V.; Brandis, A.; Salomon, Y.; McIlroy, B.; Wilson, B. C.; Pawlak, A.; Rozanowska, M.; Sarna, T.; Scherz, A. *J. Am. Chem. Soc.* **2005**, *127*, 6487–6497.
- (26) (a) Brandis, A.; Mazor, O.; Neumark, E.; Rosenbach-Belkin, V.; Salomon, Y.; Scherz, A. *Photochem. Photobiol.* **2005**, *81*, 983–993. (b) Mazor, O.; Brandis, A.; Plaks, V.;

- Neumark, E.; Rosenbach-Belkin, V.; Salomon, Y.; Scherz, A. *Photochem. Photobiol.* **2005**, *81*, 342–351.
- (27) (a) Ashur, I.; Goldschmidt, R.; Pinkas, I.; Salomon, Y.; Szweczyk, G.; Sarna, T.; Scherz, A. *J. Phys. Chem. A* **2009**, *113*, 8027–8037. (b) Kozyrev, A. N.; Chen, Y.; Goswami, L. N.; Tabaczynski, W. A.; Pandey, R. K. *J. Org. Chem.* **2006**, *71*, 1949–1960. (c) Limantara, L.; Koehler, P.; Wilhelm, B.; Porra, R. J.; Scheer, H. *Photochem. Photobiol.* **2006**, *82*, 770–780. (d) Fiedor, J.; Fiedor, L.; Kammhuber, N.; Scherz, A.; Scheer, H. *Photochem. Photobiol.* **2002**, *76*, 145–152.
- (28) Hartwich, G.; Fiedor, L.; Simonin, I.; Cmiel, E.; Schäfer, W.; Noy, D.; Scherz, A.; Scheer, H. *J. Am. Chem. Soc.* **1998**, *120*, 3675–3683.
- (29) Wasielewski, M. R. *Tetrahedron Lett.* **1977**, *18*, 1373–1376.
- (30) (a) Fukuzumi, S.; Ohkubo, K.; Zheng, X.; Chen, Y.; Pandey, R. K.; Zhan, R.; Kadish, K. M. *J. Phys. Chem. B* **2008**, *112*, 2738–2746. (b) Kunieda, M.; Tamiaki, H. *J. Org. Chem.* **2005**, *70*, 820–828. (c) Donohoe, R. J.; Frank, H. A.; Bocian, D. F. *Photochem. Photobiol.* **1988**, *48*, 531–537. (d) Schneider, E. *J. Am. Chem. Soc.* **1941**, *63*, 1477–1478.
- (31) (a) Musewald, C.; Hartwich, G.; Lossau, H.; Gilch, P.; Pöllinger-Dammer, F.; Scheer, H.; Michel-Beyerle, M. E. *J. Phys. Chem. B* **1999**, *103*, 7055–7060. (b) Musewald, C.; Hartwich, G.; Pöllinger-Dammer, F.; Lossau, H.; Scheer, H.; Michel-Beyerle, M. E. *J. Phys. Chem. B* **1998**, *102*, 8336–8342. (c) Teuchner, K.; Stiel, H.; Leupold, D.; Scherz, A.; Noy, D.; Simonin, I.; Hartwich, G.; Scheer, H. *J. Luminescence* **1997**, *72–74*, 612–614.
- (32) Vasudevan, J.; Stibrany, R. T.; Bumby, J.; Knapp, S.; Potenza, J. A.; Emge, T. J.; Schugar, H. J. *J. Am. Chem. Soc.* **1996**, *118*, 11676–11677.
- (33) Barkigia, K. M.; Miura, M.; Thompson, M. A.; Fajer, J. *Inorg. Chem.* **1991**, *30*, 2233–2236.
- (34) Donohoe, R. J.; Atamian, M.; Bocian, D. F. *J. Phys. Chem.* **1989**, *93*, 2244–2252.
- (35) Fajer, J.; Borg, D. C.; Forman, A.; Felton, R. H.; Dolphin, D.; Vegh, L. *Proc. Natl. Acad. Sci. USA* **1974**, *71*, 994–998.
- (36) Hu, S.; Mukherjee, A.; Spiro, T. G. *J. Am. Chem. Soc.* **1993**, *115*, 12366–12377.
- (37) Ruzié, C.; Krayner, M.; Balasubramanian, T.; Lindsey, J. S. *J. Org. Chem.* **2008**, *73*, 5806–5820.
- (38) Kim, H.-J.; Lindsey, J. S. *J. Org. Chem.* **2005**, *70*, 5475–5486.
- (39) Krayner, M.; Ptaszek, M.; Kim, H.-J.; Meneely, K. R.; Fan, D.; Secor, K.; Lindsey, J. S. *J. Org. Chem.* **2010**, *75*, 1016–1039.
- (40) Aravindu, K.; Krayner, M.; Kim, H.-J.; Lindsey, J. S. *New J. Chem.* **2011**, *35*, *in press*.
- (41) Buchler, J. W.; Schneehage, H. H. *Tetrahedron Lett.* **1972**, *36*, 3803–3806.
- (42) (a) Rosenfeld, A.; Morgan, J.; Goswami, L. N.; Ohulchanskyy, T.; Zheng, X.; Prasad, P. N.; Oseroff, A.; Pandey, R. K. *Photochem. Photobiol.* **2006**, *82*, 626–634. (b) Dolmans, D. E. J. G. J.; Kadambi, A.; Hill, J. S.; Waters, C. A.; Robinson, B. C.; Walker, J. P.;

- Fukumura, D.; Jain, R. K. *Cancer Res.* **2002**, *62*, 2151–2156. (c) Robinson, B. C.; Phadke, A. S. US 6,444,194 B1.
- (43) Mroz, P.; Bhaumik, J.; Dogutan, D. K.; Aly, Z.; Kamal, Z.; Khalid, L.; Kee, H. L.; Bocian, D. F.; Holten, D.; Lindsey, J. S.; Hamblin, M. R. *Cancer Lett.* **2009**, *282*, 63–76.
- (44) Kee, H. L.; Bhaumik, J.; Diers, J. R.; Mroz, P.; Hamblin, M. R.; Bocian, D. F.; Lindsey, J. S.; Holten, D. *J. Photochem. Photobiol. A: Chem.* **2008**, *200*, 346–355.
- (45) Da Silva, A. R.; Pelegrino, A. C.; Tedesco, A. C.; Jorge, R. A. *J. Braz. Chem. Soc.* **2008**, *19*, 491–501.
- (46) Dogutan, D. K.; Zaidi, S. H. H.; Thamyongkit, P.; Lindsey, J. S. *J. Org. Chem.* **2007**, *72*, 7701–7714.
- (47) Takagi, S.; Kato, Y.; Furuta, H.; Onaka, S.; Miyamoto, T. K. *J. Organomet. Chem.* **1992**, *429*, 287–299.
- (48) Cornillion, J.-L.; Anderson, J. E.; Kadish, K. M. *Inorg. Chem.* **1986**, *25*, 991–995.
- (49) (a) Lin, S.-J.; Hong, T.-N.; Tung, J.-Y.; Chen, J.-H. *Inorg. Chem.* **1997**, *36*, 3886–3891. (b) Lee, Y.-Y.; Chen, J.-H.; Hsieh, H.-Y. *Polyhedron* **2003**, *22*, 1633–1639.
- (50) Tait, C. D.; Holten, D. *Photobiochem. Photobiophys.* **1983**, *6*, 201–209.
- (51) Holten, D.; Gouterman, M.; Parson, W. W.; Windsor, M. W.; Rockley, M. G. *Photochem. Photobiol.* **1976**, *23*, 415–423.
- (52) Birks, J. B. *Photophysics of Aromatic Molecules*, Wiley-Interscience: London, 1970, pp 140–192.
- (53) (a) Gentemann, S.; Medforth, C. J.; Ema, T.; Nelson, N. Y.; Smith, K. M.; Fajer, J.; Holten, D. *Chem. Phys. Lett.* **1995**, *245*, 441–447. (b) Gentemann, S.; Nelson, N. Y.; Jaquinod, L.; Nurco, D. J.; Leung, S. H.; Medforth, C. J.; Smith, K. M.; Fajer, J.; Holten, D. *J. Phys. Chem. B* **1997**, *101*, 1247–1254. (c) Retsek, J. L.; Medforth, C. J.; Nurco, D. J.; Gentemann, S.; Chirvony, V. S.; Smith, K. M.; Holten, D. *J. Phys. Chem. B* **2001**, *105*, 6396–6411.
- (54) (a) Linnanto, J.; Korppi-Tommola, J. *Phys. Chem. Chem. Phys.* **2006**, *8*, 663–687. (b) Petit, L.; Quartarolo, A.; Adamo, C.; Russo, N. *J. Phys. Chem. B* **2006**, *110*, 2398–2404.
- (55) (a) Petke, J. D.; Maggiora, G. M.; Shipman, L. L.; Christoffersen, R. E. *Photochem. Photobiol.* **1980**, *32*, 399–414. (b) Weiss, C. Jr. *J. Mol. Spectroscopy* **1972**, *44*, 37–80.
- (56) (a) Gouterman, M. in *The Porphyrins*, Vol. 3, Dolphin, D., Ed., Academic Press: New York, 1978, pp 1–165. (b) Gouterman, M. *J. Mol. Spectroscopy* **1961**, *6*, 138–163.
- (57) Krayner, M.; Yang, E.; Diers, J. R.; Bocian, D. F.; Holten, D.; Lindsey, J. S. *New J. Chem.* **2011**, *35*, 587–601.
- (58) Kee, H. L.; Kirmaier, C.; Tang, Q.; Diers, J. R.; Muthiah, C.; Taniguchi, M.; Laha, J. K.; Ptaszek, M.; Lindsey, J. S.; Bocian, D. F.; Holten, D. *Photochem. Photobiol.* **2007**, *83*, 1125–1143.
- (59) Seybold, P. G.; Gouterman, M. *J. Mol. Spectrosc.* **1969**, *31*, 1–13.

- (60) Gradyushko, A. T.; Sevchenko, A. N.; Solovyov, K. N.; Tsvirko, M. P. *Photochem. Photobiol.* **1970**, *11*, 387–400.
- (61) Weber, G.; Teale, F. W. J. *Trans. Faraday Soc.* **1957**, *53*, 646–655.
- (62) Mass, O.; Taniguchi, M.; Ptaszek, M.; Springer, J. W.; Faries, K. M.; Diers, J. R.; Bocian, D. F.; Holten, D.; Lindsey, J. S. *New J. Chem.* **2011**, *35*, 76–88.
- (63) Kee, H. L.; Kirmaier, C.; Yu, L.; Thamyongkit, P.; Youngblood, W. J.; Calder, M. E.; Ramos, L.; Noll, B. C.; Bocian, D. F.; Scheidt, W. R.; Birge, R. R.; Lindsey, J. S.; Holten, D. *J. Phys. Chem. B* **2005**, *109*, 20433–20443.
- (64) Except for molecular mechanics and semi-empirical models, the calculation methods used in Spartan have been documented in: Shao, Y.; Molnar, L. F.; Jung, Y.; Kussmann, J.; Ochsenfeld, C.; Brown, S. T.; Gilbert, A. T. B.; Slipchenko, L. V.; Levchenko, S. V.; O'Neill, D. P.; DiStasio, R. A., Jr.; Lochan, R. C.; Wang, T.; Beran, G. J. O.; Besley, N. A.; Herbert, J. M.; Lin, C. Y.; Van Voorhis, T.; Chien, S. H.; Sodt, A.; Steele, R. P.; Rassolov, V. A.; Maslen, P. E.; Korambath, P. P.; Adamson, R. D.; Austin, B.; Baker, J.; Byrd, E. F. C.; Dachsels, H.; Doerksen, R. J.; Dreuw, A.; Dunietz, B. D.; Dutoi, A. D.; Furlani, T. R.; Gwaltney, S. R.; Heyden, A.; Hirata, S.; Hsu, C.-P.; Kedziora, G.; Khalliulin, R. Z.; Klunzinger, P.; Lee, A. M.; Lee, M. S.; Liang, W.-Z.; Lotan, I.; Nair, N.; Peters, B.; Proynov, E. I.; Pieniazek, P. A.; Rhee, Y. M.; Ritchie, J.; Rosta, E.; Sherrill, C. D.; Simmonett, A. C.; Subotnik, J. E.; Woodcock, H. L., III; Zhang, W.; Bell, A. T.; Chakraborty, A. K.; Chipman, D. M.; Keil, F. J.; Warshel, A.; Hehre, W. J.; Schaefer, H. F., III; Kong, J.; Krylov, A. I.; Gill, P. M. W.; Head-Gordon, M. *Phys. Chem. Chem. Phys.* **2006**, *8*, 3172–3191.

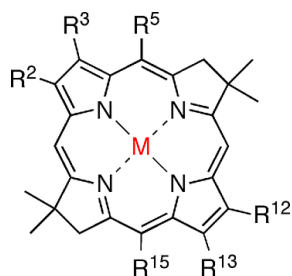
Chapter 5

Synthesis and Photophysical Properties of Metallobacteriochlorins

Reproduced in part with permission from Chen, C.Y ; Sun, E; Fan D; Taniguchi, M ; McDowell B; Yang, EK; Diers, J.R.; Bocian, D.F.; Holten, D.; Lindsey, J. S. Synthesis and Physicochemical Properties of Metallobacteriochlorins. *Inorg.Chem.* **2012**, *51*, 9443–9464. Doi: 10.1021/ic301262k. Copyright 2012 American Chemical Society.

Abstract

Access to metallobacteriochlorins is essential for investigation of a wide variety of fundamental photochemical processes, yet relatively few synthetic metallobacteriochlorins have been prepared. Members of a set of synthetic bacteriochlorins bearing 0-4 carbonyl groups (including the fully unsubstituted bacteriochlorin) were examined under two conditions: (i) standard conditions for zincation of porphyrins [$\text{Zn}(\text{OAc})_2 \cdot 2\text{H}_2\text{O}$ in DMF at 60–80 °C], and (ii) treatment in THF with a strong base (e.g., NaH or LDA) following by a metal reagent MX_n . Zincation of bacteriochlorins that bear 2-4 carbonyl groups proceeded under the former method



$M = \text{Mg, Cu, Zn, Pd, InCl}$

whereas those with 0-2 carbonyl groups proceeded with NaH or LDA/THF followed by $\text{Zn}(\text{OTf})_2$. The scope of metalation (via NaH or LDA in THF) is as follows: (a) for bacteriochlorins that bear two electron-releasing aryl groups, $M = \text{Cu, Zn, Pd, and InCl}$ (but not Mg, Al, Ni, Sn, or Au); (b) for bacteriochlorins that bear two carbonyl groups, $M = \text{Ni, Cu, Zn, Pd, Cd, InCl, and Sn}$ (but not Mg, Al or Au); and (c) a bacteriochlorin with four carbonyl groups was metalated with Mg (other metals were not examined). Altogether, 15 metallobacteriochlorins were isolated and characterized. Single-crystal X-ray analysis of 8,8,18,18-tetramethylbacteriochlorin reveals the core geometry provided by the four nitrogen atoms is rectangular; the difference in length of the two sides is $\sim 0.08 \text{ \AA}$. Electronic characteristics of (metal-free) bacteriochlorins were probed through electrochemical measurements along with density functional theory calculation of the energies of the frontier molecular orbitals. The photophysical properties (fluorescence yields, triplet yields, singlet and triplet excited-state lifetimes) of the zinc bacteriochlorins are generally similar to those of the metal-free analogues, and to those of the native chromophores bacteriochlorophyll *a* and

bacteriopheophytin *a*. The availability of diverse metallochlorins should prove useful in a variety of fundamental photochemical studies and applications.

Introduction

Naturally occurring chlorophylls and bacteriochlorophylls are essential constituents in plant and bacterial photosynthesis. Both types of hydroporphyrins contain magnesium as the central metal.¹ The introduction of different metals in tetrapyrrole macrocycles can alter the electronic,² axial-ligation,³ and photophysical⁴⁻⁶ properties of the coordination complex. The effect of metals can be seen by comparing the properties of metalloporphyrins containing magnesium, zinc, copper, or palladium, each of which is a divalent metal. Magnesium is five or six coordinate, and gives a reasonable yield of fluorescence ($\Phi_f \sim 0.1$), a long-lived excited singlet state ($\tau_s \sim 10$ ns), and a good yield of intersystem crossing to the triplet state.⁴ Zinc is four or five coordinate, and gives a lower yield of fluorescence ($\Phi_f \sim 0.03$), a shorter excited singlet state ($\tau_s \sim 2$ ns), and a higher yield of intersystem crossing to the triplet state.⁴ Copper is four coordinate and gives essentially no detectable fluorescence, a very short-lived nominal excited singlet state, and highly temperature-dependent properties of two excited-states borne from the coupling of the porphyrin triplet with the unpaired metal electron.⁵ Palladium is four coordinate and gives no detectable fluorescence, a unity yield of intersystem crossing, and a short-lived excited triplet state.⁶

A further distinction caused by metals concerns the change in optical properties. The introduction of a metal in a porphyrin typically increases the symmetry (e.g., D_{2h} to D_{4h}) and causes the spectral features in the visible region to collapse from primarily four bands (due to partially overlapping *x* and *y* transitions) to a two-banded spectrum (wherein the *x* and *y*

transitions are degenerate).⁷ The two main bands are the Q(0,0) and Q(1,0) transitions. (Weaker additional vibronic overtone bands also contribute to the spectra with or without a metal ion.) The resulting absorption of the metalloporphyrin occurs at shorter wavelength than for that of the free base porphyrin. For a chlorin, insertion of a metal does not alter the symmetry but does typically cause a hypsochromic shift in the position of the long-wavelength absorption band. An example is provided by chlorophyll *a* and pheophytin *a*, which absorb at 662 and 667 nm, respectively.¹ For a bacteriochlorin, insertion of a metal also does not alter the symmetry but typically causes a bathochromic shift in the position of the long-wavelength absorption band. An example is provided by bacteriochlorophyll *a* (Bchl *a*) and bacteriopheophytin *a* (Bph *a*), which absorb at 772 and 749 nm, respectively.¹ The ability to shift the absorption to longer wavelength upon metalation is quite attractive given the multiple motivations for access to chromophores with strong absorption in the near-infrared (NIR) spectral region. The relatively low energy of photons in NIR region (1.76–1.23 eV, 700–1000 nm) enables photochemical studies in an energy regime that has been comparatively unexplored versus studies of organic photochemistry in the ultraviolet (6.17–3.09 eV, 200–400 nm) or visible regions. Applications of NIR-active bacteriochlorins include light-harvesting for artificial photosynthesis,⁸ optical imaging^{9,10} and photodynamic therapy¹¹ of soft tissues, and fluorescent markers in clinical diagnostics.¹² In addition, selected photosynthetic organisms are now known to employ zinc-containing analogues of bacteriochlorophylls (rather than the expected magnesium).¹³ For all of these reasons, fundamental studies of diverse metallobacteriochlorins are warranted.

Despite the range of physical behavior that can be elicited with metalloporphyrins, relatively few metallobacteriochlorins have been prepared, and most that have been prepared are derived from Bchl *a*.^{14,15} While data from the naturally derived macrocycles are quite valuable,

lack of access to diverse synthetic metallobacteriochlorins has precluded wide-ranging studies of effects of peripheral substituents on spectral and photophysical properties, an approach that has been extensively pursued with porphyrins and chlorins. We have been working to develop a rational, *de novo* synthesis of bacteriochlorins.¹⁶⁻¹⁹ The resulting bacteriochlorins bear a geminal dimethyl group in each reduced, pyrroline ring to resist adventitious oxidants that otherwise could result in dehydrogenation. We recently characterized the photophysical properties of a large set of free base bacteriochlorins²⁰ derived from this synthetic approach, and also examined several indium(III) chelates thereof,²¹ but relatively few metal chelates of the synthetic bacteriochlorins have heretofore been prepared.

The metalation of bacteriochlorins – an ostensibly simple reaction – has proved more difficult than for porphyrins and chlorins. As one illustration, treatment of a chlorin–bacteriochlorin dyad with zinc acetate in CHCl_3 /methanol at room temperature for four hours afforded selective metalation of the chlorin; the resulting zinc chlorin – free base bacteriochlorin was isolated in nearly quantitative yield.⁹ As a second illustration, conditions that afford smooth zincation of the chlorin pheophytin *a* ($\text{Zn}(\text{OTf})_2$ in methanol or acetonitrile at room temperature) upon application to Bph *a* resulted in decomposition rather than metalation.²² The origin of the difficulty of metalation of bacteriochlorins remains unclear, but has been attributed to (1) diminished nucleophilicity, which decreases with increased saturation of the macrocycle (porphyrin < chlorin < bacteriochlorin),²² and (2) diminished acidity of the N-H protons, which decreases with increasing electron-richness of the ligand (porphyrin < chlorin < bacteriochlorin).²³ A factor that complicates interpretation is that many bacteriochlorins examined in metalation studies to date are derived from natural ligands of somewhat limited

stability. Regardless, the dearth of synthetic bacteriochlorins that withstand a broad range of reaction conditions has impeded a thorough investigation of these issues.

In this paper, we first summarize methods that have been used to date for metalation of bacteriochlorins, and identify correlations between methods and structural features of the bacteriochlorins. We then describe the development and application of a new method for metalation of synthetic bacteriochlorins. We then report the spectral and photophysical features of a set of metallochlorins. While no metalation procedure has yet been developed that is generically applicable to all bacteriochlorins, the present work should expand the availability of a variety of metallochlorins that have heretofore been inaccessible.

Experimental methods

Synthesis and general procedures

Experimental methods are described in detail in elsewhere.^A

Optical and photophysical characterization

Static absorption (Varian Cary 100 or Shimadzu UV-1800) and fluorescence (Spex Fluorolog Tau 2 or PTI Quantamaster 40) measurements were performed at room temperature, as were all other studies. Measurement of the fluorescence quantum yield (Φ_f) and singlet excited-state lifetimes (τ_S) and triplet yields (Φ_T) utilized dilute (μM) Ar-purged toluene and methanol solutions. Measurements of the triplet lifetimes (τ_T) lifetimes utilized Ar-purged 2-methyl tetrahydrofuran (2-MeTHF) solutions. Samples for Φ_f measurements had an absorbance ≤ 0.1 at the excitation wavelength to minimize front-face effects and similarly low absorbance in the $Q_y(0,0)$ band to minimize inner-filter effects.

Static emission measurements employed 2-4 nm excitation- and detection-monochromator bandwidths and 0.2 nm data intervals. Emission spectra were corrected for detection-system spectral response. Fluorescence quantum yields were determined relative to several different standards. These standards are (i) chlorophyll *a* in deoxygenated toluene ($\Phi_f = 0.325$),⁸⁷ which is the value measured in benzene,⁸⁸ and (ii) free base *meso*-tetraphenylporphyrin (**FbTPP**) in nondegassed toluene, for which $\Phi_f = 0.070$ was established with respect to the zinc chelate **ZnTPP** in nondegassed toluene ($\Phi_f = 0.030$),⁸⁸ consistent with prior results on **FbTPP**,⁸⁹ and (iii) 8,8,18,18-tetramethylbacteriochlorin⁹⁰ in Ar-purged toluene, for which $\Phi_f = 0.14$ was established with respect to chlorophyll *a* in benzene and **FbTPP** in toluene.

Fluorescence lifetimes were obtained using time-correlated-single-photon-counting detection on an apparatus with an approximately Gaussian instrument response function with a full-width-at-half-maximum of ~ 1 ns (Photon Technology International LaserStrobe TM-3). Samples were excited in the Soret or Q regions using excitation pulses at 337 nm from a nitrogen laser or in the blue to green spectral regions from a dye laser pumped by the nitrogen laser.

The Φ_{isc} values (triplet yields) were obtained using transient absorption spectroscopy. The extent of bleaching of the ground-state Q_x bands due to the formation of the lowest singlet excited state was measured immediately following a 130 fs flash in the $Q_y(0,0)$ band and compared with that due to the formation of the lowest triplet excited state at the asymptote of the singlet excited-state decay.^{20,91}

Electrochemistry

The electrochemical studies were performed in butyronitrile (Burdick and Jackson) using previously described instrumentation.⁹² The supporting electrolyte was 0.1 M

tetrabutylammonium hexafluorophosphate (Aldrich; recrystallized three times from methanol and dried at 110 °C in vacuo). The electrochemical cell was housed in a Vacuum Atmospheres glovebox (Model HE-93) equipped with a Dri-Train (Model 493). The $E_{1/2}$ values were obtained with square wave voltammetry (frequency 10 Hz) under conditions where the ferrocene couple has a potential of +0.19 V.

Density Functional Theory calculations

Calculations were performed with Spartan '08 for Windows version 1.2.0 in parallel mode⁹³ on a PC equipped with an Intel i7-975 cpu, 24 GB ram, and three 300 GB, 10k rpm hard drives. The calculations employed the hybrid B3LYP functional and 6-31G* basis set. The equilibrium geometries were fully optimized using the default parameters of the Spartan program.

Results

Bacteriochlorin synthesis and Bacteriochlorin metalation

The synthesis and structure characterization of all the compounds investigated in this study are described in detail in elsewhere.^A A summary of observation concerning metalation of synthetic bacteriochlorin is shown in Figure 1.

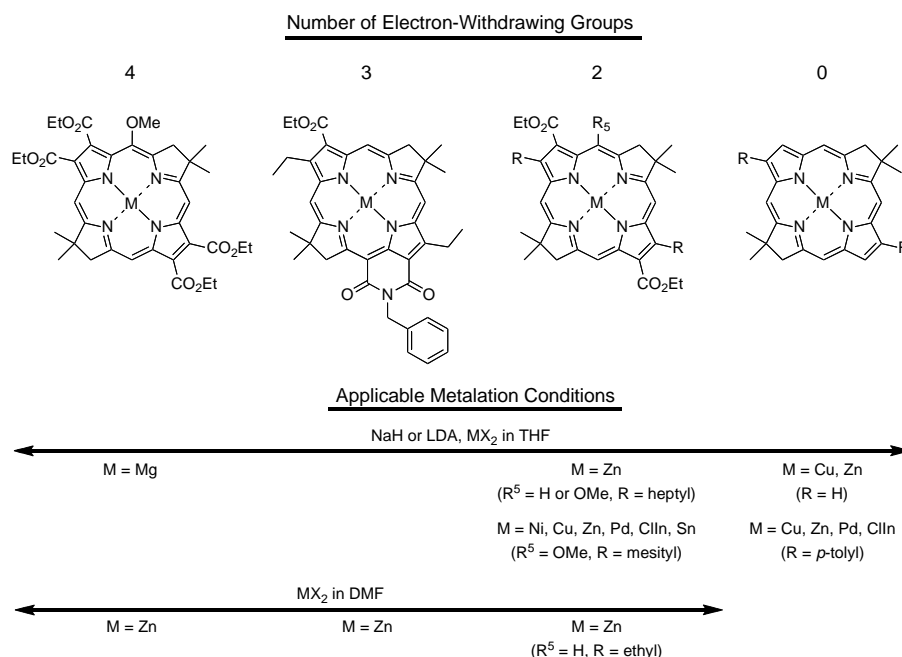


Figure 1. Summary of metalation of synthetic bacteriochlorins.^A

Structure and Physicochemical Characteristics

Structural analysis

The single-crystal X-ray structures of bacteriochlorins **BC0**, **BC0-2M**, and **CuBC0-2T** are shown in Figure 2. Note that **BC0-2M** contains 3,13-dimesityl groups whereas **CuBC0-2T** contains 2,12-di-*p*-tolyl groups. While a sizable number of photosynthetic proteins containing bacteriochlorophylls have been examined by X-ray crystallography, relatively few single-crystal X-ray studies have been carried out of bacteriochlorins. These include synthetic free base bacteriochlorins,⁶⁵ synthetic metallobacteriochlorins,^{42,52,66} and naturally derived (free base) bacteriopheophorbides.⁶⁷

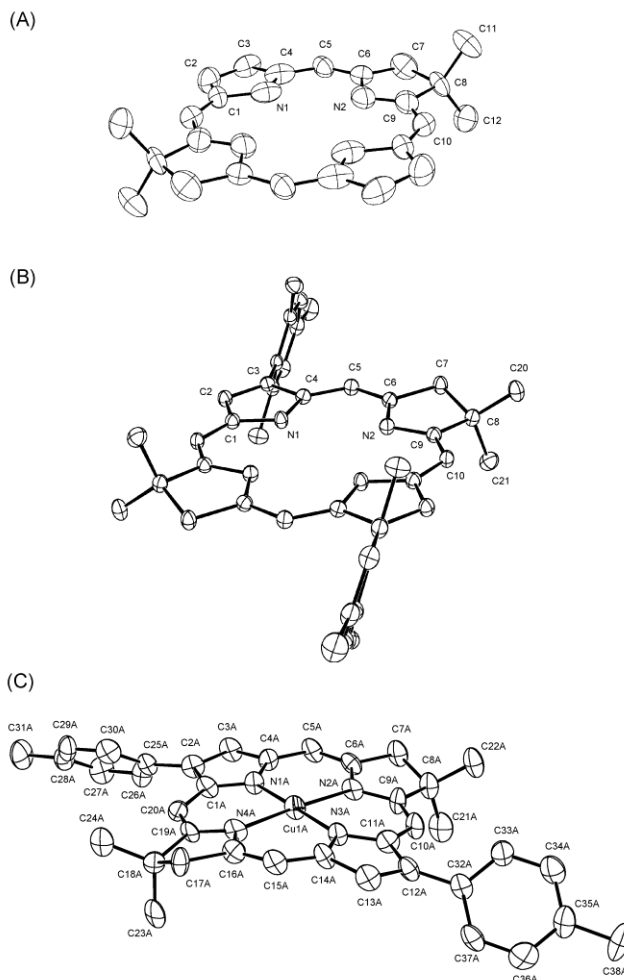


Figure 2. ORTEP drawing of (A) free base bacteriochlorin **BC0**, (B) free base bacteriochlorin **BC0-2M**, and (C) copper bacteriochlorin **CuBC0-2T** (one molecule from the unit cell).

The core shape of porphyrin (**porphine**), chlorin (**FbC**), and bacteriochlorins (**BC0** and **BC0-2M**) are shown in Figure 3. The core shape of porphine is close to square,⁶⁸ while that of chlorin **FbC** is slightly kite-shaped due to the presence of one pyrroline ring (D) and three pyrrole rings (A, B, and C).^{69,70} The core shape of bacteriochlorin **BC0** is slightly rectangular. The two pyrrole rings and two pyrroline rings that constitute a bacteriochlorin alternate upon circumambulating the macrocycle; thus, the two pyrroline rings occupy opposite corners, as do the two pyrrole rings. Introduction of two mesityl substituents at the 2- and 12-positions in **BC0-**

2M does not alter the size and shape of the core, as no significant substituent effects are observed. The core size can be evaluated by the comparison of the average distances between each of the nitrogen atoms and their centroid.⁷¹ The order of average nitrogen-centroid distances is porphine (2.055 Å) < chlorin (2.074 Å) < bacteriochlorin (2.096 Å for **BC0**, 2.095 Å for **BC0-2M**).

The core shape of the copper bacteriochlorin **CuBC0-2T** is shown in the Supporting Information (Figure S1). Copper bacteriochlorin **CuBC0-2T** is fairly planar, with the copper atom located on the least-square plane defined by the four nitrogen atoms. The average copper-centroid distance is 2.005 Å, which is shorter than that of free base bacteriochlorins **BC0** and **BC0-2M** (~2.095 Å).

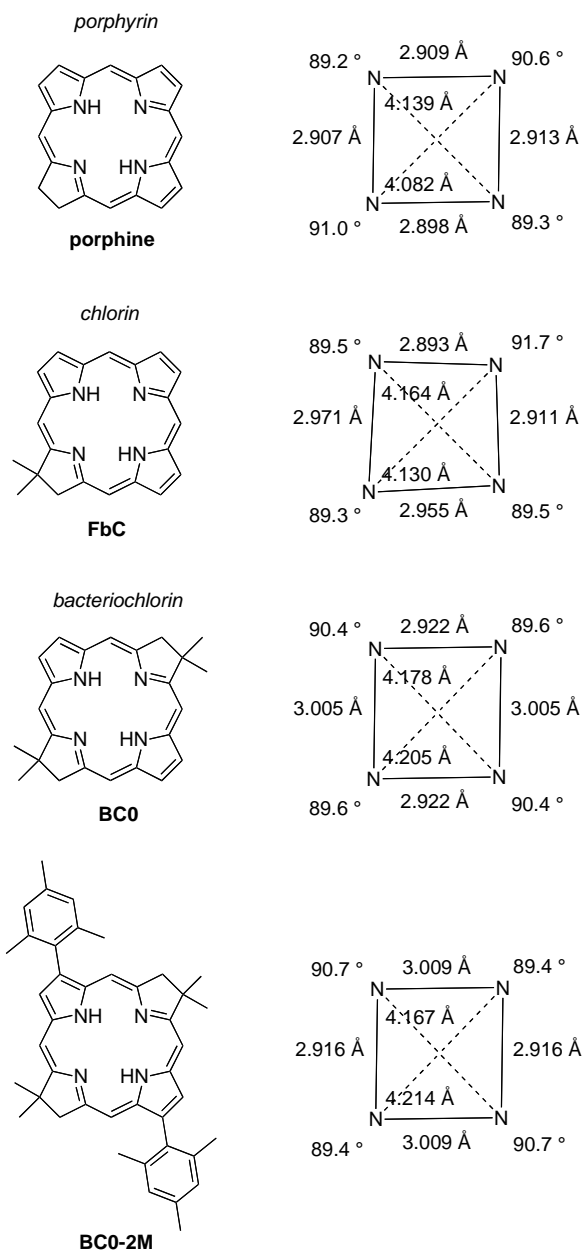


Figure 3. Comparison of core structural parameters across porphyrin, chlorin, and bacteriochlorin macrocycles.

Spectra properties

The ground-state electronic absorption spectra of the metallochlorins and the free base bacteriochlorins in toluene are shown in Figure 4 (**Zn** series) and Figure 5 (**BC0-2T** series). The spectral data including the position, intensity, and full-width at half maximum (fwhm) of the

long-wavelength absorption band (Q_y); the shift ($\Delta\lambda$) in the position of the Q_y band with respect to the free base bacteriochlorins; and intensity ratios of the Q_y to B_y bands (I_{Q_y}/I_{B_y} ratio) are listed in Table 1. Table 1 also gives spectral data for the native bacteriochlorins. In general, the absorption spectra of the synthetic metallo bacteriochlorins resemble that of the Bchl *a*, just as the spectra of the synthetic free base bacteriochlorins resemble that of the native free-base (Mg-less) analogue Bphe *a*.

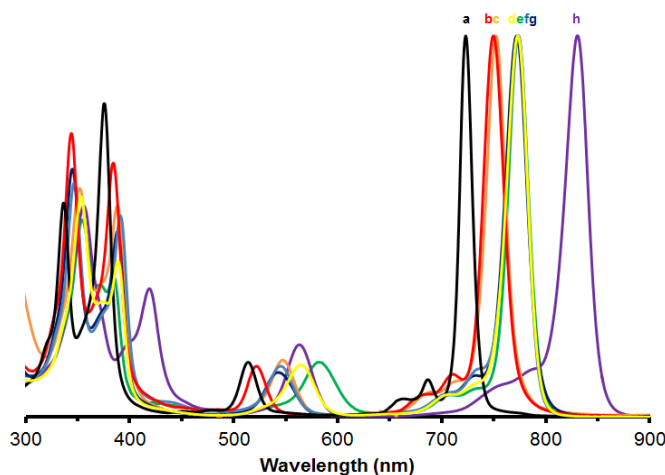


Figure 4. Absorption spectra in toluene at room temperature of bacteriochlorins (normalized at the Q_y bands). The labels in the graph are as follows: (a) **ZnBC0** (black), (b) **ZnBC0-2T** (red), (c) **ZnBC2-2H-MeO** (orange), (d) **ZnBC2-2M-MeO** (yellow), (e) **ZnBC4-MeO** (green), (f) **ZnBC2-2E** (blue), (g) **ZnBC2-2H** (dark blue), and (h) **ZnBC3-2E** (purple).

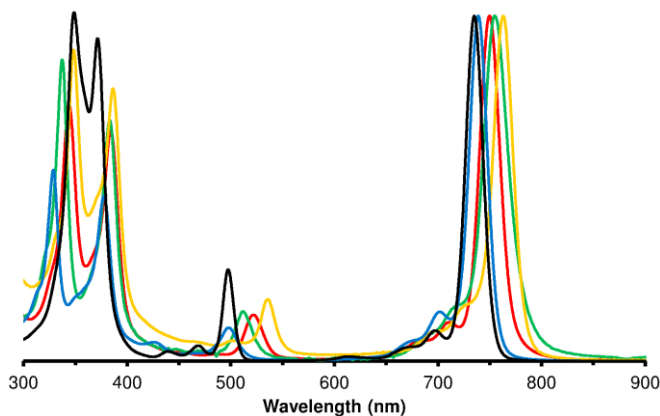


Figure 5. Absorption spectra in toluene at room temperature of bacteriochlorins (normalized at the Q_y bands). The labels in the graph are as follows: (a) **BC0-2T** (black), (b) **PdBC0-2T** (blue), (c) **ZnBC0-2T** (red), (d) **CuBC0-2T** (green), and (e) **CInBC0-2T** (orange).

Table 1. Spectral Properties of Bacteriochlorins.^a

Compound	$B_y(0,0)$ _{<i>b</i>} abs $\lambda(\text{nm})$	$B_x(0,0)$ _{<i>b</i>} abs $\lambda(\text{nm})$	$Q_x(0,0)$ abs $\lambda(\text{nm})$	$Q_y(0,0)$ abs $\lambda(\text{nm})$	$Q_y(0,0)$ abs fwhm (nm)	$Q_y(0,0)$ em $\lambda(\text{nm})$	$Q_y(0,0)$ em fwhm (nm)	ΔQ_x ^c $\Delta\lambda$ (nm)	ΔQ_y ^c $\Delta\lambda$ (nm)	I_{Q_y}/I_{B_y}
<i>Zn-BCs</i>										
ZnBC0-2T	344	384	521	749	23	756	26	22	13	1.3
ZnBC2-2M-MeO	353	389	565	773	25	780	26	27	15	1.6
ZnBC4-MeO	354	385	581	774	22	782	27	31	15	2.0
ZnBC3-2E	356	419	564	830	27	835	23	20	12	1.7
ZnBC2-2E	347	391	546	773	24	778	25	25	12	1.6
ZnBC2-2H	347	391	547	775	23	780	24	26	13	1.2
ZnBC2-2H-MeO	353	389	548	750	26	758	26	26	10	1.3
ZnBC0	336	375	514	723	14	725	18	25	10	1.7
<i>Pd-BCs</i>										
PdBC0-2T	330	379	499	739	21	745	25	0	3	1.7
PdBC2-2M-MeO	337	382	538	758	20	765	23	0	0	2.8
<i>Cu-BCs</i>										
CuBC0-2T	337	383	512	755	29	--	--	13	18	1.2
CuBC2-2M-MeO	348	390	556	780	37	--	--	18	22	1.5
CuBC0	332	378	507	728	19	--	--	18	15	1.7
<i>FbBCs</i>										
BC0-2T	351	374	499	736	20	742	23	0	0	1.0
BC2-2M-MeO	361	383	538	758	22	765	23	0	0	1.0
BC4-MeO ^d	361	368	550	759	20	763	23	0	0	1.2

BC3-2E ^d	358	408	544	818	24	823	24	0	0	1.3
BC2-2E ^d	354	383	521	761	20	764	21	0	0	0.9
BC2-2H	354	383	521	762	20	766	21	0	0	0.9
BC2-2H-MeO	357	379	522	740	18	746	21	0	0	1.1
BC0 ^d	340	365	489	713	12	716	16	0	0	0.9
<i>In-ClBCs</i>										
ClInBC0-2T ^e	350	388	539	763	23	769	31	40	27	1.1
<i>MgBCs</i>										
MgBC4-MeO	360	380	599	776	31	780	33	49	17	0.9
<i>Native BCs</i>										
BChl <i>a</i>	363	396	581	781	28	789	29	49	21	1.4
BPhe <i>a</i> ^d	362	389	532	758	31	768	27	0	0	0.7

^aIn toluene at room temperature. ^bThe nominal B_x(0,0) and B_y(0,0) absorption bands may alternate order with compound and have mixed x and y polarization. ^cThe shift of the band relative to that of the free base analogue. ^dData from ref 20. ^eData from ref 21.

The spectrum of each bacteriochlorin exhibits four absorption bands generally categorized as $B_y(0,0)$, $B_x(0,0)$, $Q_x(0,0)$, and $Q_y(0,0)$ from short to long wavelength. ($B_y(0,0)$ and $B_x(0,0)$ may reverse positions depending on the bacteriochlorin and have mixed x and y polarizations.) In general, the B bands of all bacteriochlorins examined herein fall in the region 330 to 419 nm. The Q bands of the **BC0-2T** series including the free base and all metal chelates lie at shorter wavelength (Q_x 499 to 536 nm; Q_y 737 to 763 nm) versus those of the **BC2-2M-MeO** series (Q_x 524 to 556 nm; Q_y 758 to 779 nm). For the **Zn** series, the Q bands are located at longer wavelength compared to the corresponding free base bacteriochlorins. The shifts in Q_x bands (19–34 nm) are generally more significant than those of Q_y bands (12–16 nm). The Q_y bands of the synthetic bacteriochlorins are quite intense. For **BC0-2T**, the long-wavelength maximum (732 nm) has a molar absorptivity of $\sim 120,000 \text{ M}^{-1}\text{cm}^{-1}$.¹⁶

Within the same bacteriochlorin series, the extent of the Q_x band shift increases in order of $\text{Pd} < \text{Cu} < \text{Zn}$ ($< \text{ClIn}$) chelates, while that of Q_y increases in order of $\text{Pd} < \text{Zn} < \text{Cu}$ ($< \text{ClIn}$). Each bacteriochlorin features a sharp Q_y band with fwhm in the range of 20–24 nm, except for the Cu chelates which exhibit broadened Q_y band in the range of 29–40 nm. The intensity ratios of the Q_y to B_y bands of the metallochlorins increase inversely with the increase of the wavelength shift ($\Delta\nu$) with respect to the free base bacteriochlorins in order of $(\text{ClIn}) < \text{Cu} < \text{Zn} < \text{Pd}$. For the **Zn** series, the intensity ratios of the Q_y to B_y bands fall in the range of 1.3–1.9.

The fluorescence spectrum of each zinc bacteriochlorin is dominated by a $Q_y(0,0)$ band that is only modestly (5–10 nm) shifted to longer wavelength than the $Q_y(0,0)$ absorption band and has a comparable spectral width (Table 1). This behavior is analogous to that observed for free base bacteriochlorins (Table 1 and ref 20). Similar fluorescence spectra are found for the indium chelates, as we have reported previously,²¹ and for the palladium bacteriochlorins.

However, compared to the zinc and free base bacteriochlorins, the fluorescence intensities are much weaker for the indium complexes and weaker still for the palladium complexes as described in the following.

Photophysical properties

Table 2 lists the photophysical properties of the zinc and palladium bacteriochlorins, along with representative data for the free base and indium analogues. The table also gives data for the native chromophores Bchl *a* and Bphe *a* in toluene. In comparing exact values of the photophysical characteristics of the zinc and free base bacteriochlorins, one must take into account that some of the zinc chelates may be axially ligated because they, like a few Fb complexes, were studied in THF rather than toluene for greater solubility (as indicated in Table 2 footnotes).

The zinc bacteriochlorins are quite fluorescent, with fluorescence quantum yields (Φ_f) generally in the range 0.08–0.20 with an average value of 0.13 that is comparable to that (0.15) for the free base analogues studied here or previously.²⁰ The exception is $\Phi_f = 0.033$ for the bacteriochlorin–imide **ZnBC3-2E**, which like that (0.040)²⁰ for the free base analogue is reduced due to the lower energy ($Q_y > 800$ nm; Table 1) of the singlet excited state resulting in more facile nonradiative internal conversion. The lifetimes (τ_S) of the singlet excited state for the zinc bacteriochlorins (except **ZnBC3-2E**) are in the range 2.2–4.4 ns, with an average value of 3.5 ns. These lifetimes are also similar to those for the free base analogues (3.3–4.4 ns; average 3.8 ns). The typical yield of intersystem crossing to the triplet excited state (Φ_{isc}) for the zinc bacteriochlorins is ~0.7, which is somewhat greater than the average value of ~0.5 for the free base analogues due to a modest effect of the metal ion on spin-orbit coupling. The typical Φ_f

and τ_S values for the indium chelates (0.02 and ~ 0.3 ns)²¹ are reduced and the Φ_{isc} values (~ 0.9) increased from those for the zinc chelates due to greater heavy metal enhancement of spin-orbit coupling.

The heavy metal effect (and potential d-orbital contribution) is greater still for the palladium bacteriochlorins, resulting in essentially quantitative singlet-to-triplet intersystem crossing. The consequence for **PdBC2-2M-MeO** is a very low fluorescence yield ($\Phi_f = 0.006$) and singlet lifetime ($\tau_S = 15$ ps). The two values are somewhat greater for **PdBC0-2T** for reasons that are not clear. Enhanced spin-orbit coupling also results in a progressive shortening of the lifetime of the lowest triplet excited state (τ_T) from a typical value of ~ 100 μ s for the zinc and free base bacteriochlorins to ~ 30 μ s for the indium chelates and to ~ 10 μ s for the palladium chelates.

In the case of copper bacteriochlorins (**CuBC0**, **CuBC0-2T**, **CuBC2-2M-MeO**), interactions involving the unpaired metal electron associated with the d^9 configuration of Cu(II) transform the macrocycle singlet excited state into a “singdoublet” and split the macrocycle triplet excited state into “tripdoublet” and “quartet” excited states that are close in energy, in analogy to copper porphyrins.⁷ Normal fluorescence is not expected (and none is found in the case of **CuBC2-2M-MeO**). Transient absorption studies of **CuBC0**, **CuBC0-2T**, and **CuBC2-2M-MeO** indicate essentially complete decay to the ground state with time constants of 0.3, 0.5, and 1.7 ns in THF. This time evolution likely represents deactivation of the tripdoublet/quartet excited-state manifold via a ring-to-metal charge-transfer state that has been implicated in the excited-state dynamics of copper porphyrins,⁷² but which now lies at lower energy in the corresponding bacteriochlorins due to the greater ease of macrocycle oxidation.

Table 2. Photophysical, Redox, and Molecular-Orbital Properties of Bacteriochlorins.

Compound	τ_S (ns)	Φ_f	Φ_{isc}	τ_T^c (μ s)	E_{ox}^b (V)	E_{red}^b (V)	HOMO (eV)	LUMO (eV)
<i>Zn-BCs</i>								
ZnBC0-2T	2.9	0.11	0.83	161	-0.04	-1.60	-4.26	-2.20
ZnBC2-2M-MeO	2.9	0.12	0.71	120	+0.45	-1.38	-4.55	-2.51
ZnBC4-MeO	4.4	0.13	0.80	38	+0.16	-1.10	-4.87	-2.92
ZnBC3-2E	2.2	0.033	0.28	94	+0.02	-1.12	-4.78	-2.94
ZnBC2-2E	2.6	0.08	0.71	149	-0.12	-1.42	-4.48	-2.53
ZnBC2-2H	3.5	0.14	0.60	191	0.00	-1.42	-4.47	-2.52
ZnBC2-2H-MeO	4.3	0.20	0.70	187	-0.14	-1.47	-4.48	-2.46
ZnBC0	3.4	0.10	0.67	151	-0.12	-1.68	-4.30	-2.16
<i>Pd-BCs</i>								
PdBC0-2T	0.35	0.020	>0.99	12	+0.43	-1.14	-4.36	-2.26
PdBC2-2M-MeO	0.015	0.006	>0.99	5.8	+0.29	-1.29	-4.63	-2.54
<i>Cu-BCs</i>								
CuBC0-2T				0.5 ns ^c	-0.04	-1.53	-4.25	-2.25
CuBC2-2M-MeO				1.7 ns ^c	+0.18	-1.32	-4.53	-2.55
CuBC0				0.3 ns ^c	-0.04	-1.60	-4.27	-2.18
<i>FbBCs</i>								
BC0-2T^d	3.3	0.18	0.55	163	+0.21	-1.49	-4.40	-2.22
BC2-2M-MeO	3.9	0.15	0.35	52	+0.38	-1.29	-4.65	-2.48
BC4-MeO^d	4.3	0.16	0.24	46	+0.57	-1.05	-5.00	-2.95
BC3-2E^d	1.9	0.04	0.51	85	+0.45	-0.98	-4.91	-2.99
BC2-2E^d	3.3	0.14	0.55	110	+0.29	-1.32	-4.68	-2.58
BC2-2H	3.3	0.10	0.45	110	+0.29	-1.33	-4.59	-2.52
BC2-2H-MeO	4.4	0.17	0.49	86	+0.28	-1.43	-4.60	-2.45
BC0^d	3.9	0.14	0.24	169	+0.45	-0.99	-4.46	-2.20
<i>In-ClBCs</i>								
ClInBC0-2T^e	0.21	0.016	0.9	44	+0.31	-1.25	-4.52	-2.52
<i>MgBCs</i>								
MgBC4-MeO	5.4	0.16	0.60	90			-4.86	-2.94
<i>Native BCs</i>								
BChl <i>a</i>	3.1	0.12	0.30	50			-4.75	-2.86
BPhe <i>a^d</i>	2.7	0.10	0.57	25			-4.87	-2.84

^aIn toluene at room temperature except as follows: the τ_T values for all compounds and the Φ_f , Φ_{isc} , and τ_S values for **BC2-2H**, **BC2-2H-MeO**, **ZnBC0**, **ZnBC2-2H**, **ZnBC2-2H-MeO** and **MgBC4-MeO** were determined in tetrahydrofuran. ^bFirst oxidation (E_{ox}) and first reduction (E_{red}) potentials measured in 0.1 M tetrabutylammonium hexafluorophosphate in which the ferrocene couple has an $E_{1/2}$ of 0.19 V. ^cDecay of the tripdoublet/quartet excited-state manifold in nanoseconds. ^dData from ref 20. ^eData from ref 21.

Zinc tetrapyrroles (generally porphyrins and chlorins until the present) are often exploited in photophysical and photochemical applications compared to the corresponding magnesium complexes due to a reduced propensity for demetalation. In the case of porphyrins, a sacrifice is a shorter singlet excited-state lifetime (e.g., ~2 versus ~6 ns) and fluorescence yield (~0.03 versus ~0.13). Here we have found that the zinc bacteriochlorin **ZnBC4-MeO** has Φ_f , τ_S , Φ_{isc} , and τ_T values comparable to those of the corresponding magnesium bacteriochlorin **MgBC4-MeO**. In this regard, compared to the native magnesium bacteriochlorin, Bchl *a* (Table 1),⁷³⁻⁷⁵ the zinc bacteriochlorins generally have similar Φ_f , comparable or greater τ_S , comparable Φ_{isc} , and longer τ_T values. This comparison is similar to that for the free base bacteriochlorins relative to the native metal-free bacteriochlorin Bphe *a* (Table 1).²⁰ In summary, the synthetic zinc bacteriochlorins (and the indium and palladium analogues), like the free base bacteriochlorins, exhibit photophysical characteristics suitable for a range of applications in solar-energy conversion and photomedicine.

Electrochemical and molecular orbital characteristics.

The redox properties (reduction potentials) and energies of the frontier MOs of the bacteriochlorins are listed in Table 2. Only the potentials for the first oxidation (E_{ox}) and reduction (E_{red}) (which are both reversible) are presented in the table, as these are most germane for the discussion below. It should be noted, however, that the molecules also exhibit redox processes corresponding to second oxidations and reductions. Differences in the E_{ox} and E_{red} values among the the different metallobacteriochlorins and free base analogues generally parallel those for porphyrin systems.² In prior work on a large number of chlorins,⁷⁶ good correlations were found between the E_{ox} and the HOMO energy and between the E_{red} and the LUMO energy.

Such a correlation is generally found in Table 2 and in Figure 6 , which plots the redox potentials and MO energies versus the number of electron-withdrawing groups on the bacteriochlorin.

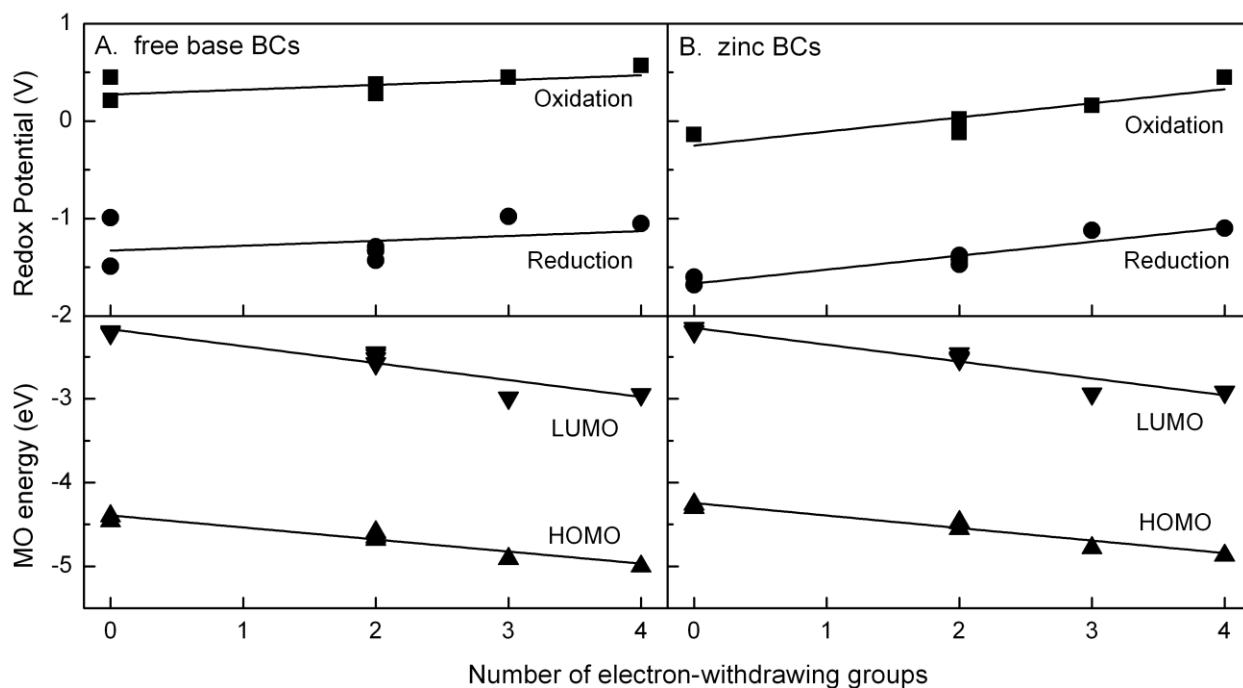


Figure 6. The effect of the number of electron-withdrawing (carbonyl) groups on the redox potentials and frontier MO energies.

Comparison of HOMO and LUMO energies of compounds **BC0**, **BC0-2T**, and **BC3-2E** listed in Table 2 with the values for their counterparts studied previously²⁰ that contain a 5-methoxy group shows that the 5-methoxy group shifts the MO energies by a relatively small amount (≤ 0.08 eV). When there is a shift in the MO energies, the shift is to slightly more negative values, indicating that the compound should be slightly harder to oxidize and easier to reduce. The data in Table 2 and Figure 6 further show that an increasing number of electron-withdrawing groups on the bacteriochlorin (affording greater ease of metalation) is reflected in a more positive E_{ox} (harder to oxidize) and a less negative E_{red} (more difficult to reduce). The one

compound that is an outlier is **BC0**. Along the same set of compounds, an increasing number of electron-withdrawing groups is reflected in shifts in the HOMO energy to more negative values (harder to oxidize) and the LUMO energy to more negative values (easier to reduce). Here, compound **BC0** is not an outlier and has essentially the same MO energies as compound **BC0-2T**. Thus, the fact that **BC0** is an outlier in the redox data may be in part a solvation (electrolyte) effect.

As expected, an increasing number of electron-withdrawing groups shifts the redox potentials and MO energies so as to make it harder to remove an electron (or electron density) and easier to add an electron (or electron density). Because metalation involves replacing two protons of the free base with a divalent metal ion, and a pair of protons is typically more electropositive than the metal ion, metalation effectively involves a net addition of electron density to the macrocycle. This property results in the correlation between the ease of metalation and the redox and MO energies.

The above comparisons are made for a set of bacteriochlorins that differ in the number and types of substituents at the same macrocycle positions. These changes cause shifts in the energies and electron densities of the HOMO and LUMO, but do not alter the identities of these two orbitals. The finding of such correlations, or even the interpretation if they are found, may be more difficult if the set of molecules differ in the sites of macrocycle substitution, and particularly if different macrocycles are involved. For example, depending on the substituent pattern, in progressing from porphyrin to chlorin (and then to bacteriochlorin), the HOMO may change from the $a_{2u}(\pi)$ orbital that has substantial electron density at the central nitrogens (and metal ion once incorporated) to the $a_{1u}(\pi)$ -like orbital that has far less electron density or even nodes at these positions. Such a switch would need to be taken into account in assessing

relationships between the ease (kinetics and thermodynamics) of metalation versus the MO and redox properties.

Conclusions and Outlook

The ability to prepare synthetic metallochlorins is essential for biomimetic studies pertaining to the roles of bacteriochlorophylls in bacterial photosynthesis and to probe the electronic interplay of peripheral substituents and central metal on photophysical properties. In this regard, the metalation of bacteriochlorins over the years has in some cases proceeded uneventfully and in other cases proved extremely difficult. In general, the reaction course for metalation of tetrapyrrole macrocycles has been interpreted in terms of a variety of parameters, including macrocycle conformation, molecular rigidity (ability to distort from a planar conformation to accommodate the incoming metal ion), nucleophilicity of the nitrogens toward the incoming metal ion, and solvent interactions that entail deprotonation of the pyrrolic NH bonds as well as coordination to the metal ion.²² Related to the ease of preparing a metal chelate is the stability of the resulting metal chelate toward demetalation. The difficulty of metalation upon moving to hydroporphyrins (porphyrin < chlorin < bacteriochlorin) has been attributed to the diminution of ligand nucleophilicity that accompanies saturation of the pyrrole rings.²² On the other hand, a careful study by Saga *et al.* of identically substituted macrocycles revealed that the ease of zinc demetalation decreased along the series porphyrin ~> chlorin >> bacteriochlorin.⁷⁷ In contrast to porphyrins, where the availability of collections of diverse macrocycles in ample quantities have enabled systematic studies of metalation and demetalation chemistry, comparable studies with bacteriochlorins to assess kinetics and thermodynamics have largely remained out of reach.

A *de novo* route to bacteriochlorins has provided a suite of macrocycles that differ in number (0-4 carbonyl groups) and type of substituents. The macrocycles provide the foundation for initiation of systematic studies of metalation methods. While a full matrix defined by metalation conditions, metal types, metal ligands, and bacteriochlorin substrates has not been performed, attempts to metalate the set of synthetic bacteriochlorins examined herein has led to the following observations:

- The difficulty of metalation of tetrapyrrole macrocycles decreases for bacteriochlorins with increasing number of electron-withdrawing groups.
- Metalation of a bacteriochlorin occurs upon treatment with a strong base (e.g., NaH or LDA) in THF followed by MX_n : (a) for bacteriochlorins that bear electron-releasing groups, $\text{M} = \text{Cu}, \text{Zn}, \text{Pd}, \text{and InCl}$; (b) for bacteriochlorins that bear two carboethoxy (electron-withdrawing) groups, $\text{M} = \text{Ni}, \text{Cu}, \text{Zn}, \text{Pd}, \text{Cd}, \text{InCl}, \text{and Sn}$ (but not Al or Au); and (c) a bacteriochlorin with four carboethoxy groups was metalated with Mg.
- Bacteriochlorins that bear ≥ 2 carbonyl groups typically can be zincated by standard porphyrin metalation conditions [$\text{Zn}(\text{OAc})_2 \cdot 2\text{H}_2\text{O}$ in DMF at 60–80 °C]

Scheer has suggested that the rate-determining step of bacteriochlorin metalation consists of deprotonation of the pyrrole N-H protons.²³ The use of a very strong base overcomes this limitation, and resembles the method developed by Arnold for preparing early transition metal chelates of porphyrins. The Arnold method entails formation and isolation of the dilithium derivative of the porphyrin as the reactive species for transmetalation upon treatment with a metal reagent.^{53,54} Such method has been applied by Stolzenberg with tetra-*p*-tolylbacteriochlorin to prepare the oxotitanyl chelate.⁵⁵ The deprotonation of the N-H protons

would be facilitated with increasing number of electron-withdrawing groups located on the pyrrole units, as observed here.

In comparing the above results with other types of tetrapyrrole macrocycles, it warrants emphasis that the (up to four) carbonyl groups were located exclusively in the pyrrole (rings A and C) and not in the pyrroline (rings B and D) units of the bacteriochlorins. By contrast, studies of chlorins can incorporate groups in the pyrrole (rings A and C), pyrroline (ring B), and pyrroline (ring D) units. In porphyrins, both pyrrole and pyrroline groups are present yet facile tautomerization typically precludes localization of a substituent in a particular heterocycle.

The studies reported herein concerning metalation of diverse synthetic bacteriochlorins – an ostensibly simple reaction – provide access to a number of the corresponding metallobacteriochlorins. One area of particular interest is the examination of dyadic (and larger) arrays comprised of free base and metallobacteriochlorins. In this regard, a review of all covalently linked arrays that contain one or more bacteriochlorins reveals only ~20 dyads prepared to date, and most of the bacteriochlorins incorporated therein have been free base species.⁸ Thus, the study of heterometalated arrays, an approach that has been widely used to probe photosynthetic-like mechanisms in synthetic multipigment architectures,⁷⁸ has largely resided outside the scope of experimentation for bacteriochlorins (but has been accessible via computational means⁷⁹). The straightforward access described herein should open the door to the study of fundamental properties, tuning NIR spectral properties, and pursuit of a range of photochemical applications of synthetic metallobacteriochlorins.

Acknowledgment.

This work was supported by grants from the Division of Chemical Sciences, Geosciences, and Biosciences, Office of Basic Energy Sciences of the U.S. Department of Energy to D.F.B. (DE-FG02-05ER15660), D.H. (DE-FG02-05ER15661) and J.S.L. (DE-FG02-96ER14632). Mass spectra were obtained at the Mass Spectrometry Laboratory for Biotechnology at North Carolina State University. Partial funding for the facility was obtained from the North Carolina Biotechnology Center and the National Science Foundation. We thank Dr. Paul Boyle for X-ray crystallographic analyses.

Supporting Information Available. Development of metalation conditions; further X-ray crystallographic information; and the synthesis and characterization of dimesitylbacteriochlorin **BC0-2M** are described in Ref A. The link information can be found in the publication reference (A).

References

- (A) Chen, C.Y.; Sun, E.; Fan, D.; Taniguchi, M.; McDowell, B.; Yang, E.K.; Diers, J.R.; Bocian, D.F.; Holten, D., and Lindsey, J. S. *Inorg. Chem.* 2012, 51, 9443–9464
- (1) Scheer, H. In *Chlorophylls and Bacteriochlorophylls. Biochemistry, Biophysics, Functions and Applications*; Grimm, B.; Porra, R. J.; Rüdiger, W.; Scheer, H., Eds., Advances in Photosynthesis and Respiration, 2006, Vol. 25; Springer, Dordrecht, The Netherlands, pp 1–26.
- (2) Felton, R. H. in *The Porphyrins*, Vol. 5, Dolphin, D., Ed., Academic Press: New York, 1978, pp 53–125.
- (3) Sanders, J. K. M.; Bampos, N.; Clyde-Watson, Z.; Darling, S. L.; Hawley, J. C.; Kim, H.-J.; Mak, C. C.; Webb, S. J. In *The Porphyrin Handbook*; Kadish, K. M., Smith, K. M., Guillard, R., Eds.; Academic Press: San Diego, CA, 2000; Vol. 3, pp 1–48.
- (4) Gradyushko, A. T.; Tsvirko, M. P. *Opt. Spectroscopy* **1971**, 31, 291–295.
- (5) Eastwood, D.; Gouterman, M. *J. Mol. Spectroscopy* **1969**, 30, 437–458.
- (6) Eastwood, D.; Gouterman, M. *J. Mol. Spectroscopy* **1970**, 35, 359–375.
- (7) Gouterman, M. in *The Porphyrins*, Vol. 3, Dolphin, D., Ed., Academic Press: New York, 1978, pp 1–165.
- (8) Lindsey, J. S.; Mass, O.; Chen, C.-Y. *New J. Chem.* **2011**, 35, 511–516.
- (9) Kee, H. L.; Nothdurft, R.; Muthiah, C.; Diers, J. R.; Fan, D.; Ptaszek, M.; Bocian, D. F.; Lindsey, J. S.; Culver, J. P.; Holten, D. *Photochem. Photobiol.* **2008**, 84, 1061–1072.
- (10) Kee, H. L.; Diers, J. R.; Ptaszek, M.; Muthiah, C.; Fan, D.; Lindsey, J. S.; Bocian, D. F.; Holten, D. *Photochem. Photobiol.* **2009**, 85, 909–920.

- (11) Huang, L.; Huang, Y.-Y.; Mroz, P.; Tegos, G. P.; Zhiyentayev, T.; Sharma, S. K.; Lu, Z.; Balasubramanian, T.; Krayner, M.; Ruzié, C.; Yang, E.; Kee, H. L.; Kirmaier, C.; Diers, J. R.; Bocian, D. F.; Holten, D.; Lindsey, J. S.; Hamblin, M. R. *Antimicrob. Agents Chemother.* **2010**, *54*, 3834–3841.
- (12) (a) Sutton, J. M.; Clarke, O. J.; Fernandez, N.; Boyle, R. W. *Bioconjugate Chem.* **2002**, *13*, 249–263. (b) Singh, S.; Aggarwal, A.; Thompson, S.; Tomé, J. P. C.; Zhu, X.; Samaroo, D.; Vinodu, M.; Gao, R.; Drain, C. M. *Bioconjugate Chem.* **2010**, *21*, 2136–2146.
- (13) (a) Wakao, N.; Yokoi, N.; Isoyama, N.; Hiraishi, A.; Shimada, K.; Kobayashi, M.; Kise, H.; Iwaki, M.; Itoh, S.; Takaichi, S.; Sakurai, Y. *Plant Cell Physiol.* **1996**, *37*, 889–893. (b) Tomi, T.; Shibata, Y.; Ikeda, Y.; Taniguchi, S.; Haik, C.; Mataga, N.; Shimada, K.; Itoh, S. *Biochim. Biophys. Acta* **2007**, *1767*, 22–30.
- (14) Kobayashi, M.; Akiyama, M.; Yamamura, M.; Kise, H.; Wakao, N.; Ishida, N.; Koizumi, M.; Kano, H.; Watanabe, T. *Z. Phys. Chem.* **1999**, *213*, 207–214.
- (15) Kobayashi, M.; Akiyama, M.; Kano, H.; Kise, H. In *Chlorophylls and Bacteriochlorophylls. Biochemistry, Biophysics, Functions and Applications*; Grimm, B.; Porra, R. J.; Rüdiger, W.; Scheer, H., Eds.; Advances in Photosynthesis and Respiration, 2006, Vol. 25; Springer: Dordrecht, The Netherlands, pp 79–94.
- (16) Kim, H.-J.; Lindsey, J. S. *J. Org. Chem.* **2005**, *70*, 5475–5486.
- (17) Krayner, M.; Balasubramanian, T.; Ruzié, C.; Ptaszek, M.; Cramer, D. L.; Taniguchi, M.; Lindsey, J. S. *J. Porphyrins Phthalocyanines* **2009**, *13*, 1098–1110.
- (18) Krayner, M.; Ptaszek, M.; Kim, H.-J.; Meneely, K. R.; Fan, D.; Secor, K.; Lindsey, J. S. *J. Org. Chem.* **2010**, *75*, 1016–1039.
- (19) Mass, O.; Lindsey, J. S. *J. Org. Chem.* **2011**, *76*, 9478–9487.
- (20) Yang, E.; Kirmaier, C.; Krayner, M.; Taniguchi, M.; Kim, H.-J.; Diers, J. R.; Bocian, D. F.; Lindsey, J. S.; Holten, D. *J. Phys. Chem. B* **2011**, *115*, 10801–10816.
- (21) Krayner, M.; Yang, E.; Kim, H.-J.; Kee, H. L.; Deans, R. M.; Sluder, C. E.; Diers, J. R.; Kirmaier, C.; Bocian, D. F.; Holten, D.; Lindsey, J. S. *Inorg. Chem.* **2011**, *50*, 4607–4618.
- (22) Orzel, L.; Kania, A.; Rutkowska-Zbik, D.; Susz, A.; Stochel, G.; Fiedor, L. *Inorg. Chem.* **2010**, *49*, 7362–7371.
- (23) Hartwich, G.; Fiedor, L.; Simonin, I.; Cmiel, E.; Schäfer, W.; Noy, D.; Scherz, A.; Scheer, H. *J. Am. Chem. Soc.* **1998**, *120*, 3675–3683.
- (24) Krayner, M.; Yang, E.; Diers, J. R.; Bocian, D. F.; Holten, D.; Lindsey, J. S. *New J. Chem.* **2011**, *35*, 587–601.
- (25) Medina, E.; Moyano, A.; Pericàs, M. A.; Riera, A. *Helv. Chim. Acta* **2000**, *83*, 972–988.

- (26) van Leusen, A. M.; Siderius, H.; Hoogenboom, B. E.; van Leusen, D. *Tetrahedron Lett.* **1972**, *13*, 5337–5340.
- (27) Brückner, C.; Posakony, J. J.; Johnson, C. K.; Boyle, R. W.; James, B. R.; Dolphin, D. J. *Porphyryns Phthalocyanines* **1998**, *2*, 455–465.
- (28) Ptaszek, M.; Bhaumik, J.; Kim, H.-J.; Taniguchi, M.; Lindsey, J. S. *Org. Process Res. Dev.* **2005**, *9*, 651–659.
- (29) Sinhababu, A. K.; Borchardt, R. T. *Tetrahedron Lett.* **1983**, *24*, 227–230.
- (30) Kim, H.-J.; Dogutan, D. K.; Ptaszek, M.; Lindsey, J. S. *Tetrahedron* **2007**, *63*, 37–55.
- (31) Balasubramanian, T.; Strachan, J.-P.; Boyle, P. D.; Lindsey, J. S. *J. Org. Chem.* **2000**, *65*, 7919–7929.
- (32) Buchler, J. W. In *Porphyryns and Metalloporphyryns*; Smith, K. M., Ed.; Elsevier: Amsterdam, 1975; pp 157–231.
- (33) Buchler, J. W. In *The Porphyryns*; Dolphin, D., Ed.; Academic Press: New York, 1978; Vol. 1, pp 389–483.
- (34) Lahiri, G. K.; Summers, J. S.; Stolzenberg, A. M. *Inorg. Chem.* **1991**, *30*, 5049–5052.
- (35) Tamiaki, H.; Yagai, S.; Miyatake, T. *Bioorg. Med. Chem.* **1998**, *6*, 2171–2178.
- (36) Sasaki, S.-I.; Tamiaki, H. *J. Org. Chem.* **2006**, *71*, 2648–2654.
- (37) Kunieda, M.; Yamamoto, K.; Sasaki, S.-I. Tamiaki, H. *Chem. Lett.* **2007**, *36*, 936–937.
- (38) Kunieda, M.; Tamiaki, H. *J. Org. Chem.* **2005**, *70*, 820–828.
- (39) Brandis, A.; Mazor, O.; Neumark, E.; Rosenbach-Belkin, V.; Salomon, Y.; Scherz, A. *Photochem. Photobiol.* **2005**, *81*, 983–993.
- (40) Kozyrev, A. N.; Chen, Y.; Goswami, L. N.; Tabaczynski, W. A.; Pandey, R. K. *J. Org. Chem.* **2006**, *71*, 1949–1960.
- (41) Fukuzumi, S.; Ohkubo, K.; Zheng, X.; Chen, Y.; Pandey, R. K.; Zhan, R.; Kadish, K. M. *J. Phys. Chem. B* **2008**, *112*, 2738–2746.
- (42) Vasudevan, J.; Stibrany, R. T.; Bumby, J.; Knapp, S.; Potenza, J. A.; Emge, T. J.; Schugar, H. J. *J. Am. Chem. Soc.* **1996**, *118*, 11676–11677.
- (43) Fajer, J.; Borg, D. C.; Forman, A.; Felton, R. H.; Dolphin, D.; Vegh, L. *Proc. Natl. Acad. Sci. USA* **1974**, *71*, 994–998.
- (44) Donohoe, R. J.; Frank, H. A.; Bocian, D. F. *Photochem. Photobiol.* **1988**, *48*, 531–537.
- (45) Donohoe, R. J.; Atamian, M.; Bocian D. F. *J. Phys. Chem.* **1989**, *93*, 2244–2252.
- (46) Scherz, A.; Salomon, Y.; Brandis, A.; Scheer, H. U.S. 6,569,846.
- (47) Hu, S.; Mukherjee, A.; Spiro T. G. *J. Am. Chem. Soc.* **1993**, *115*, 12366–12377.

- (48) Connick P. A.; Macor K. A. *Inorg. Chem.* **1991**, *30*, 4654–4663.
- (49) Strell, M.; Urumow, T. *Liebigs Ann. Chem.* **1977**, 970–974.
- (50) Wasielewski, M. R. *Tetrahedron Lett.* **1977**, *18*, 1373–1376.
- (51) Johansen, J. E.; Piermattie, V.; Angst, C.; Diener, E.; Kratky, C.; Eschenmoser, A. *Angew. Chem.* **1981**, *93*, 273–275.
- (52) Kratky, C.; Waditschatka, R.; Angst, C.; Johansen, J. E.; Plaquevent, J. C.; Schreiber, J.; Eschenmoser, A. *Helv. Chim. Acta* **1985**, *68*, 1312–1337.
- (53) (a) Arnold, J. *J. Chem. Soc., Chem. Commun.* **1990**, 976–978. (b) Brand, H.; Capriotti, J. A.; Arnold, J. *Inorg. Chem.* **1994**, *33*, 4334–4337. (c) Brand, H.; Arnold, J. *Coord. Chem. Rev.* **1995**, *140*, 137–168.
- (54) Berreau, L. M.; Hays, J. A.; Young, V. G., Jr.; Woo, L. K. *Inorg. Chem.* **1994**, *33*, 105–108.
- (55) Stolzenberg, A. M.; Haymond, G. S. *Inorg. Chem.* **2002**, *41*, 300–308.
- (56) Li, K.-L.; Guo, C.-C.; Chen, Q.-Y. *Org. Lett.* **2009**, *11*, 2724–2727.
- (57) Whitlock, H. W., Jr.; Hanauer, R.; Oester, M. Y.; Bower, B. K. *J. Am. Chem. Soc.* **1969**, *91*, 7485–7489.
- (58) Ruzié, C.; Krayner, M.; Balasubramanian, T.; Lindsey, J. S. *J. Org. Chem.* **2008**, *73*, 5806–5820.
- (59) Sharada, D. S.; Muresan, A. Z.; Muthukumaran, K.; Lindsey, J. S. *J. Org. Chem.* **2005**, *70*, 3500–3510.
- (60) (a) Lindsey, J. S.; Woodford, J. N. *Inorg. Chem.* **1995**, *34*, 1063–1069. (b) O’Shea, D. F.; Miller, M. A.; Matsueda, H.; Lindsey, J. S. *Inorg. Chem.* **1996**, *35*, 7325–7338.
- (61) (a) Fraser, R. R.; Mansour, T. S. *J. Org. Chem.* **1984**, *49*, 3443–3444. (b) March, J. *Advanced Organic Chemistry*; 4th Ed., John Wiley & Sons, Inc.: New York, p 252.
- (62) Alvarez-Bercedo, P.; Martin, R. *J. Am. Chem. Soc.* **2010**, *132*, 17352–17353.
- (63) (a) Reid, J. D.; Hunter, C. N. *J. Biol. Chem.* **2004**, *279*, 26893–26899. (b) Masuda, T. *Photosynth. Res.* **2008**, *96*, 121–143.
- (64) Robinson, L. R.; Hambricht, P. *Inorg. Chim. Acta* **1991**, *185*, 17–24.
- (65) (a) Barkigia, K. M.; Fajer, J.; Chang, C. K.; Young, R. *J. Am. Chem. Soc.* **1984**, *106*, 6457–6459. (b) Arasasingham, R. D.; Balch, A. L.; Olmstead, M. M. *Heterocycles* **1988**, *27*, 2111–2118. (c) Pandey, R. K.; Isaac, M.; MacDonald, I.; Medforth, C. J.; Senge, M. O.; Dougherty, T. J.; Smith, K. M. *J. Org. Chem.* **1997**, *62*, 1463–1472. (d) Senge, M. O.; Runge, S. *Acta Cryst.* **1998**, *C54*, 1917–1919. (e) Shea, K. M.; Jaquinod, L.; Khoury, R. G.; Smith, K. M. *Tetrahedron* **2000**, *56*, 3139–3144.

- (66) Barkigia, K. M.; Miura, M.; Thompson, M. A.; Fajer, J. *Inorg. Chem.* **1991**, *30*, 2233–2236.
- (67) (a) Barkigia, K. M.; Fajer, J.; Smith, K. M.; Williams, G. J. B. *J. Am. Chem. Soc.* **1981**, *103*, 5890–5893. (b) Barkigia, K. M.; Gottfried, D. S.; Boxer, S. G.; Fajer, J. *J. Am. Chem. Soc.* **1989**, *111*, 6444–6446. (c) Barkigia, K. M.; Gottfried, D. S. *Acta Cryst.* **1994**, *C50*, 2069–2072.
- (68) Saltsman, I.; Goldberg, I.; Balasz, Y.; Gross, Z. *Tetrahedron Lett.* **2007**, *48*, 239–244.
- (69) Taniguchi, M.; Ptaszek, M.; McDowell, B. E.; Boyle, P. D.; Lindsey, J. S. *Tetrahedron* **2007**, *63*, 3850–3863.
- (70) Taniguchi, M.; Mass, O.; Boyle, P. D.; Tang, Q.; Diers, J. R.; Bocian, D. F.; Holten, D.; Lindsey, J. S. *J. Mol. Structure* **2010**, *979*, 27–45.
- (71) Scheidt, W. R. In *The Porphyrins*; Dolphin, D., Ed., Academic Press: New York, Vol. 3, 1978, pp 463–511.
- (72) (a) Kim, D.; Holten, D.; Gouterman, M. *J. Am. Chem. Soc.* **1984**, *106*, 2793–2798. (b) Yan, X.; Holten, D. *J. Phys. Chem.* **1988**, *92*, 5982–5986.
- (73) Connolly, J. S.; Gorman, D. S.; Seely, G. R. *Ann. N. Y. Acad. Sci.* **1973**, *206*, 649–669.
- (74) Connolly, J. S.; Janzen, A. F.; Samuel, E. B. *Photochem. Photobiol.* **1982**, *36*, 559–563.
- (75) Tait, C. D.; Holten, D. *Photobiochem. Photobiophys.* **1983**, *6*, 201–209.
- (76) Kee, H. L.; Kirmaier, C.; Tang, Q.; Diers, J. R.; Muthiah, C.; Taniguchi, M.; Laha, J. K.; Ptaszek, M.; Lindsey, J. S.; Bocian, D. F.; Holten, D. *Photochem. Photobiol.* **2007**, *83*, 1125–1143.
- (77) Saga, Y.; Miura, R.; Sadaoka, K.; Hirai, Y. *J. Phys. Chem. B* **2011**, *115*, 11757–11762.
- (78) Harvey, P. D. In *The Porphyrin Handbook*; Kadish, K. M., Smith, K. M., Guillard, R., Eds.; Academic Press: San Diego, CA, 2003; Vol. 18, pp 63–250.
- (79) (a) Kobayashi, R.; Amos, R. D. *Chem. Phys. Lett.* **2006**, *420*, 106–109. (b) Erratum, **2006**, *424*, 225. (c) Dreuw, A.; Head-Gordon, M. *J. Am. Chem. Soc.* **2004**, *126*, 4007–4016. (d) Yamaguchi, Y.; Yokoyama, S.; Mashiko, S. *J. Chem. Phys.* **2002**, *116*, 6541–6548.
- (80) Srinivasan, N.; Haney, C. A.; Lindsey, J. S.; Zhang, W.; Chait, B. T. *J. Porphyrins Phthalocyanines* **1999**, *3*, 283–291.
- (81) Svec, W. A. In *The Porphyrins*; Dolphin, D. Ed., Academic Press: New York, Vol. V, 1978, pp 366–369.
- (82) Bruker-Nonius, SAINT+ version 7.07B, **2004**, Bruker-Nonius, Madison, WI 53711, USA.
- (83) Bruker-Nonius, SADABS version 2.10, **2004**, Bruker-Nonius, Madison, WI 53711, USA.

- (84) Altomare, A.; Cascarano, G.; Giacobuzzo, C.; Guagliardi, A.; Burla, M. C.; Polidori, G.; Camalli, M. *J. Appl. Cryst.* **1994**, *27*, 435.
- (85) Bruker-AXS, XL, SHELXTL version 6.12, UNIX, **2001**, Bruker-Nonius, Madison, WI 53711, USA.
- (86) Gabe, E. J.; Le Page, Y.; Charland, J.-P.; Lee, F. L.; White, P. S. *J. Appl. Cryst.* **1989**, *22*, 384–387.
- (87) Mass, O.; Taniguchi, M.; Ptaszek, M.; Springer, J. W.; Faries, K. M.; Diers, J. R.; Bocian, D. F.; Holten, D.; Lindsey, J. S. *New J. Chem.* **2011**, *35*, 76–88.
- (88) Weber, G.; Teale, F. W. J. *Trans. Faraday Soc.* **1957**, *53*, 646–655.
- (89) Seybold, P. G.; Gouterman, M. *J. Mol. Spectroscopy* **1969**, *31*, 1–13.
- (90) Gradyushko, A. T.; Sevchenko, A. N.; Solovyov, K. N.; Tsvirko, M. P. *Photochem. Photobiol.* **1970**, *11*, 387–400.
- (91) Taniguchi, M.; Cramer, D. L.; Bhise, A. D.; Kee, H. L.; Bocian, D. F.; Holten, D.; Lindsey, J. S. *New J. Chem.* **2008**, *32*, 947–958.
- (92) Kee, H. L.; Bhaumik, J.; Diers, J. R.; Mroz, P.; Hamblin, M. R.; Bocian, D. F.; Lindsey, J. S.; Holten, D. *J. Photochem. Photobiol. A: Chem.* **2008**, *200*, 346–355.
- (93) Strachan, J.-P.; Gentemann, S.; Seth, J.; Kalsbeck, W. A.; Lindsey, J. S.; Holten, D.; Bocian, D. F. *J. Am. Chem. Soc.* **1997**, *119*, 11191–11201.
- (94) Except for molecular mechanics and semi-empirical models, the calculation methods used in Spartan '08 or '10 have been documented in: Shao, Y.; Molnar, L. F.; Jung, Y.; Kussmann, J.; Ochsenfeld, C.; Brown, S. T.; Gilbert, A. T. B.; Slipchenko, L. V.; Levchenko, S. V.; O'Neill, D. P.; DiStasio, R. A., Jr.; Lochan, R. C.; Wang, T.; Beran, G. J. O.; Besley, N. A.; Herbert, J. M.; Lin, C. Y.; Van Voorhis, T.; Chien, S. H.; Sodt, A.; Steele, R. P.; Rassolov, V. A.; Maslen, P. E.; Korambath, P. P.; Adamson, R. D.; Austin, B.; Baker, J.; Byrd, E. F. C.; Dachsel, H.; Doerksen, R. J.; Dreuw, A.; Dunietz, B. D.; Dutoi, A. D.; Furlani, T. R.; Gwaltney, S. R.; Heyden, A.; Hirata, S.; Hsu, C.-P.; Kedziora, G.; Khalliulin, R. Z.; Klunzinger, P.; Lee, A. M.; Lee, M. S.; Liang, W.-Z.; Lotan, I.; Nair, N.; Peters, B.; Proynov, E. I.; Pieniazek, P. A.; Rhee, Y. M.; Ritchie, J.; Rosta, E.; Sherrill, C. D.; Simmonett, A. C.; Subotnik, J. E.; Woodcock, H. L., III; Zhang, W.; Bell, A. T.; Chakraborty, A. K.; Chipman, D. M.; Keil, F. J.; Warshel, A.; Hehre, W. J.; Schaefer, H. F., III; Kong, J.; Krylov, A. I.; Gill, P. M. W.; Head-Gordon, M. *Phys. Chem. Chem. Phys.* **2006**, *8*, 3172–3191.

Chapter 6

Photophysical Properties and Electronic Structure of Bacteriochlorin–Chalcones with Extended Near-Infrared Absorption

Reproduced with permission from Yang, EK; Ruzié, C; Krayner, M; Diers, J.R; Niedzwiedzki,DM; Kirmaier,C; Lindsey, J.S; Bocian, D.F; Holten, D. Photophysical Properties and Electronic Structure of Bacteriochlorin–Chalcones with Extended Near-Infrared Absorption. *Photochem. Photobiol.* 2013. 89. 586-604. Doi: 10.1111/php.12053. Copyright 2013 WILEY-BLACKWELL.

Abstract

Synthetic bacteriochlorins enable systematic tailoring of substituents about the bacteriochlorins chromophore and thereby provide insights concerning the native bacteriochlorophylls of bacterial photosynthesis. Nine free base bacteriochlorins (eight prepared previously and one prepared here) have been examined that bear diverse substituents at the 13- or 3,13-positions. The substituents include chalcone (3-phenylprop-2-en-1-onyl) derivatives with groups attached to the phenyl moiety, a “reverse chalcone” (3-phenyl-3-oxo-1-enyl), and extended chalcones (5-phenylpenta-2,4-dien-1-onyl, retinylidenonyl). The spectral and photophysical properties (τ_s , Φ_f , Φ_{ic} , Φ_{isc} , τ_T , k_f , k_{ic} , k_{isc}) of the bacteriochlorins have been characterized. The bacteriochlorins absorb strongly in the 780–800 nm region and have fluorescence quantum yields (Φ_f) in the range 0.05–0.11 in toluene and dimethylsulfoxide. Light-induced electron promotions between orbitals with predominantly substituent or macrocycle character or both may give rise to some net macrocycle \leftrightarrow substituent charge-transfer character in the lowest and higher singlet excited states as indicated by density functional theory (DFT) and time-dependent DFT calculations. Such calculations indicated significant participation of molecular orbitals beyond those (HOMO-1 to LUMO+1) in the Gouterman four-orbital model. Taken together, the studies provide insight into the fundamental properties of bacteriochlorins and illustrate designs for tuning the spectral and photophysical features of these NIR-absorbing tetrapyrrole chromophores.

Introduction

The development of chromophores with tunable absorption across the near-infrared (NIR) spectral region is essential for diverse applications. Light in the NIR region affords the deepest penetration in soft tissue and hence is ideal for use in photomedicine.¹⁻⁴ Absorption that can be stepped across the NIR region would complement absorption of fluorophores in the near-UV and visible regions and thereby enhance multicolor protocols.^{5,6} The ability to capture sunlight in the photon rich NIR region is essential for highly efficient bioinspired and biohybrid photosynthetic solar-conversion systems.⁷⁻⁹

Bacteriochlorophylls are nature's chromophores for absorbing sunlight in the NIR region. The native chromophores and analogs derived therefrom have limited synthetic malleability due to a nearly full complement of substituents about the perimeter of the macrocycle and susceptibility to adventitious dehydrogenation. *De novo* syntheses have recently begun to provide access to bacteriochlorins that can be tailored in a variety of ways and that are stable toward such macrocycle oxidation.¹⁰⁻¹³ Our own work has focused on creation of the bacteriochlorin skeleton wherein a geminal dimethyl group is placed in each reduced, pyrroline ring, thereby blocking adventitious pathways leading to dehydrogenated products (i.e., chlorins and porphyrins).^{14,15} The incorporation of auxochromes¹⁶ such as phenyl, vinyl and acetyl groups at select positions allows wavelength tuning of the strong NIR absorption band¹⁷⁻²⁰, known as the Q_y band.²¹ Chart 1 shows representative free base (metal-free) bacteriochlorins **B1–B11**^{14,17-20} that bear such auxochromes at the 3-position, 13-position, or both positions. Other synthetic approaches to impart a bathochromic shift of the long-wavelength band of bacteriochlorins include attachment of auxochromes²² and modification of the macrocycle skeleton.²³

The NIR absorption spectra of representative members of **B1–B11** are provided in Figure 1. In each case, a prominent fluorescence feature is found ~5 nm to longer wavelength than the Q_y absorption maximum (not shown). The free base bacteriochlorins and zinc or magnesium chelates (where available) have modest fluorescence yields (0.1–0.2), relatively long singlet excited-state lifetimes (3–5 ns), high yields of the triplet excited state (0.5–0.7) and relatively long triplet excited-state lifetimes (50–150 μ s).^{17,18,20,24}

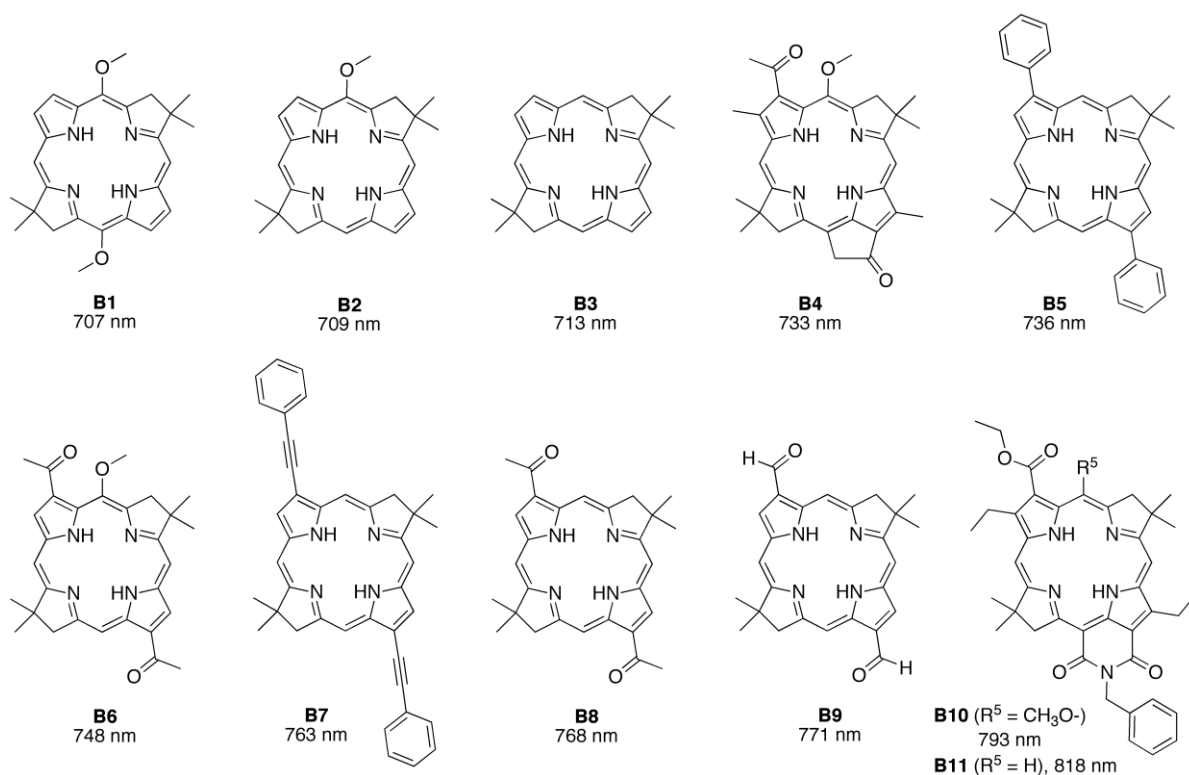


Chart 1. Representative bacteriochlorins studied previously. The position of the Q_y absorption band is indicated^{14,17–20}

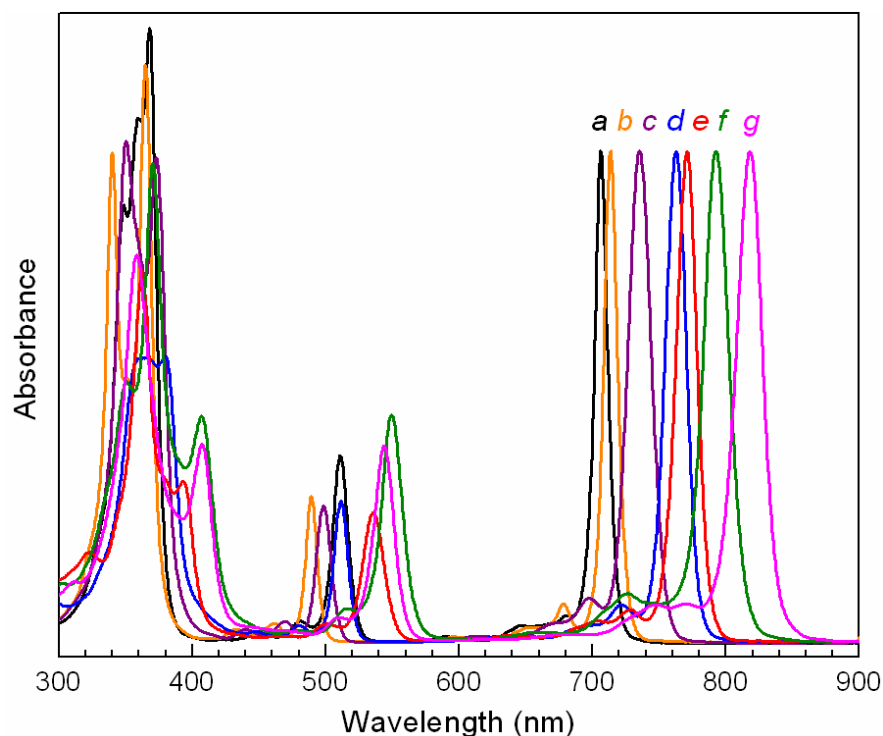


Figure 1. Absorption spectra of representative bacteriochlorins, bacteriooxophorbine, and bacteriochlorin imided studied previously, normalized in the Q_y band. The compounds (Chart 1) are **B1** (a, black), **B3** (b, orange), **B5** (c, purple), **B7** (d, blue), **B9** (e, red), **B10** (f, green), and **B11** (g, magenta).

The parent synthetic bacteriochlorin (**B3**) that bears no substituents (other than the geminal dimethyl group in each pyrroline ring) has the Q_y absorption band at 713 nm (and fluorescence at 716 nm). A substantial (58 nm) bathochromic shift to 771 nm is attained in the 3,13-diformylbacteriochlorin (**B9**). Other auxochromes (e.g., phenyl, vinyl, ethynyl, ester, acetyl) give shifts of intermediate magnitude. For a given set of 3,13-substituents, a 5-methoxy group gives a hypsochromic shift in the Q_y band of up to ~20 nm (e.g., **B6** vs **B8**, Chart 1). Combinations of these substituents afford a palette of stable synthetic bacteriochlorins with a strong, relatively sharp 15–20 nm full-width-at-half-maximum (FWHM) NIR absorption that can be stepped in ~10 nm increments from 690 to 770 nm (Figure 1). Absorption farther into the

NIR region has been obtained by incorporation of a 5-membered imide ring that spans the 12- to 15-positions of the macrocycle.¹⁸ Two representative bacteriochlorin–imides (**B10** and **B11**), with or without a 5-methoxy group, are shown in Chart 1 and have the Q_y band at 793 or 818 nm, respectively (Figure 1).

For fundamental studies as well as applications, it would be desirable to complement the existing set of 3,13-substituted bacteriochlorins that absorb in the 690–770 nm region with analogs that incorporate alternate auxochromes at the same two substituent sites to give even more bathochromic absorption shifts (similar to or exceeding those of an imide ring). One approach has been to utilize condensation reactions involving acetyl-substituted bacteriochlorins and a variety of aldehydes to prepare bacteriochlorin–Chalcones.²⁵ The name “chalcone” (*Gk* chalkos, copper ore) was given by Kostanecki and Tambor to the red-yellow condensation product of benzaldehyde and acetophenone (i.e., benzylideneacetophenone) in keeping with the names of other colored aryl ketones such as flavone and xanthone.²⁶ The enone benzylideneacetophenone is the parent member of the family of chalcones. The literature concerning chalcones is now vast; a Web of Science search on “chalcone” elicits >5000 citations owing to the importance of this motif in plant biochemistry (polyketides, flavonoids, anthocyanines)^{27–30}, and in medicinal chemistry.^{31–35} We chose chalcones as a bacteriochlorin substituent that could both be readily formed^{35–36} and might impart a bathochromic shift in the bacteriochlorin absorption spectrum.²⁵

Here we have performed a condensation of a formyl-substituted bacteriochlorin with acetophenone to prepare a reverse chalcone. The photophysical properties (in both polar and nonpolar media) and molecular-orbital (MO) characteristics of the reverse chalcone as well as the previously synthesized bacteriochlorin–chalcones are described. Collectively these studies

afford 3,13-substituted bacteriochlorins with extended NIR absorption and photophysical properties suitable for use in solar light-harvesting systems and photomedical research.

Experiment methods

3,13-Bis[(E)-3-phenylprop-1-en-2-onyl]-8,8,18,18-tetramethylbacteriochlorin (B-REV-chPh).

Following an established procedure²⁵, the reaction was carried out using a CEM Discover Synthesis Unit (CEM Corp., Matthews, NC), which was equipped with an infrared sensor for temperature monitoring. The reactions were carried out in an open vessel. Thus, a mixture of **B9** (15 mg, 0.035 mmol), acetophenone (16 μ L, 0.14 mmol), and NaOH (28 mg, 0.70 mmol) in absolute ethanol (17 mL) was reacted in an open vessel (long neck 125 mL round bottom flask) equipped with magnetic stirring and a reflux condenser and subjected to microwave irradiation at 300 W. The protocol was as follows: (1) heat from room temperature to reflux, (2) continue heating to hold at reflux for 30 min, (3) allow to cool to room temperature (~2 min), (4) check the reaction mixture by TLC analysis, and (5) repeat steps 1-4 until most of the starting material has disappeared. In so doing, the reaction mixture was heated for 2 h. The crude mixture was transferred to a round bottom flask and concentrated. The resulting crude product was dissolved in CH_2Cl_2 and washed with a saturated aqueous solution of NH_4Cl . The organic layer was separated, dried over Na_2SO_4 , concentrated under reduced pressure, and chromatographed [silica, hexanes/ CH_2Cl_2 (1:1) \rightarrow (1:9)] to afford an orange solid (<1 mg, ~4%): ^1H NMR (CDCl_3 , 300 MHz), δ -1.29 (brs, 2H), 1.97 (s, 12H), 4.44 (s, 4H), 7.58–7.75 (m, 6H), 8.19–8.35 (m, 6H), 8.63 (s, 2H), 8.99 (s, 2H), 9.07 (s, 2H), 9.25 (d, $J = 15.0$ Hz, 2H); laser-desorption mass spectrometry in the absence of a matrix³⁷ obsd 630.5; ESI-MS obsd 631.3064, calcd 631.3068 ($\text{C}_{42}\text{H}_{38}\text{N}_4\text{O}_2$); λ_{abs} (CH_2Cl_2) 333, 351, 395, 543, 800 nm.

Photophysical measurements

Measurement of the fluorescence (Φ_f) and triplet-excited-state (Φ_{isc}) quantum yields, singlet (τ_S) and triplet (τ_T) lifetimes, and transient-absorption studies unless noted otherwise, utilized dilute (μM) Ar-purged solutions at room temperature. Samples for Φ_f measurements had an absorbance <0.1 at the excitation wavelength. The Φ_f values (± 0.01) were generally determined as described previously¹⁷ with respect to two standards and the results averaged. The standards were (1) free base *meso*-tetraphenylporphyrin (**FbTPP**) in nondegassed toluene, for which $\Phi_f = 0.070$ was established with respect to the zinc chelate **ZnTPP** in nondegassed toluene ($\Phi_f = 0.030$)³⁸, consistent with prior results on **FbTPP**³⁹, and (2) 8,8,18,18-tetramethylbacteriochlorin in Ar-purged toluene, for which $\Phi_f = 0.14$ was established with respect to **FbTPP** and chlorophyll *a* (**Chl a**) in deoxygenated benzene⁴⁰ or toluene ($\Phi_f = 0.325$).

The τ_S value (± 0.1 ns) for most of the bacteriochlorins ($\tau_S \sim 1$ ns or longer) was first probed using a time-correlated single photon counting instrument that employed Soret excitation flashes derived from a nitrogen-pumped dye laser (PTI LaserStrobe) and a Gaussian instrument response function of 0.6 ns. The τ_S values measured by transient absorption are consistent with those determined via fluorescence. The τ_T values were determined using a conventional flash photolysis setup. The apparatus utilized excitation flashes (~ 5 ns, $\sim 10\text{mJ}$, 490–550 nm) from a dye laser pumped by a Q-switched Nd:YAG laser (Cobra-INDI, Spectra-Physics), continuous probe light filtered by monochromators, and a photomultiplier tube detector followed by an amplifier and digital oscilloscope with an overall instrument response function of ~ 0.1 ns.

The Φ_{isc} (triplet yield) values (± 0.07) were obtained using a transient-absorption technique in which the extent of bleaching of the ground-state Q_x and Q_y bands due to the lowest

singlet excited state was measured immediately following a ~100 fs flash (in the Q_x or Q_y bands) and compared with that due to the lowest triplet excited state at the asymptote of the singlet excited-state decay. For the Q_y region, the contribution of stimulated emission was taken into account. For both states and spectral regions, the extent of bleaching in the presence of excited-state absorption in the transient difference spectra was determined by various methods (to encompass a reasonable range of spectral shapes) including Gaussian fitting, integrations, and linear interpolation of the excited-state absorption across the ground-state bleaching region. An average value of the triplet yields obtained by these methods is reported for each bacteriochlorin.

Molecular orbital calculations

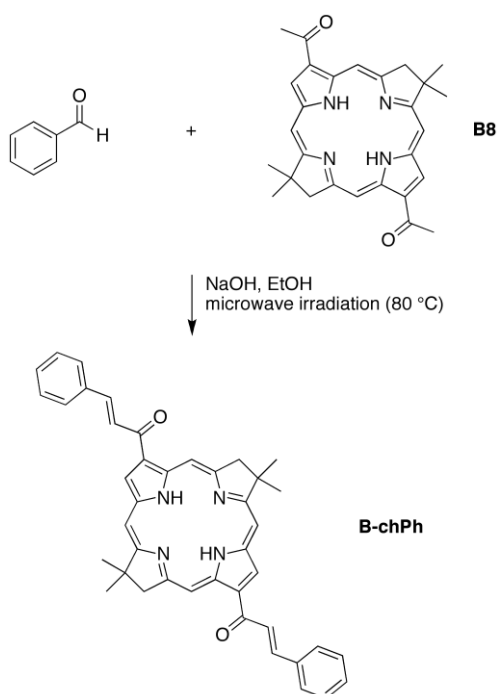
DFT calculations were performed with Spartan '10 for Windows version 1.2.0⁴¹ in parallel mode on a PC equipped with an Intel i7-975 cpu, 24 GB ram, and three 300 GB, 10k rpm hard drives. The calculations employed the hybrid B3LYP functional and basis set 6-31G*. The equilibrium geometries were fully optimized using the default parameters of the Spartan program. Molecular-orbital (MO) images were plotted from Spartan using an isovalue of 0.016.

TDDFT calculations were performed in parallel mode⁴² with Gaussian '09 version B.01 64-bit for linux using OpenSUSE version 11.4 or 12.1. One of two PC systems was used for Gaussian runs. The hardware for the first PC system used for Gaussian runs is the same as that used for the Spartan calculations and the second is a PC equipped with an intel i7-980 cpu, 24 GB ram and two 600 GB 10k rpm hard drives. Geometries used for the TDDFT calculations were from optimizations at the B3LYP/6-31G* level. TDDFT single point calculations were performed at the B3LYP/6-31G* level.

Results

Synthesis

We previously synthesized a 3,13-dibromobacteriochlorin²⁰, which provided a valuable substrate for conversion to the corresponding 3,13-diacetylbacteriochlorin **B8**²⁰ and 3,13-diformylbacteriochlorin **B9**.¹⁹ We found that treatment of the 3,13-diacetylbacteriochlorin with an aldehyde under microwave irradiation resulted in facile formation of the condensation product, namely the bacteriochlorin–chalcone **B-chPh** as shown in Scheme 1.²⁵



Scheme 1. Synthesis of a bacteriochlorin–chalcone.

The scope of the reaction encompassed a wide variety of aldehydes. The aldehydes and resulting products include the following: (1) 1,3-bis(methoxymethoxy)benzaldehyde afforded the MOM-substituted bacteriochlorin–chalcones **B-chM1** and **B-chM2** (MOM = methoxymethoxy); cleavage of the MOM group of **B-chM2** gave resorcinol-substituted bacteriochlorin–chalcone **B-**

chRsc. (2) *p*-N,N-dimethylaminobenzaldehyde afforded **B-chDma**. (3) Cinnamaldehyde afforded **B-chCin**, the vinylog of **B-chPh**. (4) Retinal afforded the retinyl-substituted bacteriochlorin–chalcones **B-chRet1** and **B-chRet2**. The bacteriochlorin–chalcones (Chart 2) exhibited a bathochromic shift of the long-wavelength absorption band (Q_y) of up to 24 nm from that of the parent 3,13-diacetylbacteriochlorin (**B8**).²⁵

The availability of diformylbacteriochlorin **B9** suggested analogous elaboration via condensation with a methyl ketone. Thus, the condensation of **B9** and acetophenone was carried out to give the bacteriochlorin–chalcone wherein the vinyl group is attached to the bacteriochlorin macrocycle and the carbonyl group is attached to the phenyl unit (Scheme 2). Such arrangement is the reverse of that for the bacteriochlorin–chalcone **B-chPh** in Scheme 1. Hence, the product shown in Scheme 2 is termed a *reversed* bacteriochlorin–chalcone, termed **B-REV-chPh**. The yields of the bacteriochlorin–chalcones shown in Scheme 1 and Chart 2 were quite reasonable, reaching as high as 58%. However, the reaction to form the reverse chalcone proceeded in low yield, with both starting material and monosubstituted bacteriochlorin (observed by laser-desorption mass spectrometry) remaining in the crude reaction mixture even after prolonged reaction time. The isolated yield of the desired **B-REV-chPh** was low (~4%), but sufficient material was obtained for spectroscopic studies (*vide infra*). The photophysical and molecular-orbital characteristics of the entire set of molecules are now described.

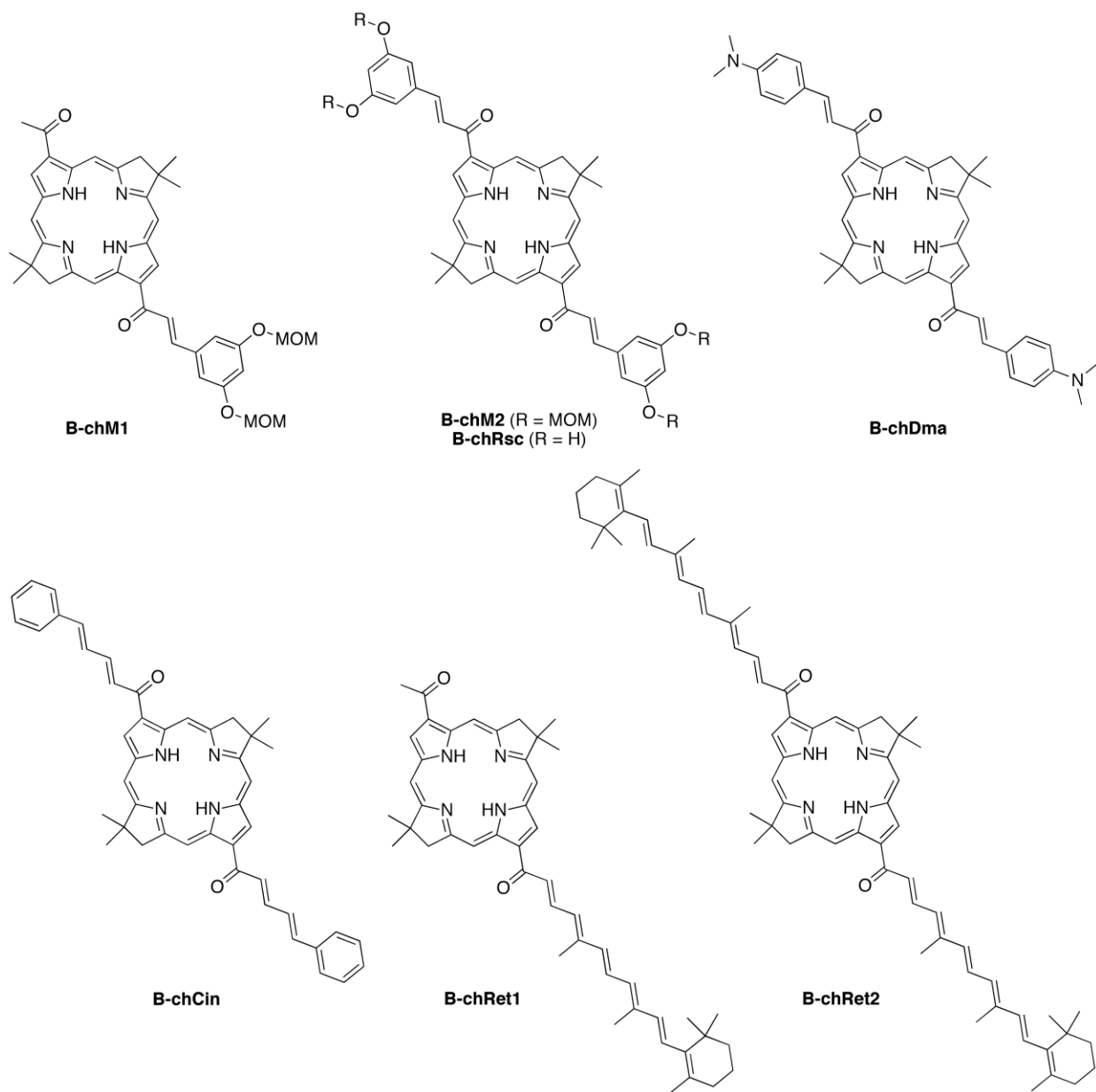
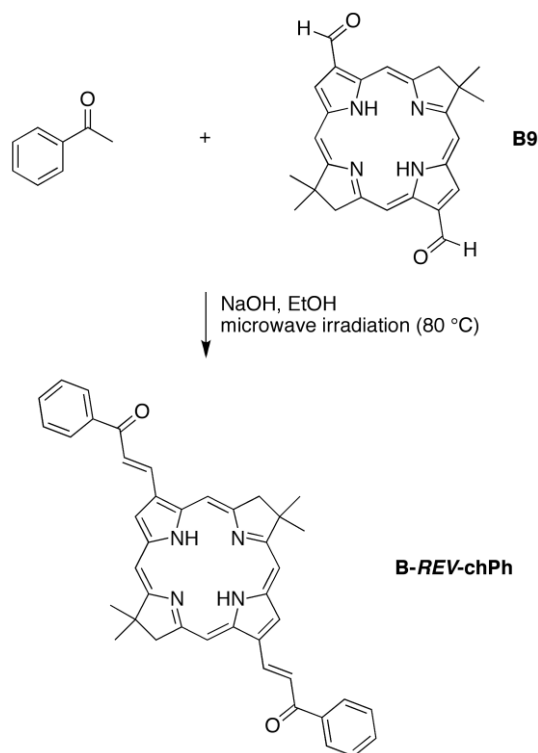


Chart 2. Bacteriochlorin–chalcones prepared previously.²⁵



Scheme 2. Synthesis of a reverse bacteriochlorin–chalcone.

Absorption spectra

The absorption spectrum of a typical bacteriochlorin²¹ such as the 3,13-substituted free base bacteriochlorins studied previously (Chart 1) is normally comprised of four main features (Figure 1). Progressing from longer to shorter wavelength these bands (and typical spectral ranges) are Q_y (690–770 nm), Q_x (520–580 nm), B_x (360–400 nm), and B_y (340–360 nm). The B_x and B_y features are also known as the Soret bands. Each of these main features is the origin transition [$Q_y(0,0)$, $Q_x(0,0)$, $B_x(0,0)$, $B_y(0,0)$], for which hereafter the (0,0) designator will not be indicated for ease of presentation. A much weaker (1,0) vibronic overtone feature can be found 1000–1500 cm^{-1} to high energy than the Q_y and Q_x origin transitions. Features in the Soret region that represent the (1,0) vibronic overtones of B_x and B_y are often partially overlapped with the origin transitions. Additional features may also contribute to the Soret-region absorption.

The Q_y absorption band is intense, with an extinction coefficient on the order of 100,000 $M^{-1}cm^{-1}$.¹⁵

The absorption spectra of the 3,13-substituted bacteriochlorin–chalcones studied here have similar overall absorption characteristics as the simpler 3,13-substituted analogs, with notable differences in detail. Spectra obtained in toluene are shown in Figures 1–3. The spectra are similar to those measured in dimethylsulfoxide (DMSO). Spectral characteristics are summarized in Table 1. The Q_y absorption band of each bacteriochlorin–chalcone bearing a single vinyl group shown in Chart 2 (i.e., except **B-chCin**) lies in the range 777–800 nm, which represents a significant bathochromic shift from the positions (690–771 nm) of the 3,13-bacteriochlorins studied previously. The latter positions include 713 nm for the unsubstituted parent **B3** and 768 nm for the diacetylbacteriochlorin **B8** (Figures 1 and 2A). The Q_y absorption bands of the bacteriochlorin–chalcones have a FWHM in the range 22–34 nm (26 nm average) in toluene and (26–38 nm) (32 nm average) in DMSO. These Q_y FWHM are greater than those of ~20 previously studied 3,13-substituted bacteriochlorins, which have widths in the range 12–25 nm (19 nm average).¹⁷ The greater FWHM in DMSO versus toluene is paralleled by a corresponding decrease in Q_y peak intensity (relative to the Soret maximum) in DMSO versus toluene. The compensating effects on bandwidth and peak height indicate that the integrated intensity (oscillator strength) of the Q_y band generally does not change appreciably with solvent. The Q_x bands lie in the range 540–550 nm (Figure 2B and 2C), which represents a bathochromic shift from the range of 489–536 nm found¹⁷ for the simpler 3,13-disubstituted analogs. The near-UV Soret absorption characteristics of the bacteriochlorin–chalcones also have notable differences compared to the simpler 3,13-substituted counterparts. For example, the Soret-region

absorption both of **B-chDma** and **B-chRet1** show overlapping features in the 330–400 region to which the B_y and B_x origin transitions contribute, plus a substantial

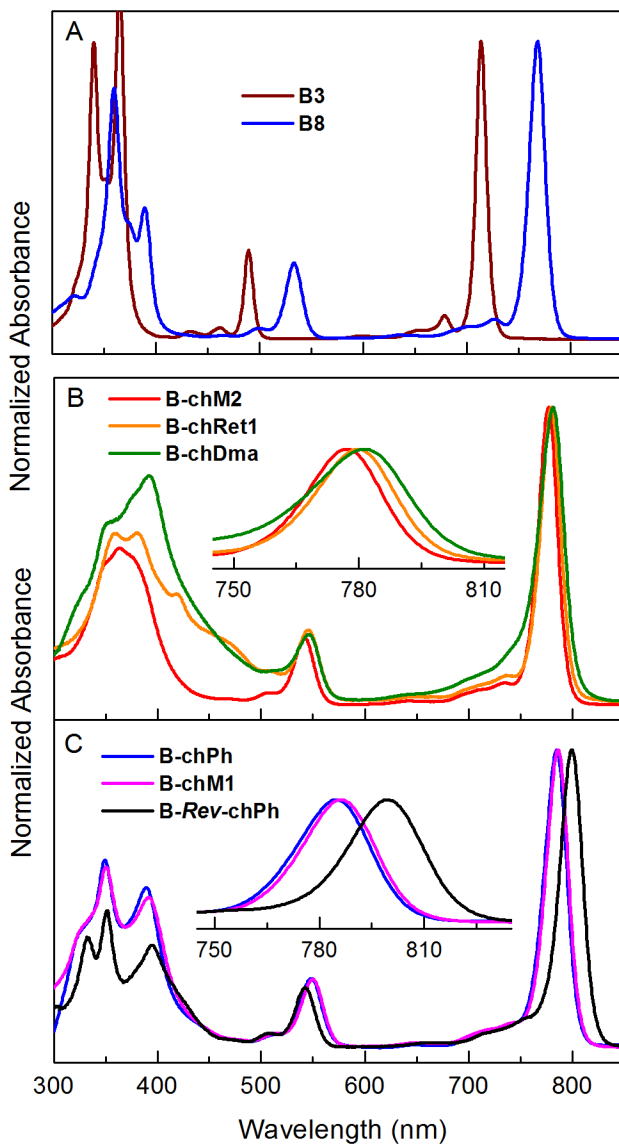


Figure 2. Absorption spectra in toluene at room temperature of reference bacteriochlorins (A) and bacteriochlorin–chalcones (B, C), normalized at the Q_y band. The insets show an expanded view of the Q_y region.

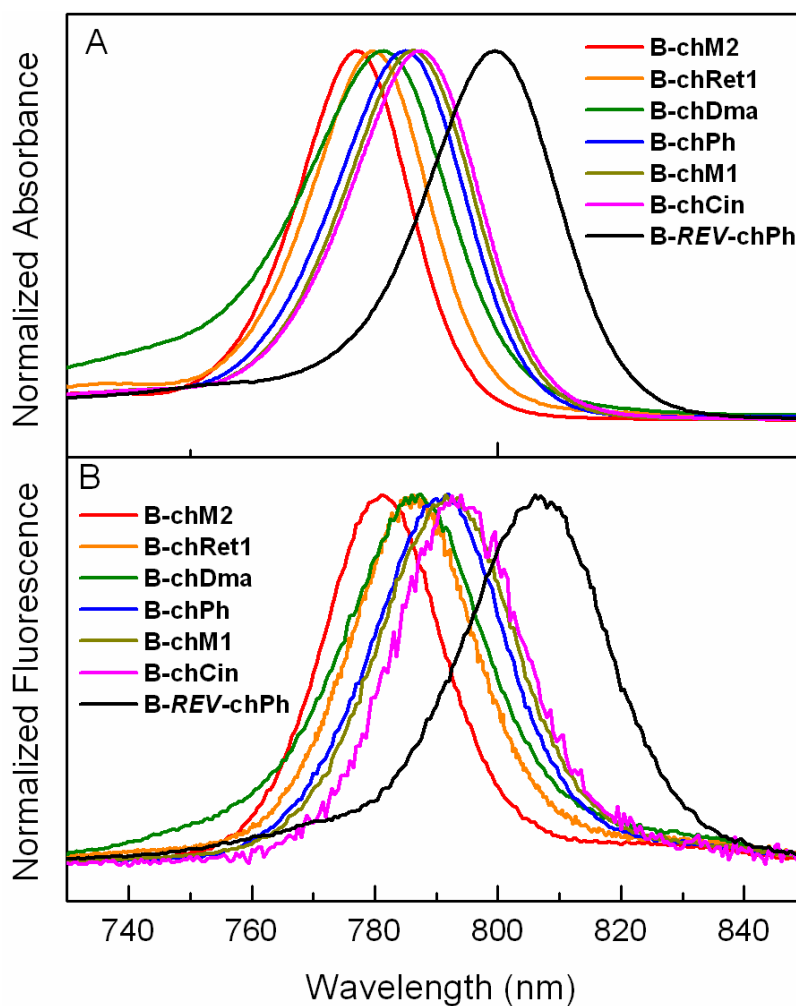


Figure 3. Q_y absorption (A) and fluorescence (B) spectra of the set of bacteriochlorin–chalcones in toluene at room temperature.

tail that contains several partially resolved features that extends into the Q_x region (Figure 2B).

The general similarity of the near-UV spectra of **B-chDma** and **B-chRet1**, and the fact that the spectrum for **B-chRet1** in this region is more complex than might be expected by the simple sum of the absorptions of a retinyl moiety plus an acetyl-containing reference bacteriochlorin (Figure 2B) has implications regarding the nature of the excited states and transitions. In particular, the macrocycle and the retinyl moiety (like the other chalcone substituents) are likely not

independent units but instead possess (higher energy) excited states of mixed parentage that give rise to the complex near-UV absorption spectrum. This point will be explored further below in conjunction with the MO calculations.

The Soret absorption of **B-chM1**, **B-chPh**, and **B-REV-chPh** do not show such a tailing absorption between the normal B and Q_x regions, but show three features (near 330, 350 and 400 nm). Clearly one or more transitions in addition to the nominal B_y and B_x contribute to the near-UV Soret absorption of the bacteriochlorin–chalcones, and the relative positions of all these bands depends on the complex. Such new contributions likely involve excited states that result from electron promotions between orbitals that have electron density on the chalcone substituents (and macrocycle), perhaps with some net charge-transfer (CT) character. Such possibilities (discussed below) make tenuous the assignment of the standard B_y and B_x tetrapyrrole transitions. For this reason, the prominent wavelength maxima (or distinct shoulders) in the Soret region are listed in Table 1 as B₁, B₂ and B₃.

In the way of a specific comparison, Figures 2B and 3A and Table 1 reveal that the Q_y band of the reverse chalcone **B-REV-chPh** is shifted 15 nm to longer wavelength than that of the normal counterpart **B-chPh** (800 versus 785 nm in both toluene and DMSO). The bathochromic shift of the Q_y band in the reverse versus normal bacteriochlorin–chalcone is accompanied by (i) an increase in intensity of the Q_y band relative to the Soret absorption and (ii) a small (~5 nm) hypsochromic shift in the Q_x band (Figure 2B). Another specific comparison indicates that the incorporation of one additional double bond in the 3,13-chalcone substituents in **B-chCin** versus **B-chPh** results in only a 2 nm bathochromic shift in the Q_y absorption band (787 versus 785 nm; Table 1).

Table 1. Spectral properties of bacteriochlorins.^a

<i>Cmpd</i>	Solvent	B ₁ abs (nm)	B ₂ abs (nm)	B ₃ abs (nm)	Q _x abs (nm)	Q _y abs (nm)	Q _y abs FWHM (nm)	I _{Q_y} / I _{B_m} ax	Q _y em (nm)	Q _y em FWHM (nm)
B3^b	Toluene	340	365		489	713	12	0.8	716	16
B8^b	Toluene	360	389		533	768	19	1.1	771	20
B-chRsc^c	MeOH	346	388	325	544	781	20	1.6	795	27
B-chM1	Toluene	350	391	330	550	786	25	1.6	792	26
	DSMO	350	391	330	546	787	31	1.3	798	33
B-chM2	Toluene	350	363	380	542	777	22	1.9	781	23
	DMSO	350	365	380	538	778	28	1.4	787	29
B-chDma	Toluene	355	391		547	782	29	1.3	787	28
B-chPh	Toluene	350	388	330	549	785	26	1.5	791	25
	DMSO	349	389	330	546	785	31	1.3	798	33
B-chCin	Toluene	354	399	336	550	787	26	1.4	794	26
	DMSO	353	400	336	548	787	32	1.1	798	34
B-REV-chPh	Toluene	350	394	332	542	800	26	2.1	808	28
	DMSO	353	396	333	542	800	33	1.5	813	34
B-chRet1	Toluene	360	381	420	545	780	23	1.7	786	24
	DMSO	361	378	419	543	780	29	1.5	790	32
B-chRet2	Toluene	352	378	420	555	792	34	0.5	796	30
	DMSO	351	379	421	551	790	38	0.4	802	38

^a Data acquired at room temperature. “sh” = shoulder. ^b From ref 17. ^c From ref 43.

Fluorescence spectra

The fluorescence spectrum of each bacteriochlorin–chalcone is dominated by the Q_y origin band. For most compounds, the Q_y fluorescence maximum is 4–7 nm to longer wavelength in DMSO than in toluene, although the Q_y absorption maximum for each complex is the same to within 1 nm in the two media. Relative to the Q_y absorption maximum (Figure 3A), the Q_y emission feature (Figure 3B) lies on the average 6 nm to longer wavelength (90 cm^{-1} to lower energy) in toluene and 10 nm to longer wavelength (160 cm^{-1} to lower energy) in DMSO. The Q_y fluorescence bands have a FWHM in the range 23–30 nm (26 nm average) in toluene and 27–38 nm (33 nm average) in DMSO, similar to the Q_y absorption band (Table 1). The FWHM of fluorescence band of the bacteriochlorin–chalcones is modestly greater than the value of 21 nm for ~20 simpler (non-chalcone) 3,13-substituted bacteriochlorins studied previously¹⁷, which have the Q_y emission feature at shorter wavelength.

Fluorescence quantum yields

The fluorescence quantum yields (Φ_f) of several bacteriochlorin–chalcones (**B-chM1**, **B-chM2**, **B-chDma**, **B-chPh** and **B-chCin**) and reverse chalcone **B-REV-chPh** are in the range 0.07–0.11 in toluene and DMSO, with an average value of 0.09 (Table 2). These values are smaller than the average Φ_f of 0.15 reported for the set of ~20 bacteriochlorins (in toluene) bearing simple 3,13 substituents (e.g., acetyl, formyl, ester, phenyl).¹⁷ The Φ_f values for bacteriochlorin–chalcones **B-chM1**, **B-chM2**, and **B-chDma** are effectively the same in DMSO versus toluene. Bacteriochlorin **B-chPh** indicates a ~30% reduction in Φ_f in DMSO versus toluene (0.08 versus 0.11). Similarly, cinnamyl derivative **B-chCin** (one additional double bond in the chalcone substituents) has an apparent ~20% reduction in Φ_f in DMSO versus toluene

(0.09 versus 0.11). A more prominent (about two-fold) reduction in Φ_f in DMSO versus toluene (0.05 versus 0.11) is observed for 13-retinyl-containing **B-chRet1**.

The fluorescence spectra shown in Figure 3B were generally obtained using at least three different excitation wavelengths across the Soret region (345–435 nm) to encompass the main spectral features and ensure that the same emission shape was obtained for each bacteriochlorin as was the case. The fluorescence yields obtained using the different excitation wavelengths were generally the same to within the experimental uncertainty. Because the different absorption features may arise from excited states that have variations in macrocycle-substituent character, these observations suggest that, independent of parentage, the energy flows in high yield to the lowest singlet excited state of the bacteriochlorin macrocycle, from which fluorescence occurs. This finding includes the retinyl-containing bacteriochlorin **B-chRet1**, which has the most extended chalcone substituent. For the latter complex, the Φ_f values in both toluene and DMSO are the same using Q_x and Soret excitation.

Singlet excited-state decay characteristics

The singlet excited-state lifetimes (τ_S) were measured by fluorescence decay (and are consistent with transient-absorption time profiles). The values for several bacteriochlorin–chalcones (**B-chM1**, **B-chM2**, **B-chDma**, and **B-chPh**) and reverse chalcone **B-REV-chPh** are in the range 2.2–2.6 ns in toluene and DMSO, with an average value of 2.5 ns (Table 2). These values are shorter than the average τ_S of 3.9 ns reported for the set of ~20 simpler (non-chalcone) 3,13-substituted bacteriochlorins.¹⁷ For several bacteriochlorin–chalcones (**B-chM1**, **B-chM2**, **B-chDma**, **B-chPh** and **B-chCin**) and reverse chalcone **B-REV-chPh**, the τ_S value is ~10% smaller in DMSO versus toluene (e.g., 2.3 ns in DMSO versus 2.5 ns in toluene for **B-chPh**). The

reduction in excited-state lifetime in a polar versus nonpolar medium is even more pronounced for the mono-retinyl–bacteriochlorin **B-chRet1** (1.5 ns in DMSO versus 2.6 ns in toluene); the approximately two-fold reduction in τ_S parallels the reduction in Φ_f noted above.

The enhanced excited-state decay of **B-chRet1** in DMSO versus toluene was explored further using the transient absorption studies using a ~ 100 fs excitation pulse (780 nm) and probing to 7.5 ns after the flash. Figure 4 shows that in both toluene and DMSO there is a smooth decay of the excited singlet state (1 ps spectrum) to form the excited triplet state (7 ns spectrum) along with ground-state recovery. There is no clear indication of any intermediates such as CT excited states along competitive decay of the singlet excited state to the ground state in DMSO. Nonetheless such states could contribute to the shorter τ_S in the polar solvent without being sufficiently populated to easily observe or could contribute directly to the singlet excited state by mixing with the normal (π, π^*) electronic configurations of the bacteriochlorin macrocycle.

Table 2. Photophysical properties of bacteriochlorins.^a

<u>Cmpd</u>	Solvent	τ_S (ns)	τ_T (μ s)	Φ_f	Φ_{isc}	Φ_{ic}	k_f^{-1} (ns)	k_{isc}^{-1} (ns)	k_{ic}^{-1} (ns)
B3^b	toluene	4.0	169	0.14	0.62	0.24	29	6.5	17
B8^b	toluene	2.9	55	0.11	0.49	0.40	26	5.9	7.3
B-chRsc^c	MeOH	3.4	78	0.02	0.66	0.32	170	5.2	10.6
B-chM1	toluene	2.4	54	0.08	0.44	0.48	30	5.5	5.0
	DSMO	2.2		0.07	0.42	0.51	31	5.2	4.3
B-chM2	toluene	2.6	72	0.08	0.60	0.32	33	4.3	8.1
	DMSO	2.6		0.07			38		
B-chDma	toluene	2.2	64	0.10	0.50	0.40	22	4.4	5.5
B-chPh	toluene	2.5	58	0.11	0.49	0.40	23	5.1	6.3
	DMSO	2.3		0.08	0.45	0.47	29	5.1	4.9
B-chCin	toluene	2.4		0.10	0.41	0.49	24	5.9	4.9
	DMSO	2.2		0.09	0.37	0.54	24	5.9	4.1
B-REV-chPh	toluene	2.4	51	0.08	0.44	0.48	30	5.5	5.0
	DMSO	2.2		0.08					
B-chRet1	toluene	2.6	65	0.11	0.48	0.41	24	5.4	6.3
	DMSO	1.5		0.05	0.36	0.59	30	4.2	2.5

^aData acquired at room temperature in Ar-purged solutions. The experimental error is ± 0.01 for the Φ_f values, ± 0.07 for Φ_{isc} values, and ± 0.1 ns for τ_S values. Triplet lifetimes were determined in tetrahydrofuran or 2-methyltetrahydrofuran. ^bFrom ref 17. ^cFrom ref 43.

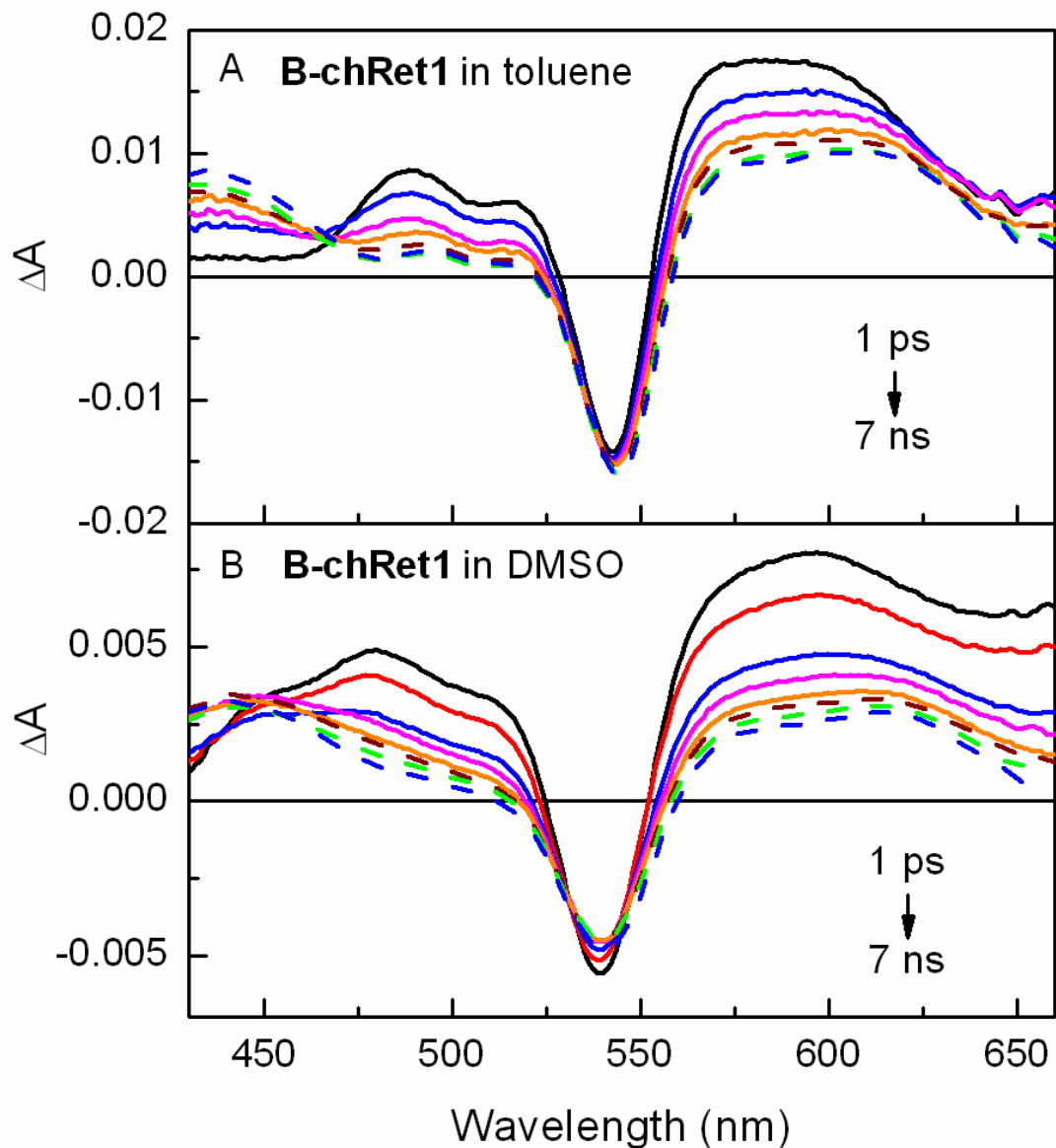


Figure 4. Transient absorption difference spectra obtained following excitation of bacteriochlorin **B-chRet1** in toluene (A) and DMSO (B) with a 120-fs excitation flash at 780 nm.

Triplet excited-state quantum yields and lifetimes

The yield of intersystem crossing from the lowest singlet to triplet excited state (Φ_{isc}), also commonly called the triplet yield (Φ_T), of each of several bacteriochlorin–chalcones (**B-chM1**, **B-chM2**, **B-chDma**, **B-chPh** and **B-chCin**) and reverse chalcone **B-REV-chPh** in

toluene is in the range 0.41–0.62 with average value of 0.48. This value is slightly lower than the average value of 0.53 for ~20 analogs bearing simple 3,13-substituents studied in toluene.¹⁷ A subgroup of the same bacteriochlorin–chalcones (**B-chM1**, **B-chPh** and **B-chCin**) in DMSO have Φ_{isc} values in the range 0.37 to 0.42 with an average value of 0.41. In particular, although within experimental uncertainty, there is consistently a ~10% lower intersystem crossing yield for the same bacteriochlorin–chalcones in DMSO versus toluene (e.g., 0.45 vs 0.49 for **B-chPh** and 0.37 versus 0.41 for **B-chCin**). The effect is greater for retinyl–bacteriochlorin **B-chRet1**, wherein Φ_{isc} drops from 0.48 in toluene to 0.36 in DMSO. These solvent effects on Φ_{isc} generally parallel reductions in τ_S values and therefore derive from the solvent dependence not of the intersystem crossing rate constant but of that for internal conversion (vide infra).

The lifetime of the lowest triplet excited state of select bacteriochlorin–chalcones (in deoxygenated THF or 2-MeTHF) was measured at room temperature using transient absorption spectroscopy. The τ_T values are in the range 51–78 μs with an average of 61 μs . These values are somewhat lower than those results found previously for a large set of bacteriochlorins bearing simple 3,13-substituents, in which the τ_T values were found to be in the range 46–190 μs with an average of 90 μs . Shorter triplet lifetimes are expected as the energy of the lowest triplet excited state moves to lower energy (in parallel with the energy of the lowest singlet excited state; Table 1). This expectation derives from the energy gap law for nonradiative decay.⁴³

Singlet excited-state decay rate constants

The observables τ_S , Φ_f , and Φ_{isc} (Table 2) for decay of the lowest-energy singlet excited state (S_1) are connected to the rate constants for $S_1 \rightarrow S_0$ spontaneous fluorescence (k_f), $S_1 \rightarrow S_0$ internal conversion (k_{ic}), and $S_1 \rightarrow T_1$ intersystem crossing (k_{isc}) via Eqs. (1) to (3).

$$\tau_S = (k_f + k_{ic} + k_{isc})^{-1} \quad (1)$$

$$\Phi_f = k_f / (k_f + k_{ic} + k_{isc}) \quad (2)$$

$$\Phi_{isc} = k_{isc} / (k_f + k_{ic} + k_{isc}) \quad (3)$$

The internal conversion yield can be calculated from Eq. (4).

$$\Phi_{ic} = 1 - \Phi_f - \Phi_{isc} \quad (4)$$

The radiative, intersystem-crossing, and internal-conversion rate constants can be calculated from the above quantities via Eq. (5), where $i = f, isc$ or ic .

$$k_i = \Phi_i / \tau_S \quad (5)$$

The Φ_{ic} , k_f , k_{isc} , and k_{ic} values obtained using Eqs. (3) to (5), along with the measured values of τ_S , Φ_f , Φ_{isc} for the bacteriochlorins are collected in Table 2.

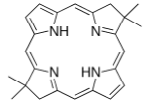
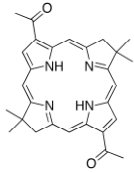
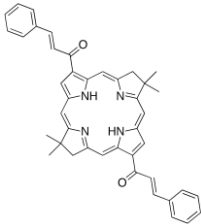
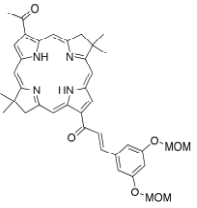
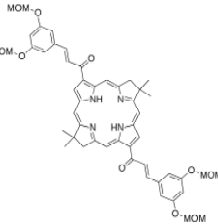
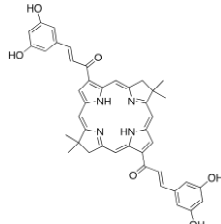
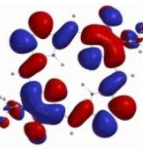
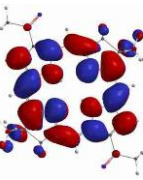
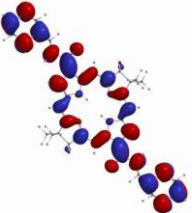
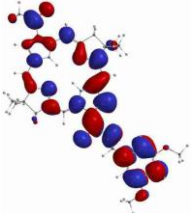
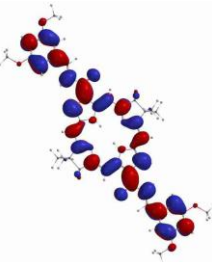
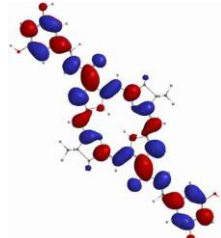
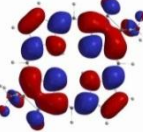
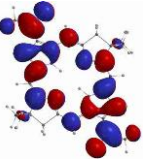
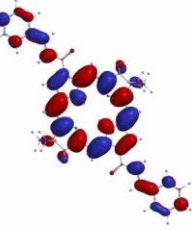
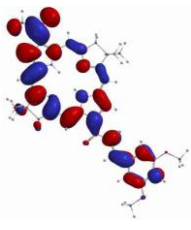
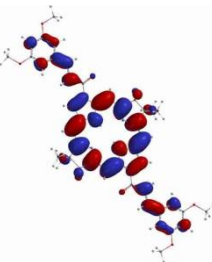
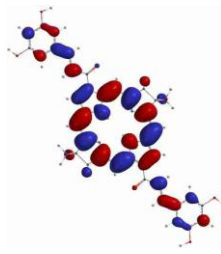
Molecular-orbital characteristics

The energies and electron-density distributions of the frontier MOs of the bacteriochlorin–chalcones (standard, reverse, extended) and reference bacteriochlorins [unsubstituted parent (**B3**) and 3,13-diacetyl complex (**B8**)] were obtained from density functional theory (DFT) calculations. Figures 5–8 show the electron-density maps and energies of the MOs spanning HOMO-5 to LUMO+4. The MO energies for all the bacteriochlorins are collected in Table 3 to facilitate comparisons.

Time-dependent DFT (TDDFT) calculations were also performed. These calculations (at the B3LYP/6-31G* level) were not used as predictors of the exact energies/wavelengths or oscillator strengths of the features spanning the near-UV to NIR absorption spectrum of the bacteriochlorins. In particular, the calculations underestimate the energies of the electronic states responsible for the main transitions by amounts typically in the range 0.2–0.6 eV. In addition, while the relative oscillator strengths of the Soret (B), Q_x and Q_y features are predicted

reasonably well for some of the bacteriochlorins, this is not true in all cases including the structurally least complex parent bacteriochlorin (**B3**). For this molecule, the predicted Q_y/B intensity ratio is off ~10-fold.

Owing to the above considerations, the TDDFT calculations were utilized qualitatively for aiding in the understanding of the likely one-electron promotions that comprise the Q_y excited state, the Q_x excited state, and the higher-energy excited states that give rise to the more complex Soret-region absorption of the bacteriochlorin–chalcones compared with the simpler bacteriochlorins. The contributors to the excited-states that are likely responsible for near-UV (Soret, B) and NIR (Q_y) absorption of the bacteriochlorin–chalcones are generally apparent via inspection of the MOs that are in energy proximity to the standard frontier MOs of simple bacteriochlorins (the MO set that underlies the four-orbital model described below). The TDDFT calculations generally identify the same contributors to the excited-state compositions. Together the MO characteristics and TDDFT predictions afford a self-consistent assessment of the physical basis for key differences and similarities in the optical properties and some photophysical characteristics of the bacteriochlorin–chalcones versus analogs that bear simple substituents at the same 3,13-positions of the macrocycle.

Cmpd	B3	B8	B-chPh	B-chM1	B-chM2	B-chRsc
Structure						
LUMO+4						
	+1.57	+0.63	-0.32	+0.67	-0.18	-0.25
LUMO+3						
	+0.96	-0.40	-1.05	-0.68	-0.98	-1.03

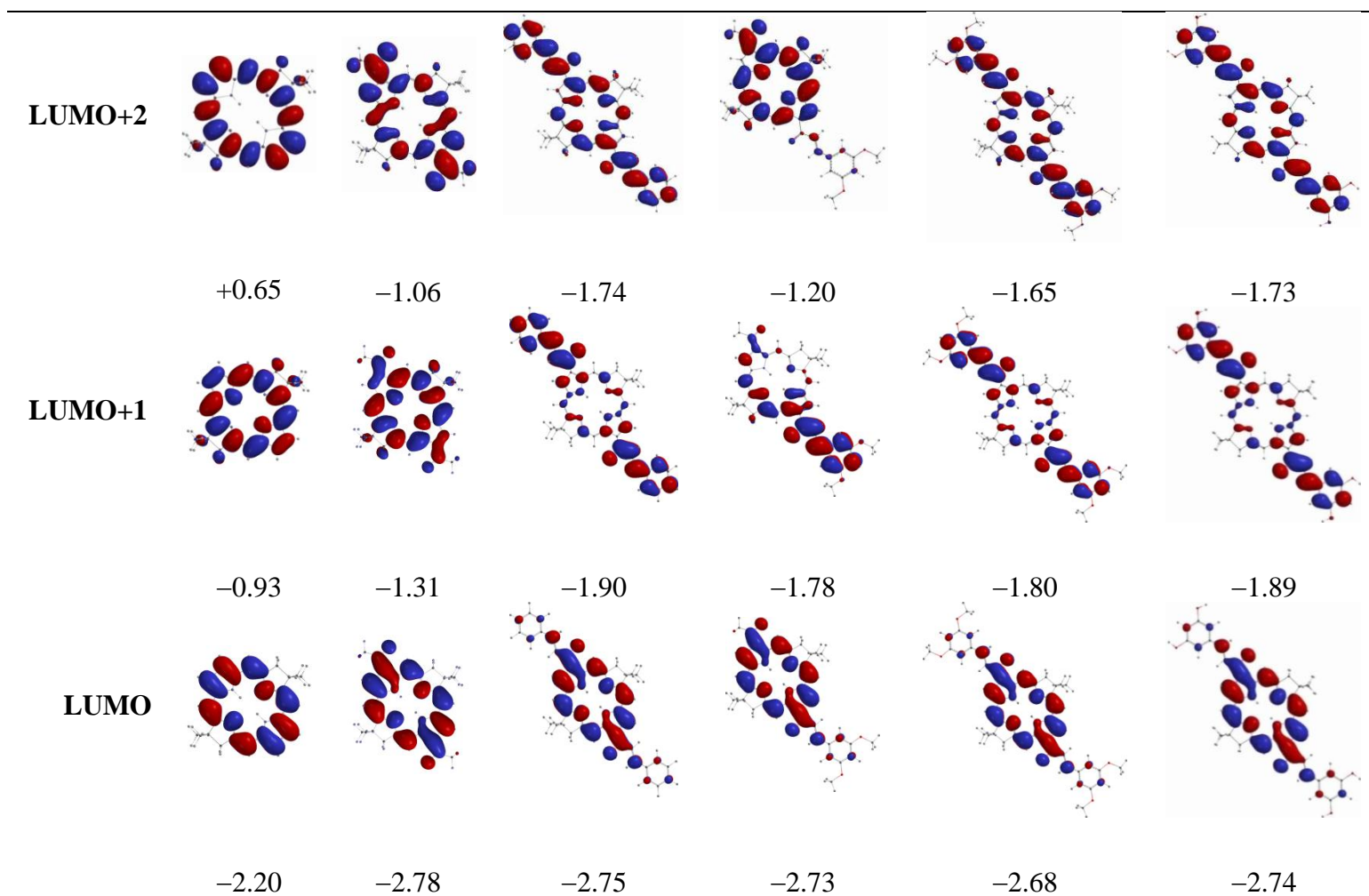
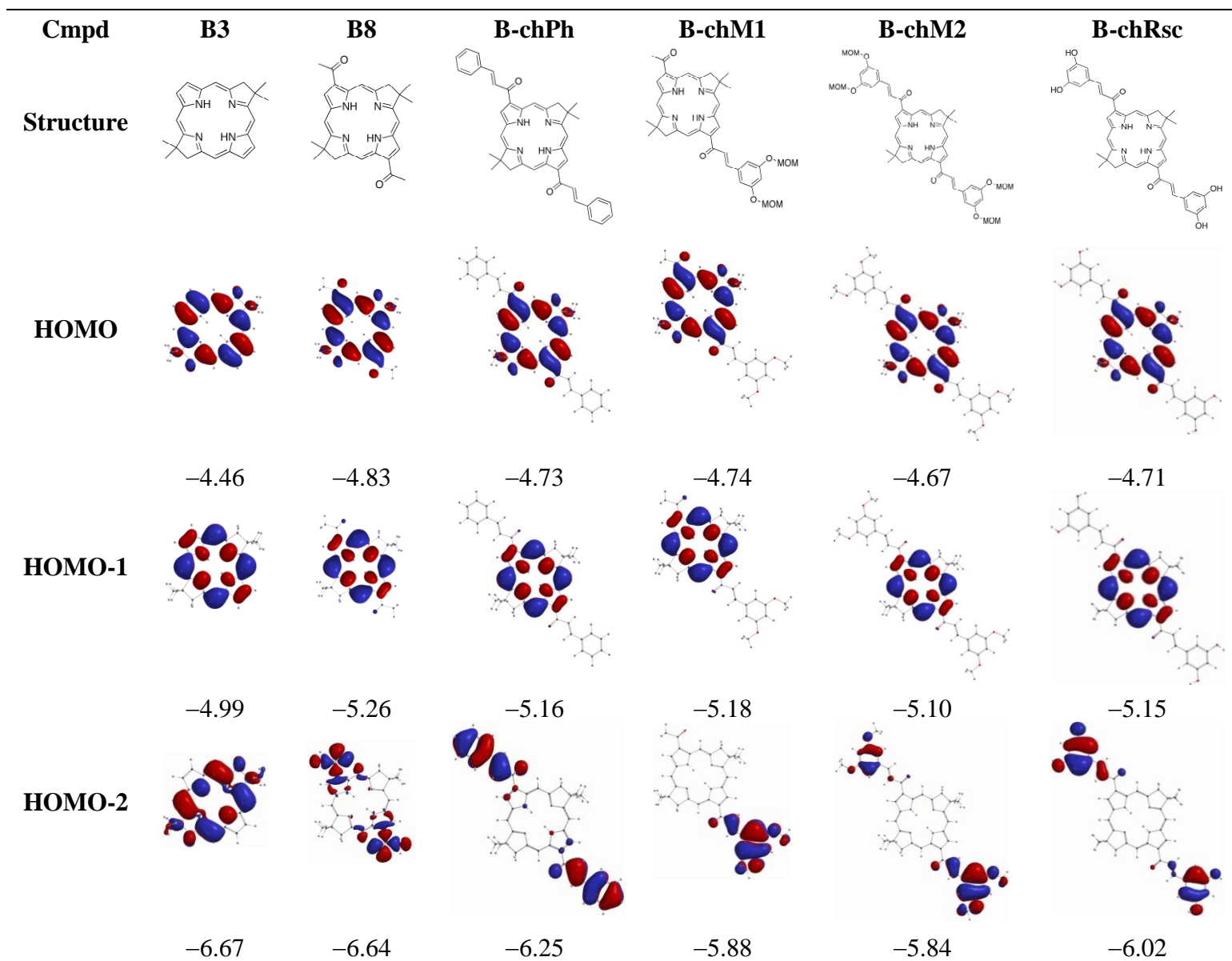


Figure 5. Characteristics of the five lowest unoccupied molecular orbitals of bacteriochlorins. The DFT calculations for **B-chM1** and **B-chM2** used $-\text{OCH}_3$ rather than $-\text{OCH}_2\text{OCH}_3$ (OMOM). The orbitals with energies indicated in red have the closest electron-density distributions to the normal macrocycle LUMO and LUMO+1 (see **B3** and **B8**).



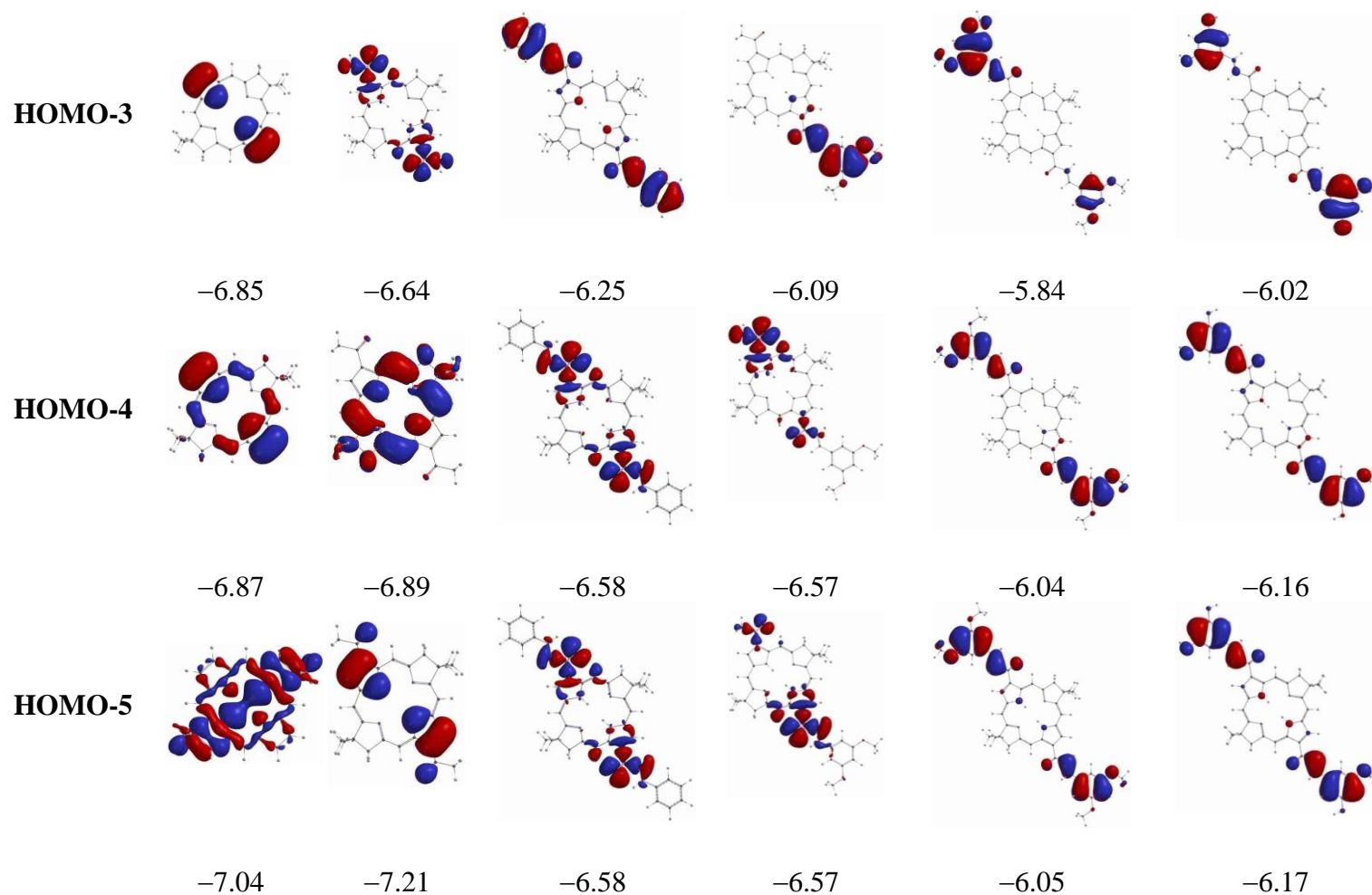
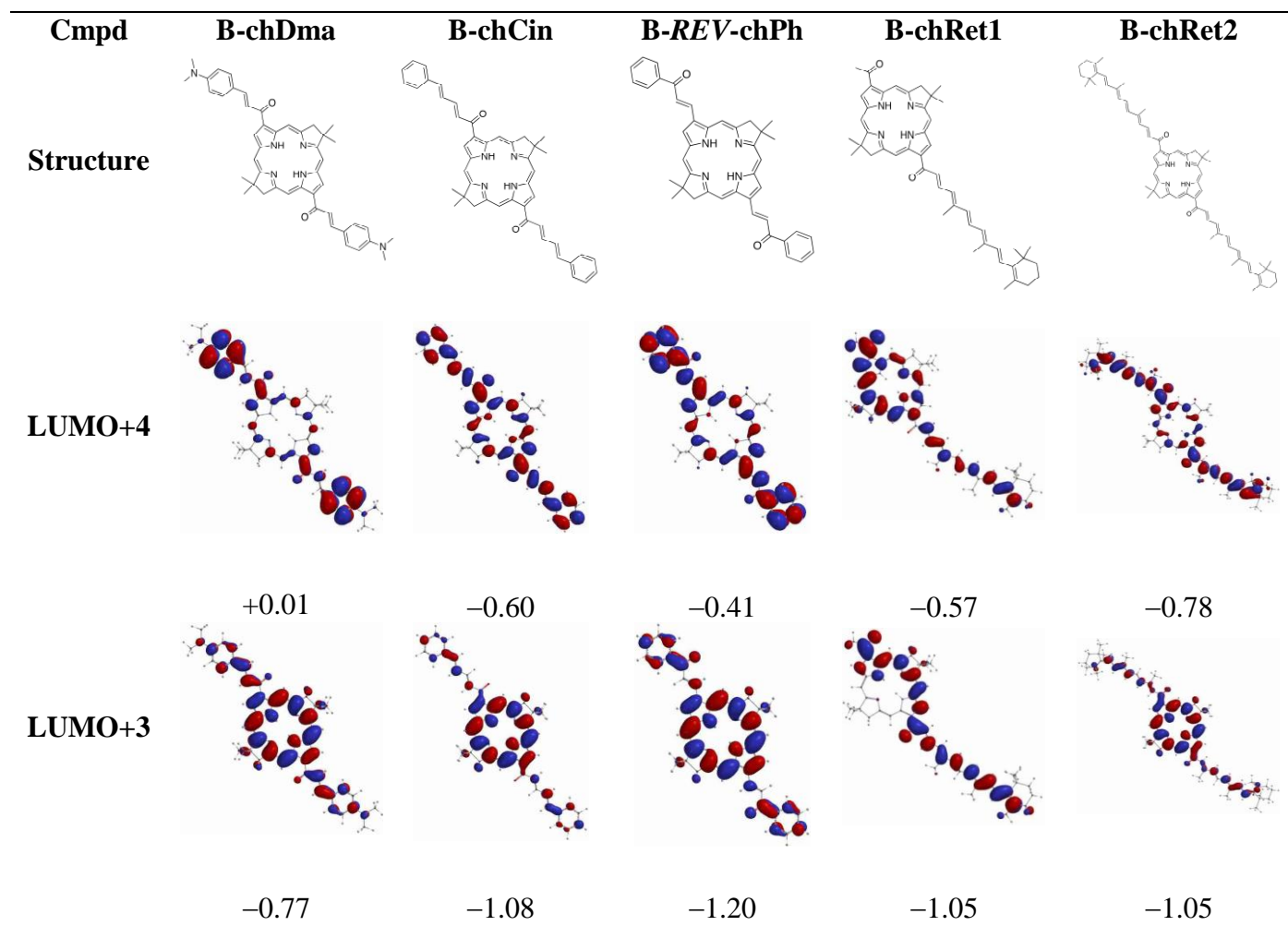


Figure 6. Characteristics of the five highest occupied molecular orbitals of bacteriochlorins. The DFT calculations for **B-chM1** and **B-chM2** used $-\text{OCH}_3$ rather than $-\text{OCH}_2\text{OCH}_3$ (OMOM). The orbitals with energies indicated in red have the closest electron-density distributions to the normal macrocycle HOMO-1 and HOMO (see **B3** and **B8**).



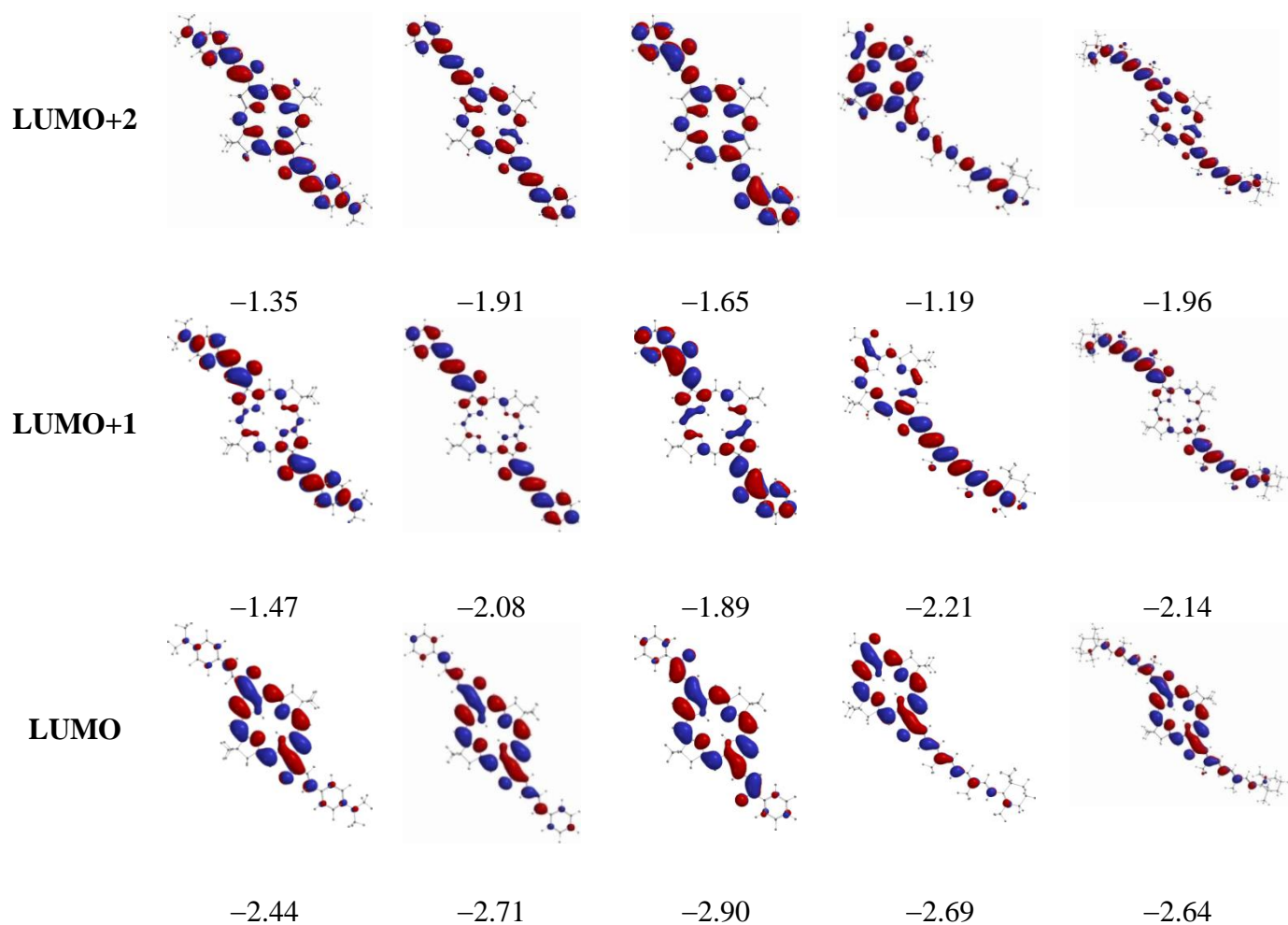
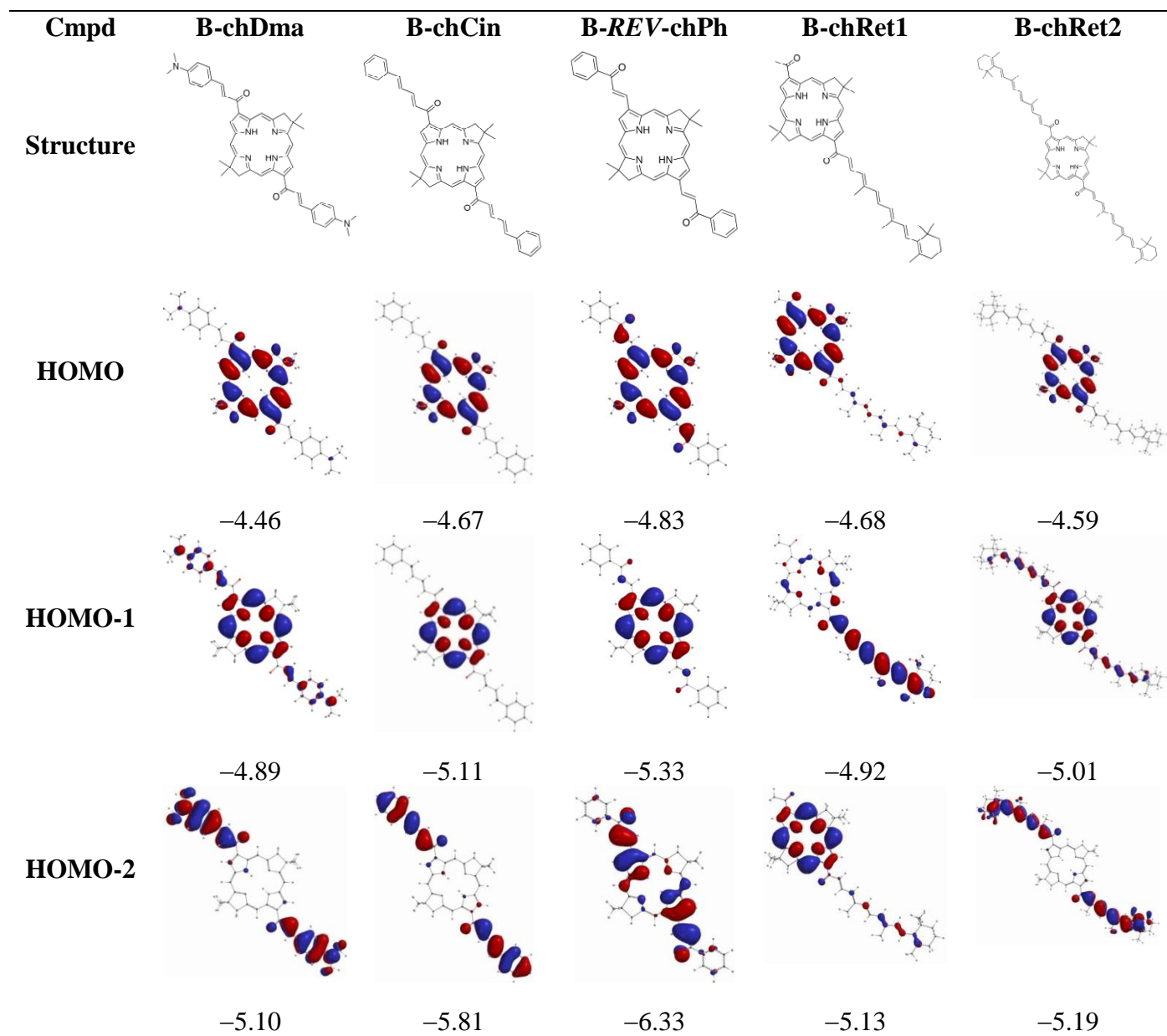


Figure 7. Characteristics of the five lowest unoccupied molecular orbitals of bacteriochlorins. The orbitals with energies indicated in red have the closest electron-density distributions to the normal macrocycle LUMO and LUMO+1 (see **B3** and **B8** of Figure 5).



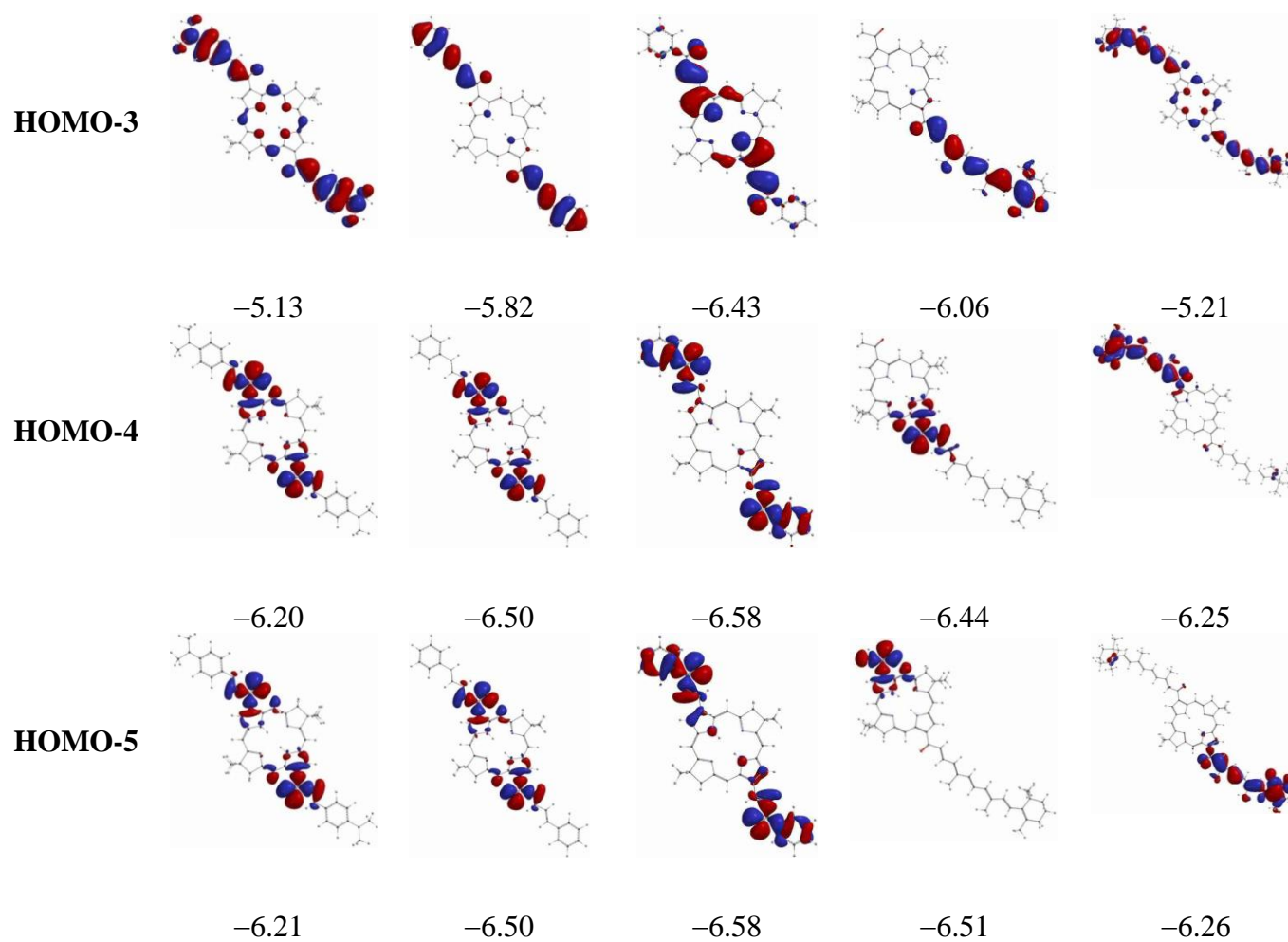


Figure 8. Characteristics of the five highest occupied molecular orbitals of bacteriochlorins. The orbitals with energies indicated in red have the closest electron-density distributions to the normal macrocycle HOMO-1 and HOMO (see **B3** and **B8** of Figure 6).

Table 3. Molecular-orbital energies of bacteriochlorins.^a

Cmpd	HOMO -5	HOMO -4	HOMO -3	HOMO -2	HOMO -1	HOMO	LUMO	LUMO +1	LUMO +2	LUMO +3	LUMO +4	H-L
B3	-7.04	-6.87	-6.85	-6.67	-4.99	-4.46	-2.20	-0.93	+0.65	+0.96	+1.57	2.26
B8	-7.21	-6.89	-6.64	-6.64	-5.26	-4.83	-2.78	-1.31	-1.06	-0.40	+0.63	2.05
B-chRsc	-6.17	-6.16	-6.02	-6.02	-5.15	-4.71	-2.74	-1.89	-1.73	-1.03	-0.25	1.97
B-chM1	-6.57	-6.57	-6.09	-5.88	-5.18	-4.74	-2.73	-1.78	-1.20	-0.68	+0.67	2.01
B-chM2	-6.05	-6.04	-5.84	-5.84	-5.10	-4.67	-2.68	-1.80	-1.65	-0.98	-0.18	1.99
B-chDma	-6.21	-6.20	-5.13	-5.10	-4.89	-4.46	-2.44	-1.47	-1.35	-0.77	+0.01	2.02
B-chPh	-6.58	-6.58	-6.25	-6.25	-5.16	-4.73	-2.75	-1.90	-1.74	-1.05	-0.32	1.98
B-chCin	-6.50	-6.50	-5.82	-5.81	-5.11	-4.67	-2.71	-2.08	-1.91	-1.08	-0.60	1.96
B-REV-chPh	-6.58	-6.58	-6.43	-6.33	-5.33	-4.83	-2.90	-1.89	-1.65	-1.20	-0.41	1.93
B-chRet1	-6.51	-6.44	-6.06	-5.13	-4.92	-4.68	-2.69	-2.21	-1.19	-1.05	-0.57	1.99
B-chRet2	-6.26	-6.25	-5.21	-5.19	-5.01	-4.59	-2.64	-2.14	-1.96	-1.05	-0.78	1.95

^aDFT calculations utilized the structures shown in Charts 1 and 2 except for the following: For **B-chM1** and **B-chM2**, -OCH₃ was used rather than -OCH₂OCH₃ (OMOM) as the terminal group on the chalcone substituent. The orbitals with energies indicated in bold italics have the closest electron-density distributions to the normal macrocycle frontier MOs, which in the four-orbital model are HOMO-1, HOMO, LUMO, and LUMO+1 (see **B3** and **B8**). The last column (H-L) lists the energy gap between the HOMO and LUMO.

Discussion

In the following sections, we first describe the context and rationale for the studies described herein. We then discuss the singlet excited-state properties of the diverse bacteriochlorins. The properties are then interpreted with insights gained from molecular-orbital calculations.

Overview

Our objectives in bacteriochlorin chemistry have been multifold. One goal is to prepare diverse substituted bacteriochlorins and learn how the nature and pattern of substituents alters the spectral and photophysical properties of these NIR absorbing tetrapyrrole chromophores.^{14,15,17–20,24,25} The knowledge gained in so doing should provide insight into the properties of native photosynthetic chromophores, but cannot readily be achieved with the native bacteriochlorophylls given their nearly full complement of substituents. A second and somewhat related goal is to learn how to tune the long-wavelength absorption band across the NIR region. The availability of a palette of such wavelength-tunable bacteriochlorins could be used in diverse studies and applications in solar-energy conversion and in photomedicine. A third goal is to develop a building block toolkit for rapid assembly of multipigment architectures that contain diverse bacteriochlorins. In contrast to the almost bewildering assortment of arrays that contain porphyrins^{44,45}, relatively few (<20) bacteriochlorin-containing arrays have been prepared.⁴⁶

The family of bacteriochlorins examined herein, which contain chalcones, extended chalcones and reverse chalcones figures prominently in each of the aforementioned objectives. The possible roles in tuning spectral properties are apparent; the possible role in a modular building block strategy resides in the fact that all such compounds can be formed via chemistry

that (1) employs basic conditions (to which the bacteriochlorins are stable), and (2) complements the most prevalent methods employed at present, which typically rely on palladium-mediated coupling reactions. Although the precursor bacteriochlorins **B8** and **B9** here were prepared using palladium-mediated reactions, chalcone chemistry may provide general advantages in various approaches to the preparation of tandem conjugates or multipigment arrays. The synthesis of normal chalcones proved substantially more efficient than that of the single reverse chalcone prepared herein. The condensation approach may be most convenient for use with polyenals such as retinal, which is available in multigram quantities yet can be sensitive to handle.⁴⁷ Other approaches to synthetic polyenes of the retinoid or carotenoid family can entail elaborate synthesis.⁴⁸

To our knowledge, only two other types of tetrapyrrole–chalcones have been prepared. One type consists of mono-chalcone analogs of **B-chPh**, **B-chCin**, and **B-chRet2** wherein a synthetic chlorin is employed in lieu of the bacteriochlorin.²⁵ A second type consists of *meso*-tetraarylporphyrins bearing one or four chalcone moieties appended via alkoxy or ester linkages to the *para*-positions of the *meso*-aryl groups.⁴⁹ The porphyrin–chalcones have been examined for cellular uptake, cytotoxicity and phototoxicity. A family of coumarin–chalcones also has been prepared and characterized spectroscopically⁵⁰, and also studied by computation.⁵¹

The inherent color yet relatively small size of chalcones has prompted a large number of synthetic^{35,36}, photophysical^{52–58}, and computational^{33,59–61} studies, predominantly of “push-pull” chalcones. As one relatively recent example, Rurack *et al.* described the synthesis and photophysical characterization of a family of push-pull chalcones of the general form shown in Chart 3.⁵³ Typical electron-donating “push” substituents included *p*-*N,N*-dimethylaniline whereas electron-withdrawing “pull” units included benzothiazole. Unlike the parent chalcone

(benzylideneacetophenone, A = D = phenyl), which absorbs broadly in the UV ($\lambda_{\text{max}} = 312 \text{ nm}$, $\epsilon = 26,700 \text{ M}^{-1}\text{cm}^{-1}$) in 95% ethanol⁶², the push-pull chalcones exhibit absorption in the visible region ($\epsilon \sim 20,000 \text{ M}^{-1}\text{cm}^{-1}$) and, in polar solvents, a strong Stokes'-shifted emission in the NIR region.⁵³ The *s-cis* configuration of the enone moiety (as displayed in each diagram herein) of the chalcones is believed to be more stable than other configurations.³³ The bacteriochlorin–chalcones examined herein include those with the bacteriochlorin attached directly to the carbonyl moiety (A site, Chart 3) and those attached to the alkene unit (D site) of the chalcone framework.

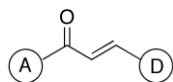


Chart 3. Push-pull chalcone architecture.

A second variation of the chalcone unit concerns extended conjugation of the alkenyl system. Thus, the extended chalcone in **B-chCin** is a conjugated dienone. A benchmark for this auxochrome – (*E,E*)-cinnamylideneacetophenone (derived from condensation of cinnamaldehyde and acetophenone) – is yellow and absorbs broadly with $\lambda_{\text{max}} = 342 \text{ nm}$ ($\epsilon = 39,000 \text{ M}^{-1}\text{cm}^{-1}$) in methanol.^{63,64} The extended chalcones **B-chRet1** and **B-chRet2** are derived by reaction of the visual chromophore retinal with the bacteriochlorin containing an acetyl group. A non-bacteriochlorin analog (**Ret-Ind**), derived from retinal and indan-1,3-dione, is shown in Chart 4.⁶⁵ **Ret-Ind** absorbs strongly in the region near 500 nm and exhibits rapid (multistep depending

on excitation energy/wavelength) excited-state decay to the ground state in < 50 ps with an overall time constant that depends on solvent polarity.⁶⁶

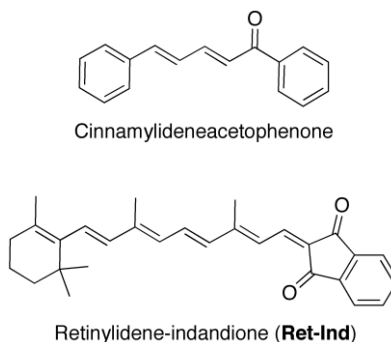


Chart 4. Benchmark extended chalcones.

Pathways and rate constants for decay of the singlet excited-state.

The measured quantities τ_S , Φ_f , and Φ_{isc} for decay of the lowest-energy singlet excited state were used to obtain values for Φ_{ic} and the rate constants for the three decay pathways of the lowest singlet excited state (k_f , k_{isc} and k_{ic}), as described in the Results section. The values for all of these fundamental photophysical properties are collected in Table 2. Here we discuss the excited-state decay rate constants for the bacteriochlorins bearing different types of substituents.

The $S_1 \rightarrow S_0$ radiative rate constants (k_f) for several bacteriochlorin–chalcones (**B-chM1**, **B-chM2**, **B-chDma**, **B-chPh**, **B-chCin**, **B-chRet1**) and reverse chalcone **B-REV-chPh** are in the range $(24 \text{ ns})^{-1}$ to $(38 \text{ ns})^{-1}$. The average value of $(26 \text{ ns})^{-1}$ for these compounds in toluene is effectively the same as the value of $(28 \text{ ns})^{-1}$ obtained in DMSO. These values are comparable to the average value of $(27 \text{ ns})^{-1}$ found previously for bacteriochlorins bearing simple 3,13-substituents.¹⁷

The $S_1 \rightarrow T_1$ intersystem-crossing rate constants for several bacteriochlorin–chalcones (**B-chM1**, **B-chM2**, **B-chDma**, **B-chPh**, **B-chCin**, and **B-chRet1**) and reverse chalcone **B-REV-chPh** are in the range $(4.2 \text{ ns})^{-1}$ to $(5.9 \text{ ns})^{-1}$. There is no systematic difference in the values for a given bacteriochlorin in toluene versus DMSO, except for retinyl–bacteriochlorin **B-chRet1** (Table 2) for which the k_{isc} value appears to modestly increase from $(5.4 \text{ ns})^{-1}$ in toluene to $(4.2 \text{ ns})^{-1}$ in DMSO. The latter effect can be understood if the lowest singlet excited state develops (more) macrocycle \leftrightarrow substituent CT character in the polar versus nonpolar solvent as a result of stabilization of contributing CT excited-state electronic configurations. A modest shift of electron density from the substituent to the macrocycle in the excited state could result in a modest increase in spin-orbit coupling, which underlies the intersystem-crossing process. In this regard, the average k_{isc} value for the 3,13-chalcone-substituted and retinyl–bacteriochlorins of $(5 \text{ ns})^{-1}$ is modestly greater than the value of $(8 \text{ ns})^{-1}$ found previously for the 3,13-substituted bacteriochlorins bearing simple substituents (e.g., acetyl, formyl, phenyl).¹⁷ The possible contribution of such CT character to the excited states is described below in conjunction with the molecular-orbital characteristics.

The third pathway for decay of the lowest singlet excited state is nonradiative internal conversion to the ground state. The rate constants for $S_1 \rightarrow S_0$ internal conversion (k_{ic}) for several bacteriochlorin–chalcones (**B-chM1**, **B-chM2**, **B-chDma**, **B-chPh**, **B-chCin**, and **B-chRet1**) and reverse chalcone **B-REV-chPh** are in the range $(2.4 \text{ ns})^{-1}$ to $(6.3 \text{ ns})^{-1}$. The average value for these compounds in toluene is $(5.9 \text{ ns})^{-1}$ and that in DMSO is $(3.6 \text{ ns})^{-1}$. The difference in average values reflects a systematic reduction in k_{ic} for the compounds in DMSO versus toluene. These differences can be seen in the following comparisons (Table 2): $(4.3 \text{ ns})^{-1}$ versus $(5.0 \text{ ns})^{-1}$ for **B-chM1**, $(4.9 \text{ ns})^{-1}$ versus $(6.3 \text{ ns})^{-1}$ for **B-chPh**, $(4.1 \text{ ns})^{-1}$ versus $(4.9 \text{ ns})^{-1}$ for **B-**

chCin, $(2.4 \text{ ns})^{-1}$ versus $(5.0 \text{ ns})^{-1}$ for **B-REV-chPh**, and $(2.5 \text{ ns})^{-1}$ versus $(6.3 \text{ ns})^{-1}$ for **B-chRet1**.

The solvent effect is greatest for the latter compound, which is the retinyl-substituted bacteriochlorin. Such effects also may be connected with an increase in excited-state CT character in the polar versus nonpolar solvent associated with stabilization of CT configurations and greater mixing with macrocycle (π, π^*) configurations in giving rise to the wavefunction for the lowest singlet excited state. Such CT configurations may enhance nonradiative deactivation by a number of mechanisms. Such mechanisms include solvent-induced displacement of the excited- versus ground-state potential-energy surfaces and enhanced Franck-Condon factors involving the internal molecular coordinates.⁴³ Such involvement of the chalcone or retinyl moiety in the lowest singlet excited state could additionally enhance nonradiative decay via isomerization or other motions of the substituent that alter interactions with the bacteriochlorin macrocycle and thus the excited-state electron-density distribution.

Molecular orbital characteristics and electronic structure

Gouterman's four-orbital model⁶⁷⁻⁶⁹ is a useful framework for understanding the effects of substituents on the optical properties of tetrapyrrole chromophores. We have applied this model to synthetic chlorins^{16,70,71} and bacteriochlorins^{17,24,72} bearing simple substituents (e.g., acetyl, formyl, vinyl, ester, ethynyl, phenyl) in various patterns about the periphery of the macrocycles. All that is required to implement this model are the energies of the four frontier MOs (HOMO-1, HOMO, LUMO, LUMO+1), which can be obtained from DFT calculations. The four-orbital model does not give absolute energies or oscillator strengths of the absorption features, but does well in assessing trends in the relative positions and relative intensities of the main optical features (Q_y , Q_x , B_x , B_y) as a function of substituent types and macrocycle sites.

Here, we use the four-orbital framework to provide a physical basis for understanding the manner in which the chalcone (normal, reverse, extended) substituents affect the absorption spectra and photophysical properties of the bacteriochlorins. As will be seen, these substituents require the consideration of additional MOs beyond the normal four-orbital set. These orbitals may place considerable electron density on the substituents, in addition to the macrocycle, and the excited states resulting from electron promotion may involve shifting of electron density between the macrocycle and the substituents.

Within the four-orbital model, the B_y and Q_y excited states are comprised of linear combinations of the (y-polarized) electronic configurations that result from HOMO \rightarrow LUMO and HOMO-1 \rightarrow LUMO+1 one-electron promotions. The B_y state reflects the symmetric combination and the Q_y state the antisymmetric combination of the configurations. For porphyrins, the B_y and B_x states have roughly 50/50 contributions of the HOMO \rightarrow LUMO and HOMO-1 \rightarrow LUMO+1 configurations. The respective constructive versus destructive interference of the two associated transition dipole moments (which have comparable strength) results in a strong B_y band in the near-UV (390–430 nm) region a very weak Q_y band in the visible (500–600 nm) region. The reduction of one pyrrole ring in chlorins and a second pyrrole ring in bacteriochlorins progressively and predominantly increases the energy of one of the two filled orbitals (the original porphyrin HOMO or HOMO-1) and the energy of one of the two unfilled orbitals (the original porphyrin LUMO or LUMO+1). Consequently, for bacteriochlorins, the Q_y state has primarily (70–90% based on TDDFT calculations) the character of the HOMO \rightarrow LUMO configuration (and 10–30% HOMO-1 \rightarrow LUMO+1) and vice versa for B_y . In parallel, the Q_y band moves to lower energy and gains intensity at the expense of the B_y band.

The excited states B_x and Q_x are similarly derived (within the four-orbital model) from configurations resulting from the (x-polarized) one-electron promotions $\text{HOMO} \rightarrow \text{LUMO}+1$ and $\text{HOMO}-1 \rightarrow \text{LUMO}$. Again, for porphyrins the B_x and Q_x states have roughly equal contributions of the two electronic configurations, resulting in strong B_x and weak Q_x bands that are in the same spectral region as (and may substantially overlap) the Q_y and B_x bands depending on the porphyrin and its metalation state. However, unlike the y-polarized states, upon progressing to chlorin and then to bacteriochlorin the energies (spectral positions) and intensities of the B_x and Q_x bands are expected to be far less affected (by pyrrole-ring reduction). Consequently in bacteriochlorins the large spectral splitting of the B_y and Q_y (compared to chlorins or porphyrins) generally causes these two bands to spectrally sandwich the less perturbed B_x and Q_x pair. Thus, the spectrum of a typical bacteriochlorin has four main features that in progressing from higher to lower energy are B_y , B_x , Q_x and Q_y , with the Q_y band in the NIR spectral region (Figure 1).

Description of the effects of the incorporation of simple 3,13-acetyl groups within the four-orbital approach will serve as a backdrop for examining the effects of 3,13-chalcone groups. The HOMO-1, HOMO, LUMO and LUMO+1 orbitals of the unsubstituted parent **B3** are shifted by 0.27–0.58 eV to more negative values upon incorporation of 3,13-acetyl groups in **B8** (Figures 5 and 6 and Table 3). Electron density resides on the acetyl groups to a different degree depending on the orbital for **B8**, but the distribution on the macrocycle in each orbital is quite similar to that in the parent **B3**. For **B8** the least electron density resides on the acetyl groups in HOMO-1 and the most in LUMO. The LUMO is stabilized the most of the four frontier MOs by addition of the 3,13-acetyl groups, resulting in a diminution of the HOMO – LUMO energy gap (Table 3) and a bathochromic shift in the Q_y band (Table 1 and Figure 9). The Q_y spectral shift

occurs because within the four-orbital model the HOMO \rightarrow LUMO is the major contributor to the Q_y excited state (with a lesser contribution from HOMO-1 \rightarrow LUMO+1). The TDDFT calculations support this picture, in which the Q_y state is calculated to be comprised primarily ($\geq 75\%$) HOMO \rightarrow LUMO and most of the remaining being HOMO-1 \rightarrow LUMO+1 for both **B3** and **B8**. Similarly, TDDFT indicates that the B_y excited state has more HOMO-1 \rightarrow LUMO+1 than HOMO \rightarrow LUMO character (consistent with the four-orbital model) along with other configurations that involve lower energy filled orbitals and/or higher energy unoccupied orbitals. These latter orbitals for **B8** have electron density on the acetyl groups (and the macrocycle). For **B3** and **B8**, the TDDFT calculations also indicate (consistent with the four-orbital model) that the Q_x state has $>90\%$ total contribution from HOMO-1 \rightarrow LUMO and HOMO \rightarrow LUMO+1. The B_x state also has substantial contribution of the same two contributions and for **B8** additional contributions of one-electron promotions between orbitals that have electron density on both the macrocycle and the acetyl groups. The result is that these two reference compounds have prototypical bacteriochlorin absorption spectra (Figure 1 and Table 1).

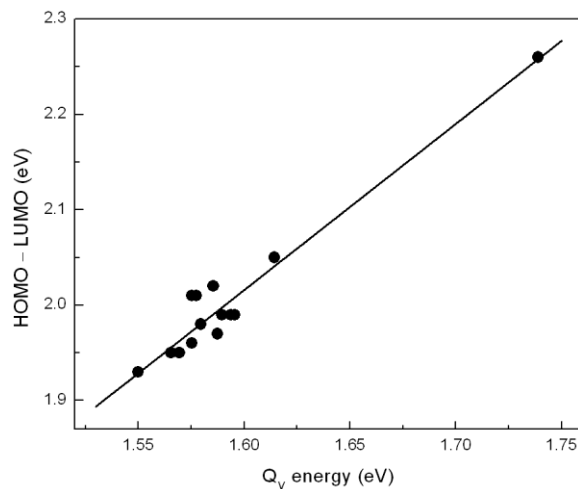


Figure 9. HOMO – LUMO energy gap versus the absorption energy of the Q_y origin band. Data are shown for compounds both in toluene and DMSO where spectra were measured in the two solvents (Table 1). The solid line is a fit to all the data.

The electron-density maps (Figures 5–8) for the normal bacteriochlorin–chalcones (**B-chPh**, **B-chM1**, **B-chM2**, **B-chRsc**, **B-chDMA**), reverse chalcone (**B-REV-chPh**) and modestly extended chalcone (**B-chCin**) generally show similar characteristics to each other. Similarities and significant differences exist for the greatly extended retinyl-containing bacteriochlorin–chalcones (**B-chRet1** and **B-chRet2**). The key points are as follows:

1. The HOMO and LUMO orbitals of the various bacteriochlorin–chalcones retain overall similar electron-density distributions on the macrocycle as in the reference compounds (**B3** and **B8**), but with electron density now residing on the substituents, much more so for the LUMO than the HOMO. The HOMO-1 orbitals of the bacteriochlorin–chalcones place little electron density on the substituents, just like reference bacteriochlorins **B3** and **B8**. Such considerations are relevant to potential shifting of electron density between macrocycle and

substituent as a result of one-electron promotions from HOMO or HOMO-1 to unoccupied MOs that have substantial chalcone-substituent character.

2. The LUMO is generally stabilized by the substituents more than the HOMO, resulting in a decrease in the HOMO – LUMO gap to an extent that depends on the bacteriochlorin (Table 3). The HOMO – LUMO gap for bacteriochlorins bearing 3,13-chalcone groups (like simple substituents) tracks the position of the Q_y absorption band (Figure 9). Again, this correlation follows because the Q_y state is expected to contain substantial HOMO \rightarrow LUMO character (within the four-orbital model). Indeed, the TDDFT calculations indicate the Q_y state for most of the bacteriochlorin–chalcones has predominantly ($\geq 75\%$) HOMO \rightarrow LUMO character.

3. The unoccupied orbitals LUMO+1 to LUMO+4 of the bacteriochlorin–chalcones are basically combinations of the normal macrocycle LUMO+1 (for **B3** or **B8**) and orbitals that have electron density spread across the chalcone substituent. Of this set (LUMO+1 to LUMO+4), the MO that has the most electron density on the macrocycle and the least on the substituents (and thus is closest in characteristics to the normal macrocycle LUMO+1) is now LUMO+3. The exception is **B-chM1**, for which this orbital is LUMO+2. Accordingly, the Soret-region absorption spectrum for the bacteriochlorin–chalcones is expected to be more complex than normal, given that for simple bacteriochlorins the B_y transition (typically the highest-energy of the main Soret-region features) in the four-orbital model has primarily HOMO-1 \rightarrow LUMO+1 character, and the B_x transition (typically the lower energy of the main Soret-region features) has substantial HOMO \rightarrow LUMO+1 character (along with substantial HOMO-1 to LUMO character). The near-UV spectrum is expected to have contributions from excited states derived in part from electron promotions from HOMO-1 and HOMO (and/or lower filled orbitals) to one or more of

the filled orbitals in the LUMO+1 to LUMO+4 set. The contribution closest to HOMO-1 \rightarrow LUMO+1 of the simple bacteriochlorins will be HOMO-1 \rightarrow LUMO+3 for most bacteriochlorin–chalcones. The TDDFT calculations indicate that some of the contributions derive from electron promotions involving filled orbitals down in energy to at least HOMO-5 and unoccupied orbitals up in energy to LUMO+4. The resulting mixed-parentage transitions often have mixed x and y polarization. Some states/transitions may have net CT character in shifting electron density between macrocycle and chalcone substituent. This analysis gives a physical basis for the more complex, multi-featured near-UV Soret-region absorption spectra of the bacteriochlorin–chalcones (Figure 2) than for bacteriochlorins that bear simple substituents (Figure 1). For these new NIR-absorbing compounds, the additional absorption transitions incorporated in the near-UV Soret region can be viewed as beneficial to the overall light-harvesting capacity.

4. The TDDFT calculations on the normal, reverse and modestly extended (cinnamyl) bacteriochlorin–chalcones indicate small (generally <10%) contributions to the Q_y excited state of one-electron promotions beyond those expected based on the four-orbital model. Again, the normal four-orbital configurations are expected to be mainly HOMO \rightarrow LUMO and HOMO-1 \rightarrow LUMO+X, where LUMO+X denotes the orbital most closely analogous to the HOMO+1 of the reference bacteriochlorins. The minor non-four-orbital contributions could potentially lend some small net substituent \leftrightarrow macrocycle CT character to the Q_y excited state depending on bacteriochlorin and potentially a mild solvent-polarity dependence of the photophysical properties. However, as noted in the Results section (Table 2), a medium-polarity dependence is not apparent for most normal, reverse and modestly extended (cinnamyl) bacteriochlorin–chalcones, and when seen is only a <15% effect. Thus, in general the bathochromically shifted

(and strong) NIR absorption attained in the synthetic bacteriochlorin–chalcones is not accompanied by significant deleterious or solvent-dependent effects on the lowest singlet excited state (Q_y) and thus the key photophysical properties.

5. For the more extended bacteriochlorin–chalcones (**B-chRet1** and **B-chRet2**), the key characteristics concerning the HOMO and LUMO are noted above for the shorter-chain chalcones. This parallelism includes the correlation of HOMO – LUMO energy gap with Q_y spectral energy/wavelength (Figure 9). **B-chRet1** and **B-chRet2** also share the characteristic noted for the shorter-chain chalcones that the LUMO+1 of reference bacteriochlorins (**B3**, **B8**) is effectively incorporated into four orbitals (LUMO+1 to LUMO+4) that have variations in electron density on the macrocycle (with the reference LUMO+1 density distribution) versus being spread across the chalcone (and retinyl) groups. The unoccupied orbital that is the closest to the normal macrocycle LUMO+1 (with the smallest electron density on the substituents) is LUMO+2 for **B-chRet1** and LUMO+3 for **B-chRet2**. Thus, as in the case of the shorter-chain and reverse bacteriochlorin–chalcones, the Soret region of **B-chRet1** and of **B-chRet2** is more complex than for the reference bacteriochlorins (Figures 1 and 2). The differences again can be understood in terms of one-electron promotions involving molecular orbitals that have various degrees of macrocycle and retinyl character that replace and/or supplement characteristic configurations of the original four-orbital set.

6. For **B-chRet1**, the macrocycle HOMO-1 of reference bacteriochlorins (and the normal, reverse, and slightly extended bacteriochlorin–chalcones) becomes the HOMO-2 for **B-chRet1** (which contains one acetyl and one retinyl group), which also has a small amount of electron density across the retinyl group. The HOMO-1 of **B-chRet1** in contrast has very little electron density on the macrocycle and is dominated by electron density on the retinyl moiety. Thus,

electron promotions from HOMO-1 of **B-chRet1** to filled orbitals that have substantial electron density on the macrocycle have the potential to contribute CT character to the resulting excited states.

7. **B-chRet2** follows a similar picture to that for **B-chRet1** except that the HOMO-1 of **B-chRet2** remains closest to the normal macrocycle HOMO-1 but acquires a modest amount of electron density along the two retinyl groups. The HOMO-2 of **B-chRet2** in contrast has little electron density on the macrocycle and a large amount of electron density on the two retinyl groups, analogous to HOMO-1 of the mono-retinyl analog **B-chRet1**.

8. For the extended chalcone analogs (**B-chRet1** and **B-chRet2**), TDDFT calculations indicate that the primary HOMO \rightarrow LUMO contribution to the Q_y excited state is supplemented by configurations that do not have simple four-orbital-model flavor. Such one-electron promotions (e.g., HOMO-1 \rightarrow LUMO and HOMO \rightarrow LUMO+1 for **B-chRet1**) could impart some macrocycle \leftrightarrow retinyl CT character on the basis of the electron-density distributions noted above (Figures 7 and 8). In this regard, the retinyl-bacteriochlorins are distinct from the numerous, less strongly coupled carotenoid–spacer–tetrapyrrole multads pioneered by the groups of Gust, Moore, and Moore, where the tetrapyrrole consists of a porphyrin⁷³, purpurin⁷⁴, or phthalocyanine.⁷⁵ Inspection of Table 2 indicates that **B-chRet1** has a 2–3-fold shorter rate constant for nonradiative internal conversion (k_{ic}) in toluene compared to the other bacteriochlorin–chalcones, and that this rate constant drops by about 3-fold again in the more polar DMSO. These findings are consistent with enhanced CT character for the Q_y state of **B-chRet1** versus the other bacteriochlorin–chalcones in toluene, with further enhancement in DMSO due to solvent stabilization of the CT configurations and thereby a greater contribution to

the Q_y wavefunction. Collectively, these considerations tie the observed photophysical behavior of **B-chRet1** to the effects of the retinyl substituents on MO characteristics and electronic structure.

In summary, the bacteriochlorin–chalcones described herein are readily synthesized, absorb strongly in the 780–800 nm region, fluoresce with small Stokes shift and quantum yields (Φ_f) in the range 0.05–0.11 and have singlet excited-state lifetimes (τ_s) in the range 1.5–2.6 ns in toluene and DMSO; the spectral features exhibit modest or no sensitivity to solvent polarity. An adequate description of the near-UV (Soret) region absorption requires significant participation of electron promotions between occupied and unoccupied molecular orbitals beyond those in the Gouterman four-orbital model, with some extent of macrocycle \leftrightarrow substituent charge-transfer character in the lowest and higher singlet excited depending on the nature of the chalcone substituent. Accordingly, the bacteriochlorin–chalcones are of fundamental interest for electronic and spectroscopic studies and represent viable architectures for light-harvesting applications, particularly where absorption across the visible and NIR regions is desirable.

Acknowledgments

This work was supported by grants from the Division of Chemical Sciences, Geosciences, and Biosciences, Office of Basic Energy Sciences of the U.S. Department of Energy to D.F.B. (DE-FG02-05ER15660), D.H. (DE-FG02-05ER15661) and J.S.L. (DE-FG02-96ER14632). Mass spectra were obtained at the Mass Spectrometry Laboratory for Biotechnology at North Carolina State University. Partial funding for the facility was obtained from the North Carolina Biotechnology Center and the National Science Foundation. Transient absorption studies were performed in the Ultrafast Laser Facility of the Photosynthetic Antenna Research Center (PARC), an Energy Frontier Research Center funded by the U.S. Department of Energy, Office of Science, Office of Basic Energy Sciences, under Award No. DE-SC0001035.

References

- (A) Yang, E.K; Ruzi , C; Krayner, M; Diers, J.R; Niedzwiedzki,DM; Kirmaier,C; Lindsey, J.S; Bocian, D.F; Holten, D. Photophysical Properties and Electronic Structure of Bacteriochlorin–Chalcones with Extended Near-Infrared Absorption. *Photochem. Photobiol.* 2013. 89. 586-604.
- (1) Agostinis, P., K. Berg, K. A. Cengel, T. H. Foster, A. W. Girotti, S. O. Gollnick, S. M. Hahn, M. R. Hamblin, A. Juzeniene, D. Kessel, M. Korbelik, J. Moan, P. Mroz, D. Nowis, J. Piette, B. C. Wilson and J. Golab (2011) Photodynamic therapy of cancer: An update. *CA Cancer J. Clin.* **61**, 250–281.
- (2) Arnaut, L. G. (2011) Design of porphyrin-based photosensitizers for photodynamic therapy. *Inorg. Photochem.* **63**, 187–233.
- (3) Kee, H. L., R. Nothdurft, C. Muthiah, J. R. Diers, D. Fan, M. Ptaszek, D. F. Bocian, J. S. Lindsey, J. P. Culver and D. Holten (2008) Examination of chlorin–bacteriochlorin energy-transfer dyads as prototypes for near-infrared molecular imaging probes. *Photochem. Photobiol.* **84**, 1061–1072.
- (4) Dawson, J. B., D. J. Barker, D. J. Ellis, E. Grassam, J. A. Cotterill, G. W. Fisher and J. W. Feather (1980) A theoretical and experimental study of light absorption and scattering by *in vivo* skin. *Phys. Med. Biol.* **25**, 695–709.
- (5) Bendall, S. C., G. P. Nolan, M. Roederer and P. K. Chattopadhyay (2012) A deep profiler’s guide to cytometry. *Trends Immunol.* **33**, 323–332.
- (6) Chattopadhyay, P. K., C.-M. Hogerkorp and M. Roederer (2008) A chromatic explosion: the development and future of multiparameter flow cytometry. *Immunology* **125**, 441–449.
- (7) Springer, J. W., P. S. Parkes-Loach, K. R. Reddy, M. Krayner, J. Jiao, G. M. Lee, D. M. Niedzwiedzki, M. A. Harris, C. Kirmaier, D. F. Bocian, J. S. Lindsey, D. Holten and P. A. Loach (2012) Biohybrid photosynthetic antenna complexes for enhanced light-harvesting. *J. Am. Chem. Soc.* **134**, 4589–4599.
- (8) Stromberg, J. R., A. Marton, H. L. Kee, C. Kirmaier, J. R. Diers, C. Muthiah, M. Taniguchi, J. S. Lindsey, D. F. Bocian, G. J. Meyer and D. Holten (2007) Examination of tethered porphyrin, chlorin, and bacteriochlorin molecules in mesoporous metal-oxide solar cells. *J. Phys. Chem. C* **111**, 15464–15478.
- (9) Hasselman, G. M., D. F. Watson, J. R. Stromberg, D. F. Bocian, D. Holten, J. S. Lindsey and G. J. Meyer (2006) Theoretical solar-to-electrical energy-conversion efficiencies of perylene-porphyrin light-harvesting arrays. *J. Phys. Chem. B* **110**, 25430–25440.
- (10) Br ckner, C., L. Samankumara and J. Ogikubo (2012) Syntheses of bacteriochlorins and isobacteriochlorins. In *Handbook of Porphyrin Science*, Vol. 17 (Edited by K. M. Kadish, K. M. Smith and R. Guilard), pp. 1–112. World Scientific, Singapore.
- (11) Grin, M. A., A. F. Mironov and A. A. Shtil (2008) Bacteriochlorophyll *a* and its derivatives: Chemistry and perspectives for cancer therapy. *Anti-Cancer Agents Med. Chem.* **8**, 683–697.

- (12) Galezowski, M. and D. T. Gryko (2007) Recent advances in the synthesis of hydroporphyrins. *Curr. Org. Chem.* **11**, 1310–1338.
- (13) Chen, Y., G. Li and R. K. Pandey (2004) Synthesis of bacteriochlorins and their potential utility in photodynamic therapy (PDT). *Curr. Org. Chem.* **8**, 1105–1134.
- (14) Krayner, M., M. Ptaszek, H.-J. Kim, K. R. Meneely, D. Fan, K. Secor and J. S. Lindsey (2010) Expanded scope of synthetic bacteriochlorins via improved acid catalysis conditions and diverse dihydrodipyrin-acetals. *J. Org. Chem.* **75**, 1016–1039.
- (15) Kim, H.-J. and J. S. Lindsey (2005) De novo synthesis of stable tetrahydroporphyrinic macrocycles: bacteriochlorins and a tetrahydrocorrins. *J. Org. Chem.* **70**, 5475–5486.
- (16) Springer, J. W., K. M. Faries, H. L. Kee, J. R. Diers, C. Muthiah, O. Mass, C. Kirmaier, J. S. Lindsey, D. F. Bocian and D. Holten (2012) Effects of substituents on synthetic analogs of chlorophylls. Part 3: The distinctive impact of auxochromes at the 7- versus 3-positions. *Photochem. Photobiol.* **88**, 651–674.
- (17) Yang, E., C. Kirmaier, M. Krayner, M. Taniguchi, H.-J. Kim, J. R. Diers, D. F. Bocian, J. S. Lindsey and D. Holten (2011) Photophysical properties and electronic structure of stable, tunable synthetic bacteriochlorins: Extending the features of native photosynthetic pigments. *J. Phys. Chem. B* **115**, 10801–10816.
- (18) Krayner, M., E. Yang, J. R. Diers, D. F. Bocian, D. Holten and J. S. Lindsey (2011) De novo synthesis and photophysical characterization of annulated bacteriochlorins. Mimicking and extending the properties of bacteriochlorophylls. *New J. Chem.* **35**, 587–601.
- (19) Ruzié, C., M. Krayner, T. Balasubramanian and J. S. Lindsey (2008) Tailoring a bacteriochlorin building block with cationic, amphipathic, or lipophilic substituents. *J. Org. Chem.* **73**, 5806–5820.
- (20) Taniguchi, M., D. L. Cramer, A. D. Bhise, H. L. Kee, D. F. Bocian, D. Holten and J. S. Lindsey (2008) Accessing the near-infrared spectral region with stable, synthetic, wavelength-tunable bacteriochlorins. *New J. Chem.* **32**, 947–958.
- (21) Kobayashi, M., M. Akiyama, H. Kano and H. Kise (2006) Spectroscopy and structure determination. In *Chlorophylls and Bacteriochlorophylls: Biochemistry, Biophysics, Functions and Applications* (Edited by B. Grimm, R. J. Porra, W. Rüdiger and H. Scheer), pp, 79–94. Springer, Dordrecht, The Netherlands.
- (22) Yu, Z. and M. Ptaszek (2012) Multifunctional bacteriochlorins from selective palladium-coupling reactions. *Org. Lett.* **14**, 3708–3711.
- (23) Samankumara, L. P., S. Wells, M. Zeller, A. M. Acuña, B. Röder and C. Brückner (2012) Expanded bacteriochlorins. *Angew. Chem. Int. Ed.* **51**, 5757–5760.
- (24) Chen, C.-Y., E. Sun, D. Fan, M. Taniguchi, B. E. McDowell, E. Yang, J. R. Diers, D. F. Bocian, D. Holten and J. S. Lindsey (2012) Synthesis and physicochemical properties of metallo-bacteriochlorins. *Inorg. Chem.* **51**, 9443–9464.
- (25) Ruzié, C., M. Krayner and J. S. Lindsey (2009) Fast and robust route to hydroporphyrin-chalcones with extended red or near-infrared absorption. *Org. Lett.* **11**, 1761–1764.

- (26) Kostanecki, S. V. and J. Tambor (1899) Ueber die sechs isomeren monooxybenzalacetophenone (monooxychalkone). *Chem. Ber.* **32**, 1921–1926.
- (27) Grotewold, E. (2006) The genetics and biochemistry of floral pigments. *Annu. Rev. Plant Biol.* **57**, 761–780.
- (28) Springob, K., J.-I. Nakajima, M. Yamazaki and K. Saito (2003) Recent advances in the biosynthesis and accumulation of anthocyanins. *Nat. Prod. Rep.* **20**, 288–303.
- (29) Austin, M. B. and J. P. Noel (2003) The chalcone synthase superfamily of type III polyketide synthases. *Nat. Prod. Rep.* **20**, 79–110.
- (30) Koes, R. E., F. Quattrocchio and J. N. M. Mol (1994) The flavonoid biosynthetic pathway in plants: function and evolution. *Bioessays* **16**, 123–132.
- (31) Sahu, N. K., S. S. Balbhadra, J. Choudhary and D. V. Kohli (2012) Exploring pharmacological significance of chalcone scaffold: A review. *Curr. Med. Chem.* **19**, 209–225.
- (32) Katsori, A.-M. and D. Hadjipavlou-Litina (2009) Chalcones in cancer: Understanding their role in terms of QSAR. *Curr. Med. Chem.* **16**, 1062–1081.
- (33) Go, M. L., X. Wu and X. L. Liu (2005) Chalcones: An update on cytotoxic and chemoprotective properties. *Curr. Med. Chem.* **12**, 483–499.
- (34) Dimmock, J. R., D. W. Elias, M. A. Beazely and N. M. Kandepu (1999) Bioactivities of chalcones. *Curr. Med. Chem.* **6**, 1125–1149.
- (35) Bukhari, S. N. A., M. Jasamai and I. Jantan (2012) Synthesis and biological evaluation of chalcone derivatives (mini review). *Mini-Rev. Med. Chem.* **12**, 1394–1403.
- (36) Dhar, D. N. *The Chemistry of Chalcones and Related Compounds*, John Wiley & Sons, Inc., New York, 1981.
- (37) Srinivasan, N., C. A. Haney, J. S. Lindsey, W. Zhang and B. T. Chait (1999) Investigation of MALDI-TOF mass spectrometry of diverse synthetic metalloporphyrins, phthalocyanines, and multiporphyrin arrays. *J. Porphyrins Phthalocyanines* **3**, 283–291.
- (38) Seybold, P. G. and M. Gouterman (1969) Porphyrins XIII: Fluorescence spectra and quantum yields. *J. Mol. Spectrosc.* **31**, 1–13.
- (39) Gradyushko, A. T., A. N. Sevchenko, K. N. Solovyov and M. P. Tsvirko (1970) Energetics of photophysical processes in chlorophyll-like molecules. *Photochem. Photobiol.* **11**, 387–400.
- (40) Weber, G. and F. W. J. Teale (1957) Determination of the absolute quantum yield of fluorescent solutions. *Trans. Faraday Soc.* **53**, 646–655.
- (41) Except for molecular mechanics and semi-empirical models, the calculation methods used in Spartan '08 or '10 have been documented in: Shao, Y., L. F. Molnar, Y. Jung, J. Kussmann, C. Ochsenfeld, S. T. Brown, A. T. B. Gilbert, L. V. Slipchenko, S. V. Levchenko, D. P. O'Neill, R. A. DiStasio Jr., R. C. Lochan, T. Wang, G. J. O. Beran, N. A. Besley, J. M. Herbert, C. Y. Lin, T. Van Voorhis, S. H. Chien, A. Sodt, R. P. Steele, V. A. Rassolov, P. E. Maslen, P. P. Korambath, R. D. Adamson, B. Austin, J. Baker, E. F. C. Byrd, H. Dachsel, R. J. Doerksen, A. Dreuw, B. D. Dunietz, A. D. Dutoi, T. R. Furlani, S.

- R. Gwaltney, A. Heyden, S. Hirata, C.-P. Hsu, G. Kedziora, R. Z. Khalliulin, P. Klunzinger, A. M. Lee, M. S. Lee, W. Liang, I. Lotan, N. Nair, B. Peters, E. I. Proynov, P. A. Pieniazek, Y. M. Rhee, J. Ritchie, E. Rosta, C. D. Sherrill, A. C. Simmonett, J. E. Subotnik, H. L. Woodcock III, W. Zhang, A. T. Bell, A. K. Chakraborty, D. M. Chipman, F. J. Keil, A. Warshel, W. J. Hehre, H. F. Schaefer III, J. Kong, A. I. Krylov, P. M. W. Gill and M. Head-Gordon (2006) Advances in methods and algorithms in a modern quantum chemistry program package. *Phys. Chem. Chem. Phys.* **8**, 3172–3191.
- (42) Frisch, M. J., G. W. Trucks, H. B. Schlegel, G. E. Scuseria, M. A. Robb, J. R. Cheeseman, G. Scalmani, V. Barone, B. Mennucci, G. A. Petersson, H. Nakatsuji, M. Caricato, X. Li, H. P. Hratchian, A. F. Izmaylov, J. Bloino, G. Zheng, J. L. Sonnenberg, M. Hada, M. Ehara, K. Toyota, R. Fukuda, J. Hasegawa, M. Ishida, T. Nakajima, Y. Honda, O. Kitao, H. Nakai, T. Vreven, J. A. Montgomery, Jr., J. E. Peralta, F. Ogliaro, M. Bearpark, J. J. Heyd, E. Brothers, K. N. Kudin, V. N. Staroverov, R. Kobayashi, J. Normand, K. Raghavachari, A. Rendell, J. C. Burant, S. S. Iyengar, J. Tomasi, M. Cossi, N. Rega, J. M. Millam, M. Klene, J. E. Knox, J. B. Cross, V. Bakken, C. Adamo, J. Jaramillo, R. Gomperts, R. E. Stratmann, O. Yazyev, A. J. Austin, R. Cammi, C. Pomelli, J. W. Ochterski, R. L. Martin, K. Morokuma, V. G. Zakrzewski, G. A. Voth, P. Salvador, J. J. Dannenberg, S. Dapprich, A. D. Daniels, Ö. Farkas, J. B. Foresman, J. V. Ortiz, J. Cioslowski and D. J. Fox (2009) *The Calculation Methods used in Gaussian '09, Revision B.01*, Gaussian, Inc., Wallingford, CT.
- (43) Birks, J. B. (1970) *Photophysics of Aromatic Molecules*, pp. 142–192. Wiley-Interscience, London.
- (44) Harvey, P. D., C. Stern and R. Guilard (2011) Bio-inspired molecular devices based on systems found in photosynthetic bacteria. In *Handbook of Porphyrin Science*, Vol. 11 (Edited by K. M. Kadish, K. M. Smith and R. Guilard), pp. 1–179. World Scientific Publishing Co., Singapore.
- (45) Harvey, P. D. (2003) Recent advances in free and metalated multiporphyrin assemblies and arrays; a photophysical behavior and energy transfer perspective. In *The Porphyrin Handbook*, Vol. 18 (Edited by K. M. Kadish, K. M. Smith and R. Guilard), pp. 63–250. Academic Press, San Diego, CA.
- (46) Lindsey, J. S., O. Mass and C.-Y. Chen (2011) Tapping the near-infrared spectral region with bacteriochlorin arrays. *New J. Chem.* **35**, 511–516.
- (47) Curley, R. W. Jr. (2012) Retinoid chemistry: Synthesis and application for metabolic disease. *Biochim. Biophys. Acta* **1821**, 3–9.
- (48) Valla, A. R., D. L. Cartier and R. Labia (2004) Chemistry of natural retinoids and carotenoids: Challenges for the future. *Curr. Org. Syn.* **1**, 167–209.
- (49) Vaz Serra, V., F. Camões, S. I. Vieira, M. A. F. Faustino, J. P. C. Tomé, D. C. G. A. Pinto, M. G. P. M. S. Neves, A. C. Tomé, A. M. S. Silva, E. F. da Cruz e Silva and J. A. S. Cavaleiro (2009) Synthesis and biological evaluation of novel chalcone-porphyrin conjugates. *Acta Chim. Slov.* **56**, 603–611.
- (50) Sun, Y.-F. and Y.-P. Cui (2008) The synthesis, characterization and properties of coumarin-based chromophores containing a chalcone moiety. *Dyes Pigments* **78**, 65–76.

- (51) Xue, Y., L. An, Y. Zheng, L. Zhang, X. Gong, Y. Qian and Y. Liu (2012) Structure and electronic spectral property of coumarin–chalcone hybrids: A comparative study using conventional and long-range corrected hybrid functionals. *Comp. Theor. Chem.* **981**, 90–99.
- (52) Fayed, T. A. and M. K. Awad (2004) Dual emission of chalcone-analogue dyes emitting in the red region. *Chem. Phys.* **303**, 317–326.
- (53) Rurack, K., J. L. Bricks, G. Reck, R. Radeaglia and U. Resch-Genger (2000) Chalcone-analogue dyes emitting in the near-infrared (NIR): Influence of donor–acceptor substitution and cation complexation on their spectroscopic properties and X-ray structure. *J. Phys. Chem. A* **104**, 3087–3109.
- (54) Rurack, K., M. L. Dekhtyar, J. L. Bricks, U. Resch-Genger and W. Rettig (1999) Quantum yield switching of fluorescence by selectively bridging single and double bonds in chalcones: Involvement of two different types of conical intersections. *J. Phys. Chem. A* **103**, 9626–9635.
- (55) Kar, S., S. Aich, S. Basu and S. Lahiri (1999) Intramolecular charge transfer in naphthalene analogues of chalcone. *Res. Chem. Intermed.* **25**, 903–913.
- (56) Wang, P. and S. Wu (1995) Spectroscopy and photophysics of bridged enone derivatives: Effect of molecular structure and solvent. *J. Photochem. Photobiol. A: Chem.* **86**, 109–113.
- (57) Wang, P. and S. Wu (1994) A study on the spectroscopy and photophysical behaviour of chalcone derivatives. *J. Photochem. Photobiol. A: Chem.* **77**, 127–131.
- (58) Wang, Y. (1985) Photophysics of polarized enones. Intramolecular charge-transfer interaction and solvent effects. *J. Phys. Chem.* **89**, 3799–3805.
- (59) Xue, Y., J. Mou, Y. Liu, X. Gong, Y. Yang and L. An (2010) An ab initio simulation of the UV/Visible spectra of substituted chalcones. *Cent. Eur. J. Chem.* **8**, 928–936.
- (60) Xue, Y. and X. Gong (2009) The conformational, electronic and spectral properties of chalcones: A density functional theory study. *J. Mol. Struct.: THEOCHEM*, **901**, 226–231.
- (61) Oumi, M., D. Maurice and M. Head-Gordon (1999) Ab initio calculations of the absorption spectrum of chalcone. *Spectrochim. Acta Part A* **55**, 525–537.
- (62) Szmant, H. H. and A. J. Basso (1952) The absorption spectra of substituted chalcones. *J. Am. Chem. Soc.* **74**, 4397–4400.
- (63) Kluge, A. F. and C. P. Lillya (1971) Molecular spectra and conformations of conjugated dienones. *J. Org. Chem.* **36**, 1977–1988.
- (64) Thomas, J. F. and G. Branch (1953) The principal absorption bands of the vinylogous series derived from benzylaldehyde and benzophenone. *J. Am. Chem. Soc.* **75**, 4793–4802.
- (65) Hashimoto, H., K. Hattori, Y. Okada, T. Yoda and R. Matsushima (1998) Molecular and crystal structures of 2-(all-*trans*-retinylidene)-indan-1,3-dione. *Jpn. J. Appl. Phys.* **37**, 4609–4615.

- (66) Kusumoto, T., D. Kosumi, C. Uragami, H. A. Frank, R. R. Birge, R. J. Cogdell and H. Hashimoto (2011) Femtosecond transient absorption spectroscopic study of a carbonyl-containing carotenoid analogue, 2-(all-*trans*-retinylidene)-indan-1,3-dione. *J. Phys. Chem. A* **115**, 2110–2119.
- (67) Gouterman, M. (1978) Optical spectra and electronic structure of porphyrins and related rings. In *The Porphyrins* Vol. 3 (Edited by D. Dolphin), pp 1–165. Academic Press, New York.
- (68) Gouterman, M. (1961) Spectra of porphyrins. *J. Mol. Spectrosc.* **6**, 138–163.
- (69) Gouterman, M. (1959) Study of the effects of substitution on the absorption spectra of porphin. *J. Chem. Phys.* **30**, 1139–1161.
- (70) Mass, O., M. Taniguchi, M. Ptaszek, J. W. Springer, K. M. Faries, J. R. Diers, D. F. Bocian, D. Holten and J. S. Lindsey (2011) Structural characteristics that make chlorophylls green: Interplay of hydrocarbon skeleton and substituents. *New J. Chem.* **35**, 76–88.
- (71) Kee, H. L., C. Kirmaier, Q. Tang, J. R. Diers, C. Muthiah, M. Taniguchi, J. K. Laha, M. Ptaszek, J. S. Lindsey, D. F. Bocian and D. Holten (2007) Effects of substituents on synthetic analogs of chlorophylls. Part 2: Redox properties, optical spectra and electronic structure. *Photochem. Photobiol.* **83**, 1125–1143.
- (72) Yang, E., J. R. Diers, Y.-Y. Huang, M. R. Hamblin, J. S. Lindsey, D. F. Bocian and D. Holten (2013) Molecular electronic tuning of photosensitizers to enhance photodynamic therapy: Synthetic dicyanobacteriochlorins as a case study. *Photochem. Photobiol.* **89**, *in press* (DOI: 10.1111/php.12021).
- (73) 74 Moore, T. A., A. L. Moore and D. Gust (2002) The design and synthesis of artificial photosynthetic antennas, reaction centres and membranes. *Phil. Trans. R. Soc. Lond. B* **357**, 1481–1498.
- (74) Savolainen, J., N. Dijkhuizen, R. Fanciulli, P. A. Liddell, D. Gust, T. A. Moore, A. L. Moore, J. Hauer, T. Backup, M. Motzkus and J. L. Herek (2008) Ultrafast energy transfer dynamics of a bioinspired dyad molecule. *J. Phys. Chem. B* **112**, 2678–2685.
- (75) Kloz, M., S. Pillai, G. Kodis, D. Gust, T. A. Moore, A. L. Moore, R. van Grondelle and J. T. M. Kennis (2012) New light-harvesting roles of hot and forbidden carotenoid states in artificial photosynthetic constructs. *Chem. Sci.* **3**, 2052–2061
- (76) Huang, Y.-Y., P. Mroz, T. Zhiyentayev, S. K. Sharma, T. Balasubramanian, C. Ruzié, M. Krayner, D. Fan, K. E. Borbas, E. Yang, H. L. Kee, C. Kirmaier, J. R. Diers, D. F. Bocian, D. Holten, J. S. Lindsey and M. R. Hamblin (2010) In vitro photodynamic therapy and quantitative structure-activity relationship studies with stable synthetic near-infrared-absorbing bacteriochlorin photosensitizers. *J. Med. Chem.* **53**, 4018–4027.

Section 3

Study of Synthetic Bacteriochlorins as Photosensitizer for Photodynamic Therapy

Collaborations

All synthetic bacteriochlorins were synthesized in the laboratory of Dr. Jonathan Lindsey at the North Carolina State University. The DFT calculations to obtain molecular orbital characteristics, and the redox potential measurements were performed in the laboratory of Dr. David Bocian at the University of California, Riverside. The PDT activity studies such as the in vitro PDT experiments, in vivo fluorescence imaging, photosensitizer uptake, localization, and reactive oxygen species detection were performed in the laboratory of Dr. Michael R. Hamblin at the Harvard Medical School.

In this dissertation, I collaborated with these researchers and the coworkers in their laboratories via my studies of the photophysical properties (including absorption, fluorescence and phosphorescence spectra, excited-state lifetimes, yields and rate constants of the excited-state decay pathways), four-orbital analyses of the optical spectra, photostability studies of bacteriochlorins for PDT, and analysis and correlation of these properties.

Chapter 7

In Vitro Photodynamic Therapy and Quantitative Structure-Activity Relationship Studies with Stable Synthetic Near-Infrared Absorbing Bacteriochlorin Photosensitizers

Reproduced in part with permission from Huang, YY; Mroz, P; Zhiyentayev, T; Sharma, SK; Balasubramanian, T; Ruzi, C; Krayner, M; Fan, D; Borbas, KE; Yang, EK; Kee, HL; Kirmaier, C; Diers, J.R; Bocian, D.F; Holten, D; Lindsey, J.S; Hamblin, M.R. In Vitro Photodynamic Therapy and Quantitative Structure-Activity Relationship Studies with Stable Synthetic Near-Infrared-Absorbing Bacteriochlorin Photosensitizers. *J. Med. Chem.* 2010, 53, 4018–4027. Doi: 10.1021/jm901908s. Copyright 2010 American Chemical Society.

Abstract

Photodynamic therapy (PDT) is a rapidly developing approach to treating cancer that combines harmless visible and near-infrared light with a nontoxic photoactivatable dye, which upon encounter with molecular oxygen generates the reactive oxygen species that are toxic to cancer cells. Bacteriochlorins are tetrapyrrole compounds with two reduced pyrrole rings in the macrocycle. These molecules are characterized by strong absorption features from 700 to >800 nm, which enable deep penetration into tissue. This report describes testing of 12 new stable synthetic bacteriochlorins for PDT activity. The 12 compounds possess a variety of peripheral substituents and are very potent in killing cancer cells *in vitro* after illumination. Quantitative structure–activity relationships were derived, and subcellular localization was determined. The most active compounds have both low dark toxicity and high phototoxicity. This combination together with near-infrared absorption gives these bacteriochlorins great potential as photosensitizers for treatment of cancer.

Introduction

Photodynamic therapy (PDT) employs a nontoxic dye termed a photosensitizer and visible light, which in the presence of oxygen produce reactive oxygen species, such as singlet oxygen, superoxide and hydroxyl radical.¹ The reactive oxygen species produced during PDT are effective in killing both malignant and normal cells via necrosis, apoptosis or autophagy depending on the cell type, structure of the photosensitizer and the light parameters chosen.²⁻⁴ PDT has the advantage of dual selectivity in that the photosensitizer can be targeted to its destination cell or tissue, and in addition the illumination can be spatially directed to the lesion.

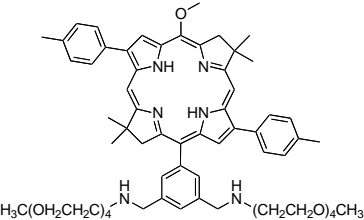
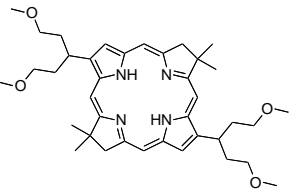
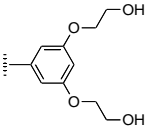
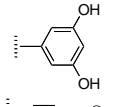
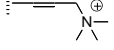
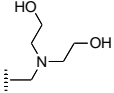
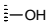
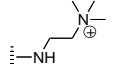
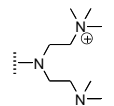
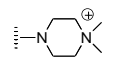
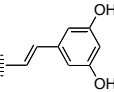
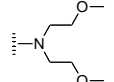
Bacteriochlorins are tetrapyrrole compounds with two opposing pyrroline (i.e., reduced pyrrole) rings. The ring structure occurs naturally in photosynthetic pigments (bacteriochlorophylls *a* and *b*) from purple photosynthetic bacteria of the orders *Rhodospirillales* and *Rhizobiales*.⁵ Reduction of two pyrrolic rings in the tetrapyrrole macrocycle has a pronounced effect on the absorption spectra. Bacteriochlorins and bacteriopurpurins have large absorption bands in the region of 720-850 nm where chlorins (one reduced ring) and porphyrins (no reduced rings) effectively do not absorb. The characteristic absorption of bacteriochlorins and bacteriopurpurins in the near-infrared spectral region is considered to be ideal for maximizing light penetration through tissue because both absorption and scattering of light at these wavelengths by endogenous entities are minimal.

During the past decade, several naturally derived bacteriochlorins have been evaluated for PDT and some of them have shown significant in vivo efficacy. The most frequently employed bacteriochlorin for PDT has been the Pd-containing bacteriopheophorbide derivative known as TOOKAD, padoporfin or WST09 that is in clinical trials for prostate cancer.⁶ A related

water soluble Pd-bacteriochlorin derivative called WST11 has been tested for PDT of mouse melanoma xenografts.⁷ A recent report has shown that the application of bacteriochlorin p6 is effective for in vitro and in vivo treatment of radiation-induced fibrosarcoma (RIF) tumors.⁸

Unfortunately, stable bacteriochlorins and bacteriopurpurins are notoriously difficult to synthesize from porphyrins or other chlorin intermediates. Many naturally occurring and naturally derived bacteriochlorins tend to be unstable in the presence of oxygen and light and are rapidly converted back to porphyrins and chlorins. To overcome these limitations, we developed a de novo synthetic pathway to stable bacteriochlorins.⁹ A key design feature of the synthetic bacteriochlorins is the use of a geminal dimethyl group in each reduced, pyrroline ring (Table 1). This geminal dimethyl group in the pyrroline rings locks-in the bacteriochlorin chromophore and precludes dehydrogenation or tautomerization processes, thereby affording a stable macrocycle. However in addition to good optical absorption properties and stability, it is necessary for a photosensitizer to also possess the appropriate molecular structure that will optimize the uptake, subcellular localization, and PDT-induced killing of cancer cells. To this end, the synthesis is compatible with a variety of groups including aryl, alkyl, and halo substituents.^{9,10,11} The introduction of halo substituents affords building blocks that can be derivatized with peripheral groups that are cationic, anionic, lipophilic, or amphipathic.^{10,12,13} Furthermore, the synthesis also affords the ability to incorporate auxochromes that allow tuning the position of the long-wavelength absorption band from ~700 to ~800 nm (with substituents tested to date).¹⁴ Taken together, the chemical robustness of the synthetic bacteriochlorins and the versatility of the synthesis provide access to the desired features of wavelength tunability and substituent tailorability (e.g., lipophilicity, molecular asymmetry) needed for PDT applications.

Table 1. Chemical structures of bacteriochlorins^a

Cmpd	
1	
2	
R	
3	
4	
5	
6	
7	
8	
9	
10	
11	
12	

^aIodide counter ions for cationic compounds omitted for clarity.

The goal of the present study was to test a group of twelve bacteriochlorins (Table 1) with varying peripheral substituents as photosensitizers for killing HeLa human cervical cancer cells and to deduce quantitative structure-function relationships. Various physicochemical properties of the molecules were also characterized to aid in the analysis of the PDT activity.

Experimental methods

Experimental informations are given in Ref A.

Results and Discussion

Molecular characteristics and logP values

A de novo synthetic pathway to bacteriochlorins that contain a geminal dimethyl group in each pyrroline ring was recently developed.⁹ This structural attribute blocks adventitious dehydrogenation and thereby affords a stable macrocycle. This synthetic route has provided the foundation for the preparation of the 12 bacteriochlorins, which are shown in Table 1. The 12 compounds encompass a range of polarity that extends from rather lipophilic (**1**, **2**, **12**) to more amphipathic (**3**, **4**, **6**, **11**) to polar (**5**, **7**, **8**, **9**, **10**). This set of compounds is valuable for examination of structure–activity relationships. Bacteriochlorin **1** contains two 3,6,9,12-tetraoxatridecylamine groups, while bacteriochlorins **2** and **12** contain symmetrically branched 1,5-dimethoxypentyl groups for solubility in lipophilic environments. Bacteriochlorins **3**, **4**, **6**, and **11** each contain four hydroxyl groups. Bacteriochlorins **4** and **11** each have four phenolic hydroxyl groups, whereas the hydroxyl groups are attached to more flexible alkyl chains in bacteriochlorins **3** and **6**. The hydroxyl groups are placed closest to the macrocycle in bacteriochlorin **4** and farthest from the macrocycle in bacteriochlorin **3**. The cationic bacteriochlorins contain either two positive charges (**5**, **8**, **10**) or four positive charges (**9**).

Bacteriochlorins **5** and **10** have substituents that are structurally more rigid than the substituents on bacteriochlorins **8** and **9**. In comparison to the cationic bacteriochlorins (**5**, **8**, **9**, **10**), bacteriochlorin **7** is expected to be anionic at physiological pH.

The measured partition coefficient (mLogP) values for relative solubility in octanol versus water were obtained experimentally by the stir-flask method, and the values were also calculated (cLogP) on the basis of the bacteriochlorin structure. A positive versus negative log *P* value reflects preferential solubilization in the octanol versus water phases, respectively. For bacteriochlorins **1–4**, **11**, and **12** there was no observable amount of bacteriochlorin in the water layer. The cationic bacteriochlorins **8–10** exhibited negative mLogP values, whereas the cationic bacteriochlorin **5** gave a mLogP value of 0.9. Bacteriochlorins **6** and **7** had mLogP values of 2.3 and 1.4, respectively. The mLogP and cLogP values are listed in Table 2.

The mLogP and cLogP values are plotted against one another in Figure 1A. The linear correlation is good ($R^2=0.78$) but not perfect. Because of the lack of a perfect correlation, a quantitative structure–activity relationship (QSAR) was constructed for each of the experiment-derived parameters that reflect PDT effectiveness (LD_{50} , cellular uptake, PDT toxicity per unit uptake) against both cLogP and mLogP. The results of the QSAR studies along with the photophysical and molecular-orbital characteristics described next give insights into the factors most important for the relative PDT effectiveness of the diverse bacteriochlorins shown in Table 1.

Table 2. Properties of Bacteriochlorins^a.

Cmpd	LD50 ^a (nM)	mlogP ^b	clogP ^c	Uptake ^d (nmol/ mg)	SF/unit uptake ^e (nmol/ mg)	Q _y (0,0) ^f absorption		Q _y (0,0) ^f fluorescence		Φ _f ^g	τ _S ^h (ns)	Φ _{isc} ^{ref i}	τ _T ^j (μs)	Orbital Energy	
						λ (nm)	fwhm (nm)	λ (nm)	fwhm (nm)					HOMO (eV)	LUMO (eV)
1	500	≥2.2	9.3 ± 1.6	3.9	0.1	732	21							-4.39	-2.20
2	100	≥2.5	6.9 ± 1.5	11.7	0.02	717	13	722	20	0.09	4.0	0.51	189	-4.36	-2.12
3	15	≥2.2	4.7 ± 1.5	10.4	0.001	732	19	738	24	0.15	3.0	0.55	159	-4.44	-2.26
4	80	≥2.5	6.8 ± 1.5	13.5	0.01	732	21	737	26	0.12	3.7	0.52	190	-4.46	-2.28
5	2000	0.9	4.2 ± 1.7	8.2	0.6	749	16	754	22	0.11	3.8	0.51	104 ^k	-4.77	-3.31
6	100	2.3	4.8 ± 1.5	8.2	0.04	718	18	724	23	0.09	3.8	0.53	190	-4.42	-2.19
7	4000	1.4	5.6 ± 1.7	0.72	0.35	734	26	742	19	0.07	3.7	0.56	70	-4.86	-2.77
8	3000	-0.5	-1.1 ±	7.7	0.88	742	23	750	25	0.13	4.0	0.48	77 ^k	-4.72	-3.34
9	800	-1.4	-5.3 ±	1.8	0.9	729	19	735	24	0.12	3.5	0.53	54 ^l	-5.04	-3.89
10	800	-1.0	-1.0 ±	1.8	1	731	21	740	28	0.12	3.8	0.50	100 ^k	-4.62	-2.45
11	200	≥1.8	7.6 ± 1.7	1.8	0.23	781	35	800	40	0.02	3.4	0.66	78	-4.72	-2.74
12	60	≥1.9	2.8 ± 1.7	15.0	0.02	727	20	733	27	0.10	3.3	0.57	105	-4.68	-2.51

^aValues taken from Figure 3. ^bMeasured value of logP. ^cCalculated value of logP. ^dValues taken from Figure 3 and apply to a bacteriochlorin concentration of 20.5 μM. ^eSurvival fraction at uptake of 0.3 nmol/(mg protein). The values are taken from Figures 2 and 3 by determining the bacteriochlorin concentration in the incubation medium necessary to produce a cell uptake of 0.3 nmol/(mg protein), and then determining the survival fractions at these bacteriochlorin concentration values after 10 J/cm² light was delivered. ^fPeak wavelength (λ) and full width at half maximum (fwhm) of spectral feature for compound in aerated methanol unless indicated otherwise. ^gFluorescence quantum yield for compound in Ar-purged methanol. ^hLifetime of the lowest singlet excited state for compound in Ar-purged methanol determined using fluorescence detection. ⁱYield of the lowest triplet excited state determined using the expression $\Phi_{isc}^{ref} = 1 - \Phi_f - k_{ic} \cdot \tau_S$, with $k_{IC} = (10 \text{ ns})^{-1}$. ^jLifetime of the lowest triplet excited state for the compound in Ar-purged 2-methyltetrahydrofuran unless indicated otherwise. ^kIn freeze-pump-thaw-degassed methanol. ^lIn freeze-pump-thaw-degassed ethanol.

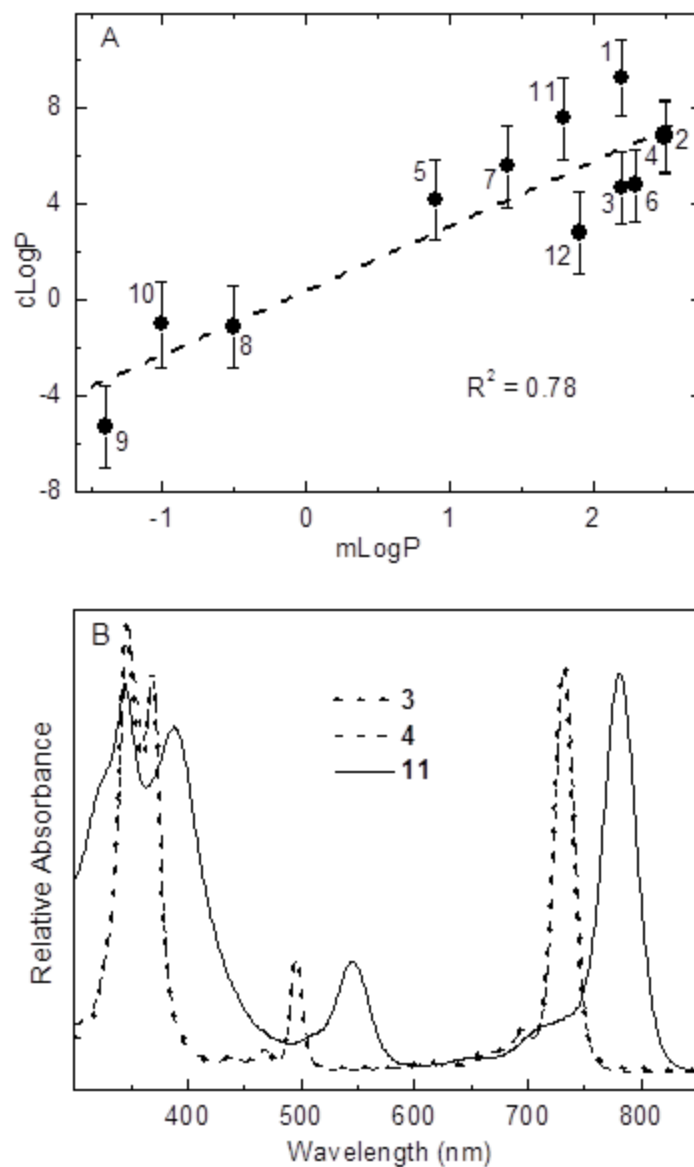


Figure 1. (A) **Octanol-water partition coefficients.** Calculated LogP (cLogP) versus measured LogP (mLogP); the line is a linear least-squares fit with an R^2 value 0.78. The data used to construct this plot are given in Table 2. The values of mLogP are lower limits for compounds **1**, **2**, **3**, **4**, **11**, and **12**. (B) **Absorption spectra.** Data is shown for representative bacteriochlorins in methanol at 295 K.

Photophysical properties

Each compound studied herein exhibits a characteristic bacteriochlorin absorption spectrum,¹⁵ with a broad near-UV Soret feature and a near-infrared Q_y band of comparable intensity. Representative spectra (for bacteriochlorins **3**, **4**, and **11** in methanol) are shown in Figure 1B. The wavelength tunability of synthetic bacteriochlorins obtained via functionalization of the 3- and 13-position has been described previously.¹⁴ The Q_y(0,0) absorption maximum of **1–12** in methanol ranges from 717 to 781 nm, and in each case the Q_y(0,0) fluorescence peak is bathochromically shifted by ≤10 nm (Table 2). The fluorescence quantum yields of these bacteriochlorins are typically 0.09–0.12. The lifetimes of the lowest singlet excited state are in the range 3–4 ns, and the lifetimes of the lowest triplet excited state are in the range 50–190 μs (both in the absence of oxygen). The triplet lifetimes are reduced to <1 μs in the presence of atmospheric oxygen, indicating facile excitedstate quenching. The yields of the lowest triplet excited state determined using a reference technique¹⁶ for **1–12** (Table 2) have an average value of 0.52 ± 0.02. This value is similar to 0.54 for bacteriopheophytin *a*.¹⁷ Overall, these results indicate that significant differences in phototoxicity of the bacteriochlorins must stem primarily from sources other than the lifetime and yield of the triplet excited state (from which the reactive oxygen species is produced).

Molecular orbital characteristics

The energies of the highest occupied molecular orbital (HOMO) and lowest unoccupied molecular orbital (LUMO) of each bacteriochlorin were obtained from DFT calculations. Table 2 shows that the HOMO energy becomes more negative along the following series: **2** (−4.36 eV) > **1** (−4.39 eV) > **6** (−4.42 eV) > **3** (−4.44 eV) > **4** (−4.46 eV) > **10** (−4.62 eV) > **12** (−4.68

eV)>**8** (-4.72 eV) ~ **11** (-4.72 eV)>**5** (-4.77 eV)>**7** (-4.86 eV)>**9** (-5.04). Along this series, the bacteriochlorins will be progressively harder to oxidize. Table 2 also shows that the LUMO energy becomes more negative along the following series:**2** (-2.12 eV)>**1** (-2.20 eV)>**6** (-2.19 eV) >**3** (-2.26 eV)>**4** (-2.28 eV)>**10** (-2.45 eV)>**12** (-2.51 eV)>**11** (-2.74 eV)>**7** (-2.77 eV)>**5** (-3.31 eV)>**8** (-3.34 eV)>**9** (-3.89). Along this series, the bacteriochlorins will be progressively easier to reduce.

A prior study of a series of zinc chlorins showed excellent linear correlations between the calculated orbital energies and measured redox potentials, with a shift in the HOMO or LUMO energy of 100 meV giving a shift in the oxidation or reduction potential on the order of 100 mV.¹⁸ These findings suggest that differences in oxidation and/or reduction potentials among the bacteriochlorins studied here may be substantial. One caveat is that the redox properties of a bacteriochlorin may differ considerably depending on the subcellular localization site. The second caveat is that the triplet excited state (T_1) redox potentials will differ from those for the ground state (S_0) by the T_1 - S_0 energy gap, which typically will vary similarly to the S_1 - S_0 energy gaps derived from $Q_y(0,0)$ spectral positions (Table 2).

With these considerations in mind, several points can be made. In a comparison of bacteriochlorins bearing aromatic alcohols, **11** will be harder to oxidize and easier to reduce than **4**, which in turn has similar redox properties to **3**. Carboxylic acid containing **7** should have redox properties comparable to **11**. Positively charged bacteriochlorins **5** and **8** will have redox properties similar to one another and oxidation potentials comparable to **11** but will be considerably easier to reduce than **11**. These anticipated differences in redox properties for this subset of compounds studied (**3** > **4** > **11** > **5** > **8** > **7**), or the entire set (**1**-**12**), show no general correlation with the relative PDT activities discussed below. The only possible connection is that

among similar bacteriochlorins (e.g., those bearing aromatic alcohols), compounds that should be easier to oxidize and harder to reduce tend to have higher activity (e.g., **3** versus **11**).

Redox and photophysical properties contribute substantially to the photochemical mechanisms (type I versus type II) of PDT activity.^{19,20} The results described above indicate that these properties do not track activity (redox) or do not change substantially (photophysics) for the 12 bacteriochlorins and thus contribute only marginally if at all to the observed differences in phototoxicity described below.

Photodynamic activity

The results of the photodynamic activity such as in Vitro PDT on HeLa cells, cellular uptake, subcellular localization, and PDT toxicity per unit uptake are described in Reference A.

Discussion

Twelve bacteriochlorins were designed and studied to probe electronic and chemical attributes that are likely to impact PDT activity. The results demonstrate that a number of these bacteriochlorins are extremely active photosensitizers. They are capable of killing cancer cells in nM concentrations (even as low as 15 nM) when combined with modest fluences (10 J/cm^2) of near-infrared (732-nm or 780-nm) light. The combination of high PDT activity with the good tissue-penetrating properties of near-infrared light suggest these compounds should be further tested in PDT especially for tumor types such as melanoma, against which traditional photosensitizers do not perform well.

Acknowledgments

This work was supported by grants from the NIH (GM36238 to J.S.L. and AI050875 to M.R.H.) and by a Burroughs-Wellcome fellowship (to M.K.), and the Jimmy V. NCSU Cancer Therapeutics Training Program. Y-Y.H. and T.B. were supported by a grant (R41AI072854) from the National Institute of Allergy and Infectious Diseases to NIRvana Pharmaceuticals, Inc. P.M. was partially supported by Genzyme-Partners Translational research Grant. Characterization of the photophysical and redox properties of the bacteriochlorins described herein were initially motivated by solar-energy studies and supported by grants from the Division of Chemical Sciences, Geosciences and Biosciences Division, Office of Basic Energy Sciences of the U.S. Department of Energy to D.F.B. (DE-FG02-05ER15660) and D.H. (DE-FG02-05ER15661).

Supporting Information Available

The link information is given in Ref A.

References

- (A) Huang YY, Mroz P, Zhiyentayev T, Sharma SK, Balasubramanian T, Ruzi C, Krayner M, Fan D, Borbas KE, Yang E, Kee HL, Kirmaier C, Diers JR, Bocian DF, Holten D, Lindsey JS, Hamblin MR. In Vitro Photodynamic Therapy and Quantitative Structure-Activity Relationship Studies with Stable Synthetic Near-Infrared-Absorbing Bacteriochlorin Photosensitizers. *J. Med. Chem.* 2010, 53, 4018–4027.
- (1) Hamblin MR, Mroz P. *Advances in Photodynamic Therapy: Basic, Translational and Clinical.* Artech House; Norwood, MA: 2008.
- (2) Castano AP, Demidova TN, Hamblin MR. Mechanisms in photodynamic therapy: part one—photosensitizers, photochemistry and cellular localization. *Photodiagn. Photodyn. Ther.* 2004;1:279–293.
- (3) Castano AP, Demidova TN, Hamblin MR. Mechanisms in photodynamic therapy: part three—photosensitizer pharmacokinetics, biodistribution, tumor localization and modes of tumor destruction. *Photodiagn. Photodyn. Ther.* 2005;2:91–106.
- (4) Castano AP, Demidova TN, Hamblin MR. Mechanisms in photodynamic therapy: part two—cellular signalling, cell metabolism and modes of cell death. *Photodiagn. Photodyn. Ther.* 2005;2:1–23.
- (5) Lapouge K, Naveke A, Gall A, Ivancich A, Seguin J, Scheer H, Sturgis JN, Mattioli TA, Robert B. Conformation of bacteriochlorophyll molecules in photosynthetic proteins from purple bacteria. *Biochemistry.* 1999;38:11115–11121.
- (6) Trachtenberg J, Weersink RA, Davidson SR, Haider MA, Bogaards A, Gertner MR, Evans A, Scherz A, Savard J, Chin JL, Wilson BC, Elhilali M. Vascular-targeted photodynamic therapy (padoporfin, WST09) for recurrent prostate cancer after failure of external beam radiotherapy: a study of escalating light doses. *BJU Int.* 2008;102:556–562.

- (7) Mazor O, Brandis A, Plaks V, Neumark E, Rosenbach-Belkin V, Salomon Y, Scherz A. WST11, a novel water-soluble bacteriochlorophyll derivative; cellular uptake, pharmacokinetics, biodistribution and vascular-targeted photodynamic activity using melanoma tumors as a model. *Photochem. Photobiol.* 2005;81:342–351.
- (8) Chen Y, Potter WR, Missert JR, Morgan J, Pandey RK. Comparative in vitro and in vivo studies on long-wavelength photosensitizers derived from bacteriopurpurinimide and bacteriochlorin p6: fused imide ring enhances the in vivo PDT efficacy. *Bioconjugate Chem.* 2007;18:1460–1473.
- (9) Kim HJ, Lindsey JS. De novo synthesis of stable tetrahydro-porphyrinic macrocycles: bacteriochlorins and a tetradehydrocorrin. *J. Org. Chem.* 2005;70:5475–5486.
- (10) Ruzié C, Kraymer M, Balasubramanian T, Lindsey JS. Tailoring a bacteriochlorin building block with cationic, amphipathic, or lipophilic substituents. *J. Org. Chem.* 2008;73:5806–5820.
- (11) Borbas KE, Ruzié C, Lindsey JS. Swallowtail bacteriochlorins. Lipophilic absorbers for the near-infrared. *Org. Lett.* 2008;10:1931–1934
- (12) Fan D, Taniguchi M, Lindsey JS. Regioselective 15-bromination and functionalization of a stable synthetic bacteriochlorin. *J. Org. Chem.* 2007;72:5350–5357.
- (13) Ruzié C, Kraymer M, Lindsey JS. Fast and robust route to hydroporphyrin-chalcones with extended red or near-infrared absorption. *Org. Lett.* 2009;11:1761–1764
- (14) Taniguchi M, Cramer DL, Bhise AD, Kee HL, Bocian DF, Holten D, Lindsey JS. Accessing the near-infrared spectral region with stable, synthetic, wavelength-tunable bacteriochlorins. *New J. Chem.* 2008;32:947–958.
- (15) Kobayashi M, Akiyama M, Kano H, Kise H. Spectroscopy and Structure Determination. In: Grimm B, Porra RJ, Rüdiger W, Scheer H, editors. *Chlorophylls and Bacteriochlorophylls: Biochemistry, Biophysics, Functions and Applications*. Vol. 25. Springer; Dordrecht, The Netherlands: 2006. pp. 79–94. *Advances in Photosynthesis and Respiration*.
- (16) Kee HL, Bhaumik J, Diers JR, Mroz P, Hamblin MR, Bocian DF, Lindsey JS, Holten D. Photophysical characterization of imidazolium-substituted Pd(II), In(III), and Zn(II) porphyrins as photosensitizers for photodynamic therapy. *J. Photochem. Photobiol., A.* 2008;200:346–355.
- (17) Holten D, Gouterman M, Parson WW, Windsor MW, Rockley MG. Electron transfer from photoexcited singlet and triplet bacteriochlorophyll. *Photochem. Photobiol.* 1976;23:415–420.
- (18) Kee HL, Kirmaier C, Tang Q, Diers JR, Muthiah C, Taniguchi M, Laha JK, Ptaszek M, Lindsey JS, Bocian DF, Holten D. Effects of substituents on synthetic analogs of chlorophylls. Part 2: Redox properties, optical spectra and electronic structure. *Photochem. Photobiol.* 2007;83:1125–1143.
- (19) Ochsner M. Photophysical and photobiological processes in the photodynamic therapy of tumours. *J. Photochem. Photobiol., B.* 1997;39:1–18.

- (20) Mroz P, Bhaumik J, Dogutan DK, Aly Z, Kamal Z, Khalid L, Kee HL, Bocian DF, Holten D, Lindsey JS, Hamblin MR. Imidazole metalloporphyrins as photosensitizers for photodynamic therapy: role of molecular charge, central metal and hydroxyl radical production. *Cancer Lett.* 2009;282:63–76.
- (21) Henderson BW, Bellnier DA, Greco WR, Sharma A, Pandey RK, Vaughan LA, Weishaupt KR, Dougherty TJ. An in vivo quantitative structure–activity relationship for a congeneric series of pyropheophorbide derivatives as photosensitizers for photodynamic therapy. *Cancer Res.* 1997;57:4000–4007.
- (22) Margaron P, Gregoire MJ, Scasnar V, Ali H, van Lier JE. Structure–photodynamic activity relationships of a series of 4-substituted zinc phthalocyanines. *Photochem. Photobiol.* 1996;63:217–223
- (23) MacDonald IJ, Morgan J, Bellnier DA, Paszkiewicz GM, Whitaker JE, Litchfield DJ, Dougherty TJ. Subcellular localization patterns and their relationship to photodynamic activity of pyropheophorbide-a derivatives. *Photochem. Photobiol.* 1999;70:789–797.
- (24) Buytaert E, Dewaele M, Agostinis P. Molecular effectors of multiple cell death pathways initiated by photodynamic therapy. *Biochim. Biophys. Acta.* 2007;1776:86–107.
- (25) Pogue BW, Ortel B, Chen N, Redmond RW, Hasan T. A photobiological and photophysical-based study of phototoxicity of two chlorins. *Cancer Res.* 2001;61:717–724.
- (26) Kessel D, Luguya R, Vicente MG. Localization and photodynamic efficacy of two cationic porphyrins varying in charge distributions. *Photochem. Photobiol.* 2003;78:431–435.
- (27) Rancan F, Wiehe A, Nobel M, Senge MO, Omari SA, Bohm F, John M, Roder B. Influence of substitutions on asymmetric dihydroxychlorins with regard to intracellular uptake, subcellular localization and photosensitization of Jurkat cells. *J. Photochem. Photobiol., B.* 2005;78:17–28
- (28) Trivedi NS, Wang HW, Nieminen AL, Oleinick NL, Izatt JA. Quantitative analysis of Pc 4 localization in mouse lymphoma (LY-R) cells via double-label confocal fluorescence microscopy. *Photochem. Photobiol.* 2000;71:634–639
- (29) Sasnouski S, Pic E, Dumas D, Zorin V, D'Hallewin MA, Guillemin F, Bezdetsnaya L. Influence of incubation time and sensitizer localization on meta-tetra(hydroxyphenyl)chlorin (mTHPC)-induced photoinactivation of cells. *Radiat. Res.* 2007;168:209–217.
- (30) Szokalska A, Makowski M, Nowis D, Wilczynski GM, Kujawa M, Wojcik C, Mlynarczuk-Bialy I, Salwa P, Bil J, Janowska S, Agostinis P, Verfaillie T, Bugajski M, Gietka J, Issat T, Glodkowska E, Mrowka P, Stoklosa T, Hamblin MR, Mroz P, Jakobisiak M, Golab J. Proteasome inhibition potentiates antitumor effects of photodynamic therapy in mice through induction of endoplasmic reticulum stress and unfolded protein response. *Cancer Res.* 2009;69:4235–4243.
- (31) Kraymer M, Ptaszek M, Kim HJ, Meneely KR, Fan D, Secor K, Lindsey JS. Expanded scope of synthetic bacteriochlorins via improved acid catalysis conditions and diverse dihydrodipyrin-acetals. *J. Org. Chem.* 2010;75:1016–1039

- (32) Weber G, Teale FW. Determination of the absolute quantum yield of fluorescent solutions. *Trans. Faraday Soc.* 1957;53:646–655.
- (33) Gradyushko AT, Sevchenko AN, Solovyov KN, Tsvirko MP. Energetics of photophysical processes in chlorophyll-like molecules. *Photochem. Photobiol.* 1970;11:387–400
- (34) Kong J, White CA, Krylov AI, Sherrill D, Adamson RD, Furlani TR, Lee MS, Lee AM, Gwaltney SR, Adams TR, Ochsenfeld C, Gilbert AT, Kedziora GS, Rassolov VA, Maurice DR, Nair N, Shao Y, Besley NA, Maslen PE, Dombroski JP, Daschel H, Zhang W, Korambath PP, Baker J, Byrd EF, Van Voorhis T, Oumi M, Hirata S, Hsu C-P, Ishikawa N, Florian J, Warshel A, Johnson BG, Gill PM, Head-Gordon M, Pople JA. Q-Chem 2.0: a high performance ab initio electronic structure program package. *J. Comput. Chem.* 2000;21:1532–1548.
- (35) Perry VP. Cultivation of large cultures of HeLa cells in horse serum. *Science.* 1955;121:805
- (36) He P, Ahn JC, Shin JI, Hwang HJ, Kang JW, Lee SJ, Chung PS. Enhanced apoptotic effect of combined modality of 9-hydroxyphorbide alpha-mediated photodynamic therapy and carboplatin on AMC-HN-3 human head and neck cancer cells. *Oncol. Rep.* 2009;21:329–334.
- (37) Lobner D. Comparison of the LDH and MTT assays for quantifying cell death: validity for neuronal apoptosis? *J. Neurosci. Methods.* 2000;96:147–152.
- (38) Merlin JL, Azzi S, Lignon D, Ramacci C, Zeghari N, Guillemin F. MTT assays allow quick and reliable measurement of the response of human tumour cells to photodynamic therapy. *Eur. J. Cancer.* 1992;28A:1452–1458.
- (39) Hamblin MR, Miller JL, Ortel B. Scavenger-receptor targeted photodynamic therapy. *Photochem. Photobiol.* 2000;72:533–540.

Chapter 8

Synthetic Bacteriochlorins Overcome the Resistance of Melanoma to Photodynamic Therapy

Reproduced in part with permission from Mroz, P; Huang, YY; Szokalska, A; Zhiyentayev, T; Janjua, S; Nifli, AP; Sherwood, ME; Ruzié, C; Borbas, KE; Fan, D; Krayner, M; Balasubramanian, T; Yang, EK; Kee, HL; Kirmaier, C; Diers, J.R; Bocian, D.F; Holten, D; Lindsey, J.S; Hamblin, M.R. Stable. Synthetic Bacteriochlorins Overcome The Resistance of Melanoma to Photodynamic Therapy. *FASEB J.* 2010, *24*, 3160–3170. Doi:10.1096/fj.09-152587. Copyright 2010 The Federation of American Societies for Experimental Biology.

Abstract

Cutaneous malignant melanoma remains a therapeutic challenge, and patients with advanced disease have limited survival. Photodynamic therapy (PDT) has been successfully used to treat many malignancies, and it may show promise as an antimelanoma modality. However, high melanin levels in melanomas can adversely affect PDT effectiveness. Herein the extent of melanin contribution to melanoma resistance to PDT was investigated in a set of melanoma cell lines that markedly differ in the levels of pigmentation; 3 new bacteriochlorins successfully overcame the resistance. Cell killing studies determined that bacteriochlorins are superior at ($LD_{50} \approx 0.1 \mu\text{M}$) when compared with controls such as the FDA-approved Photofrin ($LD_{50} \approx 10 \mu\text{M}$) and clinically tested LuTex ($LD_{50} \approx 1 \mu\text{M}$). The melanin content affects PDT effectiveness, but the degree of reduction is significantly lower for bacteriochlorins than for Photofrin. Microscopy reveals that the least effective bacteriochlorin localizes predominantly in lysosomes, while the most effective one preferentially accumulates in mitochondria. Interestingly all bacteriochlorins accumulate in melanosomes, and subsequent illumination leads to melanosomal damage shown by electron microscopy. Fluorescent probes show that the most effective bacteriochlorin produces significantly higher levels of hydroxyl radicals, and this is consistent with the redox properties suggested by molecular-orbital calculations. The best *in vitro* performing bacteriochlorin was tested *in vivo* in a mouse melanoma model using spectrally resolved fluorescence imaging and provided significant survival advantage with 20% of cures ($P < 0.01$).

Keywords: melanoma, photodynamic therapy, multidrug resistance, melanosomes, bacteriochlorins, electron microscopy

Introduction

Malignant melanoma is a cancer that arises from melanocytes, the specialized pigmented cells that are found predominantly in the skin. Although melanoma accounts for only 4% of skin cancer cases, it causes 79% of all skin cancer related deaths. If diagnosed early, melanoma can be cured by surgical resection with about 80% effectiveness for thin lesions. However, once metastases occur, it is largely refractory to existing therapies. The National Comprehensive Cancer Network¹ recommends a plethora of treatments for stage III and local recurrence of melanoma that include, intralesional injection of BCG or interferon, and local ablation therapy or radiation therapy. Only interferon alfa-2b has been shown to have a reproducible benefit². Other potential immunotherapies include vaccines or high-dose bolus interleukin-2 alone or in combination with chemotherapy³. Naylor *et al.*⁴ are used topical 5% imiquimod cream and irradiation of skin metastases with a continuous-wave 810-nm laser to widen the response to distant non-irradiated lesions.

Photodynamic therapy (PDT) uses a non-toxic dye molecule or photosensitizer that absorbs a photon of an appropriate wavelength of light to form an excited triplet state⁵. The excited molecule can then transfer energy to the (triplet) ground state of molecular oxygen to produce the highly cytotoxic singlet oxygen (Type II reaction), or undergo electron transfer (Type I reaction) with the ultimate formation of reactive oxygen species. Such species are the superoxide radical anion or hydroxyl radicals that can oxidize important biological molecules such as proteins, lipids and nucleic acids.

There are 3 main mechanisms that make PDT an effective anti-cancer procedure: (1) direct tumor killing by the reactive oxygen species, (2) tumor-associated vascular damage, and

(3) activation of anti-tumor immune response. The prevailing view is that all three mechanisms are necessary for the optimal tumor damage.

Melanins are the principal surface pigments that play a major role in photoprotection.^{6,7} Melanin synthesis is initiated with the enzymatic hydroxylation of the L-tyrosine to L-dihydroxyphenylalanine (L-DOPA) and oxidation of L-DOPA to DOPAquinone. DOPAquinone is subsequently transformed to melanin in a series of reactions accelerated by enzymes and metal cations. Numerous stimuli are able to alter melanogenesis or the production of melanin by cultured melanocytes.^{8,9} The type of melanin produced depends on the cellular genotype and environmental factors, resulting in the black pigment eumelanin, the reddish to yellow pigment pheomelanin or the mixed melanin that contains both components.¹⁰ Consequently melanomas can vary from non-pigmented tumors that have no melanin whatsoever, through moderately pigmented to highly pigmented tumors, and their pigmentation level is proportional to the degree of differentiation and inversely proportional to the growth rate.^{11,12}

Bacteriochlorins are tetrapyrrole macrocycles that contain alternating pyrrole and pyrroline (i.e., reduced pyrrole) rings. The macrocycle structure occurs naturally in photosynthetic pigments (bacteriochlorophylls *a* and *b*) found in purple photosynthetic bacteria.¹³ The presence of the reduced rings in the tetrapyrrole macrocycle has a pronounced effect on the absorption spectra. Bacteriochlorins have intense absorption bands in the region of 720-850 nm, allowing for deeper light penetration through tissue and bypassing the melanin absorption.

During the past decade, several naturally occurring or naturally derived bacteriochlorins have been evaluated in PDT applications, and some of them have shown significant *in vivo* efficacy.^{14,15} However, naturally occurring bacteriochlorins have the following drawbacks:

limited synthetic malleability, susceptibility to unwanted dehydrogenation, a requirement for harsh conditions for the modification of functional groups already present in the macrocycle.

To overcome the aforementioned limitations of naturally occurring bacteriochlorins, a *de novo* synthetic pathway to stable bacteriochlorins has been developed.¹⁶ A key design feature of the synthetic bacteriochlorins is a geminal-dimethyl group in each reduced, pyrroline ring that locks-in the bacteriochlorin chromophore and precludes dehydrogenation or tautomerization processes. This structural feature dramatically increases the chemical stability and eliminates susceptibility to degradative aerobic oxidation.

In this report, three synthetic bacteriochlorins in combination with 730-nm illumination from a diode laser were tested and the results compared with those for the clinically approved photosensitizer Photofrin (630 nm absorption) and with lutetium texaphyrin (LuTex), which is an established near-infrared absorbing photosensitizer.¹⁷ These studies utilized a series of human and mouse melanoma cell lines that differ in the pigmentation levels. The selected compounds performed significantly better when compared to Photofrin or LuTex, even in highly pigmented cells and led to a significant survival advantage and 20% of cures in an *in vivo* model. A preliminary account of this work has been presented at International Photodynamic Association Conference as a proceedings paper.¹⁸

The results presented here suggest that PDT may be a promising therapeutic option to treat melanoma patients and to prevent relapse of the disease. PDT has been shown to have the potential to induce an anti-tumor immune response capable of destroying well-established tumors as well as distant metastases.¹⁹ It is therefore of utmost importance to establish effective PDT treatment regimens of melanoma in order to be able to explore the possible immunological benefits in patients. PDT may never replace surgery for localized melanoma. Nevertheless it may

be an effective treatment option for skin-disseminated tumors, unresectable melanomas, mucosal and ocular tumors as well as for patients with stage III and IV melanoma.

Experiment methods

Photophysical measurements and molecular orbital characteristics

Photophysical measurements were performed as described previously.²³ The quantum yield and lifetime measurements utilized Ar-purged solutions (methanol or 2-methyltetrahydrofuran) except that the triplet lifetime for **3** was determined using a deoxygenated (by free-pump-thaw) aqueous Cremophor micellar solution. Fluorescence yields were determined with respect to 8,8,18,18-tetramethylbacteriochlorin²⁴ in Ar-purged toluene, for which $\Phi_f = 0.125$ was established with respect to chlorophyll *a* in benzene [$\Phi_f = 0.325$]²⁵ and free base tetraphenylporphyrin toluene [$\Phi_f = 0.090$]²⁶ using Soret and Q_x excitation.

Density functional theory calculations were performed with Spartan '08 for Windows (Wavefunction, Irvine, CA, USA; ref. 27) using the hybrid B3LYP functional and 6-31G* basis set; equilibrium geometries were fully optimized using the default program parameters.

Synthesis and photodynamic activity

Experimental informations are given in Ref A.

Results

Photophysical properties

The detailed photophysical properties of the bacteriochlorins **1–3** are given in Table S1 of the Supplementary Materials. The compounds exhibit a narrow range of near-infrared absorption maxima (721–737 nm; Figure 1), fluorescence yields (0.093–0.18), and lifetimes of

the lowest singlet excited state (3.7–4.8 ns). The lifetimes of the lowest triplet excited state are (180–200 μ s) for **2** and **3**, ~55 μ s for the analogs of **1**, and 20 μ s for the standard photosensitizer LuTex, all in the absence of molecular oxygen. The triplet lifetimes are reduced to <1 μ s in the presence of atmospheric oxygen, indicating facile excited-state quenching. The yields of the triplet excited state (0.41–0.53) are similar to the value of 0.54 for the naturally occurring bacteriopheophytin *a*.³¹ These results indicate that any significant differences in phototoxicity of **1–3** must derive primarily from sources other than the lifetime and yield of the triplet excited state (from which the reactive oxygen species is produced).

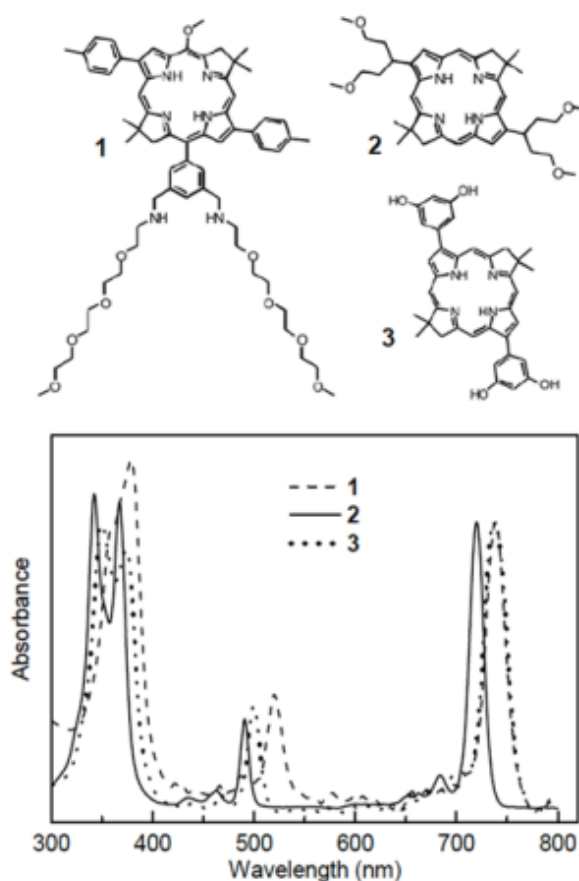


Figure 1. Molecular structures and absorption spectra (normalized at the Q_y band) for the bacteriochlorins **1**, **2**, and **3** in DMSO at room temperature. Spectral characteristics are listed in Table S1.

Molecular orbital characteristics

As indicated in Table S1 of the Supplementary Materials, the highest occupied molecular orbital (HOMO) energy becomes more negative along the following series: **2** (−4.36 eV) < **1** (−4.39 eV) < **3** (−4.46 eV). The lowest unoccupied molecular orbital (LUMO) energy becomes more negative along the same series: **2** (−2.12) < **1** (−2.20) < **3** (−2.28). Thus, **3** should be harder to oxidize and easier to reduce than **1**, which in turn should be harder to oxidize and easier to reduce than **2**. A prior study of a series of zinc chlorins showed excellent linear correlations between the calculated orbital energies and measured redox potentials (32). These results suggest the shifts in oxidation and reduction potentials for the bacteriochlorins studied here (i.e., **2** versus **3**) are likely to be on the order of 100 mV.

The above values reflect differences in ground-state (S_0) properties. The lowest triplet excited state (T_1) will be both a more potent oxidizing and reducing agent than S_0 by the T_1 – S_0 energy gap. This gap should be the same to within ~0.05 eV for bacteriochlorins **1–3** due to their similar structure, comparable S_1 energies, and comparable LUMO-HOMO energy gaps (Table S1 of SI). Thus, the trends in the redox characteristics for T_1 for **1–3** will track those given above for S_0 . Since **3** and not **1** is the most potent PDT agent tested, these findings suggests that if a Type I (electron-transfer) mechanism is operative, then the reduction of the bacteriochlorin T_1 excited state is involved. If **1** had been the best photosensitizer, then oxidation (rather than reduction) of the T_1 excited state would occur.

Effectiveness of bacteriochlorin-mediated PDT against C-mel melanoma cells

The effectiveness of **1**, **2** and **3** was tested against the highly pigmented human melanoma cell line, C-mel. There was no dark toxicity after 24 h incubation in any case. All compounds

tested were effective in producing PDT-induced loss of mitochondrial activity in a dose-dependent and light-dependent manner against C-mel cells (Figure 2A). The order of effectiveness is **3** > **2** > **1**. Bacteriochlorin **3** kills over two logs of C-mel cells at a remarkably low 0.25 μM and $5\text{J}/\text{cm}^2$ of light, as measured by mitochondrial activity. The order of relative C-mel cell uptake values of **1**, **2**, and **3** after 24 h incubation (Figure 2B) is **3** >> **2** > **1**. This trend broadly correlates with the order of PDT effectiveness, except that there is a large difference in PDT effectiveness between **2** and **1**, and only a small difference in cell uptake.

Effects of melanin content on PDT effectiveness with bacteriochlorin photosensitizers.

The effectiveness of the best performing bacteriochlorin, **3**, was then tested in three variants of the pigmented mouse melanoma cell line B16 that had very different levels of pigmentation. The absorption spectra between 300 and 700-nm showing the melanin levels in these three cell lines as well as the morphology are shown in Figure S2 of the Supplementary Materials. B16-G4F lacks the α -MSH receptor and has low melanin levels (OD at 400 nm of 0.055) (33). B16F1 has moderate levels of melanin (OD at 400nm of 0.5214); however, after growth for 7 days in low glucose-containing medium the melanin level was greatly increased (B16F1 LG, OD at 400 nm of 1.1841) (34). Figure 2C shows that the extent of killing correlates well with the amount of intracellular melanin pigment: the B16G4F was effectively eradicated after incubation with **3** and illumination with $10\text{J}/\text{cm}^2$ of 730-nm light ($\text{LD}_{50} \approx 0.1\ \mu\text{M}$), while the moderately pigmented B16F1 needed somewhat more **3** ($\text{LD}_{50} \approx 0.2\ \mu\text{M}$), and even the highly pigmented B16F1 LG was still effectively killed by **3** ($\text{LD}_{50} \approx 0.5\ \mu\text{M}$), as measured by mitochondrial activity assay. Cellular uptake values of **3** by the different B16 variants showed no significant differences (data not shown) suggesting that differences in PDT killing were solely due to differences in melanin content.

Results were obtained for comparison of the effectiveness of Photofrin-mediated PDT on the same three cell lines (Figure 2D). Photofrin mediated PDT was much less effective against B16G4F than bacteriochlorin **3**, as shown by the higher concentration needed ($LD_{50} \approx 3 \mu\text{M}$) but nevertheless significant PDT killing was observed. The effectiveness of Photofrin was dramatically reduced in the case of B16F1 ($LD_{50} \approx 10 \mu\text{M}$) and completely abolished in B16F1 LG cells (no LD_{50}).

The effectiveness of **3**, Photofrin and LuTex were compared via a photosensitizer dose-variation experiment using a single light fluence (10 J/cm^2). Figure 2E shows that the clinically approved Photofrin was hardly able to kill any pigmented B16F10 melanoma cells even at $10 \mu\text{M}$ ($LD_{50} \approx 10 \mu\text{M}$), while LuTex could kill 90% at $5 \mu\text{M}$ ($LD_{50} \approx 1 \mu\text{M}$), and the extremely effective **3** could kill 98% at only $1 \mu\text{M}$ ($LD_{50} \approx 0.1 \mu\text{M}$). Values for photosensitizer uptake by B16F10 cells (Figure 2F) show that Photofrin actually had the largest uptake while the uptake of **3** was only slightly higher than LuTex (although the PDT killing was markedly higher). To confirm that the MTT assay correctly reported cell death, the survival fractions after PDT with **3** and Photofrin as determined by the MTT assay were compared with those found using the crystal violet (CV) assay that measures cellular integrity (see Figure S1 of Supplementary Materials). The killing assessed by MTT was somewhat higher than that found with CV but overall the dose response was very similar. Moreover, transmission electron micrographs confirmed complete cellular destruction after PDT with **3** (Figure S1 of Supplementary Materials).

More results to elucidate PDT effectiveness which are intracellular localization of the bacteriochlorins, isolation of melanosomes, melanosome destruction by PDT using near-infrared light, reactive oxygen species production, and bacteriochlorin-PDT on pigmented melanoma in mice are recorded in ref A.

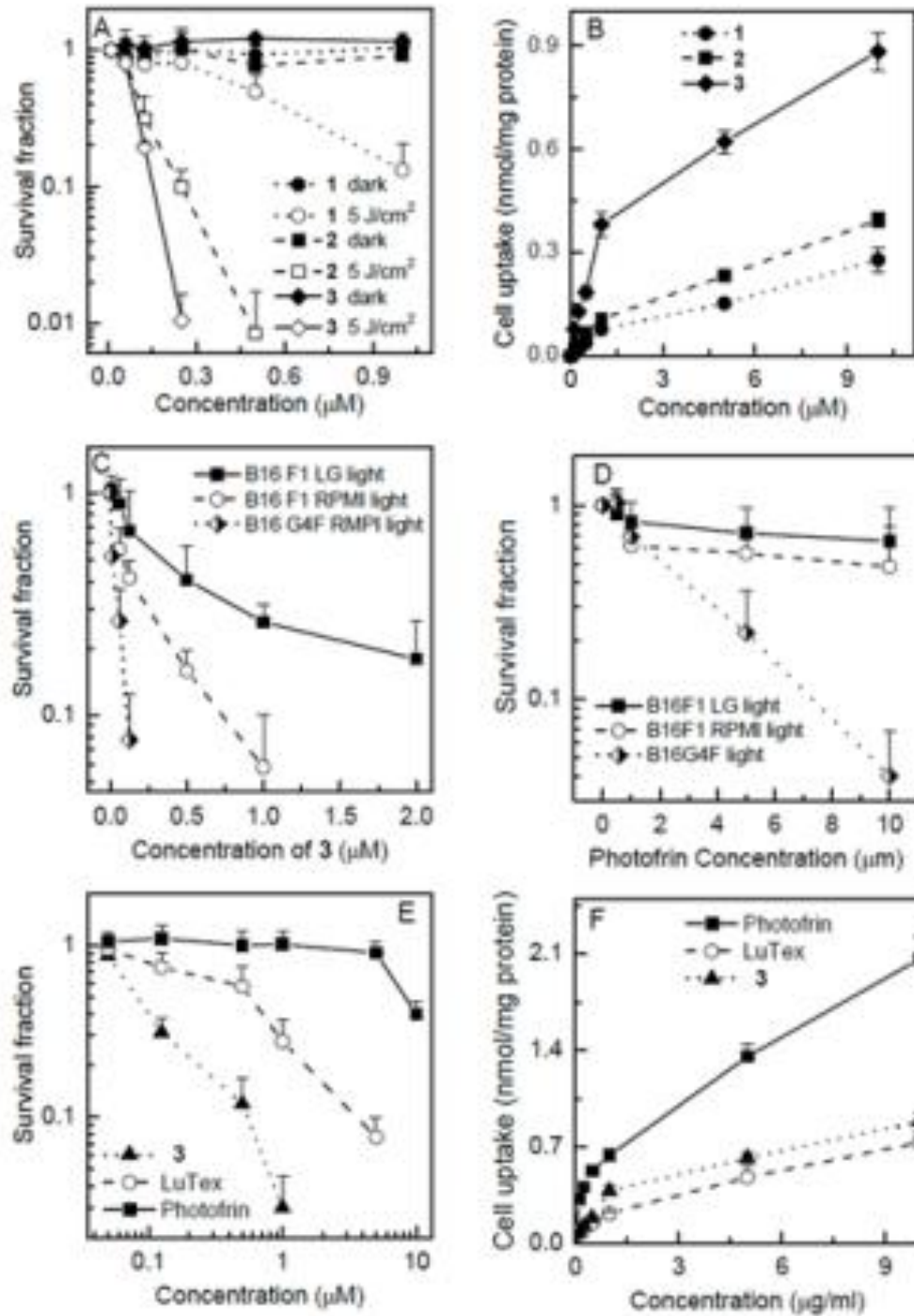


Figure 2. (A) *In vitro* PDT effectiveness of **1**, **2** and **3** in human melanoma cell line, C-mel. (B) Cellular uptake of **1**, **2**, and **3** after 24 h incubation with C-mel cells. (C) Effectiveness of 5J/cm² PDT with **3** and (D) Photofrin against differently pigmented variants of B16 mouse melanoma cells. (E) Comparison of PDT effectiveness on B16F10 melanoma cells mediated by **3**, LuTex, and Photofrin. (F) B16F10 cellular uptake of **3**, LuTex and Photofrin.

Discussion

This report has demonstrated that innovative synthetic stable bacteriochlorins, which absorb light in the near-infrared spectral region, are highly active photosensitizers against melanoma both *in vitro* and *in vivo*. There have been suggestions that melanoma is one of the most resistant types of cancer to PDT because photoactivating light is absorbed by intracellular melanin rather than by the photoactive photosensitizer that is localized within the melanoma cells.

The examined synthetic bacteriochlorins when combined with 730-nm light are significantly better at killing both pigmented and non-pigmented melanoma cells compared to the FDA-approved Photofrin and 635-nm light and another near-infrared absorbing photosensitizer LuTex. Moreover, the bacteriochlorins examined herein, particularly **2** and **3**, are effective at significantly lower concentrations (bacteriochlorin < 0.5 μM versus Photofrin > 6 μM), thereby reducing side effects.

Regarding the mechanism of PDT for the bacteriochlorins studied herein, *in vitro* experiments performed with fluorescent probes for singlet oxygen and for hydroxyl radical reveal no difference between **2** and **3** in singlet oxygen generation but that **3** produces significantly more hydroxyl radicals than **2**. The finding of similar singlet oxygen production for **2** and **3** is consistent with the comparable photophysical characteristics (Table S1). The finding that **3** produces more hydroxyl radicals than **2** is consistent with the expected difference in redox properties of the two compounds on the basis of the molecular-orbital calculations. In particular, bacteriochlorin **3** should be easier to reduce (and harder to oxidize) than **2** (and **1**).

A Type I mechanism that fits the latter results requires that the triplet excited state of the bacteriochlorin receives an electron from an endogenous substrate that acts as a reducing agent,

and subsequently passes the electron to O₂ leading to formation of superoxide radical ion and subsequently to hydroxyl radicals (or other reactive species). This mechanism, as opposed to the well-understood Type II mechanism (which involves energy transfer from the excited bacteriochlorin triplet to ground state triplet oxygen ³O₂ to form reactive singlet oxygen ¹O₂), is in keeping with prior work on a set of imidazole-substituted porphyrins.^{23,28} This type of electron-transfer mechanism has been also proposed as one mode of PDT activity of the palladium bacteriochlorin TOOKAD.⁴² These considerations suggest that the greater PDT efficacy of **3** compared to **2** (or **1**) may derive from enhanced activity of **3** via a Type I mechanism that generates hydroxyl radicals (and/or another reactive species), perhaps supplementing singlet oxygen formation via a Type II mechanism.

Discussion about localization and comparison with commercial photosensitizers is recorded in detail in elsewhere.^A

Conclusions

The lack of development of PDT as a therapy for melanoma is thought to be due to ineffectiveness of methodologies using presently available photosensitizers and to the optical quenching of the activating light by the melanin pigment. The results presented here show that there is high promise for future clinical application of synthetic bacteriochlorins in PDT of pigmented melanoma.

Supplementary Material: An additional description of some methods, along with additional results and figures is provided in supplementary materials as noted in ref (A).

Acknowledgments

This work was supported by grants from the NIH (R01GM36238 to J.S.L. and R01AI050875 to M.R.H.), a Burroughs-Wellcome fellowship (to M.K.), and the Jimmy V.

NCSU Cancer Therapeutics Training Program. P.M. and T.B. were supported by a grant (R41AI072854) from the National Institute of Allergy and Infectious Diseases to NIRvana Pharmaceuticals, Inc. P.M. was partly supported by Genzyme-Partners Translational research Grant. A.S. was supported by the Foundation for Polish Science, International Union Against Cancer and European Structural Fund: “Mazowieckie Stypendium Doktoranckie”. Characterization of the photophysical and redox properties of the bacteriochlorins described herein was initially motivated by solar-energy studies and supported by grants from the Division of Chemical Sciences, Geosciences and Biosciences Division, Office of Basic Energy Sciences of the U.S. Department of Energy to D.F.B. (DE-FG02-05ER15660) and D.H. (DE-FG02-05ER15661). We are grateful to Pharmacyclics, Inc. for the gift of LuTex and loan of 730-nm laser, and to QLT, Inc. for the gift of Photofrin.

References

- (A) P. Mroz, YY Huang, A Szokalska, T Zhiyentayev, S Janjua, AP Nifli, M E. Sherwood, C Ruzié, K. E Borbas, D Fan, M Krayner, T Balasubramanian, Ek Yang, H L Kee, Christine Kirmaier, James R. Diers, David F. Bocian, Dewey Holten, Jonathan S. Lindsey, and M R. HamblinStable. Synthetic Bacteriochlorins Overcome The Resistance of Melanoma to Photodynamic therapy.2010 .*The FASEB Journal* vol. 24 no. 9 3160-3170
- (1) National Comprehensive Cancer Network, Inc Fort Washington, PA, USA: National Comprehensive Cancer Network, Inc.; *The NCCN Clinical Practice Guidelines in Oncology™ Melanoma* (Version, V. I. 2010) 2009
- (2) Kirkwood J M, Strawderman M H, Ernstoff M S, Smith T J, Borden E C, Blum R H. Interferon alfa-2b adjuvant therapy of high-risk resected cutaneous melanoma: the Eastern Cooperative Oncology Group Trial EST 1684. *J Clin Oncol.* 1996;14:7–17.
- (3) Cummins D L, Cummins J M, Pantle H, Silverman M A, Leonard A L, Chanmugam A. Cutaneous malignant melanoma. *Mayo Clin Proc.* 2006;81:500–507.
- (4) Naylor M F, Chen W R, Teague T K, Perry L A, Nordquist R E. In situ photoimmunotherapy: a tumour-directed treatment for melanoma. *Br J Dermatol.* 2006;155:1287–1292.
- (5) Castano A P, Demidova T N, Hamblin M R. Mechanisms in photodynamic therapy: part one—photosensitizers, photochemistry and cellular localization. *Photodiagn Photodyn Ther.*2004;1:279–293.
- (6) Slominski A, Paus R, Schadendorf D. Melanocytes as “sensory” and regulatory cells in the epidermis. *J Theor Biol.* 1993;164:103–120.
- (7) Slominski A, Tobin D J, Shibahara S, Wortsman J. Melanin pigmentation in mammalian skin and its hormonal regulation. *Physiol Rev.* 2004;84:1155–1228.
- (8) Slominski A, Wortsman J, Carlson A J, Matsuoka L Y, Balch C M, Mihm M C. Malignant melanoma. *Arch Pathol Lab Med.* 2001;125:1295–1306

- (9) Riley P A. Melanogenesis and melanoma. *Pigment Cell Res.* 2003;16:548–552
- (10) Simon J D, Peles D, Wakamatsu K, Ito S. Current challenges in understanding melanogenesis: bridging chemistry, biological control, morphology, and function. *Pigment Cell Melanoma Res.*2009;22:563–579.
- (11) Carlson J A, Ross J S, Slominski A, Linette G, Mysliborski J, Hill J, Mihm M., Jr Molecular diagnostics in melanoma. *J Am Acad Dermatol.* 2005;52:743–775; quiz 775–748.
- (12) Suzuki I, Cone R D, Im S, Nordlund J, Abdel-Malek Z A. Binding of melanotropic hormones to the melanocortin receptor MC1R on human melanocytes stimulates proliferation and melanogenesis. *Endocrinology.* 1996;137:1627–1633
- (13) Lapouge K, Naveke A, Gall A, Ivancich A, Seguin J, Scheer H, Sturgis J N, Mattioli T A, Robert B. Conformation of bacteriochlorophyll molecules in photosynthetic proteins from purple bacteria. *Biochemistry.* 1999;38:11115–11121.
- (14) Trachtenberg J, Weersink R A, Davidson S R, Haider M A, Bogaards A, Gertner M R, Evans A, Scherz A, Savard J, Chin J L, Wilson B C, Elhilali M. Vascular-targeted photodynamic therapy (padoporfin, WST09) for recurrent prostate cancer after failure of external beam radiotherapy: a study of escalating light doses. *BJU Int.* 2008;102:556–562.
- (15) Mazor O, Brandis A, Plaks V, Neumark E, Rosenbach-Belkin V, Salomon Y, Scherz A. WST11, a novel water-soluble bacteriochlorophyll derivative; cellular uptake, pharmacokinetics, biodistribution and vascular-targeted photodynamic activity using melanoma tumors as a model. *Photochem Photobiol.* 2005;81:342–351.
- (16) Kim H J, Lindsey J S. De novo synthesis of stable tetrahydroporphyrinic macrocycles: bacteriochlorins and a tetrahydrocorrin. *J Org Chem.* 2005;70:5475–5486.
- (17) Yeung P F. Motexafin lutetium (Pharmacyclics) *IDrugs.* 2001;4:351–359.
- (18) Mroz P, Huang Y-Y, Janjua S, Zhiyentayev T, Ruzié C, Borbas K, Fan E D, Krayner M, Balasubramanian T, Kang E, Kee K H, Holten L D, Lindsey S J, Hamblin M R. New stable synthetic bacteriochlorins for photodynamic therapy of melanoma. *Proc SPIE.*2009;7380:73802S.
- (19) Castano A P, Mroz P, Hamblin M R. Photodynamic therapy and anti-tumour immunity. *Nat Rev Cancer.* 2006;6:535–545.
- (20) Fan D, Taniguchi M, Lindsey J S. Regioselective 15-bromination and functionalization of a stable synthetic bacteriochlorin. *J Org Chem.* 2007;72:5350–5357.
- (21) Borbas K E, Ruzie C, Lindsey J S. Swallowtail bacteriochlorins. Lipophilic absorbers for the near-infrared. *Org Lett.* 2008;10:1931–1934.

- (22) Ruzié C, Krayer M, Balasubramanian T, Lindsey J S. Tailoring a bacteriochlorin building block with cationic, amphipathic, or lipophilic substituents. *J Org Chem.* 2008;73:5806–5820.
- (23) Kee H L, Bhaumik J, Diers J R, Mroz P, Hamblin M R, Bocian D F, Lindsey J S, Holten D. Photophysical characterization of imidazolium-substituted Pd(II), In(III), and Zn(II) porphyrins as photosensitizers for photodynamic therapy. *J Photochem Photobiol A.*2008;200:346–355.
- (24) Taniguchi M, Cramer D L, Bhise A D, Kee H L, Bocian D F, Holten D, Lindsey J S. Accessing the near-infrared spectral region with stable, synthetic, wavelength-tunable bacteriochlorins. *New J Chem.* 2008;32:947–958.
- (25) Weber G, Teale F W J. Determination of the absolute quantum yield of fluorescent solutions. *Trans Faraday Soc.* 1957;53:646–655.
- (26) Gradyushko A T, Sevchenko A N, Solovyov K N, Tsvirko M P. Energetics of photophysical processes in chlorophyll-like molecules. *Photochem Photobiol.* 1970;11:387–400.
- (27) Shao Y, Molnar L F, Jung Y, Kussmann J, Ochsenfeld C, Brown S T, Gilbert A T B, Slipchenko L V, Levchenko S V, O'Neill D P, DiStasio R A, Jr, Lochan R C, Wang T, Beran G J O, Besley N A, Herbert J M, Lin C Y, Van Voorhis T, Chien S H, Sodt A, Steele R P, Rassolov V A, Maslen P E, Korambath P P, Adamson R D, Austin B, Baker J, Byrd E F C, Dachsel H, Doerksen R J, Dreuw A, Dunietz B D, Dutoi A D, Furlani T R, Gwaltney S R, Heyden A, Hirata S, Hsu C-P, Kedziora G, Khalliulin R Z, Klunzinger P, Lee A M, Lee M S, Liang W Z, Lotan I, Nair N, Peters B, Proynov E I, Pieniazek P A, Rhee Y M, Ritchie J, Rosta E, Sherrill C D, Simmonett A C, Subotnik J E, Woodcock H L, III, Zhang W, Bell A T, Chakraborty A K, Chipman D M, Keil F J, Warshel A, Hehre W J, Schaefer H F, Kong J, Krylov A I, Gill P M W, Head-Gordon M. Advances in methods and algorithms in a modern quantum chemistry program package. *Phys Chem Chem Phys.* 2006;8:3172–3191.
- (28) Mroz P, Bhaumik J, Dogutan D K, Aly Z, Kamal Z, Khalid L, Kee H L, Bocian D F, Holten D, Lindsey J S, Hamblin M R. Imidazole metalloporphyrins as photosensitizers for photodynamic therapy: role of molecular charge, central metal and hydroxyl radical production. *Cancer Lett.*2009;282:63–76.
- (29) Orlow S J, Boissy R E, Moran D J, Pifko-Hirst S. Subcellular distribution of tyrosinase and tyrosinase-related protein-1: implications for melanosomal biogenesis. *J Invest Dermatol.*1993;100:55–64.
- (30) Sapan C V, Lundblad R L, Price N C. Colorimetric protein assay techniques. *Biotechnol Appl Biochem.* 1999;29:99–108.

- (31) Price M, Reiners J J, Santiago A M, Kessel D. Monitoring singlet oxygen and hydroxyl radical formation with fluorescent probes during photodynamic therapy. *Photochem Photobiol.* 2009;85:1177–1181.
- (32) Setsukinai K, Urano Y, Kakinuma K, Majima H J, Nagano T. Development of novel fluorescence probes that can reliably detect reactive oxygen species and distinguish specific species. *J Biol Chem.* 2003;278:3170–3175.
- (33) Su J, Zhang J, Liu L, Huang Y, Mason R P. Exploring feasibility of multicolored CdTe quantum dots for in vitro and in vivo fluorescent imaging. *J Nanosci Nanotechnol.* 2008;8:1174–1177.
- (34) Chang S K, Rizvi I, Solban N, Hasan T. In vivo optical molecular imaging of vascular endothelial growth factor for monitoring cancer treatment. *Clin Cancer Res.* 2008;14:4146–4153.
- (35) Holten D, Gouterman M, Parson W W, Windsor M W, Rockley M G. Electron transfer from photoexcited singlet and triplet bacteriopheophytin. *Photochem Photobiol.* 1976;23:415–420.
- (36) Kee H L, Kirmaier C, Tang Q, Diers J R, Muthiah C, Taniguchi M, Laha J K, Ptaszek M, Lindsey J S, Bocian D F, Holten D. Effects of substituents on synthetic analogs of chlorophylls. Part 2: Redox properties, optical spectra and electronic structure. *Photochem Photobiol.* 2007;83:1125–1143.
- (37) Solca F F, Chluba-de Tapia J, Iwata K, Eberle A N. B16–G4F mouse melanoma cells: an MSH receptor-deficient cell clone. *FEBS Lett.* 1993;322:177–180.
- (38) Nakayasu M, Saeki H, Tohda H, Oikawa A. Effects of sugars on melanogenesis in cultured melanoma cells. *J Cell Physiol.* 1977;92:49–55.
- (39) Orlow S J. Melanosomes are specialized members of the lysosomal lineage of organelles. *J Invest Dermatol.* 1995;105:3–7.
- (40) Kuroda T S, Itoh T, Fukuda M. Functional analysis of slac2-a/melanophilin as a linker protein between Rab27A and myosin Va in melanosome transport. *Methods Enzymol.* 2005;403:419–431.
- (41) Hong L, Garguilo J, Anzaldi L, Edwards G S, Nemanich R J, Simon J D. Age-dependent photoionization thresholds of melanosomes and lipofuscin isolated from human retinal pigment epithelium cells. *Photochem Photobiol.* 2006;82:1475–1481.
- (42) Ashur I, Goldschmidt R, Pinkas I, Salomon Y, Szewczyk G, Sarna T, Scherz A. Photocatalytic generation of oxygen radicals by the water-soluble bacteriochlorophyll derivative WST11, noncovalently bound to serum albumin. *J Phys Chem A.* 2009;113:8027–8037.

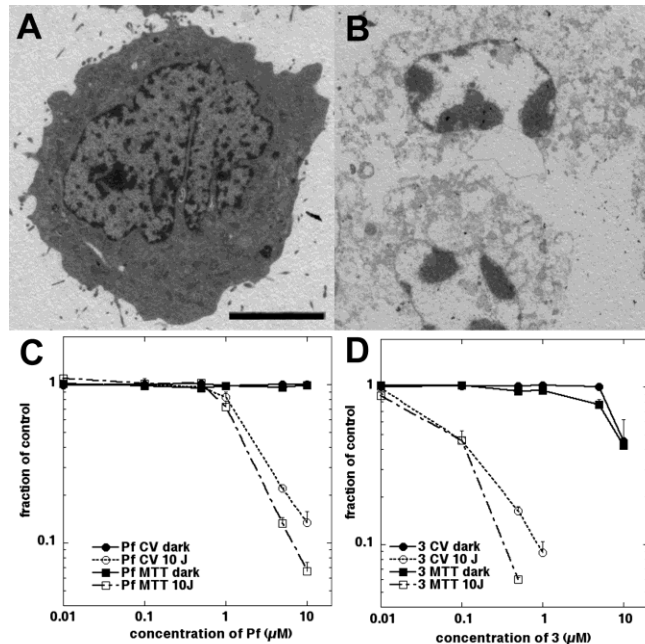
- (43) Chen K G, Valencia J C, Lai B, Zhang G, Paterson J K, Rouzaud F, Berens W, Wincovitch S M, Garfield S H, Leapman R D, Hearing V J, Gottesman M M. Melanosomal sequestration of cytotoxic drugs contributes to the intractability of malignant melanomas. *Proc Natl Acad Sci U S A*. 2006;103:9903–9907.
- (44) Chen K G, Valencia J C, Gillet J P, Hearing V J, Gottesman M M. Involvement of ABC transporters in melanogenesis and the development of multidrug resistance of melanoma. *Pigment Cell Melanoma Res*. 2009;22:740–749.
- (45) Safaei R, Larson B J, Cheng T C, Gibson M A, Otani S, Naerdemann W, Howell S B. Abnormal lysosomal trafficking and enhanced exosomal export of cisplatin in drug-resistant human ovarian carcinoma cells. *Mol Cancer Ther*. 2005;4:1595–1604.
- (46) Safaei R, Katano K, Larson B J, Samimi G, Holzer A K, Naerdemann W, Tomioka M, Goodman M, Howell S B. Intracellular localization and trafficking of fluorescein-labeled cisplatin in human ovarian carcinoma cells. *Clin Cancer Res*. 2005;11:756–767.
- (47) Szakacs G, Gottesman M M. Comparing solid tumors with cell lines: implications for identifying drug resistance genes in cancer. *Mol Interv*. 2004;4:323–325.
- (48) Liu W, Baer M R, Bowman M J, Pera P, Zheng X, Morgan J, Pandey R A, Oseroff A R. The tyrosine kinase inhibitor imatinib mesylate enhances the efficacy of photodynamic therapy by inhibiting ABCG2. *Clin Cancer Res*. 2007;13:2463–2470.
- (49) Liu Y, Hong L, Wakamatsu K, Ito S, Adhyaru B, Cheng C Y, Bowers C R, Simon J D. Comparison of structural and chemical properties of black and red human hair melanosomes. *Photochem Photobiol*. 2005;81:135–144.
- (50) Slominski A, Zbytek B, Slominski R. Inhibitors of melanogenesis increase toxicity of cyclophosphamide and lymphocytes against melanoma cells. *Int J Cancer*. 2009;124:1470–1477.
- (51) Brozyna A A, VanMiddlesworth L, Slominski A T. Inhibition of melanogenesis as a radiation sensitizer for melanoma therapy. *Int J Cancer*. 2008;123:1448–1456.
- (52) Castano A P, Mroz P, Wu M X, Hamblin M R. Photodynamic therapy plus low-dose cyclophosphamide generates antitumor immunity in a mouse model. *Proc Natl Acad Sci U S A*. 2008;105:5495–5500.
- (53) Dellian M, Richert C, Gamarra F, Goetz A E. Photodynamic eradication of amelanotic melanoma of the hamster with fast acting photosensitizers. *Int J Cancer*. 1996;65:246–248.
- (54) Buseti A, Soncin M, Jori G, Rodgers M A. High efficiency of benzoporphyrin derivative in the photodynamic therapy of pigmented malignant melanoma. *Br J Cancer*. 1999;79:821–824.

- (55) Biolo R, Jori G, Soncin M, Rihter B, Kenney M E, Rodgers M A. Effect of photosensitizer delivery system and irradiation parameters on the efficiency of photodynamic therapy of B16 pigmented melanoma in mice. *Photochem Photobiol.* 1996;63:224–228.
- (56) Woodburn K W, Fan Q, Kessel D, Luo Y, Young S W. Photodynamic therapy of B16F10 murine melanoma with lutetium texaphyrin. *J Invest Dermatol.* 1998;110:746–751.
- (57) Mennel S, Barbazetto I, Meyer C H, Peter S, Stur M. Ocular photodynamic therapy—standard applications and new indications (part 1). Review of the literature and personal experience. *Ophthalmologica.* 2007;221:216–226.
- (58) Sheleg S V, Zhavrid E A, Khodina T V, Kochubeev G A, Istomin Y P, Chalov V N, Zhuravkin I N. Photodynamic therapy with chlorin e(6) for skin metastases of melanoma. *Photodermatol Photoimmunol Photomed.* 2004;20:21–26.

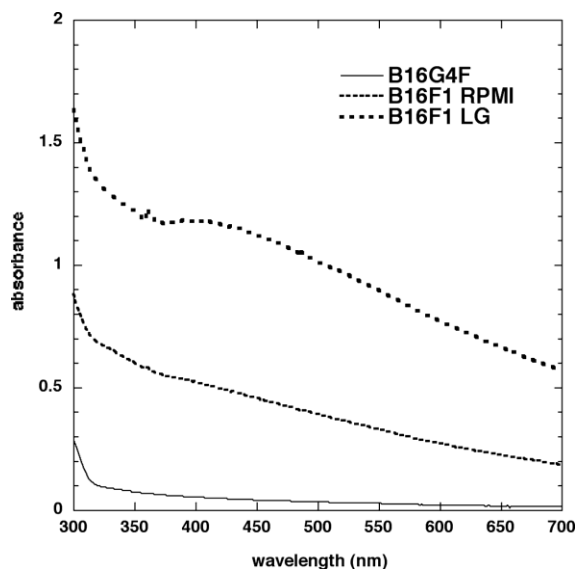
Supplementary materials

Materials and methods

Photosensitizers



Supplementary Figure 1. TEM micrographs of morphological changes observed after PDT with 2. A) Control, non-treated cells; B) B16F10 melanoma cells 8h after PDT with bacteriochlorin 2. Scale bar is 5 μm . Comparison of Photofrin (C) and bacteriochlorin 3 (D) PDT killing effects measured by MTT metabolic assay and also by crystal violet (CV) cellular integrity assays.



Supplementary figure 2 Visible absorption spectra of cell lysates containing equal numbers of melanoma cells of B16G4F (low melanin), B16F1 growing in RPMI medium (moderate melanin) and B16F1 growing in low glucose DMEM medium (high melanin).

Other photoactivity supplementary are described in ref A.

Photophysical measurements

All photophysical measurements were performed on samples of the bacteriochlorin in Ar-purged solutions at room temperature unless noted otherwise. Static absorption (Cary 100) and fluorescence (Spex Fluorolog2) measurements were performed using dilute (μM) non-Ar-purged solutions.⁵ Solutions with an absorbance of ≤ 0.15 at the Soret-band excitation wavelength were used for the fluorescence spectral, quantum yield and lifetime measurements. The lifetime of the lowest singlet excited state (τ_S) for a given compound was obtained using a fluorescence phase-modulation technique.⁶

Fluorescence quantum yields (Φ_f) were measured with respect to 8,8,18,18-tetramethylbacteriochlorin⁷ using Ar-purged solutions. The value of $\Phi_f = 0.125$ for the latter compound in toluene was established with respect to chlorophyll *a* in benzene [$\Phi_f = 0.325$]⁸ and free base tetraphenylporphyrin toluene [$\Phi_f = 0.090$]⁹ using several excitation wavelengths

spanning the Soret and Q_x absorption bands. Yields of the lowest excited triplet state (Φ_{isc}) were determined for compounds in methanol or 2-methyltetrahydrofuran using a transient-absorption technique.⁵ The lifetimes of the lowest energy triplet excited state (τ_T) for compounds in Ar-purged 2-methyltetrahydrofuran (MeTHF) were determined using a setup described previously.⁵ The triplet lifetime for **3** was also measured in an aqueous Cremophor micellar solution that was deoxygenated by repeated freeze-pump-thaw cycles on a vacuum line (< 1 micron pressure).

Table S1. Photophysical Properties and Molecular-Orbital Energies of Bacteriochlorins.^a

Cmpd	Q _y (0,0) ^b absorption		Q _y (0,0) ^b fluorescence		Φ_f^c	τ_s^d (ns)	Φ_{isc}^e	τ_T^f (μ s)	Orbital Energy	
	λ (nm)	fwhm (nm)	λ (nm)	fwhm (nm)					HOMO (eV)	LUMO (eV)
1	739	23	739	24	0.16 ^g	4.1 ^g	0.51 ^g	55 ^g	-4.39	-2.20
2	721	15	727	21	0.093	4.0	0.58	180	-4.36	-2.12
3	737	24	745	20	0.12	3.7	0.41	200 ^h	-4.46	-2.28

^aAll measurements performed on compounds at room temperature. ^bPeak wavelength (λ) and full width at half maximum (fwhm) of spectral feature for compound in aerated solution of DMSO, except the fluorescence data for **1** is for the compound in methanol. ^cFluorescence quantum yield for compound in Ar-purged methanol. ^dLifetime of the lowest singlet excited state for compound in Ar-purged methanol determined using fluorescence detection. ^eMeasured yield of the lowest triplet excited state for the compound in Ar-purged methanol. ^fLifetime of the lowest triplet excited state for the compound in Ar-purged MeTHF unless indicated otherwise. ^gThe average values from two analogs of **1** have the following characteristics (all measurements in Ar-purged toluene except for τ_T which utilized the compound in Ar-purged MeTHF): $\Phi_f = 0.14$, $\tau_s = 3.4$ ns, $\Phi_{isc} = 0.53$, $\tau_T = 45$ μ s for 8,8,18,18-tetramethyl-2,12-di-*p*-tolylbacteriochlorin (determined here; $\Phi_f = 0.18$, $\tau_s = 4.8$ ns, $\Phi_{isc} = 0.50$, $\tau_T = 65$ μ s for 5-methoxy-8,8,18,18-tetramethyl-2,12-di-*p*-tolylbacteriochlorin determined previously (9)). ^hThe triplet lifetime of **3** in deoxygenated (by freeze-pump-thaw procedure) aqueous Cremophore micellar solution is 190 μ s.

References

- (A) P. Mroz, YY Huang, A Szokalska, T Zhiyentayev, S Janjua, AP Nifli, M E. Sherwood, C Ruzié, K. E Borbas, D Fan, M Kraye, T Balasubramanian, Ek Yang, H L Kee, Christine Kirmaier, James R. Diers, David F. Bocian, Dewey Holten, Jonathan S. Lindsey, and M R. Hamblin. Synthetic Bacteriochlorins Overcome The Resistance of Melanoma to Photodynamic therapy. 2010 .*The FASEB Journal* vol. 24 no. 9 3160-3170
- (1) Fan, D., Taniguchi, M., and Lindsey, J. S. (2007) Regioselective 15-bromination and functionalization of a stable synthetic bacteriochlorin. *J Org Chem* 72, 5350-5357
- (2) Borbas, K. E., Ruzie, C., and Lindsey, J. S. (2008) Swallowtail bacteriochlorins. Lipophilic absorbers for the near-infrared. *Org Lett* 10, 1931-1934
- (3) Ruzie, C., Kraye, M., Balasubramanian, T., and Lindsey, J. S. (2008) Tailoring a bacteriochlorin building block with cationic, amphipathic, or lipophilic substituents. *J Org Chem*
- (4) Kim, H. J., and Lindsey, J. S. (2005) De novo synthesis of stable tetrahydroporphyrinic macrocycles: bacteriochlorins and a tetrahydrocorrin. *J Org Chem* 70, 5475-5486
- (5) Kee, H. L., Bhaumik, J., Diers, J. R., Mroz, P., Hamblin, M. R., Bocian, D. F., Lindsey, J. S., and Holten, D. (2008) Photophysical characterization of imidazolium-substituted Pd(II), In(III), and Zn(II) porphyrins as photosensitizers for photodynamic therapy. *J Photochem Photobiol A* 200, 346-355
- (6) Kee, H. L., Kirmaier, C., Yu, L., Thamyongkit, P., Youngblood, W. J., Calder, M. E., Ramos, L., Noll, B. C., Bocian, D. F., Scheidt, W. R., Birge, R. R., Lindsey, J. S., and Holten, D. (2005) Structural control of the photodynamics of boron-dipyrrin complexes. *J Phys Chem B* 109, 20433-20443
- (7) Taniguchi, M., Cramer, D. L., Bhise, A. D., Kee, H. L., Bocian, D. F., Holten, D., and Lindsey, J. S. (2008) Accessing the near-infrared spectral region with stable, synthetic, wavelength-tunable bacteriochlorins. *New J Chem* 32, 947-958
- (8) Weber, G., and Teale, F. W. J. (1957) Determination of the absolute quantum yield of fluorescent solutions. *Trans. Faraday Soc* 53, 646-655
- (9) Gradyushko, A. T., Sevchenko, A. N., Solovyov, K. N., and Tsvirko, M. P. (1970) Energetics of photophysical processes in chlorophyll-like molecules. *Photochem Photobiol* 11, 387-400
- (10) Kong, J., White, C. A., Krylov, A. I., Sherrill, D., Adamson, R. D., Furlani, T. R., Lee, M. S., Lee, A. M., Gwaltney, S. R., Adams, T. R., Ochsenfeld, C., Gilbert, A. T. B., Kedziora, G. S., Rassolov, V. A., Maurice, D. R., Nair, N., Shao, Y., Besley, N. A., Maslen, P. E., Dombroski, J. P., Daschel, H., Zhang, W., Korambath, P. P., Baker, J., Byrd, E. F. C., Van Voorhis, T., Oumi, M., Hirata, S., Hsu, C.-P., Ishikawa, N., Florian, J., Warshel, A., Johnson, B. G., Gill, P. M. W., Head-Gordon, M., and Pople, J. A. (2000) Q-Chem 2.0: a high-performance ab initio electronic structure program package. *J. Computational Chem* 21, 1532-1548

Chapter 9

Stable synthetic bacteriochlorins for photodynamic therapy: role of bis-cyano peripheral groups, central metal substitution (2H, Zn, Pd), and Cremophor EL delivery.

Reproduced in part with permission from Huang, YY; Balasubramanian, T; Yang, EK; Luo, D; Diers, J.R; Bocian, D.F; Lindsey, J. S; Holten, D; Hamblin, MR. Stable Synthetic Bacteriochlorins for Photodynamic Therapy: Role of Dicyano Peripheral Groups, Central Metal Substitution (2H, Zn, Pd), and Cremophor EL Delivery. *ChemMedChem*. 2012, 7, 2155–2167. Doi: 10.1002/cmdc.201200351. Copyright 2012 WILEY-VCH.

Abstract

A series of four stable synthetic bacteriochlorins was tested for photodynamic therapy (PDT) on HeLa cells *in vitro*. The parent bacteriochlorin (**BC**), dicyano derivative (**(NC)₂BC**) and corresponding zinc chelate (**(NC)₂BC-Zn**) and palladium chelate (**(NC)₂BC-Pd**) were studied. Direct dilution of a solution of bacteriochlorin in an organic solvent into serum-containing medium was compared with the dilution of bacteriochlorin in Cremophor EL (CrEL) micelles into the same medium. CrEL generally reduced aggregation (as indicated by absorption and fluorescence) and increased activity up to 10-fold (depending on bacteriochlorin) although it decreased cellular uptake. The order of PDT activity against HeLa human cancer cells after 24 h incubation and illumination with 10 J/cm² of NIR light is (**(NC)₂BC-Pd**) (LD50 = 25 nM) > (**(NC)₂BC**) > (**(NC)₂BC-Zn**) ≈ **BC**. Subcellular localization was in the endoplasmic reticulum, mitochondria and lysosomes depending on the bacteriochlorin. (**(NC)₂BC-Pd**) showed PDT-mediated damage to mitochondria and lysosomes, and the greatest production of hydroxyl radicals as determined using a hydroxyphenylfluorescein probe. The incorporation of cyano substituents provides an excellent motif for the enhancement of the photoactivity and photostability of bacteriochlorins as PDT photosensitizers.

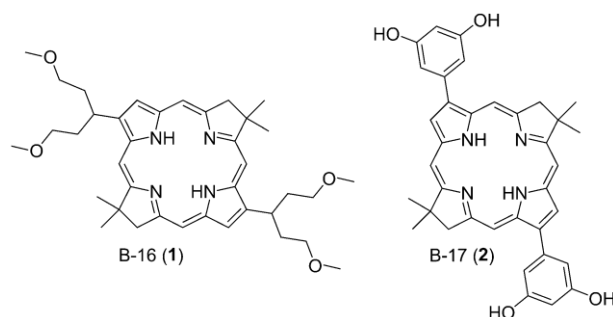
Introduction

Photodynamic therapy (PDT) is a rapidly developing cancer therapy that utilizes the combination of a non-toxic dye termed a photosensitizer (PS) and harmless visible or near-infrared (NIR) light to kill cancer cells and destroy tumors by generating reactive oxygen species (ROS), such as singlet oxygen, superoxide and hydroxyl radical.¹ PDT has the advantage of dual selectivity in that the PS can be targeted to its destination cell or tissue and the illumination can be spatially directed to the lesion. The ROS produced during PDT are effective in killing both malignant and normal cells via necrosis, apoptosis or autophagy depending on the cell type, structure of the PS and the light parameters chosen.

Bacteriochlorins are tetrapyrrole compounds with two opposing pyrrole (reduced pyrrole) rings. The ring structure occurs naturally in photosynthetic pigments (bacteriochlorophylls *a* and *b*) from purple photosynthetic bacteria of the orders *Rhodospirillales* and *Rhizobiales*. Reduction of two pyrrolic rings in the tetrapyrrole macrocycle has a pronounced effect on the absorption spectrum. Bacteriochlorins and bacteriopurpurins have large absorption bands in the NIR spectral region of 720–850 nm where chlorins (one reduced ring) and porphyrins (no reduced rings) effectively do not absorb. The characteristically large absorption of bacteriochlorins and bacteriopurpurins in the NIR is considered to be ideal for maximizing light penetration through tissue because both absorption and scattering of light at these wavelengths by endogenous chromophores are minimal.

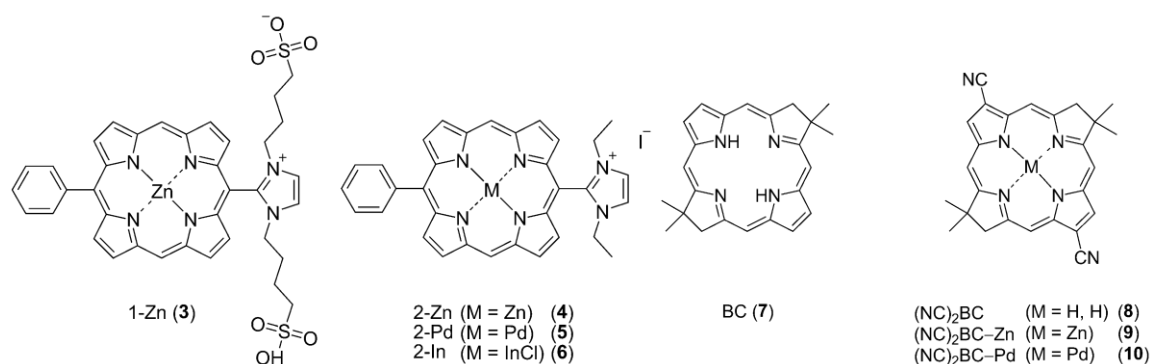
A disadvantage of many naturally occurring bacteriochlorin derivatives is their instability both in the dark and in the light. A *de novo* synthetic route has been developed that affords bacteriochlorins that are stabilized against adventitious oxidation by the presence of a pair of geminal dimethyl groups.² This route has been used to prepare bacteriochlorins containing a

variety of positively charged substituents, groups to impart water solubility, and groups that generally vary in hydrophobicity/hydrophilicity. The bacteriochlorins were employed as PS to test PDT activity against B16 mouse melanoma cells,³ HeLa human cervical cancer cells⁴ and microbial cells (Gram-positive, Gram-negative bacteria and yeast)⁵ *in vitro*. A number of the bacteriochlorins showed high PDT efficacy (e.g., LD50 < 100 nM) against the targeted cell lines, including bacteriochlorins B-16(1) and B-17(2).^{3,4} The reasons for the high PDT efficacy include the following: 1) the chemical characteristics such as lipophilicity ensure that these compounds are highly taken up by the targeted cells and subsequently localize in sensitive intracellular compartments such as mitochondria and endoplasmic reticulum (ER); 2) the long-wavelength absorption band with large extinction coefficient and the good triplet yield ensures that the incident light is optimally used to produce cell killing even with pigmented cells such as melanoma.



Despite the favorable results, some of the compounds studied previously were more readily photobleached than others. This finding indicated that improvements in photostability should be sought to enhance the efficacy of the synthetic bacteriochlorins for use in a variety of PDT protocols. Furthermore, each bacteriochlorin employed was the metal-free (free base) form. PDT efficacy of tetrapyrroles and related macrocycles (porphyrins, chlorins, bacteriochlorins, phthalocyanines, etc.) often depends on the metalation state,⁶ as was found for a set of

imidazolium-substituted metalloporphyrins(1-Zn(3) and 2-M, where M=Zn (4), Pd (5), or InCl (6)).⁷ Therefore, in the present study the PDT efficacy of a group of free-base and metal-substituted bacteriochlorins bearing electron-withdrawing cyano-groups was examined (7-10). The goal was to determine if such substituents and/or the presence or the nature of the central metal ion would enhance photostability and/or alter other physicochemical properties to give even greater efficacy for killing HeLa human cervical cancer cells.



Many hydrophobic molecules such as the present bacteriochlorins are poorly soluble in biological media. Cell uptake should be optimum if the chemical/solubility properties of the PS allow for efficient transport through cellular and subcellular boundaries as well as reasonable solubility in both the cellular space and the delivery vehicle. The formation of molecular aggregates can diminish uptake (due to mobility constraints) and reduce PDT activity (due to rapid nonradiative deactivation of the photoexcited PS). Nonradiative deactivation accompanying aggregation also reduces the ability to probe cellular localization via confocal microscopy because fluorescence is generally dramatically quenched. For these reasons Cremophor EL micellar preparation was studied as a delivery vehicle for the compounds.

Experimental methods

Photostability

Photostability measurements utilized excitation light obtained from a 300W Xenon lamp (Model R300-3 lamp and PS300-1 power supply; ILC Technologies, Sunnyvale, CA) that passed through a 70-cm path cell containing deionized water followed by a monochromator with a 10-nm bandpass. The light intensity at the sample position was measured using a calibrated diode and optometer (Models 221 and S471, United Detector Technologies, San Diego, CA) and was typically $\sim 5 \text{ mW/cm}^2$ at the wavelength (720-750 nm) of the NIR absorption maximum of the bacteriochlorin ($A \sim 0.5$ in 1 cm). The solutions contained ambient (atmospheric) O_2 and were stirred using a micro magnetic bar at the bottom of the cuvette during illumination.

Synthesis and PDT activities

Experimental informations are given in Ref A.

Results

Absorption spectra

The bacteriochlorin PS under study are relatively insoluble in water, which prompted use of two approaches toward solubilization for cell uptake experiments. The procedures are as follows: (1) direct dilution (denoted dd) of bacteriochlorin from organic solvent (5 mM solutions in DMA or THF) into complete culture media containing supplemental 10% FBS and (2) encapsulation into CrEL micelles and dilution of this suspension at a bacteriochlorin concentration of approximately 500 μM into complete medium. Figure 1 shows the absorption spectra for the four PS at 10 μM using these two delivery vehicles compared with the spectra determined in pure methanol. All four compounds show good solubility in methanol, toluene, and a number of other organic media. However, **BC** (7) and **(NC)₂BC** (8) show significant

aggregation using direct dilution into complete medium, which is markedly reduced using CrEL encapsulation prior to dilution into complete medium (Figure 1a,b). The metallobacteriochlorins **(NC)₂BC-Zn** (9) and **(NC)₂BC-Pd** (10) were significantly less aggregated after direct dilution and therefore the effect of CrEL was less pronounced (Figure 1c,d). Synthetic bacteriochlorins such as those studied here absorb strongly in the NIR region, with a molar absorptivity at the NIR maximum (called the Q_y band) of ~120,000 M⁻¹cm⁻¹.²

Photodynamic activity

The best way to compare the phototoxicity of a group of PS having very different activities is to vary the concentration over several orders of magnitude and to determine the cell survival fraction with a single light dose. The results of such studies with the directly diluted PS at concentrations up to 5 μM are shown in Figure 2a. Because PS may exhibit some dark toxicity when used at high concentrations, a dark control was used for each data point. Dark toxicity was negligible (greater than 85% survival at the highest PS concentration tested). The order of effectiveness for PDT activity was as follows: **(NC)₂BC-Pd** > **(NC)₂BC** > **(NC)₂BC-Zn** ≈ **BC**. The most active PS delivered by direct dilution, **(NC)₂BC-Pd**, had an LD50 value of 25 nM. **(NC)₂BC** was intermediate in activity with a LD50 of 60 nM, while the least active PS, **BC** and **(NC)₂BC-Zn**, had LD50 values equal to or greater than 1 μM (Table 1).

The analogous data with CrEL formulated PS are shown in Figure 2b. Note that dark toxicity was significantly higher for this formulation than for the direct dilution; accordingly, the highest concentration that could be tested was 1 μM. **(NC)₂BC-Zn** in CrEL approached 50% dark toxicity at 1 μM, while **BC** showed 30% dark toxicity. The PDT effectiveness of all four PS was improved by CrEL encapsulation. **(NC)₂BC-Zn** showed the most substantial improvement in that CrEL gave a 17-fold decrease in the LD50 concentration from 1 μM to 60

nM, while **BC** gave a 5-fold decrease from 1.8 μM to 350 nM. Only small (<3-fold) improvements were displayed by the more active PS, **(NC)₂BC** and **(NC)₂BC-Pd** (Table 1).

The next test concerned the potential effect of CrEL encapsulation on the rate at which the cells took up the PS and therefore became photosensitive. The study used a series of incubation times ranging from 30 min to 24 h along with the same PS concentration of 500 nM and the same delivered light fluence of 10 J/cm². The results are shown in Figure 3. In all cases, CrEL encapsulation significantly reduced the incubation time required to produce light-mediated cell killing. The greatest reduction in incubation time (and increase in cell killing) was found for **BC** (Figure 3a) where CrEL allowed more killing to be achieved after 30 min versus that after 24 h with direct dilution. For **(NC)₂BC-Zn** (Figure 3c) there was also a reduction in the incubation time needed to produce killing that was not apparent with direct dilution. For **(NC)₂BC** and **(NC)₂BC-Pd**, where the equivalent PS concentration with direct dilution did produce killing, CrEL encapsulation shortened the required incubation time (Figure 3b,d).

Table 1. PDT activity and photostability of the bacteriochlorins.^a

Compound	LD50 dd ^b	LD50 CrEL ^b	LD90 dd ^b	LD90 CrEL ^b	Uptake dd ^c	Uptake CrEL ^c	Efficacy/ uptake dd ^d	Efficacy/ uptake CrEL ^d	Photo- stability DMA ^e	Photo- stability CrEL ^e
	(nM)	(nM)	(nM)	(nM)	(nmol/ mg)	(nmol/ mg)				
BC	1800	60	3000	120	5.27	3.70	1.00	7.32	0.13	0.11
(NC)₂BC	60	25	300	100	4.26	3.32	37.11	114.29	0.91	0.90
(NC)₂BC-Zn	1000	350	2000	350	2.12	2.07	4.47	76.38	0.52	0.04
(NC)₂BC-Pd	25	18	90	40	4.77	2.32	79.55	227.15	0.83	0.94

^aAll measured quantities were obtained at room temperature. ^bValues taken from Figure 2; dd reflects direct dilution of the DMA stock solution of the PS into complete medium, and CrEL reflects dilution of the micellar solution into complete medium. ^cValues taken from Figure 4 and apply to an incubation time of 24 h and bacteriochlorin concentration of 500 nM. ^dEfficacy corrected for uptake. The uptake values for BC, (NC)₂BC and (NC)₂BC-Zn were determined by fluorescence spectroscopy, while those for (NC)₂BC-Pd were determined by absorption spectroscopy. The values are calculated by dividing the reciprocal of the LD50 by the uptake value, and then normalizing to the value for the direct dilution of BC. ^eFraction of the initial Qy absorbance remaining after 100 J/cm² illumination for dimethylacetamide (DMA) and CrEL micellar solutions. **B-16** and **B-17** have photostability values in DMA of 0.02 and 0.09, respectively, and in CrEL of 0.10 at 70 J/cm² and 0.22 at 50 J/cm².

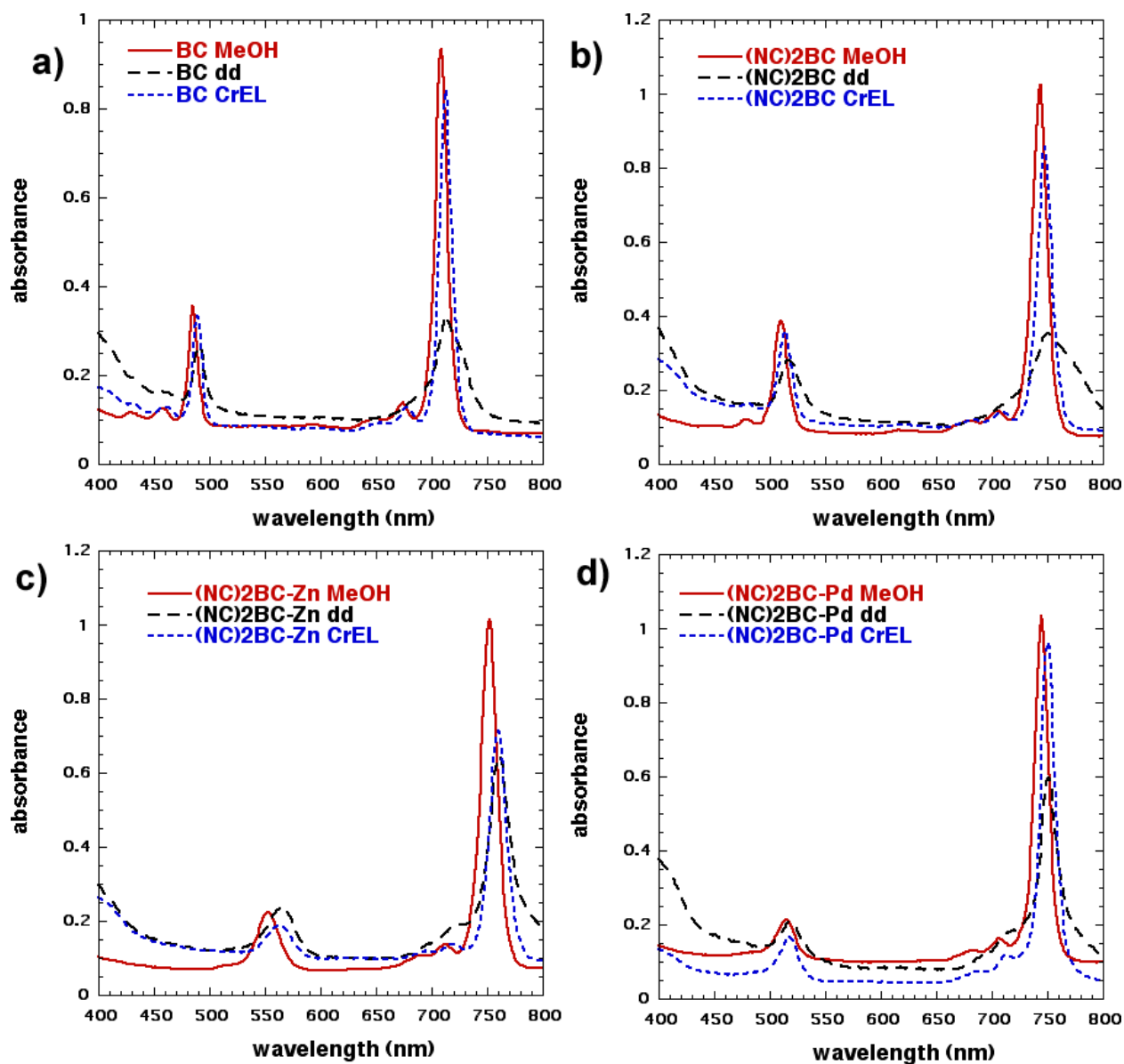


Figure 1. Absorption spectra of the four bacteriochlorins. Spectra were measured at 10 μ M concentration of bacteriochlorin in pure methanol (solid red), in a solution obtained by direct dilution (dd) of a 5 mM DMA or THF stock solution of bacteriochlorin into complete medium containing 10% FBS (black dotted), or in a solution obtained by dilution of a 500 μ M CrEL micellar stock solution of bacteriochlorin into complete medium containing 10% FBS (blue dashed). A BC; B (NC)₂BC; C (NC)₂BC-Zn; and D (NC)₂BC-Pd.

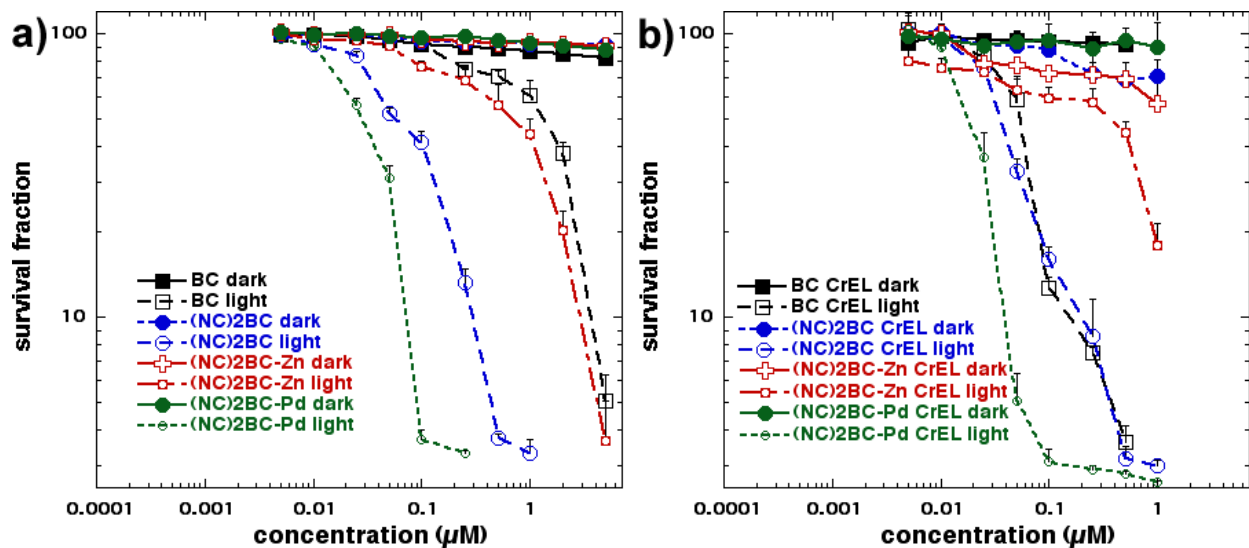


Figure 2. Relative effectiveness as photosensitizers and effect of Cremophor. The bacteriochlorins were incubated with HeLa cells at a wide range of concentrations for 24 h, followed by illumination (or not) with 10 J/cm^2 NIR light and a MTT assay 24 h later. (a) Direct dilution (dd) into complete medium from 5 mM DMA solution. (b) Dilution into complete medium from 500 μM CrEL solution.

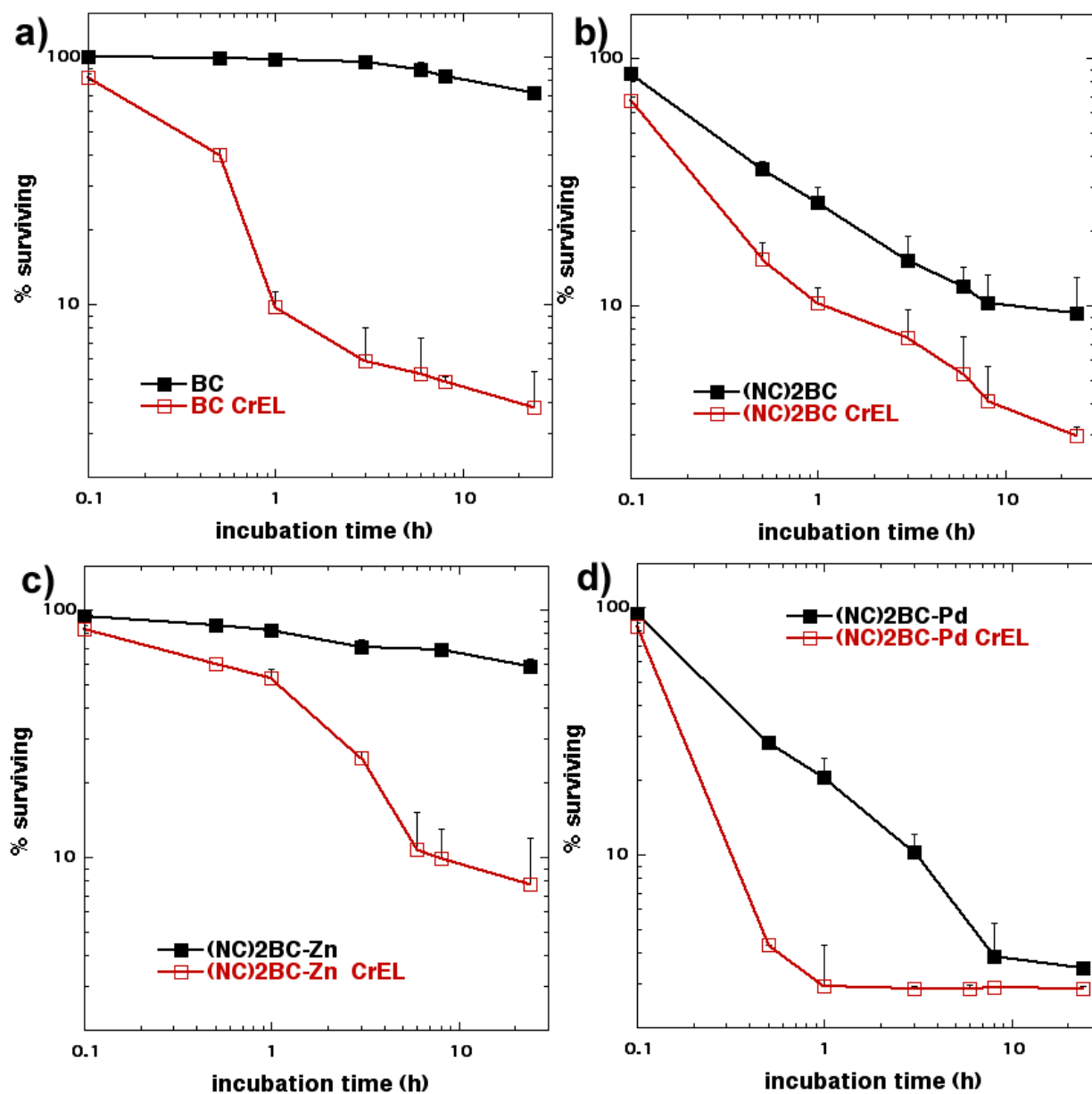


Figure 3. Effect of incubation time and delivery vehicle on efficacy of cell killing. a) BC(7); b) (NC)₂BC(8); c) (NC)₂BC-Zn (9); and d) (NC)₂BC-Pd(10). HeLa cells were incubated with the four bacteriochlorins (500 nM each) delivered either by direct dilution (black) or in CrEL micelles (red) for time periods from 30 min to 24 h followed by 10 J/cm² NIR light and a MTT assay 24 h later.

Photostability

The photostability of the four bacteriochlorins under study, **BC**, **(NC)₂BC**, **(NC)₂BC-Zn**, **(NC)₂BC-Pd** was investigated and compared with the results for PDT activity of representative synthetic bacteriochlorins that were investigated previously (**B-16** and **B-17**).^{7b} The bacteriochlorins were studied in DMA and aqueous CrEL micelles, and for both media in the presence of atmospheric O₂. Table 1 gives the fraction of the peak NIR (Q_y) absorbance remaining as a function of incident light fluence up to 100 J/cm² for the four bacteriochlorins. A decrease in Q_y absorbance parallels the progressive decrease in the entire (300–900 nm) absorption spectrum with little or no sign of features due to a chromophoric photoproduct. The diminution of the absorption profile was often accompanied by an increase in the absorption baseline, particularly at wavelengths shorter than 500 nm and increasing toward the near-UV region indicative of light scattering. These combined observations suggest that photoaggregation contributes to photoinstability. In some cases, depending on compound and medium, weak absorptions due to photoproducts (likely open-chain tetrapyrroles) are also observed.

The data in Table 1 show that **(NC)₂BC** and **(NC)₂BC-Pd** are substantially more photostable than **(NC)₂BC-Zn** and **BC** and have ≤15% loss of absorbance at 100 J/cm² illumination in both media. The bacteriochlorins **(NC)₂BC** and **(NC)₂BC-Pd** are also substantially more photostable than the previously studied bacteriochlorins **B-16** (1) and **B-17** (2), which in DMA give residual Q_y absorbance values of 0.02 and 0.09, and in CrEL of 0.10 at 70 J/cm² and 0.22 at 50 J/cm², respectively.

More results to elucidate PDT effectiveness which are subcellular localization, photosensitizer uptake, and reactive oxygen species generation are given in ref A.

Discussion

Motivation and overview

This study has demonstrated structure-function relationships among PS consisting of a set of bacteriochlorins characterized by variations in 1) peripheral substituent pattern (unsubstituted or with 3,13-dicyano groups) and 2) metalation state (free base or Pd²⁺ or Zn²⁺ chelate). Our previous studies of tailored synthetic bacteriochlorins has afforded molecules that show quantitative structure-activity relationships with regard to charge and lipophilicity (logP),⁴ and that are well suited for a range of PDT applications including treatments for microbial infections⁵ and for melanoma.³ Bacteriochlorins B16(1) and B17(2) are representative compounds that proved efficacious against HeLa cancer cells with LD50 of ≤ 100 nM.⁴ However, the photostability of these compounds in the PDT milieu was less than optimal, and photobleaching could therefore prove problematic in some PDT protocols.

meso-Tetraaryl bacteriochlorins bearing halogens (F, Cl) in the *ortho*-aryl positions and sulfo substituents in the *meta*-aryl positions have been reported to afford a pronounced increase in photostability due to the electron-withdrawing character of the substituents.⁸ Here, we found that peripheral cyano groups markedly increase the PDT activity compared to the analog that lacks these substituents. For example, among the two free base bacteriochlorins, (NC)₂BC is more active than BC. The central Pd²⁺ ion of (NC)₂BC-Pd increases activity over (NC)₂BC, and (NC)₂BC is in turn more active than the zinc chelate (NC)₂BC-Zn (Table 1). The origin of these differences must now be examined.

Photostability

A goal of this study was to determine if incorporation of 3,13-dicyano substituents on a bacteriochlorin could improve photostability over analogues studied previously (B-16, and B-

17), including those that have good PDT activity. The results demonstrate that **(NC)₂BC-Pd** and **(NC)₂BC** are more photostable and more photoactive than **(NC)₂BC-Zn** and **BC** (Table 1). Furthermore, as noted above, **(NC)₂BC-Pd** and **(NC)₂BC** are clearly more photostable than previously studied bacteriochlorins **B-16** and **B17**, at least in the solvent systems studied (DMA and CrEL), although the activities are comparable or only modestly better (LD50 < 100 nM). It can be seen that photostability depends on the medium to a degree depending on the compound.

Although the photostability of a PS is highly desirable, direct connections with activity are difficult and likely need to take into account additional factors such as the mutual solubility/solubilization characteristics of the solvate/solvent and potential mechanisms of photoaggregation, which appears to contribute (among with formation of photoproducts such as open-chain tetrapyrrole) to photoinstability. Furthermore, photobleaching has been proposed to be beneficial in clinical applications by providing a wider safety margin against normal tissue damage.³⁰ The relationships between the excited-state properties that influence photostability (via photoaggregation or photoproduct formation) and photoactivity (via the ability to perform Type-1 photochemistry) will be explored in a subsequent paper, drawing on a broad range of bacteriochlorin and porphyrin PS and media conditions that are beyond the scope of the present study.

Further discussions about localization, cellular uptake and distribution, delivery vehicle and mechanisms of reactive oxygen species production are described in detail elsewhere.^A

Acknowledgments

This work was supported by a grant from the NIH (R01AI050875 to M.R.H. and the JimmyV NCSU Cancer Therapeutics Training Program. Y-Y.H. and T.B. were supported by a grant (R41AI072854) from the National Institute of Allergy and Infectious Diseases to NIRvana Pharmaceuticals, Inc. XX. The content is solely the responsibility of the authors and does not necessarily represent the official views of the NIAID or the NIH. Characterization of the photophysical, redox and molecular-orbital properties of the bacteriochlorins described herein

was initially motivated by solar-energy studies and supported by grants from the Division of Chemical Sciences, Geosciences and Biosciences Division, Office of Basic Energy Sciences of the U.S. Department of Energy to D.F.B. (DE-FG02-05ER15660) and D.H. (DE-FG02-05ER15661).

References

- (A) Ying-Ying Huang, Thiagarajan Balasubramanian, Eunkyung Yang, Dianzhong Luo, James R. Diers, David F. Bocian, Jonathan S. Lindsey, Dewey Holten, and Michael R. Hamblin. Stable Synthetic Bacteriochlorins for Photodynamic Therapy: Role of Dicyano Peripheral Groups, Central Metal Substitution (2H, Zn, Pd), and Cremophor EL Delivery. *ChemMedChem*. 2012. 7.2155-2167
- (1) Agostinis, P., et al. *CA Cancer J Clin*. 2011, 61, 250-281.
- (2) a) Kim, H.-J. and J.S. Lindsey. *J Org Chem*. 2005, 70, 5475–5486; b) Ruzié, C., et al. *J Org Chem*. 2008, 73, 5806-5820; c) Taniguchi, M., et al. *New J Chem*. 2008, 32, 947-958.
- (3) Mroz, P., et al. *Faseb J*. 2010, 24, 3160-3170.
- (4) Huang, Y.Y., et al. *J Med Chem*. 2010, 53, 4018–4027.
- (5) Huang, L., et al. *Antimicrob Agents Chemother*. 2010, 54, 3834-3841.
- (6) a) Nyman, E.S. and P.H. Hynninen. *J Photochem Photobiol B*. 2004, 73, 1-28; b) Ethirajan, M., et al. *Chem Soc Rev*. 2011, 40, 340-362; c) Josefsen, L.B. and R.W. Boyle. *Met Based Drugs*. 2008, 2008, 276109; d) Fukuzumi, S., et al. *J Phys Chem B*. 2008, 112, 2738-2746; e) Rosenfeld, A., et al. *Photochem Photobiol*. 2006, 82, 626-634; f) Chen, Y., et al. *J Med Chem*. 2005, 48, 3692-3695.
- (7) a) Kee, H.L., et al. *J Photochem Photobiol A*. 2008, 200, 346-355; b) Mroz, P., et al. *Cancer Lett*. 2009, 282, 63-76.
- (8) a) Dabrowski, J.M., et al. *ChemMedChem*. 2010, 5, 1770-1780; b) Dabrowski, J.M., et al. *ChemMedChem*. 2011, 6, 465-475; c) Dabrowski, J.M., et al. *Free Radic Biol Med*. 2012, 52, 1188-1200.
- (9) a) Plati, J., O. Bucur, and R. Khosravi-Far. *Integr Biol (Camb)*. 2011, 3, 279-296; b) Danial, N.N. *Oncogene*. 2008, 27 Suppl 1, S53-70.
- (10) Sparreboom, A., et al. *Anal Biochem*. 1998, 255, 171-175.
- (11) Zhao, F.K., et al. *Biochem Biophys Res Commun*. 1989, 159, 1359-1367.
- (12) Brand, L. and J.R. Gohlke. *Annu Rev Biochem*. 1972, 41, 843-868.
- (13) Kessel, D. *Photochem Photobiol*. 1992, 56, 447-451.
- (14) Woodburn, K., et al. *Photochem Photobiol*. 1994, 60, 154-159.

- (15) Morgan, A.R., et al. *Cancer Res.* 1988, 48, 194-198.
- (16) Kessel, D., A. Morgan, and G.M. Garbo. *Photochem Photobiol.* 1991, 54, 193-196.
- (17) Patel, S. and A. Datta. *Photochem Photobiol.* 2009, 85, 725-732.
- (18) Liu, J.Y., et al. *Met Based Drugs.* 2008, 2008, 284691.
- (19) Lee, P.P., et al. *Tetrahedron lett.* 2005, 46, 1551-1554.
- (20) Decreau, R., et al. *J Photochem Photobiol B.* 1999, 48, 48-56.
- (21) Obochi, M.O., R.W. Boyle, and J.E. van Lier. *Photochem Photobiol.* 1993, 57, 634-640.
- (22) Garcia-Diaz, M., et al. *J Control Release.* 2012, epub ahead of print.
- (23) Eggener, S.E. and J.A. Coleman. *Sci World J.* 2008, 8, 963-973.
- (24) Huang, Z., et al. *Photochem Photobiol Sci.* 2007, 6, 1318-1324.
- (25) a) Moore, C.M., D. Pendse, and M. Emberton. *Nat Clin Pract Urol.* 2009, 6, 18-30; b) Davidson, S.R., et al. *Phys Med Biol.* 2009, 54, 2293-2313.
- (26) Vakrat-Haglili, Y., et al. *J Am Chem Soc.* 2005, 127, 6487-6497.
- (27) Ashur, I., et al. *J Phys Chem A.* 2009, 113, 8027-8037.
- (28) Silva, E.F., et al. *Chemistry.* 2010, 16, 9273-9286.
- (29) a) Price, M., et al. *Photochem Photobiol.* 2009, 85, 1177-1181; b) Setsukinai, K., et al. *J Biol Chem.* 2003, 278, 3170-3175; c) Price, M. and D. Kessel. *J Biomed Opt.* 2010, 15, 051605.
- (30) Krammer, B. and K. Plaetzer. *Photochem Photobiol Sci.* 2008, 7, 283-289.
- (31) Krayner, M., et al. *J Org Chem.* 2010, 75, 1016-1039.
- (32) Perry, V.P. *Science.* 1955, 121, 805.
- (33) Merlin, J.L., et al. *Eur J Cancer.* 1992, 28A, 1452-1458.
- (34) a) Brunk, U.T., et al. *Free Radic Biol Med.* 1997, 23, 616-626; b) Ditaranto, K., T.L. Tekirian, and A.J. Yang. *Neurobiol Dis.* 2001, 8, 19-31.

Chapter 10

Stable Synthetic Cationic Bacteriochlorins as Selective Antimicrobial Photosensitizer

Copyright © American Society for Microbiology. Reproduced in part with permission from [Huang, L; Huang, YY; Mroz, P; Tegos, G.P; Zhiyentayev, T; Sharma, SK; Lu, Z; Balasubramanian, T; Krayner, M; Ruzié, C; **Yang, EK**; Kee, HL; Kirmaier, C; Diers, J.R; Bocian, D.F; Holten, D; Lindsey, S.J; Hamblin, M.R. Stable Synthetic Cationic Bacteriochlorins As Selective Antimicrobial Photosensitizers. *Antimicrobial Agents and Chemotherapy (AAC)*. **2010**, 54, 3834–3841. doi : 10.1128/AAC.00125-10]

Abstract

Photodynamic inactivation is a rapidly developing antimicrobial treatment that employs a non-toxic photoactivatable dye or photosensitizer in combination with harmless visible light to generate reactive oxygen species that are toxic to cells. Tetrapyrroles (e.g., porphyrins, chlorins, bacteriochlorins) are a class of photosensitizers that exhibit promising characteristics to serve as broad-spectrum antimicrobials. In order to bind to and efficiently penetrate into all classes of microbial cells, tetrapyrroles should have structures that contain (i) one or more cationic charge(s) or (ii) a basic group. In this report, we investigate the use of new stable synthetic bacteriochlorins that have a strong absorption band in the range 720–740 nm, which is in the near-infrared spectral region. Four bacteriochlorins with 2, 4 or 6 quaternized ammonium groups, or 2 basic amine groups, were compared for light-mediated killing against a Gram-positive bacterium (*Staphylococcus aureus*), a Gram-negative bacterium (*Escherichia coli*), and a dimorphic fungal yeast (*Candida albicans*). Selectivity was assessed by determining phototoxicity against human HeLa cancer cells under the same conditions. All 4 compounds were highly active (6 logs of killing at 1 μ M or less) against *S. aureus* and showed selectivity for bacteria over human cells. Increasing the cationic charge increased activity against *E. coli*. Only the compound with basic groups was highly active against *C. albicans*. Supporting photochemical and theoretical characterization studies indicate (i) the four bacteriochlorins have comparable photophysical features in homogeneous solution and (ii) the anticipated redox characteristics do not correlate with cell-killing ability. These results support the interpretation that the disparate biological activities observed stem from cellular binding and localization effects rather than intrinsic electronic properties. These findings further establish cationic bacteriochlorins as extremely active and selective near-infrared activated antimicrobial photosensitizers, and the results

provide fundamental information on structure-activity relationships for antimicrobial photosensitizers.

Introduction

Photodynamic therapy (PDT) employs a nontoxic dye termed a photosensitizer and low-intensity visible light, which in the presence of molecular oxygen produces reactive oxygen species, such as singlet oxygen, superoxide, and hydroxyl radicals.¹⁵ PDT has the advantage of dual selectivity in that the photosensitizer can be targeted to a destination cell or tissue, and in addition the illumination can be spatially directed to the lesion.^{7,48} PDT has its origins over a hundred years ago in the discovery of light-mediated killing of microorganisms³⁵, but since then has been principally developed as a treatment for cancer⁸ and age-related macular degeneration.⁵⁸ Photodynamic inactivation (PDI) is the term used to describe the use of PDT to inactivate an unwanted entity such as a microbial cell.

There has been a relentless rise in antibiotic resistance over many years in most regions of the world and in many different classes of microbial cells.⁴¹ In recent times the phenomenon has become even more worrying, with concerns that hitherto fairly trivial infections could again become untreatable as in the days before antibiotics were discovered.³ In fact the present time has been termed the “end of the antibiotic era”.¹ The rise in multidrug resistance among microbial pathogens has motivated an international search for alternative antimicrobial strategies, particularly those which could be applied to infections in wounds and burns.³²

PDI has attracted attention as a possible alternative treatment for localized infections.^{14,19,27} In this treatment, the photosensitizer is topically or locally applied to the infected tissue and, after a relatively short time interval, light is delivered to the area. Depending

on the effectiveness of the antimicrobial photosensitizer, up to three logs of bacterial or fungal cells can be killed without causing unacceptable damage to the host tissue.¹¹ PDI is thought to be equally effective against multi-drug resistant as against naïve species⁴⁹, and in addition the PDI treatment itself is unlikely to cause resistance to arise.²⁶ It should be noted that the lack of development of resistance after PDT is generally difficult to prove experimentally but can be shown in particular instances.

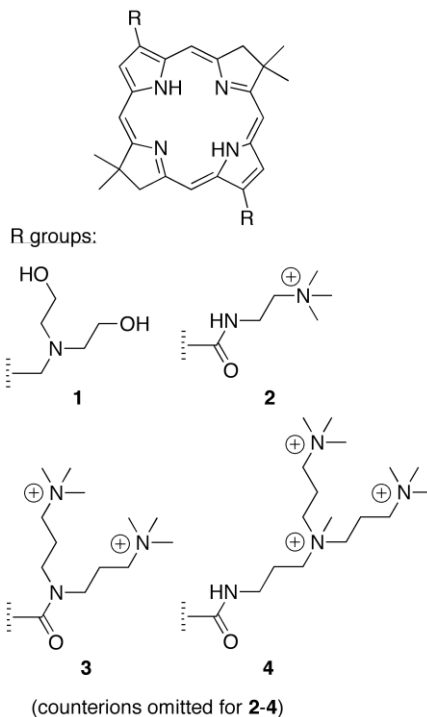


Figure 1. Bacteriochlorin photosensitizer

Gram-negative bacteria are resistant to PDI with many commonly used photosensitizers that readily lead to phototoxicity for Gram-positive species.²⁹ On the other hand, photosensitizers bearing a cationic charge^{31,33,37} or the use of agents that increase the permeability of the outer membrane³⁸ are known to increase the efficacy of killing of gram-negative

organisms. The ideal photosensitizer for killing bacteria should possess an overall cationic charge and preferably multiple cationic charges.^{16,52}

Photosensitizers based on the bacteriochlorin backbone have been studied as potential PDT-agents for cancer and non-oncological applications.^{10,43,46,55} The large absorption feature in the near-infrared spectral region, which is characteristic of bacteriochlorins, is considered to be ideal for maximizing light penetration through tissue. This is so because both absorption and scattering of light in the 700–800 nm region are minimal.^{40,42} However, in addition to good optical properties, it is necessary for a photosensitizer molecule to possess the appropriate structural characteristics that will optimize the binding to and penetration into microbial cells. For antimicrobial applications, the effective molecular features are likely to include the presence of positively charged substituents such as quaternized ammonium groups.

A de novo synthetic pathway to bacteriochlorins that contain a geminal dimethyl group in each pyrroline ring has been developed recently.²² This structural attribute blocks adventitious dehydrogenation (to form the chlorin) and thereby affords a stable macrocycle. This synthetic route has provided a number of bacteriochlorin building blocks, which provided modular access to bacteriochlorins **1–4** (Figure 1). The four molecules were designed to allow investigation of the structure activity relationship among differently charged bacteriochlorins. Bacteriochlorin **1** is a neutral species with two basic amino groups; bacteriochlorins **2–4** contain 2, 4, or 6 cationic charges, respectively. The synthesis of bacteriochlorins **1–3** has been reported⁴⁴, and the synthesis of **4** will be described herein. The photophysical and molecular-orbital characteristics of all four bacteriochlorins have been investigated as part of this study. The goals of the present study were to (i) test bacteriochlorins **1–4** as antimicrobial photosensitizers against a panel of human pathogens of different taxonomic classifications, and (ii) determine selectivity of the four

bacteriochlorins for killing microbial cells versus mammalian (human cancer) cells using the same incubation time and other experimental conditions.

Experimental methods

Photophysical measurements

Photophysical measurements were performed as described previously.²⁰ Measurement of the fluorescence (Φ_f) and triplet-excited-state (Φ_{isc}) quantum yields and singlet (τ_S) and triplet (τ_T) lifetimes utilized Ar-purged solutions (methanol or 2-methyltetrahydrofuran) except that the τ_T values for **2** in methanol and **3** in ethanol utilized rigorously degassed (by freeze-pump-thaw) solutions. The Φ_f values were determined with respect to 8,8,18,18-tetramethylbacteriochlorin (**50**) in Ar-purged toluene, for which $\Phi_f = 0.125$ was established with respect to chlorophyll *a* in benzene ($\Phi_f = 0.325$)⁵⁶ and free base tetraphenylporphyrin in toluene ($\Phi_f = 0.09$)¹² using Soret and Q_x excitation. Triplet yields were determined using a reference technique to facilitate comparisons (20). First, a value of $\Phi_{isc} = 0.57$ was measured for **3**. This value along with the Φ_f and τ_S values for this compound (Table 1) give a value of $k_{ic} = (11.4 \text{ ns})^{-1}$ for the rate constant for internal conversion of the lowest singlet excited state to the ground state via the expression $k_{ic} = (\tau_S)^{-1}[1 - \Phi_f - \Phi_{isc}]$. This value is in good agreement with the average value of $k_{ic} = (10 \text{ ns})^{-1}$ obtained for a number of analogous 3,13-substituted synthetic bacteriochlorins (unpublished work). This k_{ic} value was used to obtain the triplet yield for each of the bacteriochlorins using the expression $\Phi_{isc}^{ref} = 1 - \Phi_f - k_{ic} \cdot \tau_S$ (Table 1).

Other experimental detail containing synthesis and PDT activity is shown in Ref A.

Results

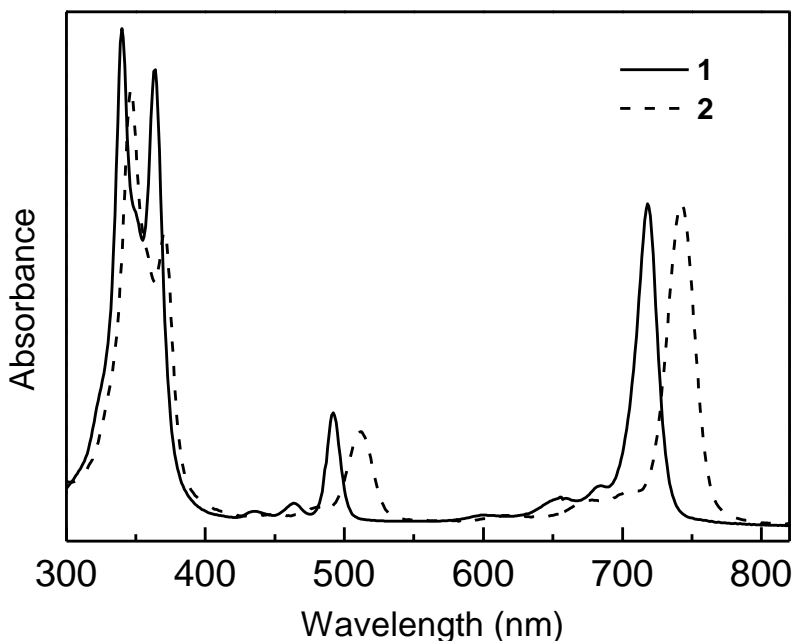


Figure 2. Absorption spectra of bacteriochlorins. 1(solid line) and 2 (dashed line) in methanol at room temperature. The long wavelength near-infrared feature is the Qy(0,0)band.

*PDI studies against Gram-positive *S. aureus**

The best way to compare the phototoxicity of a group of photosensitizers with very different potencies is to vary the concentration over several orders of magnitude and determine the survival fraction with and without (dark toxicity) a single light dose. Figure 3 displays the survival fraction curves obtained against the Gram-positive bacterium *S. aureus* incubated for 30 minutes using bacteriochlorins **1–4** with and without illumination (10 J/cm^2 732-nm laser light). The non-cationic bacteriochlorin **1** produces 1 log of killing at 100 nM, almost 6 logs at 1 μM , and eliminates the cells at higher concentrations (Figure 3A). The most effective compound is the bis-cationic bacteriochlorin **2**, which kills a remarkable 5 logs at 100 nM and eliminates the population at 1 μM (Figure 3B). No dark toxicity is observed. Less effective than **2** are the

tetrakis-cationic bacteriochlorin **3** (Figure 3C) and the hexakis-cationic bacteriochlorin **4** (Figure 3D), both of which have a small amount of phototoxicity at 100 nM and kill 5 logs at 1 μ M. Again no dark toxicity is seen.

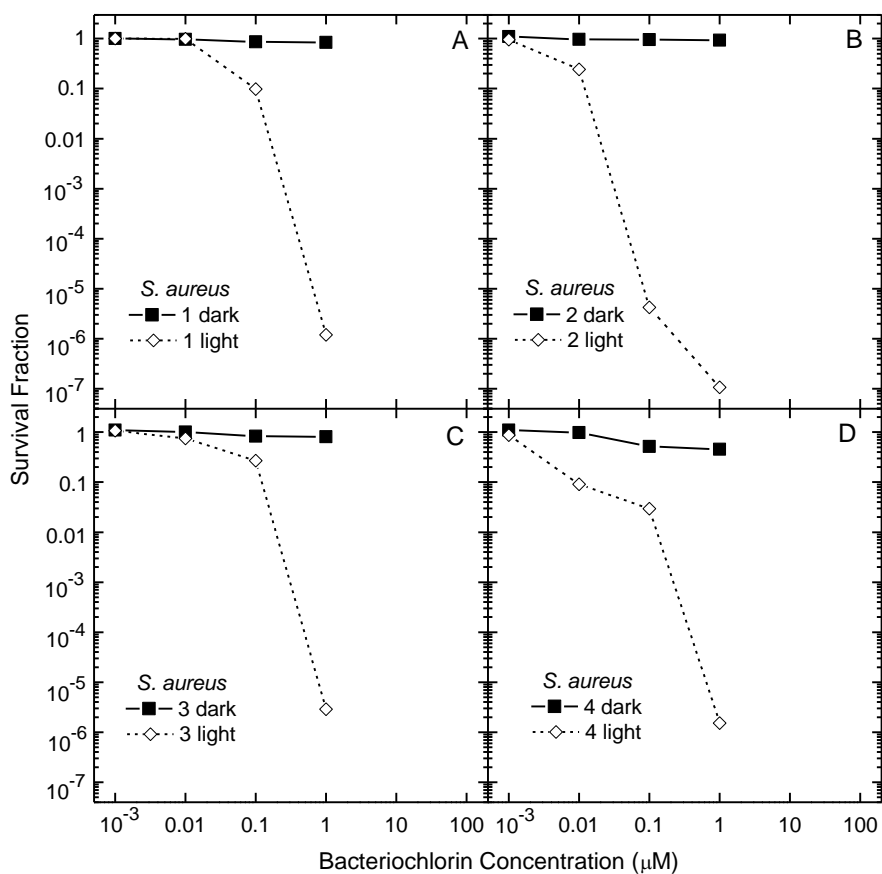


Figure 3. Survival fraction against photosensitizer concentration for the photodynamic killing of *S. aureus* cells. Cell suspensions of 10⁸/mL were incubated for 30 min with different concentrations of bacteriochlorins 1 (A); 2 (B); 3 (C) and 4 (D) followed by illumination with 10 J/cm² of 732-nm laser light.

PDI studies against Gram-negative E. coli

The non-cationic bacteriochlorin **1** shows no effects (no phototoxicity and no dark toxicity) against the Gram-negative *E. coli* (Figure 4A). The bis-cationic bacteriochlorin **2**, however, is effective against *E. coli*, killing 1 log at 1 μ M, 3 logs at 10 μ M and eliminating the

population at 100 μM (Figure 4B). Modest dark toxicity (up to 1 log) is observed at the highest concentrations. The tetrakis-cationic bacteriochlorin **3** is significantly more effective, killing 4 logs at 1 μM , almost 6 logs at 10 μM and eliminating the cells at 100 μM (Figure 4C). The hexakis-cationic bacteriochlorin **4** is even more powerful, killing 1.5 logs at 100 nM and eliminating the cells at 1 μM (Figure 4D). Interestingly, neither bacteriochlorin **3** nor **4** displays dark toxicity

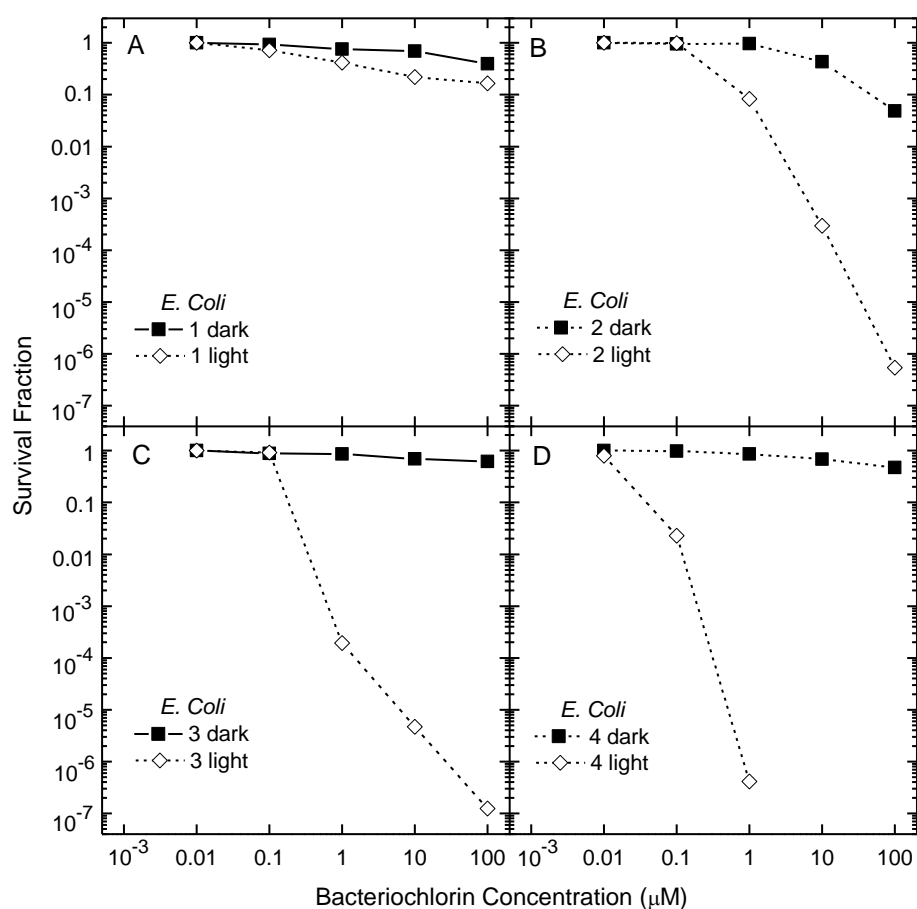


Figure 4. Survival fraction against photosensitizer concentration for the photodynamic killing of *E. coli* cells. Cell suspensions of $10^8/\text{mL}$ were incubated for 30 min with different concentrations of bacteriochlorins **1** (A); **2** (B); **3** (C) and **4** (D) followed by illumination with $10 \text{ J}/\text{cm}^2$ of 732-nm laser light.

PDI studies against fungal yeast *C. albicans*

The only bacteriochlorins that exhibits a high degree of phototoxicity against the eukaryotic fungal yeast cell *C. albicans* is the non-cationic bacteriochlorin **1** (Figure 5A). This compound displays 4 logs of killing at 10 μM and gives total elimination (>6 logs killing) at 100 μM . A much lower degree of phototoxicity is observed with the bis-cationic bacteriochlorin **2** with 1–2 logs of killing at 10–100 μM (Figure 5B). Neither the tetrakis-cationic bacteriochlorin **3** (Figure 5C) nor the hexakis-cationic bacteriochlorin **4** (Figure 5D) show any PDI effect whatsoever. The only dark toxicity towards *C. albicans* is 2 logs in the case of bacteriochlorin **1** at 100 μM (Figure 5A).

Confocal microscopy was carried out to confirm that the non-cationic bacteriochlorin **1** is effective at killing *Candida* cells because it is able to penetrate inside the cell while the quaternized bacteriochlorin **2** cannot. Figure 6A shows *C. albicans* incubated with 100 μM bacteriochlorin **1** for 30 min. The bacteriochlorin fluorescence is false colored red and the autofluorescence from the *Candida* cells is false colored green. It can be seen that the basic bacteriochlorin **1** penetrates into the interior of the yeast cells (Figure 6A), while the bis-cationic bacteriochlorin **2** under the same conditions gives much less fluorescence, and none was visible inside the yeast cells (Figure 6B).

PDI studies against mammalian cells

In order to answer the question whether these bacteriochlorins might exhibit selective killing of microbial (bacterial or fungal) cells versus the host mammalian cells, experiments were performed using a human cancer cell line (HeLa) and the same short incubation time (30 minutes). Tetrapyrroles are thought to be taken up rapidly into microbial cells, but much more

slowly into mammalian cells. In order to carry out a fair comparison (because the microbial cells were incubated in serum-free medium) two different incubation media were used. These were complete medium 10% fetal bovine serum and also RPMI medium without serum. All three cationic bacteriochlorins (2, Figure 7B; 3, Figure 7C; and

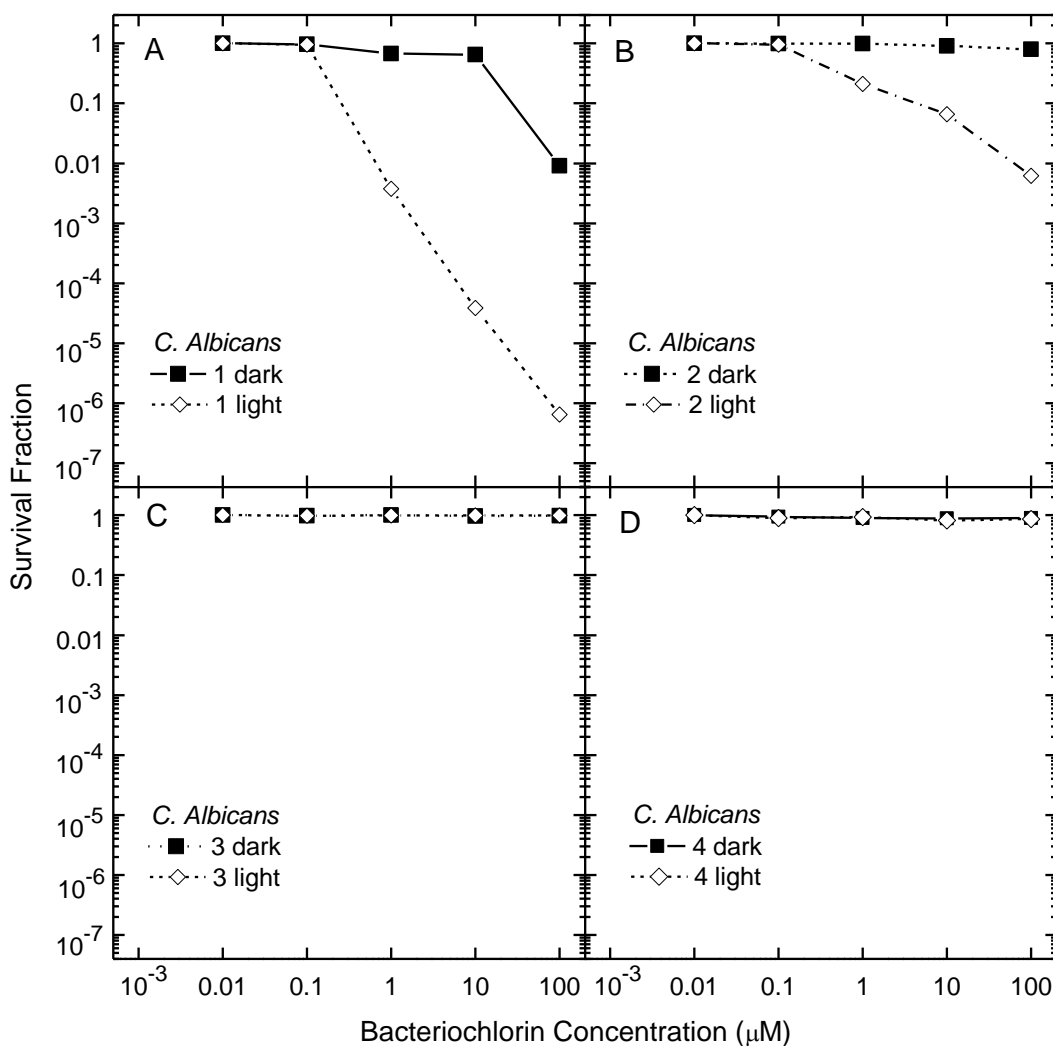


Figure 5. Survival fraction against photosensitizer concentration for the photodynamic killing of *C. albicans* cells. Cell suspensions of $10^7/\text{mL}$ were incubated for 30 min with different concentrations of bacteriochlorins 1 (A); 2 (B); 3 (C) and 4 (D) followed by illumination with $10 \text{ J}/\text{cm}^2$ of 732-nm laser light.

4, Figure 7D) exhibit minimal PDT killing of HeLa cells, only exhibiting significant phototoxicity above $5 \mu\text{M}$. By contrast the non-quaternized bacteriochlorin 1 (Figure 7A) shows

much greater (at least 50 times) phototoxicity with significant killing observed at only 100 nM. Although the MTT assay is only capable of measuring 2.5 logs of cell killing, the same y axis was used in Fig. 3 to 5 and 7 to emphasize the observed selectivity of the bacteriochlorins for microbial over mammalian cells. In contrast to expectations, the PDT killing of HeLa cells by compounds 2 to 4 after incubation in serum-free medium was actually lower than that found with conventional serum-containing medium (Fig. 7B to D). It was expected that the uptake of bacteriochlorins into the cells might be higher when there was no competition for binding from serum proteins, but apparently this was not the case. The only case where the killing was higher after incubation in serum-free medium was that of the dark toxicity (not PDT) for compound 1 (Fig. 7A).

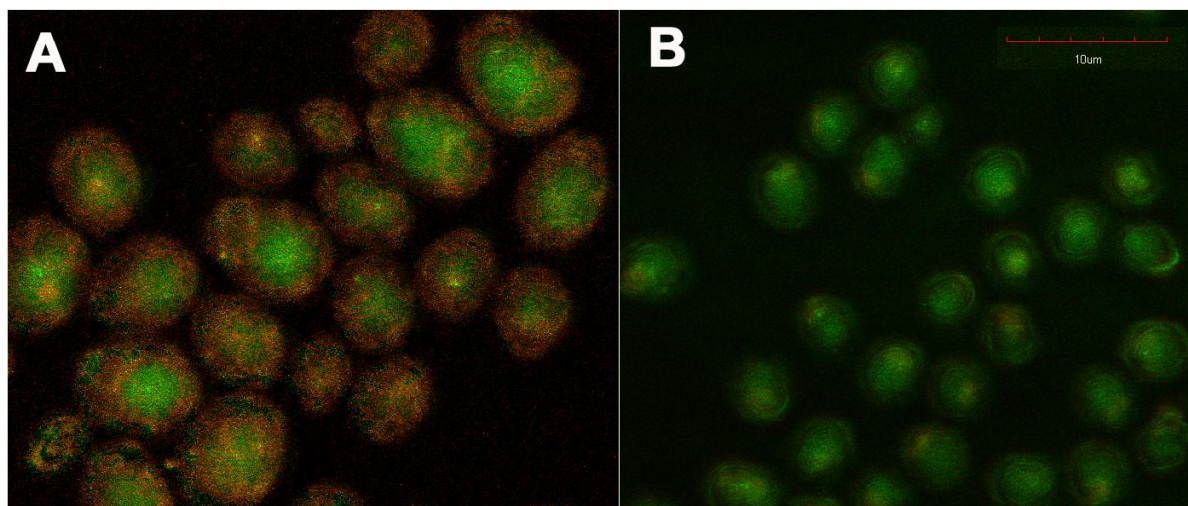


Figure 6. Two color confocal fluorescence micrographs. *C. albicans* cells were incubated for 30 min with 100 μ M of bacteriochlorin 1 (A) or 2 (B). Autofluorescence is colored green and near-infrared bacteriochlorin fluorescence is colored red. The scale bar is 10 μ m.

Photophysical properties

Each compound exhibits a characteristic bacteriochlorin absorption spectrum²³ with a

broad near-UV Soret (B) feature and a long-wavelength Q_y feature of comparable intensity in the near-infrared spectral region; absorption spectra for bacteriochlorins **1** and **2** are shown in Figure 1. The wavelength tunability of synthetic bacteriochlorins via functionalization of the 3- and 13-position has been reported previously.⁵⁰ The Q_y absorption maximum of bacteriochlorins **1–4** in methanol are in the range 718–742 (Table 1). Lifetimes of the singlet state are in the range 3.5–4.0 ns, and the lifetimes of the lowest triplet excited state are in the range 54–90 μ s (all in the absence of oxygen). The triplet lifetimes are reduced to <1 μ s in the presence of atmospheric oxygen, indicating facile excited-state quenching. The yields of the excited triplet state are in the range 0.48–0.53. These values are comparable to that of 0.54 for bacteriopheophytin *a*.¹⁷

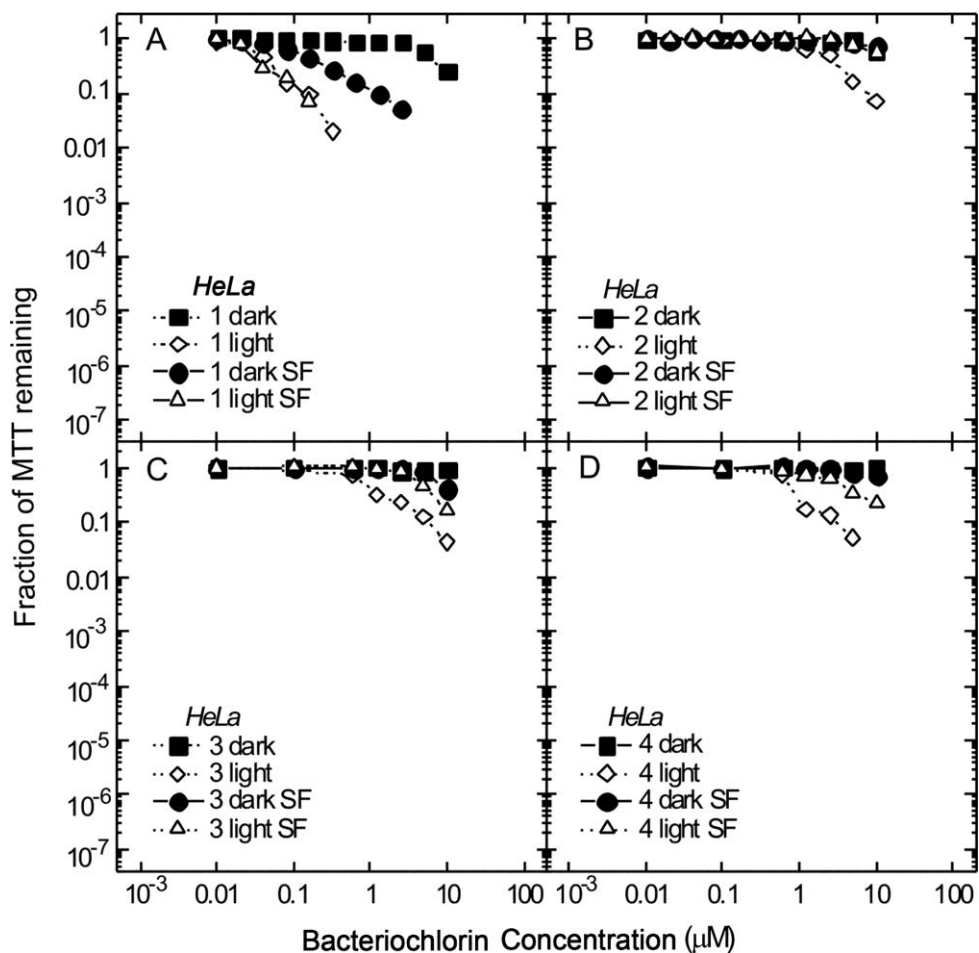


Figure 7. Survival fraction against photosensitizer concentration for the photodynamic killing of HeLa cells. Cells (5,000/well) were incubated in complete medium or in serum free medium (SF) for 30 min with different concentrations of compounds 1(A), 2(B), 3(C), and 4(D) followed by illumination (light) or not (dark) with 10 J/cm^2 of 732-nm laser light. Viability was determined 24h later by MIT assay.

Table 1. Chemical and photophysical properties of bacteriochlorins ^a

Cmpd	Partition Coefficient		Q _y absorption ^b		Q _y fluorescence ^b		Φ _f ^c	τ _S ^d (ns)	Φ _{isc} ^{ref e}	τ _T ^f (μs)	Orbital Energy	
	mLogP ^g	cLogP ^h	λ (nm)	fwhm (nm)	λ (nm)	fwhm (nm)					HOMO (eV)	LUMO (eV)
1	+2.3	+4.8 ± 1.5	718	18	724	23	0.095	3.8	0.53	190 ⁱ	-4.42	-2.19
2	-0.5	-1.1 ± 1.7	742	23	750	25	0.13	4.0	0.48	77 ^j	-4.72	-3.34
3	-1.4	-5.3 ± 1.7	729	19	735	24	0.12	3.5	0.53	54 ^k	-5.05	-3.89
4	-1.7	-5.8 ± 1.7	740	24	750	25					-4.56	-3.92

^a All data measured for compounds at room temperature. ^bPeak wavelength (λ) and full width at half maximum (fwhm) of spectral feature for compound in aerated methanol. ^cFluorescence quantum yield for compound in Ar-purged methanol. ^dLifetime of the lowest singlet excited state for compound in Ar-purged methanol determined using fluorescence detection. ^eYield of the lowest triplet excited state determined using the expression $\Phi_{isc}^{ref} = 1 - \Phi_f - k_{ic} \cdot \tau_S$, with $k_{ic} = (10 \text{ ns})^{-1}$ as described in the text. ^fLifetime of the lowest triplet excited state. ^gMeasured log P. ^hCalculated log P. ⁱIn Ar-purged 2-methyltetrahydrofuran. ^jIn freeze-pump-thaw-degassed methanol. ^kIn freeze-pump-thaw-degassed ethanol.

Molecular orbital characteristics

The energies of the highest occupied molecular orbital (HOMO) and lowest unoccupied molecular orbital (LUMO) of each bacteriochlorin were obtained from DFT calculations. Table 1 shows that the HOMO energy becomes more negative along the following series: **1** (-4.42 eV) > **3** (-4.56 eV) > **2** (-4.72 eV) > **4** (-5.05 eV). Along this series, the bacteriochlorins will be progressively harder to oxidize. Table 1 also shows that the LUMO energy becomes more negative along the following series: **1** (-2.19 eV) > **2** (-3.34 eV) > **3** (-3.89 eV) > **4** (-3.92 eV). Along this series, the bacteriochlorins will be progressively easier to reduce.

A prior study of a series of zinc chlorins showed excellent linear correlations between the calculated orbital energies and measured redox potentials, with a shift in the HOMO or LUMO energy of 100 meV giving a shift in the oxidation or reduction potential of on the order of 100 mV.²¹ These findings suggest that differences in ground-state (S_0) oxidation and/or reduction potentials among the bacteriochlorins studied here may be substantial. The one caveat is that the redox properties of a bacteriochlorin may differ considerably depending on the sub-cellular localization site. A second caveat is that the triplet excited state (T_1) redox potentials will differ from those for the ground-state (S_0) by the $T_1 - S_0$ energy gap, which typically will vary similarly to the $S_1 - S_0$ energy gaps derived from $Q_y(0,0)$ spectral positions (Table 1). Potential connections between redox and PDI activity are given below.

Discussion

The present report has demonstrated that stable, synthetic cationic bacteriochlorins are highly promising candidate photosensitizers for antimicrobial PDT. The new method for bacteriochlorin synthesis^{22,24} provides compounds with *gem*-dimethyl groups in the reduced pyrrole rings at the 8 and 18 positions. This substitution pattern locks-in the bacteriochlorin macrocycle by preventing the oxidation reactions that typically occur with derivatives of naturally occurring bacteriochlorins. These reactions lead to instabilities encountered with many other bacteriochlorins previously tested for PDT activity. The versatility of the 3,13-disubstituted bacteriochlorin building blocks enables macrocycles with a variety of substituent patterns to be prepared, including the set of quaternized compounds that were studied herein.

A large number of publications have pointed out the necessity of using cationic charged photosensitizers to efficiently mediate photodynamic inhibition (PDI) of Gram-negative bacteria; however, reports that have compared structure-function relationships of photosensitizers against three different classes of microbial cell (Gram-positive bacteria, Gram-negative bacteria, and fungal yeast) are less common.³⁰ One striking result from the present investigation is that the photosensitizer structure that gives the maximum PDI effect is different for each class of microbial cell.

All four compounds tested were highly active against the Gram-positive *S. aureus* (Figure 3). The bis-quaternized bacteriochlorin **2** was most effective, producing a remarkable 5 logs of killing at 100 nM. The other three compounds (basic, tetrakis-quaternized and hexakis-quaternized) exhibited comparable levels of cell killing that were lower than **2** but still quite substantial (>5 logs at 1 μ M). One explanation of this finding is that there exists an optimum

level of cationic charge necessary both to bind to bacterial anionic phosphate groups and to also allow penetration into the bacterial cell wall where the reactive oxygen species produced upon illumination can do most damage. Levels of cationic charge less than this optimum value (for instance the properties of bacteriochlorin **1**) will not lead to sufficient binding, or cationic charges greater than this optimum value (for instance bacteriochlorins **3** and **4**) will lead to the binding being too strong to allow photosensitizer penetration to the bacterial interior. A similar finding has been presented in two other reports by one of our groups involving comparisons of conjugates between chlorin(e6) and different sizes of polylysine chains¹⁶ or different sizes of polyethylenimine chains.⁵¹ In both cases the smallest conjugate with the least cationic charges has the greatest PDI effect against *S. aureus*, while the largest conjugate with the most cationic charges was the most effective against *E. coli*. Maisch et al.²⁸ also found that a porphyrin with two cationic groups was a better photosensitizer against *S. aureus* than a molecule with four such groups.

A more straightforward structure-function relationship is found here for the effect of the bacteriochlorins against the Gram-negative *E. coli* (Figure 4). In particular, the greater the number of cationic quaternized groups the greater the PDI effect. Bacteriochlorin **4** with six cationic groups kills measurable numbers of cells at 100 nM and eliminates the population at 1 μ M. Bacteriochlorin **3** (4 cationic groups) kills 4 logs at 1 μ M, while bacteriochlorin **2** (2 cationic groups) kills only 1 log at 1 μ M, and bacteriochlorin **1** (no cationic groups) has no killing effect at all.

The fungal yeast *C. albicans* displays yet another structure-function relationship (Figure 5). Only the non-cationic bacteriochlorin **1** has a high PDI killing effect, namely elimination of the population (> 6 logs) at 100 μ M. The bis-cationic bacteriochlorin **2** shows a measurable 1–2

logs of killing at $\geq 1 \mu\text{M}$, while bacteriochlorins with four (**3**) or six (**4**) cationic groups give no killing effect at all. The microscopy studies suggest that the non-cationic bacteriochlorin **1** is able to penetrate to the interior of the fungal cells, while the cationic bacteriochlorin **2** cannot; this difference in localization and uptake explains the much greater fungicidal effect of **1**. The similarity of the structure-function relationships between *Candida* and HeLa cells is presumably due to the fact that fungal cells are eukaryotic and to some extent resemble mammalian cells in their overall cellular structure. Because both types of cells are classified as eukaryotes, they have many component features in common, including plasma membrane, nucleus and nuclear membrane, mitochondria, endoplasmic reticulum, Golgi apparatus and cytoskeleton.

While many authors have reported that *Candida* cells are susceptible to PDT with cationic photosensitizers^{9,25,36}, there are other reports that photosensitizers commonly used to kill cancer cells, such as Photofrin⁵, are also effective against yeast cells. Further study is necessary to understand the precise structural features of photosensitizer molecules for optimal PDT of fungal cells, while preserving selectivity over the host mammalian cells. The overall goal of antimicrobial PDT is to be able to kill microbes that are infecting tissue after local application of the photosensitizer solution to the infected area and subsequent illumination. Thus, it is necessary to also study the PDT killing of mammalian cells that would comprise the host tissue. To this end, a human cancer cell line (HeLa cells) was investigated using the same incubation time (30 min) employed for the microbial cells. The structure-function relationship was to some extent similar to that found for *C. albicans* with only the basic bacteriochlorin (**1**) giving any significant level of killing at concentrations lower than $1 \mu\text{M}$. Therefore, selective PDT killing of bacteria compared to mammalian cells is accomplished with quaternized bacteriochlorins with

the bis-cationic compound giving the highest selectivity for *S. aureus* and the hexakis cationic compound giving the highest selectivity for *E. coli*.

To our knowledge there has been only one prior investigation of bacteriochlorins as antimicrobial photosensitizers. Schastak et al.⁴⁵ compared the photodynamic killing of *S. aureus*, MRSA, *E. coli* and *Pseudomonas aeruginosa* using a meso-substituted tetramethylpyridinium bacteriochlorin versus that with a chorin(e6) derivative called Photolon. The cationic bacteriochlorin was able to kill both Gram-positive and Gram-negative bacteria, while the anionic Photolon was only able to kill Gram-positive species. Several groups have studied bacteriochlorins to kill cancer cells and to treat tumors in vivo. The long-wavelength light between 700 and 800 nm that is absorbed by bacteriochlorins is believed to be ideally suited to penetrate living tissue due to reduced absorption by tissue chromophores and reduced Mie scattering.⁵³ The large extinction coefficient ($>100,000 \text{ M}^{-1}\text{cm}^{-1}$) typical of the bacteriochlorin Q_y band is also advantageous for strong absorption of near-infrared light by the photosensitizer. The Pd-containing bacteriochlorins known as TOOKAD (13, 57) and Stakel (2) have been extensively investigated in laboratory studies, and, in addition, TOOKAD has been studied in clinical trials of PDT for prostate cancer.⁵⁴

The photophysical studies and DFT calculations indicate that the activity differences observed among bacteriochlorins **1–4** must stem from cellular binding and localization effects rather than photochemical properties. Indeed, the yield of the triplet excited state (from which the reactive oxygen species is produced) is essentially identical (0.48–0.53) for the four bacteriochlorins, and in each cases the lifetime is reduced to $<1 \mu\text{s}$ in the presence of atmospheric oxygen, indicating facile excited-state quenching. Moreover, there is no specific correlation between the anticipated differences in redox properties (based on the molecular-

orbital energies) for the four bacteriochlorins and their PDI activity against any of the organisms studied. The only broad trend is that **1** or **2** are typically more active than **3** or **4**, which all other things being equal would favor a mechanism of activity that involves reduction rather than oxidation of the photoexcited bacteriochlorin to the extent that electron transfer is involved.

In conclusion, bacteriochlorins with constitutive cationic charges provided by quaternized ammonium groups are highly active antibacterial photosensitizers. The hexakis-cationic bacteriochlorin **4** is capable of eliminating (>6 logs killing) both Gram-positive (*S. aureus*) and Gram-negative (*E. coli*) bacteria at the remarkably low concentration of 1 μ M. Good selectivity (4-5 logs) for bacteria over mammalian cells is observed. Only the non-quaternized bacteriochlorin **1** shows good PDT killing of the yeast (*C. albicans*), and selectivity over mammalian cells is lower in this case because both cell types are eukaryotic organisms.

Acknowledgments

This work was supported by grants from the NIH (R01AI050875 to M.R.H. and R01GM36238 to J.S.L.), a Burroughs-Wellcome fellowship (to M.K), and the Jimmy V. NCSU Cancer Therapeutics Training Program. L.H., Y-Y.H. and T.B. were supported by a grant (R41AI072854) from the National Institute of Allergy and Infectious Diseases to NIRvana Pharmaceuticals, Inc. P.M. was partly supported by Genzyme-Partners Translational Research Grant. G.P.T was partly supported by a Massachusetts Technology Transfer Center Award. Characterization of the photophysical and redox properties of the bacteriochlorins described herein was initially motivated by solar-energy studies and supported by grants from the Division of Chemical Sciences, Geosciences and Biosciences Division, Office of Basic Energy Sciences of the U.S. Department of Energy to D.F.B. (DE-FG02-05ER15660) and D.H. (DE-FG02-05ER15661).

We thank Aaron Mitchell, Department of Microbiology, Columbia University, New York, NY, for the gift of DAY286 reference strain of *C. albicans*. We thank Jie (Jenny) Zhao and Margaret E. Sherwood, Wellman Center for Photomedicine, Massachusetts General Hospital for help with confocal microscopy.

References

- (A) Huang, L; Huang, YY; Mroz, P; Tegos, G.P; Zhiyentayev, T; Sharma, SK; Lu, Z; Balasubramanian, T; Krayner, M; Ruzié, C; **Yang, EK**; Kee, HL; Kirmaier, C; Diers, J.R; Bocian, D.F; Holten, D; Lindsey, S.J; Hamblin, M.R. Stable Synthetic Cationic Bacteriochlorins As Selective Antimicrobial Photosensitizers. *Antimicrobial Agents and Chemotherapy (AAC)*. **2010**, *54*, 3834–3841.
- (1) Bell, S. G. 2003. Antibiotic resistance: is the end of an era near? *Neonatal Netw* 22:47-54.
- (2) Berdugo, M., R. A. Bejjani, F. Valamanesh, M. Savoldelli, J. C. Jeanny, D. Blanc, H. Ficheux, A. Scherz, Y. Salomon, D. BenEzra, and F. Behar-Cohen. 2008. Evaluation of the new photosensitizer Stakel (WST-11) for photodynamic choroidal vessel occlusion in rabbit and rat eyes. *Invest Ophthalmol Vis Sci* 49:1633-44.
- (3) Carmeli, Y. 2008. Strategies for managing today's infections. *Clin Microbiol Infect* 14 Suppl 3:22-31.
- (4) Carmichael, J., W. G. DeGraff, A. F. Gazdar, J. D. Minna, and J. B. Mitchell. 1987. Evaluation of a tetrazolium-based semiautomated colorimetric assay: assessment of chemosensitivity testing. *Cancer Res* 47:936-42.
- (5) Chabrier-Rosello, Y., T. H. Foster, N. Perez-Nazario, S. Mitra, and C. G. Haidaris. 2005. Sensitivity of *Candida albicans* germ tubes and biofilms to photofrin-mediated phototoxicity. *Antimicrob Agents Chemother* 49:4288-95.
- (6) Demidova, T. N., and M. R. Hamblin. 2005. Effect of cell-photosensitizer binding and cell density on microbial photoinactivation. *Antimicrob. Agents Chemother.* 49:2329-2335.
- (7) Demidova, T. N., and M. R. Hamblin. 2004. Photodynamic therapy targeted to pathogens. *Int.J.Immunopathol.Pharmacol.* 17:245-254.
- (8) Dolmans, D. E., D. Fukumura, and R. K. Jain. 2003. Photodynamic therapy for cancer. *Nat Rev Cancer* 3:380-7.
- (9) Foley, J. W., X. Song, T. N. Demidova, F. Jilal, and M. R. Hamblin. 2006. Synthesis and properties of benzo[a]phenoxazinium chalcogen analogues as novel broad-spectrum antimicrobial photosensitizers. *J Med Chem* 49:5291-9.
- (10) Fukuzumi, S., K. Ohkubo, X. Zheng, Y. Chen, R. K. Pandey, R. Zhan, and K. M. Kadish. 2008. Metal Bacteriochlorins Which Act as Dual Singlet Oxygen and Superoxide Generators. *J Phys Chem B*.
- (11) Gad, F., T. Zahra, K. P. Francis, T. Hasan, and M. R. Hamblin. 2004. Targeted photodynamic therapy of established soft-tissue infections in mice. *Photochem Photobiol Sci* 3:451-8.
- (12) Gradyushko, A. T., A. N. Sevchenko, K. N. Solovyov, and M. P. Tsvirko. 1970. Energetics of photophysical processes in chlorophyll-like molecules. *Photochem Photobiol* 11:387–400.

- (13) Gross, S., A. Gilead, A. Scherz, M. Neeman, and Y. Salomon. 2003. Monitoring photodynamic therapy of solid tumors online by BOLD-contrast MRI. *Nat Med* 9:1327-31.
- (14) Hamblin, M. R., and T. Hasan. 2004. Photodynamic therapy: a new antimicrobial approach to infectious disease? 3:436-450.
- (15) Hamblin, M. R., and P. Mroz. 2008. *Advances in Photodynamic Therapy: Basic, Translational and Clinical*. Artech House, Boston, MA.
- (16) Hamblin, M. R., D. A. O'Donnell, N. Murthy, K. Rajagopalan, N. Michaud, M. E. Sherwood, and T. Hasan. 2002. Polycationic photosensitizer conjugates: effects of chain length and Gram classification on the photodynamic inactivation of bacteria. *J Antimicrob Chemother* 49:941-951.
- (17) Holten, D., M. Gouterman, W. W. Parson, M. W. Windsor, and M. G. Rockley. 1976. Electron transfer from photoexcited singlet and triplet bacteriopheophytin. *Photochem Photobiol* 23:415-20.
- (18) Jett, B. D., K. L. Hatter, M. M. Huycke, and M. S. Gilmore. 1997. Simplified agar plate method for quantifying viable bacteria. *Biotechniques* 23:648-50.
- (19) Jori, G., C. Fabris, M. Soncin, S. Ferro, O. Coppellotti, D. Dei, L. Fantetti, G. Chiti, and G. Roncucci. 2006. Photodynamic therapy in the treatment of microbial infections: basic principles and perspective applications. *Lasers Surg Med* 38:468-81.
- (20) Kee, H. L., J. Bhaumik, J. R. Diers, P. Mroz, M. R. Hamblin, D. F. Bocian, J. S. Lindsey, and D. Holten. 2008. Photophysical characterization of imidazolium-substituted Pd(II), In(III), and Zn(II) porphyrins as photosensitizers for photodynamic therapy. *J Photochem Photobiol A* 200:346-355.
- (21) Kee, H. L., C. Kirmaier, Q. Tang, J. R. Diers, C. Muthiah, M. Taniguchi, J. K. Laha, M. Ptaszek, J. S. Lindsey, D. F. Bocian, and D. Holten. 2007. Effects of substituents on synthetic analogs of chlorophylls. Part 2: Redox properties, optical spectra and electronic structure. *Photochem Photobiol* 83:1125-43.
- (22) Kim, H. J., and J. S. Lindsey. 2005. De novo synthesis of stable tetrahydroporphyrinic macrocycles: bacteriochlorins and a tetrahydrocorrin. *J Org Chem* 70:5475-86.
- (23) Kobayashi, M., M. Akiyama, H. Kano, and H. Kise. 2006. Chlorophylls and Bacteriochlorophylls: Biochemistry, Biophysics, Functions and Applications, p. 79-94. In B. Grimm, R. J. Porra, W. Rüdiger, and H. Scheer (ed.), *Advances in Photosynthesis and Respiration*, vol. 25. Springer, Dordrecht, The Netherlands.
- (24) Kong, J., C. A. White, A. I. Krylov, D. Sherrill, R. D. Adamson, T. R. Furlani, M. S. Lee, A. M. Lee, S. R. Gwaltney, T. R. Adams, C. Ochsenfeld, A. T. B. Gilbert, G. S. Kedziora, V. A. Rassolov, D. R. Maurice, N. Nair, Y. Shao, N. A. Besley, P. E. Maslen, J. P. Dombroski, H. Daschel, W. Zhang, P. P. Korambath, J. Baker, E. F. C. Byrd, T. Van Voorhis, M. Oumi, S. Hirata, C.-P. Hsu, N. Ishikawa, J. Florian, A. Warshel, B. G. Johnson, P. M. W. Gill, M. Head-Gordon, and J. A. Pople. 2000. Q-Chem 2.0: a high-performance ab initio electronic structure program package. *J. Computational Chem* 21:1532-1548.

- (25) Lambrechts, S. A., M. C. Aalders, and J. Van Marle. 2005. Mechanistic study of the photodynamic inactivation of *Candida albicans* by a cationic porphyrin. *Antimicrob Agents Chemother* 49:2026-34.
- (26) Lauro, F. M., P. Pretto, L. Covolo, G. Jori, and G. Bertoloni. 2002. Photoinactivation of bacterial strains involved in periodontal diseases sensitized by porphycene-polylysine conjugates. *Photochem Photobiol Sci* 1:468-70.
- (27) Maisch, T. 2007. Anti-microbial photodynamic therapy: useful in the future? *Lasers Med Sci* 22:83-91.
- (28) Maisch, T., C. Bosl, R. M. Szeimies, N. Lehn, and C. Abels. 2005. Photodynamic effects of novel XF porphyrin derivatives on prokaryotic and eukaryotic cells. *Antimicrob Agents Chemother* 49:1542-52.
- (29) Malik, Z., H. Ladan, and Y. Nitzan. 1992. Photodynamic inactivation of Gram-negative bacteria: problems and possible solutions. *J. Photochem. Photobiol. B* 14:262-6.
- (30) Mantareva, V., V. Kussovski, I. Angelov, E. Borisova, L. Avramov, G. Schnurpfeil, and D. Wohrle. 2007. Photodynamic activity of water-soluble phthalocyanine zinc(II) complexes against pathogenic microorganisms. *Bioorg Med Chem* 15:4829-35.
- (31) Merchat, M., G. Bertolini, P. Giacomini, A. Villanueva, and G. Jori. 1996. Meso-substituted cationic porphyrins as efficient photosensitizers of gram-positive and gram-negative bacteria. *J. Photochem. Photobiol. B* 32:153-7.
- (32) Michel, M., and L. Gutmann. 1997. Methicillin-resistant *Staphylococcus aureus* and vancomycin-resistant enterococci: therapeutic realities and possibilities. *Lancet* 349:1901-6.
- (33) Minnock, A., D. I. Vernon, J. Schofield, J. Griffiths, J. H. Parish, and S. B. Brown. 2000. Mechanism of uptake of a cationic water-soluble pyridinium zinc phthalocyanine across the outer membrane of *Escherichia coli*. *Antimicrob Agents Chemother* 44:522-7.
- (34) Mizzoni, R. H., M. A. Hennessey, and C. R. Scholz. 1954. Polyamine salts with autonomic blocking properties. *J. Am. Chem. Soc.* 76:2414-2417.
- (35) Moan, J., and Q. Peng. 2003. An outline of the hundred-year history of PDT. *Anticancer Res* 23:3591-600.
- (36) Munin, E., L. M. Giroldo, L. P. Alves, and M. S. Costa. 2007. Study of germ tube formation by *Candida albicans* after photodynamic antimicrobial chemotherapy (PACT). *J Photochem Photobiol B*.
- (37) Nitzan, Y., R. Dror, H. Ladan, Z. Malik, S. Kimel, and V. Gottfried. 1995. Structure-activity relationship of porphines for photoinactivation of bacteria. *Photochem. Photobiol.* 62:342-7.
- (38) Nitzan, Y., M. Gutterman, Z. Malik, and B. Ehrenberg. 1992. Inactivation of gram-negative bacteria by photosensitized porphyrins. *Photochem. Photobiol.* 55:89-96.
- (39) Nobile, C. J., and A. P. Mitchell. 2005. Regulation of cell-surface genes and biofilm formation by the *C. albicans* transcription factor Bcr1p. *Curr Biol* 15:1150-5.

- (40) Oertel, M., S. I. Schastak, A. Tannapfel, R. Hermann, U. Sack, J. Mossner, and F. Berr. 2003. Novel bacteriochlorine for high tissue-penetration: photodynamic properties in human biliary tract cancer cells in vitro and in a mouse tumour model. *J Photochem Photobiol B* 71:1-10.
- (41) Owens, R. C., Jr. 2008. Antimicrobial stewardship: concepts and strategies in the 21st century. *Diagn Microbiol Infect Dis* 61:110-28.
- (42) Rovers, J. P., M. L. de Jode, and M. F. Grahn. 2000. Significantly increased lesion size by using the near-infrared photosensitizer 5,10,15,20-tetrakis (m-hydroxyphenyl)bacteriochlorin in interstitial photodynamic therapy of normal rat liver tissue. *Lasers Surg Med* 27:235-40.
- (43) Rovers, J. P., M. L. de Jode, H. Rezzoug, and M. F. Grahn. 2000. In vivo photodynamic characteristics of the near-infrared photosensitizer 5,10,15,20-tetrakis(M-hydroxyphenyl) bacteriochlorin. *Photochem Photobiol* 72:358-64.
- (44) Ruzie, C., M. Krayner, T. Balasubramanian, and J. S. Lindsey. 2008. Tailoring a bacteriochlorin building block with cationic, amphipathic, or lipophilic substituents. *J Org Chem* 73:5806-20.
- (45) Schastak, S., B. Gitter, R. Handzel, R. Hermann, and P. Wiedemann. 2008. Improved photoinactivation of gram-negative and gram-positive methicillin-resistant bacterial strains using a new near-infrared absorbing meso-tetrahydroporphyrin: a comparative study with a chlorine e6 photosensitizer photolon. *Methods Find Exp Clin Pharmacol* 30:129-33.
- (46) Schuitmaker, J. J., J. A. van Best, J. L. van Delft, T. M. Dubbelman, J. A. Oosterhuis, and D. de Wolff-Rouendaal. 1990. Bacteriochlorin a, a new photosensitizer in photodynamic therapy. In vivo results. *Invest Ophthalmol Vis Sci* 31:1444-50.
- (47) Sherman, F. 1991. Getting started with yeast. *Methods Enzymol* 194:3-21.
- (48) Solban, N., I. Rizvi, and T. Hasan. 2006. Targeted photodynamic therapy. *Lasers Surg Med*.
- (49) Tang, H. M., M. R. Hamblin, and C. M. Yow. 2007. A comparative in vitro photoinactivation study of clinical isolates of multidrug-resistant pathogens. *J Infect Chemother* 13:87-91.
- (50) Taniguchi, M., D. L. Cramer, A. D. Bhise, H. L. Kee, D. F. Bocian, D. Holten, and J. S. Lindsey. 2008. Accessing the near-infrared spectral region with stable, synthetic, wavelength-tunable bacteriochlorins. *New J Chem* 32:947-958.
- (51) Tegos, G. P., M. Anbe, C. Yang, T. N. Demidova, M. Satti, P. Mroz, S. Janjua, F. Gad, and M. R. Hamblin. 2006. Protease-stable polycationic photosensitizer conjugates between polyethyleneimine and chlorin(e6) for broad-spectrum antimicrobial photoinactivation. *Antimicrob Agents Chemother* 50:1402-10.
- (52) Tegos, G. P., T. N. Demidova, D. Arcila-Lopez, H. Lee, T. Wharton, H. Gali, and M. R. Hamblin. 2005. Cationic fullerenes are effective and selective antimicrobial photosensitizers. *Chem. Biol.* 12:1127-1135.

- (53) Torricelli, A., A. Pifferi, P. Taroni, E. Giambattistelli, and R. Cubeddu. 2001. In vivo optical characterization of human tissues from 610 to 1010 nm by time-resolved reflectance spectroscopy. *Phys Med Biol* 46:2227-37.
- (54) Trachtenberg, J., R. A. Weersink, S. R. Davidson, M. A. Haider, A. Bogaards, M. R. Gertner, A. Evans, A. Scherz, J. Savard, J. L. Chin, B. C. Wilson, and M. Elhilali. 2008. Vascular-targeted photodynamic therapy (padoporfin, WST09) for recurrent prostate cancer after failure of external beam radiotherapy: a study of escalating light doses. *BJU Int* 102:556-62.
- (55) van Duijnhoven, F. H., J. P. Rovers, K. Engelmann, Z. Krajina, S. F. Purkiss, F. A. Zoetmulder, T. J. Vogl, and O. T. Terpstra. 2005. Photodynamic therapy with 5,10,15,20-tetrakis(m-hydroxyphenyl) bacteriochlorin for colorectal liver metastases is safe and feasible: results from a phase I study. *Ann Surg Oncol* 12:808-16.
- (56) Weber, G., and F. W. J. Teale. 1957. Determination of the absolute quantum yield of fluorescent solutions. *Trans. Faraday Soc* 53:646-655.
- (57) Woodhams, J. H., A. J. MacRobert, M. Novelli, and S. G. Bown. 2006. Photodynamic therapy with WST09 (Tookad): quantitative studies in normal colon and transplanted tumours. *Int J Cancer* 118:477-82.
- (58) Wormald, R., J. Evans, L. Smeeth, and K. Henshaw. 2005. Photodynamic therapy for neovascular age-related macular degeneration. *Cochrane Database Syst Rev* 4:CD002030.

Chapter 11

Molecular Electronic Tuning of Photosensitizers to Enhance Photodynamic Therapy: Synthetic Dicyanobacteriochlorins as a Case Study

Reproduced with permission from Yang, EK; Ruzié, C; Krayner, M; Diers, J.R; Niedzwiedzki,DM; Kirmaier,C; Lindsey, J.S; Bocian, D.F; Holten, D. Photophysical Properties and Electronic Structure of Bacteriochlorin–Chalcones with Extended Near-Infrared Absorption. *Photochem. Photobiol.* 2013. 89. 605-618. Doi:10.1111/php.12021. Copyright 2013 WILEY-BLACKWELL.

Abstract

Photophysical, photostability, electrochemical, and molecular-orbital characteristics are analyzed for a set of stable dicyanobacteriochlorins that are promising photosensitizers for photodynamic therapy (PDT). The bacteriochlorins are the parent compound (**BC**), dicyano derivative (**(NC)₂BC**) and corresponding zinc (**(NC)₂BC-Zn**) and palladium chelate (**(NC)₂BC-Pd**). The order of PDT activity against HeLa human cancer cells *in vitro* is **(NC)₂BC-Pd** > **(NC)₂BC** > **(NC)₂BC-Zn** \approx **BC**. The near-infrared absorption feature of each dicyanobacteriochlorin is bathochromically shifted 35–50 nm (748–763 nm) from that for **BC** (713 nm). Intersystem crossing to the PDT-active triplet excited state is essentially quantitative for **(NC)₂BC-Pd**. Phosphorescence from **(NC)₂BC-Pd** occurs at 1122 nm (1.1 eV). This value and the measured ground-state redox potentials fix the triplet excited-state redox properties, which underpin PDT activity via Type-1 (electron-transfer) pathways. A perhaps counterintuitive (but readily explicable) result is that of the three dicyanobacteriochlorins, the photosensitizer with the shortest triplet lifetime (7 μ s), **(NC)₂BC-Pd**, has the highest activity. Photostabilities of the dicyanobacteriochlorins and other bacteriochlorins studied recently are investigated and discussed in terms of four phenomena: aggregation, reduction, oxidation, and chemical reaction. Collectively, the results and analysis provide fundamental insights concerning the molecular design of PDT agents.

Introduction

Photodynamic therapy (PDT) is an emerging treatment approach that uses a non-toxic photosensitizer and harmless visible or near-infrared (NIR) light to kill diseased cells by generating reactive oxygen species, such as singlet oxygen, superoxide and hydroxyl radicals.¹ To enhance the efficacy and selectivity of response, molecular tuning of the chemical and electronic-structure characteristics of photosensitizers is employed to produce (1) favorable photophysical properties; (2) chemical and photochemical stability; (3) preferential delivery to the destination tissue or cell type, including subcellular compartments; and (4) production of reactive oxygen species that are especially lethal to the target cell.

An important consideration is to choose or tune the photosensitizer to have strong absorption in the NIR region where light penetration through tissue is maximal because both absorption and scattering of light at these wavelengths by endogenous chromophores are minimal. In this regard, bacteriochlorins and related macrocycles are ideal because of the intense NIR (720–850 nm) absorption resulting from the reduction of two pyrrolic rings in the tetrapyrrole macrocycle compared to chlorins (one reduced ring, modestly intense red absorption) and porphyrins (no reduced rings and weak or no red or NIR absorption). Naturally occurring bacteriochlorins or derivatives thereof, such as **WST9** (Tookad) and **WST11** (Chart 1) can have high PDT efficacy but have drawbacks due to instability (in the dark and in the light) and limitations on molecular tailoring because nearly all sites about the perimeter of the macrocycle already bear substituents.

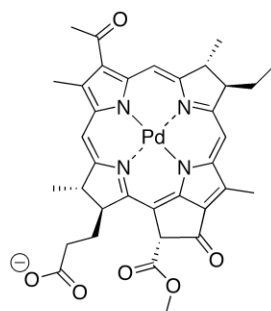
A *de novo* synthetic route has been developed to access bacteriochlorins that are stabilized against adventitious oxidation by the presence of a geminal dimethyl group in each

reduced ring.²⁻⁴ This route has been used to prepare bacteriochlorins containing a variety of positively charged substituents, groups to impart water solubility, and/or groups that can vary the balance between hydrophobicity and hydrophilicity. The PDT activity of these bacteriochlorins has been tested against B16 mouse melanoma cells⁵, HeLa human cervical cancer cells⁶ and microbial cells (Gram-positive, Gram-negative bacteria and yeast)⁷ *in vitro*. A number of these synthetic bacteriochlorins are highly efficacious (i.e., LD50 \leq 100 nM) for cell killing against human cancer cell lines. Representative structures are shown in Chart 2. The bacteriochlorins employed are all the metal-free (free base) forms. The PDT efficacy of tetrapyrrole chromophores (e.g., porphyrins, chlorins, bacteriochlorins, phthalocyanines) often depends on the metalation state,⁸ as was found for a set of imidazole-substituted metalloporphyrins (Chart 3) targeted against HeLa and CT26 cancer cells.^{9,10}

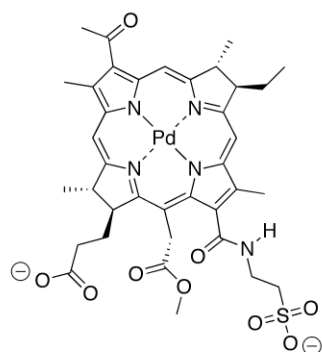
Some of the synthetic bacteriochlorins are more readily photobleached than others. Photobleaching is defined as loss of absorption of the bacteriochlorin, and can stem from a variety of causes (oxidation, reduction, aggregation, chemical reaction). Understanding the interplay of molecular structure and origin of photobleaching in principle could lead to improvements in photostability and thereby afford increased PDT activity.

Recently we synthesized and examined the PDT efficacy against HeLa cancer cells of a set of free base and metal-substituted bacteriochlorins bearing electron-withdrawing, cyano-groups (Chart 4).¹¹ In addition to photoactivity, analyses were performed of cellular uptake, subcellular distribution, and the propensity of the compounds to form singlet oxygen (Type-2 photochemistry) or hydroxyl radicals (Type-1 photochemistry). The dicyanobacteriochlorins show (1) the same trend in efficacy with metal ion (e.g., Pd²⁺ > Zn²⁺) as determined for the imidazole-substituted (and other) porphyrins, (2) increased photostability, and (3) efficacies

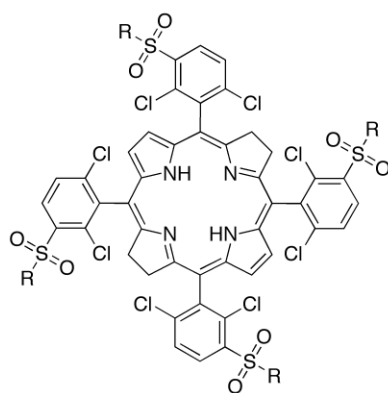
comparable to or surpassing those of the best of the synthetic bacteriochlorins studied previously and other common PDT agents.



WST9



WST11



TDCPBS

Chart 1. Representative native bacteriochlorin derivatives (**WST9** = Tookad, **WST11**)^{20,21} and a synthetic bacteriochlorin (**TDCPBS**)^{27,28} that have been examined in PDT studies.

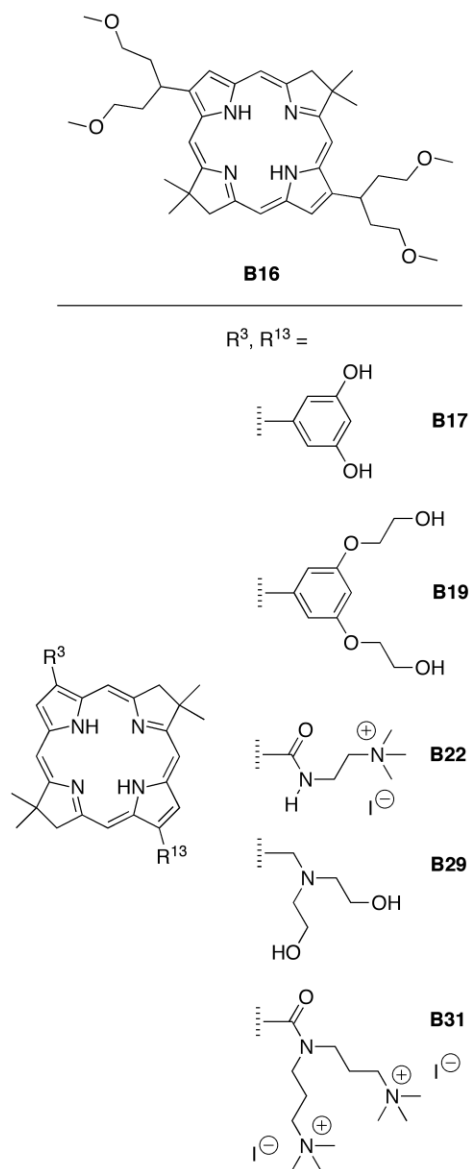


Chart 2. Representative synthetic bacteriochlorins examined previously for PDT activity.⁵⁻⁷

In the present work, the photophysical, redox, and molecular-orbital characteristics of the unsubstituted and dicyanobacteriochlorins are presented along with more extensive photostability data. This information allows analysis of the recent results¹¹ concerning photoactivity and reactive oxygen species production in terms of fundamental electronic

properties, including excited-state redox potentials. To increase the generality of the findings, the analysis is extended to include results on the imidazole-substituted porphyrins and representative synthetic bacteriochlorins studied previously, for which photostability characteristics are presented here for the first time. The collective findings provide fundamental insights into the design and electronic tuning of bacteriochlorin photosensitizers for enhanced PDT efficacy.

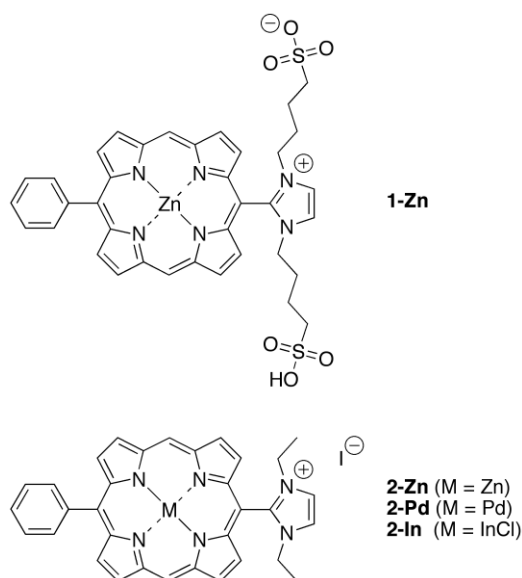


Chart 3. Imidazole-substituted porphyrins examined previously for PDT activity.^{9,10}

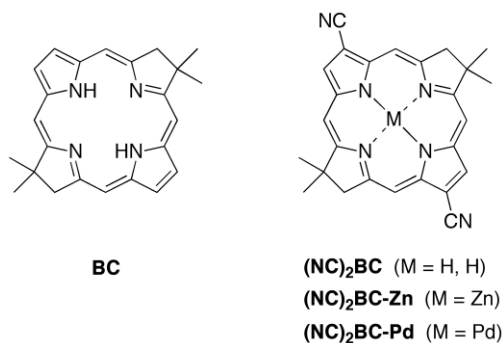


Chart 4. Synthetic bacteriochlorins examined recently for PDT activity.¹¹

Experimental methods

Photosensitizers

The syntheses of BC^4 , $(\text{NC})_2\text{BC}^3$, and $(\text{NC})_2\text{BC-Zn}^3$ have been described. The synthesis of $(\text{NC})_2\text{BC-Pd}$ will be reported elsewhere. Absorption and emission studies indicate that samples of $(\text{NC})_2\text{BC-Pd}$ studied herein contain <1% of the free base $(\text{NC})_2\text{BC}$ starting material. Photofrin and Verteporfin (liposomal benzoporphyrin derivative, BPD) were gifts from QLT, Inc. (Vancouver, Canada) and Lutex was a gift from Pharmacyclics, Inc. (Sunnyvale, CA).

Photophysical characterization

Static absorption (Varian Cary 100 or Shimadzu UV-1800) and fluorescence (Spex Fluorolog Tau 2 or PTI Quantamaster 40) measurements were performed at room temperature, as were all other studies. Determination of the fluorescence quantum yield (Φ_f), singlet excited-state lifetimes (τ_s) and triplet yields (Φ_T) utilized dilute (μM) Ar-purged toluene and methanol solutions. Measurements of the triplet lifetimes (τ_T) utilized Ar-purged 2-methyl tetrahydrofuran solutions. Samples for Φ_f measurements had an absorbance ≤ 0.1 at the excitation wavelength to minimize front-face effects and similarly low absorbance in the $Q_y(0,0)$ band to minimize inner-filter effects.

Static emission measurements employed 2–4 nm excitation- and detection-monochromator bandwidths and 0.2-nm data intervals. Emission spectra were corrected for detection-system spectral response. Some measurements employed an extended NIR sensitive detector that drives a lock-in amplifier frequency-referenced to the rate of chopping of the excitation light prior to the excitation monochromator. Fluorescence quantum yields were

determined relative to several different standards. These standards are (1) chlorophyll *a* in deoxygenated toluene ($\Phi_f = 0.325$),¹² which is the value measured in benzene,¹³ (2) free base *meso*-tetraphenylporphyrin (**FbTPP**) in nondegassed toluene, for which $\Phi_f = 0.070$ was established with respect to the zinc chelate **ZnTPP** in nondegassed toluene ($\Phi_f = 0.030$),¹⁴ a value consistent with prior results on **FbTPP**,¹⁵ and (3) 8,8,18,18-tetramethylbacteriochlorin⁴ in Ar-purged toluene, for which $\Phi_f = 0.14$ was established with respect to chlorophyll *a* in benzene and **FbTPP** in toluene.

Singlet-excited state lifetimes (τ_s) for all compounds except **(NC)₂BC-Pd** were obtained using time-correlated-single-photon-counting detection on an apparatus with an approximately Gaussian instrument response function with a full-width-at-half-maximum of ~ 1 ns (Photon Technology International LaserStrobe TM-3). Samples were excited in the Soret or Q_x regions using excitation pulses at 337 nm from a nitrogen laser or in the blue to green spectral regions from a dye laser pumped by the nitrogen laser. The τ_s value for **(NC)₂BC-Pd** was obtained by ultrafast transient absorption spectroscopy, probing disappearance of the bleaching in the Q_y ground-state absorption band and excited-state absorption features following excitation in the Q_x band with an ~ 130 fs excitation flash.¹⁶ The τ_T values were similarly determined using transient absorption spectroscopy, probing the decay of bleaching of the Soret band and excited-state absorption features following excitation in the Q_x band with ~ 5 ns pulses from a Q-switched Nd:YAG laser (532 nm) or a dye laser pumped by the Nd:YAG laser.^{9,16}

The Φ_{isc} values (triplet yields) were obtained using transient absorption spectroscopy. The extent of bleaching of the ground-state Q_x bands due to the formation of the lowest singlet excited state was measured immediately following a 130 fs flash in the $Q_y(0,0)$ band and

compared with that due to the formation of the lowest triplet excited state at the asymptote of the singlet excited-state decay.^{9,16}

Photostability studies

Photostability measurements utilized excitation light obtained from a 300W Xenon lamp (Model R300-3 lamp and PS300-1 power supply; ILC Technologies, Sunnyvale, CA) that passed through a 70 cm path cell containing deionized water followed by a monochromator with a 10 nm bandpass. The light intensity at the sample position was measured using a calibrated diode and optometer (Models 221 and S471, United Detector Technologies, San Diego, CA) and was typically $\sim 5 \text{ mW/cm}^2$ at the wavelength (720–750 nm) of the NIR absorption maximum of the bacteriochlorin sample ($A \sim 0.5$ in 1 cm). The solutions contained ambient (atmospheric) O_2 or had the O_2 removed by purging with Ar for ~ 1 h or by repeated freeze-pump-thaw cycles on a high vacuum line that achieved a vacuum of $< 10^{-6}$ Torr. The O_2 was removed from all aqueous micellar solutions via the latter method. Samples were stirred using a micro magnetic bar at the bottom of the cuvette during illumination.

Electrochemistry

Electrochemical studies were performed using previously described instrumentation.¹⁷ The solvent was butyronitrile (Burdick and Jackson) containing 0.1 M tetrabutylammonium hexafluorophosphate (Aldrich; recrystallized three times from methanol and dried at 110 °C in vacuo) as the supporting electrolyte. The electrochemical cell was housed in a glovebox. The $E_{1/2}$ values were obtained with square wave voltammetry (frequency 10 Hz) under conditions where the ferrocene couple has a potential of +0.19 V.

Density Functional Theory calculations

DFT calculations were performed with Spartan '10 for Windows version 1.2.0 in parallel mode on a PC equipped with an Intel i7-975 cpu, 24 GB ram, and three 300 GB, 10k rpm hard drives.¹⁸ The calculations employed the hybrid B3LYP functional and basis sets 6-31G* and LACVP (the former for atoms H to Kr and lan12dz for atoms Kr and above). The equilibrium geometries were fully optimized using the default parameters of the Spartan program. Molecular orbital images were plotted using an isovalue of 0.016.

Results and discussions

Sensitizer Activity, Uptake, Localization, and Reactive oxygen species production

In our recent study¹¹, the PDT activity against HeLa cancer cells *in vitro* was studied using the parent bacteriochlorin (**BC**), dicyano derivative (**(NC)₂BC**) and the corresponding zinc chelate (**(NC)₂BC-Zn**) and palladium chelate (**(NC)₂BC-Pd**) (Chart 4). The photosensitizers were delivered either by (1) direct dilution (denoted “dd”) of a solution of bacteriochlorin in an organic solvent [5 mM in *N,N*-dimethylacetamide (DMA) or tetrahydrofuran (THF)] into serum-containing complete culture medium or (2) encapsulation into aqueous Cremophore EL micelles (CrEL) followed by dilution into the same complete medium. For both delivery methods, the order of PDT activity against HeLa cells after incubation for 24 h and illumination with 10 J/cm² of NIR light is **(NC)₂BC-Pd** > **(NC)₂BC** > **(NC)₂BC-Zn** > **BC**. As can be seen from Table 1, the LD50 values improve using CrEL versus direct dilution only modestly for **(NC)₂BC-Pd** (18 versus 25 nM) and **(NC)₂BC** (25 versus 60 nM) but significantly for **(NC)₂BC-Zn** (60 versus 1000 nM) and **BC** (350 versus 1800 nM).

Values for the uptake of 5 μ M bacteriochlorin at different time points in the incubation medium are also given in Table 1. The highest uptake using direct dilution is found for **BC** and **(NC)₂BC-Pd**, followed by **(NC)₂BC** and **(NC)₂BC-Zn**. The use of CrEL substantially decreases the uptake of **(NC)₂BC-Pd**, **(NC)₂BC** and **BC** but has little effect for **(NC)₂BC-Zn**. Table 1 also gives the PDT efficacy per unit uptake, obtained by dividing the reciprocal of the LD50 value by the uptake value and then normalizing to the value of **BC** using direct dilution. The tabulated values of efficacy corrected for uptake for both delivery motifs show the same order as the tabulated values for activity alone: **(NC)₂BC-Pd** > **(NC)₂BC** > **(NC)₂BC-Zn** > **BC**. Thus, although cell uptake certainly influences the overall PDT activity, other factors appear to dominate. In this regard, the greater efficacy of **(NC)₂BC-Pd** versus **(NC)₂BC-Zn** parallels our prior results on imidazole-substituted metalloporphyrins (Chart 3) wherein **2-Pd** is more active than **2-Zn**, exhibiting LD50 values of 55 nM and 833 nM under the excitation conditions employed.^{9,10} The studies on the dicyanobacteriochlorins complement and extend this prior work by inclusion of a free base analogue, providing additional information for analysis of activity.

Fluorescence microscopy studies reveal that subcellular localization of the unsubstituted and dicyanobacteriochlorins is in the endoplasmic reticulum, mitochondria and lysosomes depending on the compound. The least active compound, **BC**, is found mainly in the endoplasmic reticulum and lysosomes, and the next compound, **(NC)₂BC-Zn**, is also found mainly in lysosomes with little evidence for association with mitochondria. The second most active bacteriochlorin, **(NC)₂BC**, localizes mainly in the endoplasmic reticulum and mitochondria. The most active compound, **(NC)₂BC-Pd**, also targets mitochondria (and lysosomes) as deduced by the damage done by PDT activity monitored after illumination. The results suggest that the propensity for mitochondrial targeting contributes to the relative PDT

efficacy of the four bacteriochlorins. Mitochondria are considered to be an important PDT target because of the vital cellular functions performed, including regulation of metabolism, cell-cycle control development, and induction of apoptotic cell death after mitochondrial damage.

The propensities of the bacteriochlorins to produce singlet oxygen by energy transfer (Type-2 mechanism) or hydroxyl radical by electron transfer (Type-1 mechanism) were probed using fluorescent dyes sensitive to the particular reactive oxygen species. Of the four bacteriochlorins, **(NC)₂BC-Pd** produces the most singlet oxygen and also the most hydroxyl radicals, with the balance favoring the latter (Type-1 photochemistry). The next active compound, **(NC)₂BC**, also produces a relatively high ratio of hydroxyl radicals to singlet oxygen. The two least active photosensitizers, **(NC)₂BC-Zn** and **BC**, give low ratios hydroxyl radicals versus singlet oxygen and therefore carry out less Type-1 than Type-2 photochemistry. In summary, the most active bacteriochlorins (against HeLa cells) produce the greatest amounts of hydroxyl radicals. Similar results were found previously for the imidazole-substituted porphyrins (Chart 3), for which **2-Pd** produces more hydroxyl radicals and, as noted above, has greater PDT activity than **2-Zn**¹⁰.

Initial results of photobleaching studies obtained previously¹¹ on the four bacteriochlorins are also given in Table 1. Listed is the fraction of the NIR $Q_y(0,0)$ absorbance remaining after 100 J/cm² of illumination in the same optical band. Values are given for the compounds in DMA and CrEL solutions in the presence of ambient O₂ and for the latter in the absence of O₂. The most active compounds, **(NC)₂BC-Pd** and **(NC)₂BC**, are the most photostable, with typically >90% of the Q_y absorbance remaining even in the presence of ambient O₂. The two lesser active compounds, **(NC)₂BC-Zn** and **BC**, show lower photostability in the presence of O₂ and marked improvement if O₂ is removed from the solution. Below, more extensive

measurements of the photostability of the dicyanobacteriochlorins are presented and compared with those for representative synthetic bacteriochlorins whose PDT activity (but not photostability) have been studied previously.

Absorption and Fluorescence spectra

Figure 1A shows the absorption spectra for **BC**, **(NC)₂BC**, **(NC)₂BC-Zn**, and **(NC)₂BC-Pd** in toluene. The wavelengths of all the major absorption features for the bacteriochlorins in toluene and methanol are given in Table 2. For each bacteriochlorin the spectral positions are similar in the two solvents, and the same is found for the compounds in DMA and in CrEL solutions. All four compounds show good solubility in the four media.

Figure 1B focuses on the NIR absorption feature, the Q_y(0,0) band. This band for the metal-free dicyanobacteriochlorin **(NC)₂BC** is substantially (35 nm) hypsochromically shifted versus the parent bacteriochlorin **BC** (748 versus 713 nm in toluene). The incorporation of the central Pd²⁺ ion of **(NC)₂BC-Pd** slightly bathochromically shifts the band to 751 nm while the Zn²⁺ of **(NC)₂BC-Zn** causes a larger shift to 761 nm. Figure 1B shows that the corresponding Q_y(0,0) fluorescence band for each bacteriochlorin lies only 2–5 nm to longer wavelength than the Q_y(0,0) absorption maximum (Table 2).

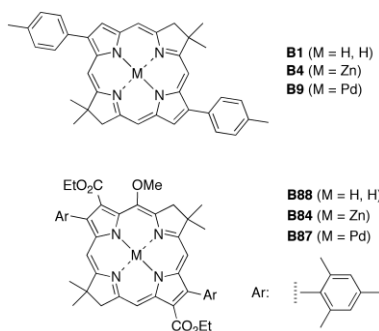


Chart 5. Two sets of synthetic bacteriochlorins prepared and studied recently.¹⁹

Table 1. PDT activity, photostability and photophysical properties of the bacteriochlorins.^a

Compound	LD50 dd	LD50 CrEL	Uptake dd	Uptake CrEL	Efficacy /uptake dd ^b	Efficacy /uptake CrEL ^b	Photo- stability DMA ^c	Photo- stability CrEL ^c	Photo- stability CrEL no O ₂ ^c	Φ_f	τ_S	Φ_T	τ_T
	(nM)	(nM)	(nmol/ mg)	(nmol/ mg)							(ns)		(μ s)
<i>Unsubstituted & dicyano BCs</i>													
BC	1800	350	5.3	3.7	1.0	7.3	0.13	0.11	0.54	0.14	4.0	0.62	169
(NC)₂BC	60	25	4.3	3.3	37.1	114.3	0.91	0.90		0.15	4.1	0.43	84
(NC)₂BC-Zn	1000	60	2.1	2.1	4.5	76.4	0.52	0.04	0.67	0.15	3.9	0.63	121
(NC)₂BC-Pd	25	18	4.8	2.3	79.6	227.2	0.83	0.94		≤ 0.007	0.02	0.99	7
<i>Representative prior studied</i>													
B16	100		11.7		8.1		0.02	0.01	0.56	0.11	3.6	0.40	190
B17	80		13.5		8.8		0.09	0.21	0.71	0.08	3.7	0.56	198
B19	15		0.001		632400					0.15	3.0	0.55	159
B22	3000		7.7		0.4		0.60	0.11 ^d	0.76	0.11	4.0	0.48	77
B29	100		8.2		11.6		0.09	0.11 ^d	0.78	0.10	3.8	0.53	190
B31	800		1.8		6.6		0.02	0.05 ^d	0.73	0.09	3.5	0.53	54

^aAll measured quantities were obtained at room temperature. Data for **B16-B31** are taken from refs (5) and (6). LD50 and uptake data for the unsubstituted and dicyano bacteriochlorins are taken from ref (11). For the LD50, uptake, and efficacy/uptake values, “dd” reflects direct dilution of the DMA stock solution of the photosensitizer into complete medium and CrEL reflects dilution of the micellar solution into complete medium. Measurements of the fluorescence yields (Φ_f), singlet excited state lifetimes (τ_S) and triplet yields (Φ_T) employed Ar-purged toluene solutions and of the triplet lifetimes (τ_T) Ar-purged THF solutions. ^bCalculated by dividing the reciprocal of the LD50 by the uptake value and normalizing to the value for **BC** dd. ^cPhotostability as measured by the percentage of the initial Q_y absorbance remaining after 100 J/cm² fluence of light given at that wavelength. ^dThe values are reached at ≤ 50 J/cm² fluence.

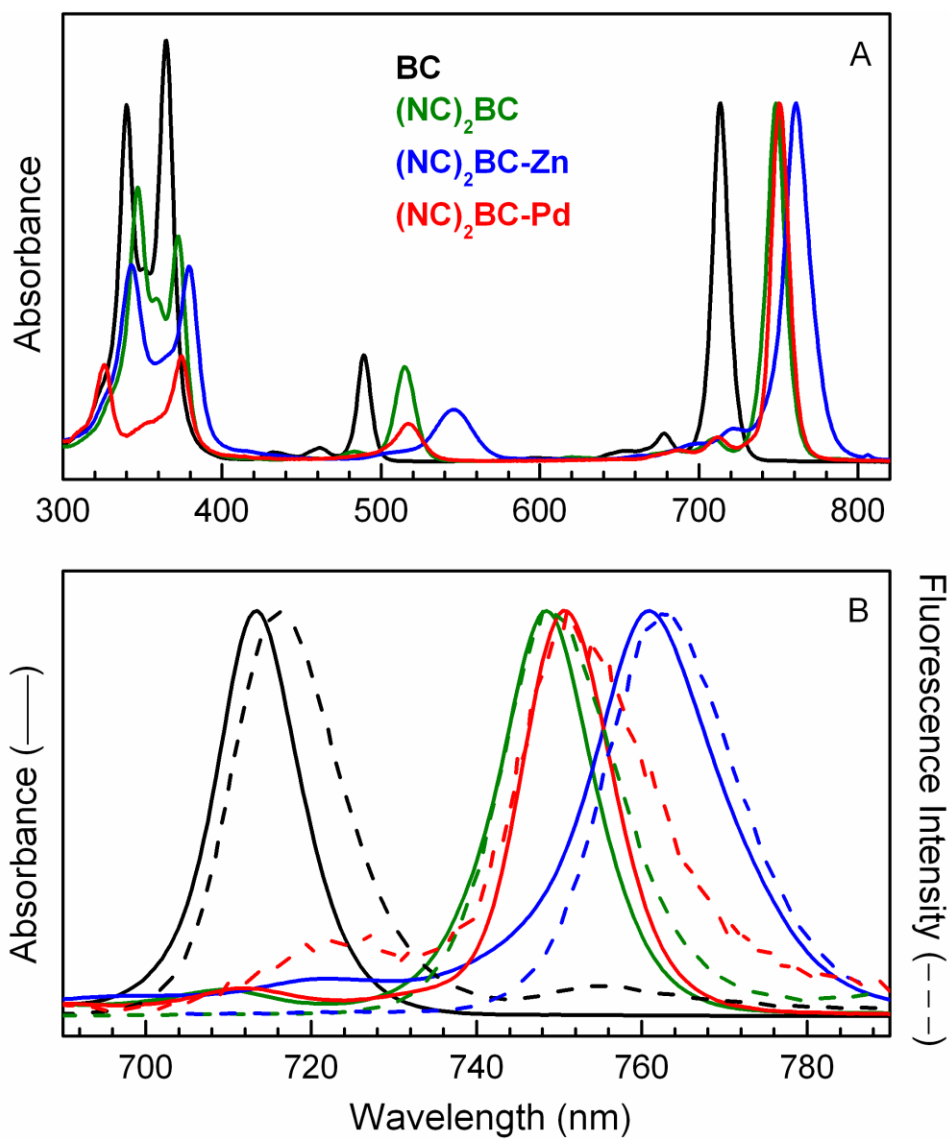


Figure 1. Absorption spectra (solid) and fluorescence spectra (dashed) of bacteriochlorins in toluene: **BC** (black), $(NC)_2BC$ (green), $(NC)_2BC-Zn$ (blue), $(NC)_2BC-Pd$ (red). Panel A shows the full near-UV to NIR absorption spectrum. Panel B focuses on the NIR (Q_y) region of the absorption spectra and the companion fluorescence spectra.

Table 2. Absorption and fluorescence properties of dicyanobacteriochlorins.^a

Cmpd	Solvent	B _y abs (nm)	B _x abs (nm)	Q _x abs (nm)	Q _y abs (nm)	Q _y em (nm)	Q _y /I _B	Φ _s	τ _S (ns)
BC	Tol	340	365	489	713	716	0.85	0.14	4.0
	MeOH	335	359	485	708	712	0.72	0.095	4.1
(NC)₂BC	Tol	347	372	515	748	752	1.3	0.15	4.1
	MeOH	342	367	510	743	747	1.3	0.095	4.1
(NC)₂BC-Zn	Tol	343	380	546	761	763	1.8	0.15	3.9
	MeOH	341	374	553	752	757	1.9	0.15	4.1
(NC)₂BC-Pd	Tol	326	374	518	751	753	3.4	0.007	0.023
	MeOH	323	371	514	744	749	2.8	0.007	

^aAll measurements were made at room temperature.

Fluorescence yields, Singlet excited-state lifetimes, and Triplet yields

Compounds **BC**, **(NC)₂BC** and **(NC)₂BC-Zn** have similar singlet excited-state lifetimes ($\tau_S = 3.9\text{--}4.1$ ns) and fluorescence quantum yields ($\Phi_f = 0.14\text{--}0.15$). The results are summarized in Tables 1 and 2. The lifetime of **(NC)₂BC-Pd** is dramatically reduced ($\tau_S = 23$ ps) as is the fluorescence yield ($\Phi_f \leq 0.007$). The latter value is an upper limit because the possibility cannot be excluded that some of the weak emission derives from trace demetalated analogue **(NC)₂BC**,

which has spectral overlap with **(NC)₂BC-Pd**. Indeed, based on the relative τ_S values, one would have expected a Φ_f value of ~ 0.0008 for **(NC)₂BC-Pd**. The Φ_f and τ_s values of **BC**, **(NC)₂BC** and **(NC)₂BC-Zn** are comparable to those that we have found recently for synthetic free base bacteriochlorins (see e.g., Table 1)^{5-7,16,19} and zinc bacteriochlorins¹⁹ bearing a number of substituent patterns. The results for **(NC)₂BC-Pd** are in keeping with values for two other synthetic palladium bacteriochlorins¹⁹, and palladium-substituted bacteriochlorophyll and the corresponding sulfonato derivative.^{20,21}

The reduced τ_S and Φ_f values for **(NC)₂BC-Pd** (like other palladium tetrapyrroles) derives from heavy-metal (and perhaps d-orbital) enhancement of singlet-to-triplet intersystem-crossing, which in turn makes the latter process virtually quantitative ($\Phi_T = 0.99$). The yield of intersystem crossing (i.e., the triplet yield) for **(NC)₂BC-Pd** can be compared with 0.63 for **(NC)₂BC-Zn** and 0.43 for **(NC)₂BC** (Table 1). The Φ_T value for **BC** (0.62) is greater than that for **(NC)₂BC**, reflecting the effect of the cyano-groups to draw electron density from the macrocycle and thereby diminish spin-orbit coupling, which underlies the intersystem-crossing process. The Φ_T values obtained here for the dicyanobacteriochlorins are consistent with the results of prior studies on synthetic bacteriochlorins, which give average yields of ~ 0.5 for free base bacteriochlorins, ~ 0.7 for zinc chelates, ~ 0.8 for indium chelates, and ~ 1 for palladium chelates.^{11-13,16,19} Essentially quantitative intersystem crossing is also found for palladium-substituted bacteriochlorophyll and derivatives thereof.^{20,21} These values for bacteriochlorins can be compared with the typical triplet yields of 0.7–0.8, 0.8–0.9 and 0.9–1 for free base, zinc, and palladium porphyrins such as tetraphenylporphyrins and imidazolium porphyrins.^{9,22}

These comparisons show that one can expect a maximal enhancement factor in triplet yield of ~1.5 for porphyrins and ~2 for bacteriochlorins upon changing the metalation state (i.e., palladium versus free base). The data in Table 1 indicate that PDT activity, as judged by LD50 or related measures that account for uptake, show variations in activity of one or two orders of magnitude. Although heavy metal (e.g., palladium) substitution may not give a significant gain in PDT efficacy due to an increased triplet yield, activity could be enhanced via accompanying changes in more critical characteristics, such as ground- and excited-state redox properties, shorter T_1 lifetimes, and altered axial ligation, as discussed previously⁹ and below.

Phosphorescence spectra and Triplet excited-state energies

Figure 2 shows an emission scan for **(NC)₂BC-Pd** in deoxygenated THF at room temperature; the scan was collected using a detection system with extended NIR sensitivity. The spectrum shows fluorescence (747 nm) close in position to that found in toluene (753 nm; Figure 1B) as well as weak phosphorescence at 1122 nm. The phosphorescence is verified as originating from **(NC)₂BC-Pd** using excitation spectra and is completely quenched (as expected) if the solution contains ambient O₂. Phosphorescence was not observed for **(NC)₂BC-Zn** under the same conditions, and is expected to be much weaker.

Because of the rather small number of reports of bacteriochlorin phosphorescence, this emission was also measured for two other recently synthesized palladium chelates (**B9** and **B87**) for which the other photophysical properties have been obtained recently.¹⁹ The structures of these palladium bacteriochlorins and their zinc and free base analogues are shown in Chart 5. The phosphorescence, verified by excitation spectra, occurs at 1114 nm for **B9** and 1118 nm for **B87**, similar to 1122 nm for **(NC)₂BC-Pd**. Each wavelength corresponds to a triplet excited-

state (T_1) energy of 1.11 eV. The latter value is lower than that of the singlet excited state (S_1) for the three bacteriochlorins by 0.56, 0.52 and 0.54 eV, respectively.

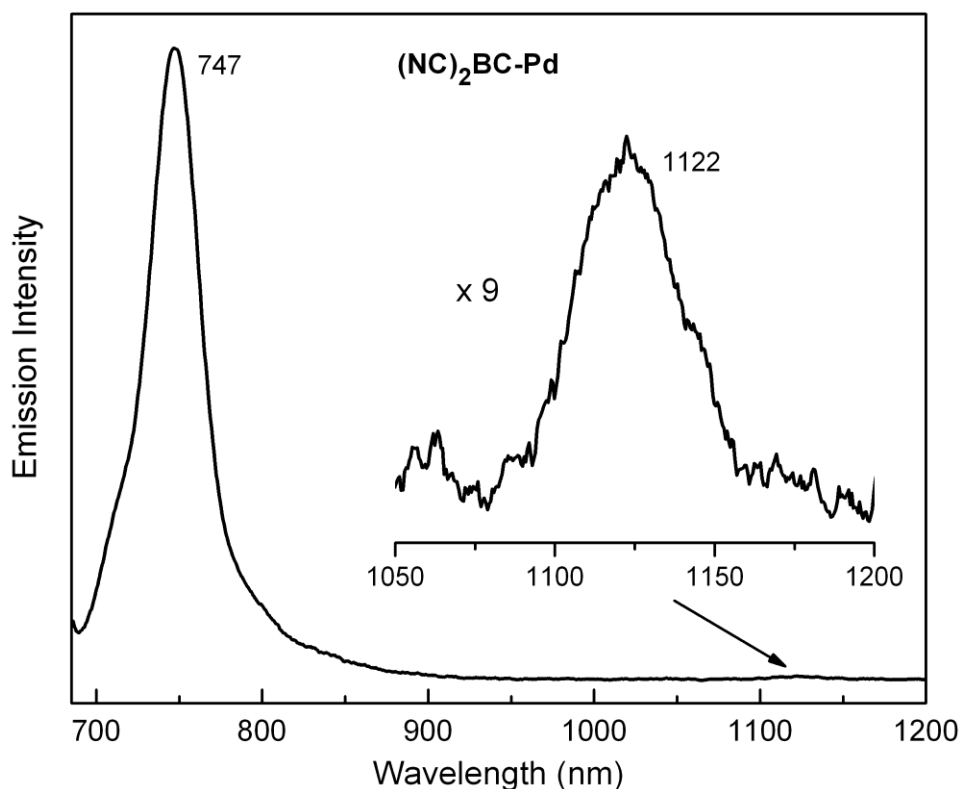


Figure 2. Emission spectrum of $(NC)_2BC-Pd$ in 2-methyltetrahydrofuran. The band at 747 nm is fluorescence and the band at 1122 nm is phosphorescence. The spectra were acquired using excitation in the Soret band (374 nm). The phosphorescence was also observed using excitation in the Q_y band (740 nm).

The above-noted phosphorescence wavelengths, T_1 energies and S_1-T_1 energy gaps for the three synthetic palladium bacteriochlorins are within the span of most reported values. The compounds include bacteriochlorophyll (BChl) and its zinc- and palladium-substituted analogues (1170–1221 nm, 1.01–1.06 eV; 0.56–0.58 eV), the free base analogue bacteriopheophytin (1097 nm; 1.13 eV; 0.50 eV), zinc tetraphenylbacteriochlorin (1157 nm; 1.07 eV; 0.57 eV), and free base tetraphenylbacteriochlorin (1053 nm; 1.17 eV; 0.50 eV) (23,24). Similar T_1 energies (1.15

and 1.22 eV) have been determined for two chlorinated tetrasulfonatophenylbacteriochlorins using photoacoustic spectroscopy.²⁵ The T_1 energies for the latter two compounds could be slightly lower than reported because the analysis assumed that internal conversion is effectively zero (i.e., $\Phi_f + \Phi_T = 1$) whereas recent results on a large group of free base bacteriochlorins indicate that this nonradiative pathway typically has at least twice the quantum yield as fluorescence.¹⁶ The triplet energy of 1.30 eV for free base tetraphenylbacteriochlorin²² is modestly higher than the above-noted phosphorescence energy of 1.17 eV.²⁴ Elucidation of triplet excited-state energies is important for deducing excited-state redox potentials and assessing PDT mechanisms as discussed recently^{22,25} and below.

Triplet excited-state lifetimes

The lifetime of the lowest triplet excited state (τ_T) in deoxygenated solution is in the range 80–170 μs for **BC**, **(NC)₂BC**, and **(NC)₂BC-Zn** but is dramatically reduced to 7 μs for **(NC)₂BC-Pd** (Table 1). Similar triplet lifetimes (3–10 μs) have been reported for other synthetic palladium bacteriochlorins¹⁹ and for palladium-substituted bacteriochlorophylls.^{20,21} The shorter lifetimes of the palladium versus zinc or free base bacteriochlorins can be attributed to heavy-atom enhancement of both triplet excited-state decay pathways (phosphorescence emission and non-radiative intersystem crossing). The triplet lifetime is reduced to <1 μs for each of the bacteriochlorins in the presence of ambient O_2 , consistent with the added contribution of the energy/electron-transfer processes that underlie the formation of the reactive oxygen species for PDT.

The results of the present study of metal-containing dicyanobacteriochlorins along with the findings in our prior studies of free base bacteriochlorins^{5–7} and imidazole-substituted

porphyrins^{9,10} show no clear correlation between triplet lifetime and PDT activity (Table 1). In fact, a seemingly counterintuitive result is that of the three dicyanobacteriochlorins, the photosensitizer with the shortest triplet lifetime (7 μ s), **(NC)₂BC-Pd**, has the highest activity. The same is true concerning imidazole-substituted porphyrins **2-Pd** (~10 μ s) versus **2-Zn** (~6 ms) studied previously.^{9,10} The synthetic palladium tetrapyrroles, like native bacteriochlorophyll-derived **WST9** (Tookad) and **WST11**, apparently have such favorable general characteristics (e.g., uptake/distribution, reactive oxygen species production) that a triplet lifetime of ≤ 10 μ s allows sufficient encounters with O₂ to attain high PDT activity.²² A possible advantage to such short triplet lifetimes in reducing photobleaching is described below.

Photostability

The photostability properties of the four bacteriochlorins under study [**BC**, **(NC)₂BC**, **(NC)₂BC-Zn**, **(NC)₂BC-Pd**] (Chart 4) were measured, as were those of representative synthetic bacteriochlorins whose PDT activity was investigated previously (**B16**, **B17**, **B19**, **B22**, **B29**, **B31**; Chart 2).⁵⁻⁷ The photostability properties of several standard PDT agents (Lutex, Photofrin, benzoporphyrin derivative BPD)²⁶ were also examined. Each compound was studied in multiple media [e.g., toluene, DMA, dimethylsulfoxide (DMSO), methanol (MeOH), ethanol (EtOH), acetonitrile (MeCN), CrEL] both in the presence and absence of ambient O₂. The absorbance spectrum (350–900 nm) was monitored as a function of incident light fluence (up to 100 J/cm²) in the Q_y(0,0) band, and in most cases the fluorescence spectrum was followed as well. In each case, the fraction of the initial peak Q_y(0,0) absorbance as a function of light fluence was plotted. Table 1 gives the value at 100 J/cm² for a number of bacteriochlorins in DMA and CrEL in the

presence of ambient O₂ and CrEL in the absence of O₂. Representative spectra and plots are shown in Figures 3–6.

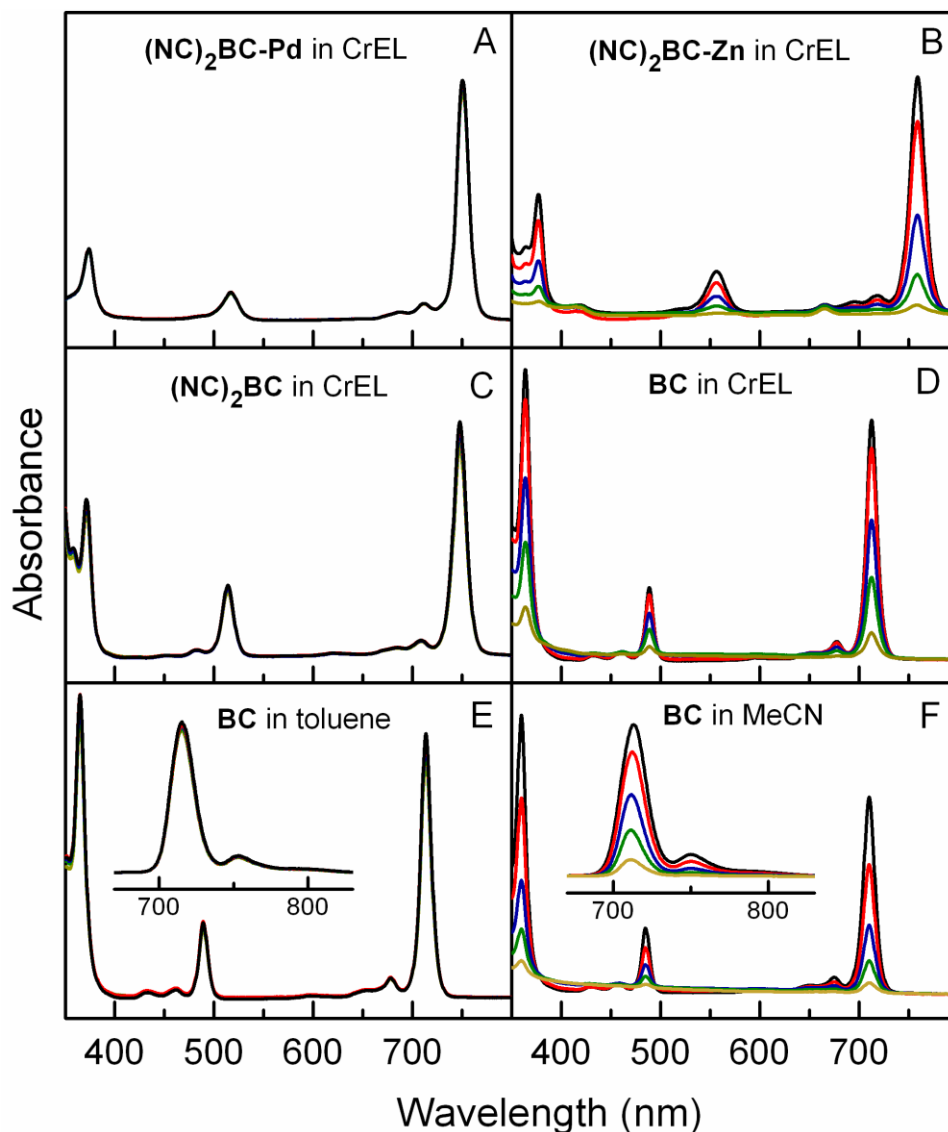


Figure 3. Photobleaching studies showing the absorption spectrum of bacteriochlorins in media containing ambient O₂ as a function of the fluence of the light delivered at the Q_y maximum (720–750 nm). The following fluences (J/cm²) are shown in each panel: 0 (black), 5 (red), 25 (blue), 50 (green) and 100 (dark yellow). The insets to panels E and F show the corresponding fluorescence spectra elicited by excitation in the Q_x band (480–530 nm) for the same fluences used during acquisition of the absorption spectra.

Photobleaching is defined operationally as loss of absorption of the bacteriochlorin in the entire near-UV-to-NIR spectral region. Photobleaching can stem from a variety of sources, including reduction, oxidation, aggregation, or chemical reaction, which are referred to as photoreduction, photooxidation, photoaggregation, and photodegradation, respectively. Photoreduction and photooxidation may in part be reversed (by electron transfer with a species in the environment), as can photoaggregation (by dissociation), whereas photodegradation is typically irreversible. One photodegradation pathway entails [2 + 2] cycloaddition of the ground-state bacteriochlorin with singlet oxygen (formed by energy transfer from the triplet excited-state bacteriochlorin) followed by ring opening to give a bilin species.

One of the goals with the dicyanobacteriochlorins (Chart 4)¹¹ was to improve photostability compared to the previously studied synthetic bacteriochlorins. The results bear out the success of that endeavor. The spectra in Figures 3A and 3C, the plots in Figures 4A, and the values in Table 1 show that **(NC)₂BC-Pd** and **(NC)₂BC** in the presence of ambient O₂ are extremely stable. The solutions retain ≥90% of the NIR absorbance in CrEL and ≥83% in DMA after exposure to 100 J/cm² of NIR light. In contrast, the previously studied bacteriochlorins **B16**, **B17**, **B22**, **B29**, and **B31**, as well as the parent unsubstituted compound **BC** in the same media, have ≤20% absorbance remaining after illumination with 100 J/cm² (in some cases at ≤50 J/cm²) in the presence of ambient O₂ and 50–80% after removal of O₂ (Figures 3 and 4 and Table 1). Thus, for CrEL and DMA solutions, **(NC)₂BC-Pd** and **(NC)₂BC** in the presence of ambient O₂ are more photostable than the other bacteriochlorins even after stability has been markedly improved by the removal of O₂ (Figure 4). Bacteriochlorins **(NC)₂BC-Pd** and **(NC)₂BC** are also modestly more stable than common PDT agents²⁶ Photofrin and Lutex and considerably more stable than benzoporphyrin derivative (BPD) (Figures 4A and 4F).

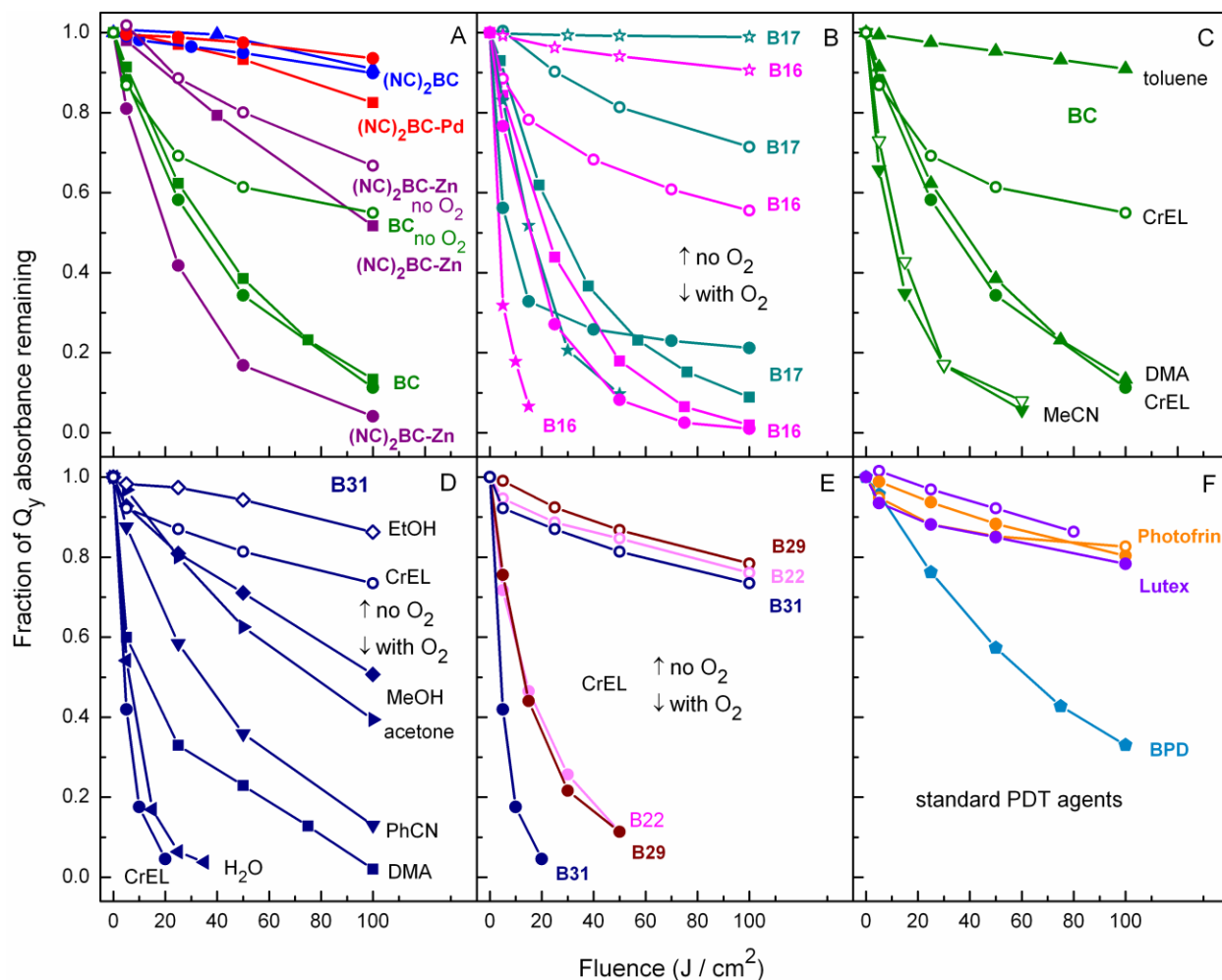


Figure 4. Photostability of bacteriochlorins and standard PDT agents in various media in the presence (closed symbols) or absence (open symbols) of atmospheric O_2 . The absorbance at the maximum of the NIR $Q_y(0,0)$ absorption band (720–750 nm) relative to that prior to illumination is plotted as a function of the fluence of incident light in that band. The panels are organized as follows: (A) unsubstituted and dicyanobacteriochlorins in CrEL and DMA, (B) **B16** and **B17** in CrEL, DMA and DMSO, (C) **BC** in various media, (D) **B31** in various media, (E) **B22**, **B29** and **B31** in CrEL, (F) standard PDT agents. The data for the bacteriochlorins are colorized as follows: $(NC)_2BC$ -Pd (red), $(NC)_2BC$ -Zn (purple), $(NC)_2BC$ (blue), **BC** (green), **B16** (magenta), **B17** (dark cyan), **B22** (light magenta), **B29** (wine), **B31** (navy blue). The data for the standard PDT agents are colorized as follows: Photofrin (orange), Lutex (violet), benzporphyrin derivative (BPD, sky blue). The symbols for the media are as follows: CrEL (circles), *N,N*-dimethylacetamide (DMA, squares), dimethylsulfoxide (DMSO, stars), acetonitrile (MeCN, down triangles), MeCN/ H_2O = 50/50 (pentagons), ethanol (EtOH, diamonds), methanol (MeOH, diamonds), toluene (up triangles), acetone (right triangles), benzonitrile (PhCN, down triangles), H_2O (left triangles).

The zinc chelate **(NC)₂BC-Zn** in DMA and CrEL both in the presence and absence of O₂ is less photostable than **(NC)₂BC-Pd** and **(NC)₂BC** in these media containing O₂ (Figure 3B and 4A). **(NC)₂BC-Zn** has comparable stability to the previously studied bacteriochlorins and **BC** in CrEL (with or without O₂) but is typically more stable in DMA (Table 1). In effect, the incorporation of a zinc ion counteracts the photostability enhancement obtained upon incorporation of the dicyano-groups; in contrast, a palladium ion can have a synergistic effect. These findings can be understood in terms of the redox properties of the chromophores, as described below. Collectively, the results show that the incorporation of (electron-withdrawing) cyano groups at the 3,13-positions, along with the appropriate choice of metalation state, provide an excellent design for improving photostability of bacteriochlorin photosensitizers. Chlorine atoms, which also are electron-withdrawing, have been incorporated at the *ortho*-positions of the aryl rings in synthetic *meso*-tetraarylbacteriochlorins to improve photostability (Chart 1).^{27,28}

Prior studies of the photodegradation of bacteriochlorophyll *a* and derivatives show that the process is highly solvent dependent and requires O₂. Typical photoproducts include chlorins such as 2-acetylchlorophyll *a* and other derivatives formed by two-electron oxidation of the macrocycle, bilin-like open-chain tetrapyrroles likely formed via addition of singlet oxygen and ring opening, and other species that have no featured absorption in the visible region.^{21,29} The geminal dimethyl groups in the synthetic bacteriochlorins are incorporated to avoid dehydrogenation to form chlorins and porphyrins^{2,3}, which when observed are produced in such low yield that the expected features are cleanly resolved only via fluorescence. Bacteriochlorin **B16** in DMA with ambient O₂ after prolonged illumination gives such an example, showing a weak fluorescence feature at ~640 nm (Figure 6C, inset) with no corresponding sharp feature in the absorption spectrum (Figure 6A). This example also reveals broad weak absorption and

fluorescence-centered features around 600 nm that could represent open-chain tetrapyrrolic photoproducts.

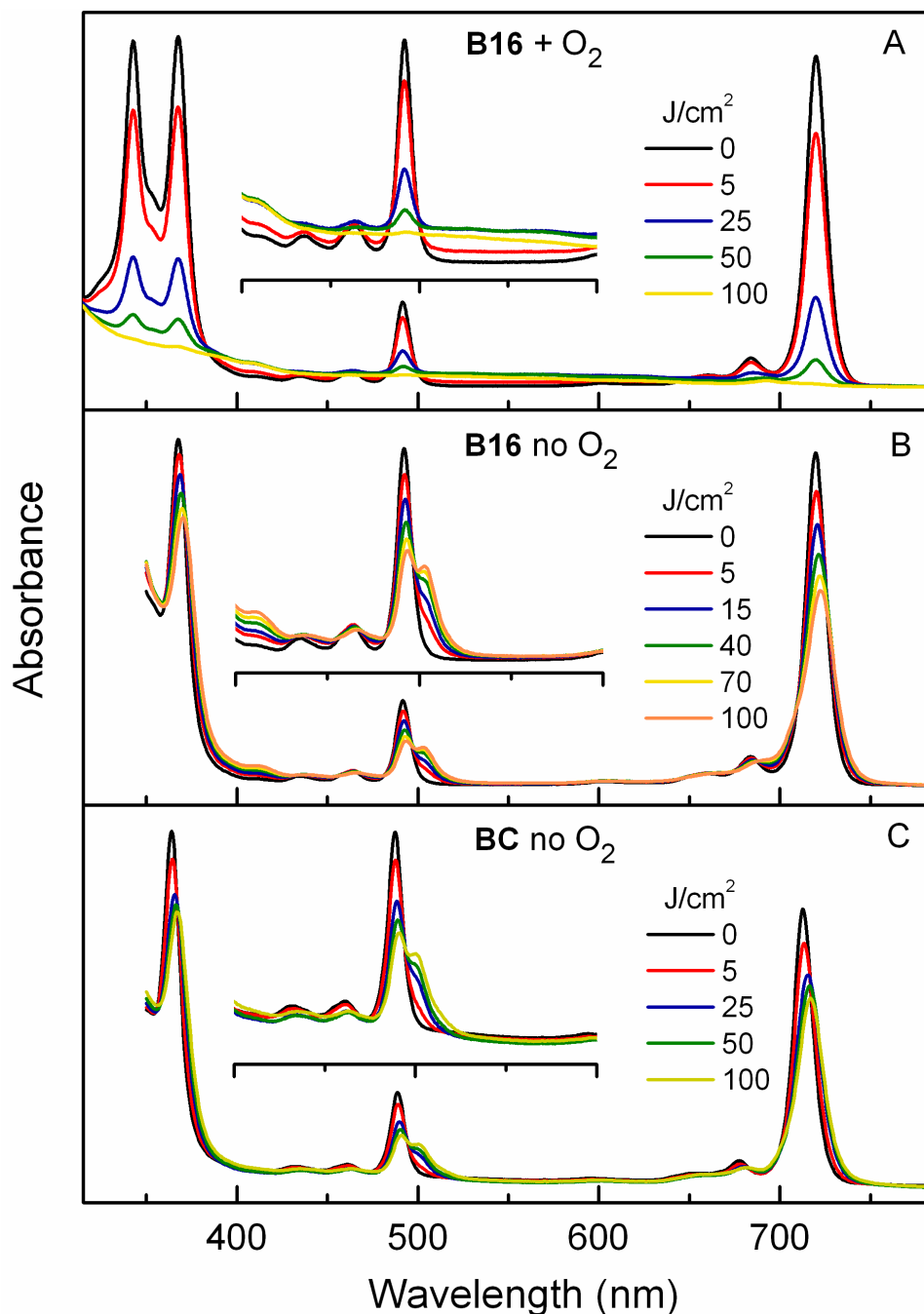


Figure 5. Photobleaching studies in aqueous micellar solutions (CrEL) of **B16** with ambient O₂ (A), **B16** with no O₂ (B), and **BC** with no O₂ (C) showing the absorption spectrum as a function of light fluence (J/cm^2) in the Q_y band (~720 nm). The insets to each panel show expanded views of the 400–600 nm region. The absorbance scale is 0–0.8 in each panel.

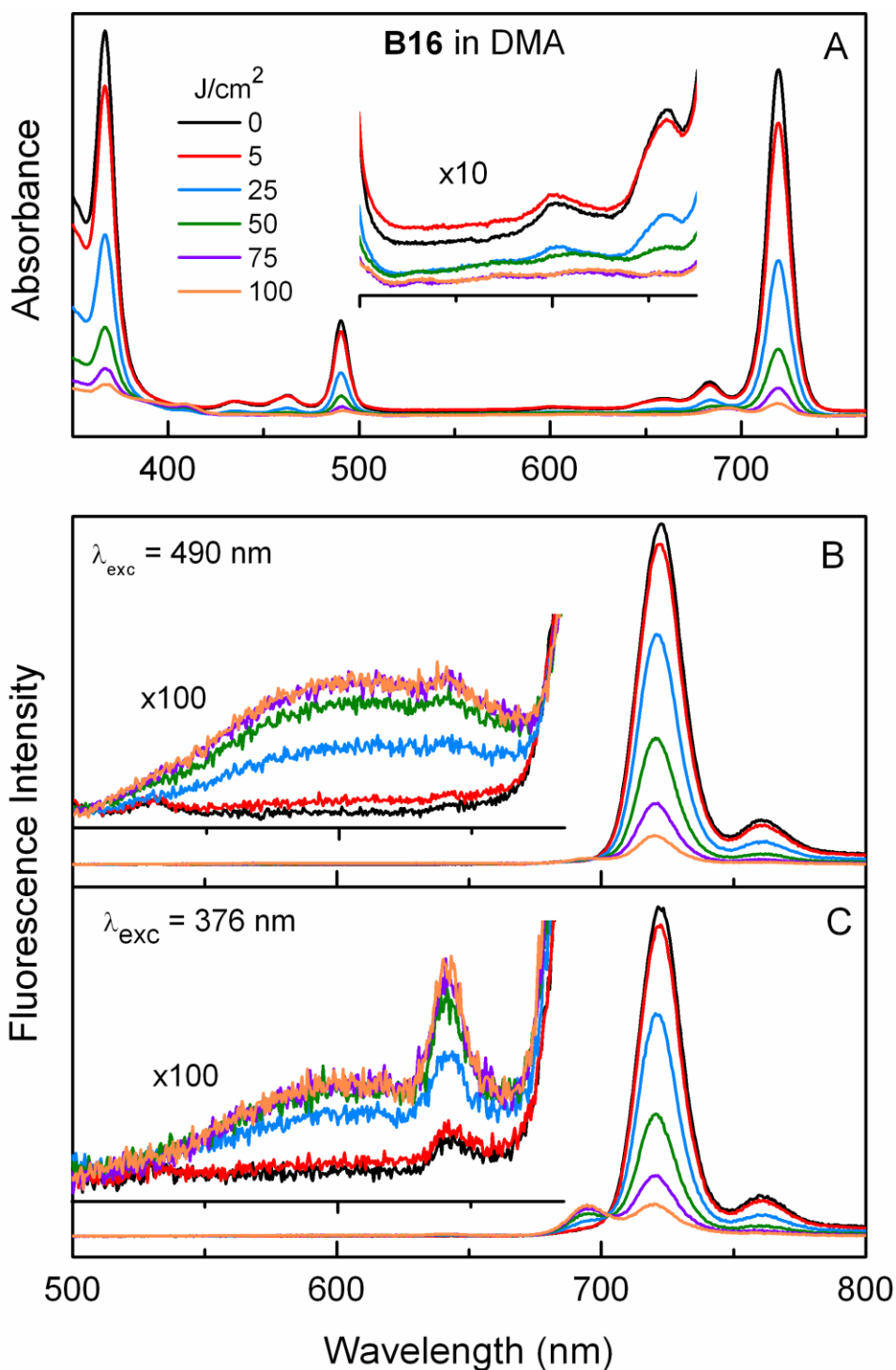


Figure 6. Photobleaching studies of **B16** in *N,N*-dimethylacetamide (DMA) with ambient O₂ showing the absorption spectra (A) and fluorescence spectra using excitation at the 490-nm Q_x-band maximum (B) or at 376 nm on the long-wavelength side of the Soret band (C) as a function of light fluence (J/cm^2) in the Q_y band (720 nm): 0 (black), 5 (red), 25 (blue), 50 (green), 75 (purple) and 100 (dark yellow). The insets to each panel show expanded views of certain regions of each spectrum. The absorbance scale is 0–0.6 in panel (A).

Generally the photobleaching of the synthetic bacteriochlorins (bearing geminal dimethyl groups) is evidenced by decrease in the entire near-UV-to-NIR absorption spectrum along with a similar disappearance of fluorescence. The diminution of the absorption profile is often accompanied by an apparent increase in the baseline, particularly at wavelengths shorter than 500 nm and increasing toward the near-UV region. This behavior is illustrated by the absorption spectra for **(NC)₂BC-Zn**, **BC**, and **B16** in CrEL with ambient O₂ obtained after 100 J/cm² illumination (Figures 3B, 3D, and 5A; dark yellow). The featureless spectral profiles could reflect formation of nondescript photoproducts analogous to those for bacteriochlorophyll *a*²⁹ or light scattering due to photoaggregation. The analogous profiles for **B16** and **BC** in CrEL in the absence of O₂ (Figures 5B and 5C) show Soret, Q_x and Q_y features that are decreased in intensity, broadened, and bathochromically shifted after prolonged illumination. This behavior could reflect the formation of small aggregates (possibly as small as dimers) that are partially soluble and remain suspended in the micellar environment. The ability of CrEL to reduce aggregation or aid disaggregation underlies the motivation for its use as a delivery vehicle for the bacteriochlorins.^{6,11} Aggregates may play a positive role in PDT by serving as reservoirs to provide fresh photosensitizer in place of those that have undergone irreversible photodegradation.²⁹

A relationship between photobleaching and the solubilization characteristics of the bacteriochlorin in a given medium is illustrated by the behavior of unsubstituted bacteriochlorin **BC** in several media in the presence of ambient O₂ (Figures 3D, 3E, 3F, and 4C). The photostability is poor in the CrEL (as noted above), MeCN and DMA but excellent in toluene, where 93% of the absorbance remains after 100 J/cm² illumination. Thus, in the (nonpolar) medium in which it is expected to be the most soluble, the highly nonpolar bacteriochlorin **BC**

shows photostability that rivals that of dicyanobacteriochlorins **(NC)₂BC-Pd** and **(NC)₂BC** (Figures 3A, 3C, 3E and 4). Solubility characteristics may also contribute to the marked medium dependence of photobleaching of the charged bacteriochlorin **B31** (Chart 2 and Figure 4E). Solvent polarity can also impact photooxidation contributions to photobleaching via the concentration of ambient O₂ in the medium and stabilization of electron-transfer products. Collectively, these results and considerations suggest that the photostability of a photosensitizer may be much different in organic solvents, delivery media, and the cellular milieu.

A contribution of a photoaggregation mechanism to the observed photobleaching could occur by several pathways. One pathway is an extension of excimer formation³⁰ whereby a bacteriochlorin in the T₁ state associates with another bacteriochlorin in the ground state and so on to associate more chromophores. Such a pathway raises the possibility that photobleaching could be reduced for photosensitizers that have shorter T₁ lifetimes (such as palladium tetrapyrroles) and thus provide less time for such diffusional encounters. A second pathway would involve electron transfer from a bacteriochlorin in the T₁ excited state to O₂ (or another electron acceptor) to form the bacteriochlorin π -cation radical. Interaction of the latter species with a ground-state bacteriochlorin would form a dimeric complex, analogous to formation of the monocation dimer of magnesium octaethylporphyrin³¹, and so on to associate more chromophores. Dimer (and aggregate) formation would be enhanced because the monomer cation radical has a half-filled HOMO and thus the bonding orbital of the interacting chromophore pair would be filled and the higher energy antibonding orbital would be half-filled (or empty), thereby giving a net bonding interaction that would not occur for two neutral species (where both orbitals are filled). The bacteriochlorin π -cation radical in the latter mechanism is

presumably an intermediate in more common photooxidation pathways for degradation (e.g., to form chlorins). Thus, it is possible that multiple photobleaching pathways may be intertwined.

Electrochemical and Molecular-orbital characteristics of the dicyanobacteriochlorins

The first oxidation potential (E_{ox}) and first reduction potential (E_{red}) of the four bacteriochlorins [**BC**, **(NC)₂BC**, **(NC)₂BC-Zn**, **(NC)₂BC-Pd**] were measured and are listed in Table 3. The table also gives the energy of the highest occupied molecular orbital (E_{HOMO}) and the lowest unoccupied molecular orbital (E_{LUMO}) obtained from DFT calculations for each photosensitizer. Electron densities (and energies) of the four frontier molecular orbitals for each of these four bacteriochlorins are shown in Figure 7. Studies of a large number of chlorins have shown essentially linear relationships between E_{ox} and E_{HOMO} and between E_{red} and E_{LUMO} .³² As E_{ox} becomes more positive, E_{HOMO} becomes more negative, and the molecule is harder to oxidize. As E_{red} becomes less negative, E_{LUMO} becomes more negative, and the molecule is easier to reduce. For comparison Table 3 also lists redox and MO data for two other sets of free base, zinc and palladium bacteriochlorins investigated recently.¹⁹ The Table also gives data acquired here or previously⁹ for imidazole-substituted porphyrins and tetraphenylporphyrins.

Incorporation of the two cyano groups of **(NC)₂BC** make the molecule harder to oxidize than **BC** ($E_{\text{ox}} = 0.60$ versus 0.09 V; $E_{\text{HOMO}} = -5.22$ versus -4.45 V). Similarly, the two cyano groups of **(NC)₂BC** make the molecule easier to reduce than **BC** ($E_{\text{red}} = -1.10$ versus -1.67 V; $E_{\text{LUMO}} = -3.10$ versus -2.20 V). Compared to **(NC)₂BC**, zinc chelate **(NC)₂BC-Zn** is significantly easier to oxidize (+29 mV) and only slightly harder to reduce (+4 mV); these redox-potential shifts are in concert with the relative magnitudes and signs (to less negative values) of the energy shifts in the HOMO (+15 meV) and LUMO (+3 meV). Compared to **(NC)₂BC**,

palladium chelate **(NC)₂BC-Pd** is slightly easier to oxidize (+8 mV) and also slightly easier to reduce (+7 mV); the former tracks the small shift to less negative HOMO energy (+6 meV) whereas the latter is not paralleled by the virtually unchanged LUMO energy (-1 meV). In summary, the data in Table 3 show that of the three dicyanobacteriochlorins, **(NC)₂BC-Zn** is the easiest to oxidize (although it is harder to oxidize than **BC**) and **(NC)₂BC-Pd** is the easiest to reduce (and is also easier to reduce than **BC**).

Figure 8A plots the orbital energies (Table 3) versus the cell-killing LD50 values (Table 1) for the bacteriochlorins obtained using direct dilution into the complete culture medium. A qualitatively similar plot is obtained using the LD50 values when the bacteriochlorins were first encapsulated in micelles upon treatment with CrEL before dilution into the complete culture medium. Figure 8B plots the redox potentials of the T₁ excited state versus LD50 values. The excited-state redox potentials are obtained from the ground-state redox potentials and the T₁ energies (Table 3). The correlations with LD50 are discussed below.

Table 3. Spectral, state-energy, redox, and molecular-orbital properties of the bacteriochlorins.^a

Compound	Q _y ^b	Q _y ^c	T ₁	S ₁ ^d	T ₁ ^e	S ₁ -T ₁	S ₀		T ₁		Orbital ^h	
	abs	flu	phos	energy	energy	energy	Redox ^f Potentials		Redox ^g Potentials		Energy	
	(nm)	(nm)	(nm)	(eV)	(eV)	(eV)	E _{ox} (V)	E _{red} (V)	T ₁ E _{ox} (V)	T ₁ E _{red} (V)	HOMO (eV)	LUMO (eV)
<i>DicyanoBC set</i>												
BC	713	716		1.74	1.20		+0.09	-1.67	-1.11	-0.47	-4.45	-2.20
(NC)₂BC	748	752		1.65	1.11		+0.60	-1.10	-0.51	+0.01	-5.22	-3.10
(NC)₂BC-Zn	761	763		1.63	1.09		+0.31	-1.14	-0.78	-0.05	-5.08	-3.07
(NC)₂BC-Pd	751	753	1122	1.65	1.11	0.54	+0.52	-1.03	-0.59	+0.08	-5.16	-3.11
<i>Other FbBCs</i>												
B16	717	722		1.71							-4.36	-2.12
B17	731	737		1.68							-4.46	-2.28
<i>Ref BC-T set</i>												
B1 (Fb)	736	742		1.68	1.12		+0.21	-1.49	-0.91	-0.37	-4.40	-2.22
B4 (Zn)	749	756		1.65	1.09		-0.04	-1.60	-1.13	-0.51	-4.26	-2.20
B9 (Pd)	739	745	1114	1.67	1.11	0.56	+0.43	-1.14	-0.68	-0.03	-4.36	-2.26
<i>Ref BC-MME set</i>												
B88 (Fb)	758	765		1.63	1.11		+0.38	-1.29	-0.73	-0.18	-4.65	-2.48
B84 (Zn)	773	780		1.60	1.08		+0.08	-1.41	-1.00	-0.33	-4.55	-2.51

B87 (Pd)	758	765	1118	1.63	1.11	0.52	+0.29	-1.29	-0.82	-0.18	-4.63	-2.54
<i>Imidazole porphyrins</i>												
1-Zn	576	579	738	2.14	1.68	0.47					-4.97	-2.35
2-Zn	576	579	738	2.14	1.68	0.46	+0.36	-1.39	-1.32	+0.29	-5.72 ⁱ	-2.81 ⁱ
2-Pd	547	550	672	2.25	1.84	0.42					-5.81 ^j	-2.83 ^j
<i>Ref porphyrins</i>												
FbTPP	647	650		1.91	1.47 ^k	0.44	+0.83	-1.45	-0.64	+0.02	-4.90	-2.20
ZnTPP	588	599	784	2.08	1.58	0.51	+0.56	-1.58	-1.02	0	-4.96	-2.12
PdTPP	553	560	696	2.21	1.78	0.45	+0.82	-1.61	-0.96	+0.17	-5.36	-2.42

^aProperties of bacteriochlorins. All measured quantities were obtained at room temperature. ^bPeak wavelength of the Q_y(0,0) absorption band in toluene. ^cPeak wavelength of the Q_y(0,0) fluorescence band in toluene. ^dEnergy of the S₁ excited state calculated from the average energy positions of the Q_y(0,0) absorption and fluorescence bands in the prior two columns. ^eEnergy of the T₁ excited state determined by phosphorescence for values indicated in normal font. The values in italics for the free base and zinc bacteriochlorins were obtained from the S₁ energy by assuming the same S₁-T₁ energy gap as in the palladium analogue. ^fGround-state redox potentials measured in butyronitrile/0.1 M *n*-BuN₄PF₆ versus FeCp₂/FeCp₂⁺ = +0.19 V. ^gRedox potentials for the T₁ excited state calculated from the ground state redox potentials and the T₁ energy. ^hFrontier molecular orbital energies from DFT calculations obtained using the 6-31G* basis set except for **(NC)₂BC-Pd**, for which the LACVP basis set was used. For **PdTPP** and **ZnTPP** the values listed are for the C₂ symmetry structures, which are slightly lower in energy than the C₄ symmetry structures. ⁱThe HOMO and LUMO energies listed for **2-Zn** were calculated using the actual iodide counterion; for comparison, the values calculated using a chloride counterion are -5.58 and -2.67 eV, respectively. ^jThe HOMO and LUMO energies listed for **2-Pd** were calculated using the actual iodide counterion; for comparison, the values calculated using a chloride counterion are -5.67 and -2.68 eV, respectively. ^kFrom refs (22) and (34).

Excited-state redox properties and Reactive oxygen species production

Until recently it has been generally accepted that singlet oxygen (formed by energy transfer; i.e., Type-2 photochemistry) is the major mediator of toxicity in PDT. Studies have now shown that hydroxyl radicals, superoxide and other species formed by electron transfer (Type-1 photochemistry) also play an important role in PDT activity depending on the photosensitizer and specific disease or cell type. The palladium analogues of bacteriochlorophyll *a* (**WST9** and **WST11**; Chart 1) produce superoxide and hydroxyl radicals.^{20,21,33} Synthetic free base *meso*-tetraaryl bacteriochlorins (particularly halogenated sulfonamide analogues; Chart 1) also produce superoxide and hydroxyl radicals as well as the Type-2 product singlet oxygen.^{25,27} It has been suggested that the latter bacteriochlorins may be expected to produce both Type-1 and Type-2 photoproducts whereas porphyrins give significantly less electron-transfer (Type-1) products because porphyrins are harder to oxidize than bacteriochlorins.^{22,25}

The diverse free base synthetic bacteriochlorins shown in Chart 2 and free base and metal-containing dicyanobacteriochlorins (Chart 4) that are the subject of the present study also produce hydroxyl radicals as well as singlet oxygen.^{5,6,7,11} As noted above, the most active dicyanobacteriochlorin (**(NC)₂BC-Pd**) and the second most active analogue (**(NC)₂BC**) give a higher ratio of hydroxyl radicals versus singlet oxygen upon illumination, whereas the reverse is true for (**(NC)₂BC-Zn**) and **BC**. Indeed, (**(NC)₂BC-Pd**) has greater PDT efficacy and a much greater propensity to produce hydroxyl radicals than (**(NC)₂BC-Zn**). In a prior study of imidazole-substituted metalloporphyrins (Chart 3), the palladium chelate (**2-Pd**) was similarly found to have greater PDT activity and produce much more hydroxyl radicals than the zinc analogue (**2-Zn**).¹⁰

The parallelism in relative photoactivity and hydroxyl-radical formation for the palladium versus zinc chelates of the dicyanobacteriochlorins and imidazole-substituted porphyrins gives insights into fundamental mechanistic issues. In particular, the palladium chelates of both the dicyanobacteriochlorins and porphyrins are found (or expected) to be harder to oxidize and easier to reduce than the zinc chelates (both in the ground state and the T_1 states). These findings together with general comparisons of the excited-state redox properties of bacteriochlorins versus porphyrins, and the effects of the dicyano substituents of the bacteriochlorins on photoactivity (and photostability), must be considered collectively in assessing the mechanisms of production of reactive oxygen species via Type-1 photochemistry (e.g., hydroxyl radical formation) for these tetrapyrroles.

The Type-1 mechanism is virtually always thought to involve photooxidation of the photosensitizer (P) in the T_1 excited state (P^T) by electron transfer to O_2 via Eqn. (1A).



A number of reaction sequences have been considered for the subsequent formation of hydrogen peroxide and hydroxyl radicals from the superoxide ion ($O_2^{-\bullet}$).^{10,20–22,25,33} The one-electron oxidized photosensitizer is then returned to the starting condition by electron transfer from endogenous electron donor (D) [Eqn. (1B)]. The endogenous electron donor has been proposed to be human serum albumin for the palladium bacteriochlorophyll *a* derivatives, where complexes between the two species underlie a proposed photocatalytic role of such photosensitizers via Eqns. (1A) and (1B).²¹ Photosensitizer oxidation mechanisms involving Eqn. (1A) would generally imply that photoactivity should track the T_1 excited-state oxidation

potential of the photosensitizer. Therefore, more potent photosensitizers should be easier to oxidize in the T₁ excited state than less efficacious compounds, all other factors being equal.

An alternative mechanism is photoreduction of the photosensitizer in the T₁ excited state by an endogenous electron donor (D) followed by electron transfer from the photosensitizer anion to O₂, to again produce superoxide ion, via Eqns. (2A) and (2B).



Subsequent dark reactions of superoxide ion leading to hydrogen peroxide and hydroxyl radicals and other reactive oxygen species would proceed just as in the photooxidation mechanism described above [Eqn. (1A)]. Additionally, hydroxyl radicals potentially can be formed more directly from hydrogen peroxide and the reduced photosensitizer produced in Eqn. 2A.¹⁰ The photoreduction mechanism [(Eqns. (2A) plus (2B))] would also give a photocatalytic role for the photosensitizer in an analogous manner (to that noted above via the photooxidation pathway) for human serum albumin (as the electron donor) and palladium bacteriochlorophyll *a* derivatives (as photosensitizer).²¹ Furthermore, ascorbate has been proposed to perform a similar role as a sacrificial electron donor to tetrapyrrole photosensitizers in the P^T state [(Eqn. 2A)] or P^{•+} forms [(Eqn. (1A)).²² Photosensitizer reduction mechanisms involving Eqn. (2A) would generally imply that photoactivity should track the T₁ excited-state reduction potential of the photosensitizer. Therefore, more potent photosensitizers should be easier to reduce in the T₁ excited state than less efficacious compounds, all other factors being equal.

We have considered these two alternative mechanisms (photosensitizer oxidation and reduction) previously in the study of imidazole-substituted palladium versus zinc porphyrins.^{9,10} The photoreduction pathway rather than the photooxidation pathway seems to best explain the findings that porphyrin **2-Pd** produces more hydroxyl radicals and is more efficacious than **2-Zn** (Chart 3). This follows because based on the T_1 energies and ground-state redox potentials for these compounds and **PdTPP** and **ZnTPP** (Table 3 and ref (35)), the **2-Pd** is expected to be ~150 mV easier to reduce and ~50 mV harder to oxidize than **2-Zn** in the T_1 state. Similarly, for the dicyanobacteriochlorins, **(NC)₂BC-Pd** is ~130 mV easier to reduce and ~190 mV harder to oxidize than **(NC)₂BC-Zn** in the T_1 state.

The latter trend can be extended to the entire set of unsubstituted and dicyanobacteriochlorins (Chart 4 and Table 3). The T_1 reduction potential becomes less negative or more positive (the excited bacteriochlorin becomes easier to reduce) in the order **BC** (-0.47 V) > **(NC)₂BC-Zn** (-0.05) > **(NC)₂BC** (0.01) > **(NC)₂BC-Pd** (0.08). The T_1 oxidation potential becomes more negative (the excited bacteriochlorin becomes easier to oxidize) in the order **(NC)₂BC** (-0.51 V) > **(NC)₂BC-Pd** (-0.59 V) > **(NC)₂BC-Zn** (-0.78 V) > **BC** (-1.11 V). Figure 8B shows the excited-state redox potentials versus LD50 (using the direct-dilution medium). A similar plot is obtained using the LD50 values obtained using CrEL delivery. Good correlations are seen for both the T_1 oxidation and reduction potentials, although the implications for activity are, at first glance, reversed. Increasing PDT activity (decreasing LD50) correlates with greater ease of reduction and greater difficulty of oxidation.

The simplest interpretation of the parallel findings for the dicyanobacteriochlorins and imidazole-substituted porphyrins is that the photoreduction of the T_1 excited state contributes significantly to inherent PDT efficacy (i.e., reactive oxygen species production once the

photosensitizer is excited). However, at least two additional factors must be considered as follows.

(1) The absolute (and relative) rates of electron transfer will ultimately depend on the relationship between net free energy change for the excited-state electron-transfer reaction (which depends on the T_1 redox potentials) and the total reorganization energy involving the photosensitizer, O_2 , and the medium. In other words, depending on where electron transfer for a particular photosensitizer is on this curve (i.e., the Marcus plot), an increase in the free-energy driving force for the process (via a change in redox potentials or T_1 energy) could either increase or decrease the rate of the reaction. The standard considerations given above consider that a greater magnitude of the free energy change implies an increased rate and yield of electron transfer.

(2) The overall PDT activity via the Type-1 mechanism may not be dictated by the rates and yields of electron transfer (or the Type-2 contribution by the rates and yields of energy transfer) if the limiting factor is photostability. In this regard, it is normally thought that photoactivity proceeds via photooxidation [Eqn. (1A)] and most electron-transfer routes to photobleaching proceed via a similar mechanism. In particular, for a bacteriochlorin the excited-state oxidation process in Eqn. (1A) involves one-electron oxidation of the macrocycle to form the π -cation radical, and ultimately formation of a typical chlorin photoproduct by two-electron oxidation.^{21,29} Even if formation of chlorin does not proceed via the bacteriochlorin π -cation radical, the general reasoning seems to be that, within the context of a Type-1 mechanism, both PDT activity and photobleaching proceed via a photooxidation (rather than photoreduction) pathway.

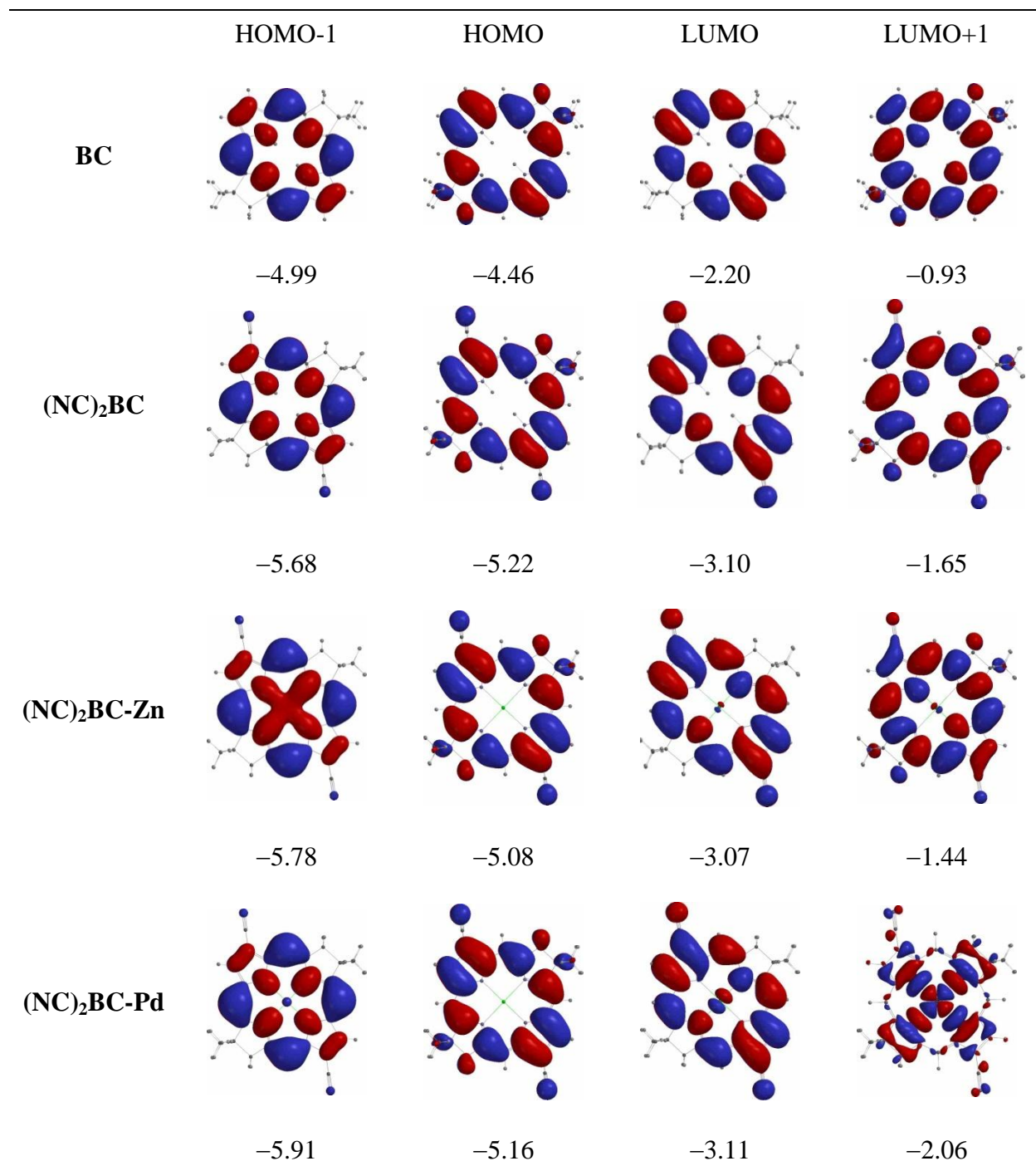


Figure 7. Electron densities and energies of frontier molecular orbitals. The DFT calculations employed basis sets 6-31G* for **BC**, **(NC)₂BC**, and **(NC)₂BC-Zn** and LACVP* for **(NC)₂BC-Pd**. Effectively the same electron densities and the same MO energies (-5.74, -5.09, -3.09, -1.45 eV) were obtained for **(NC)₂BC-Zn** using LACVP*. The LUMO+2 for **(NC)₂BC-Pd** has similar macrocycle electron density and energy (-1.41 eV) as the LUMO+1 for the other molecules.

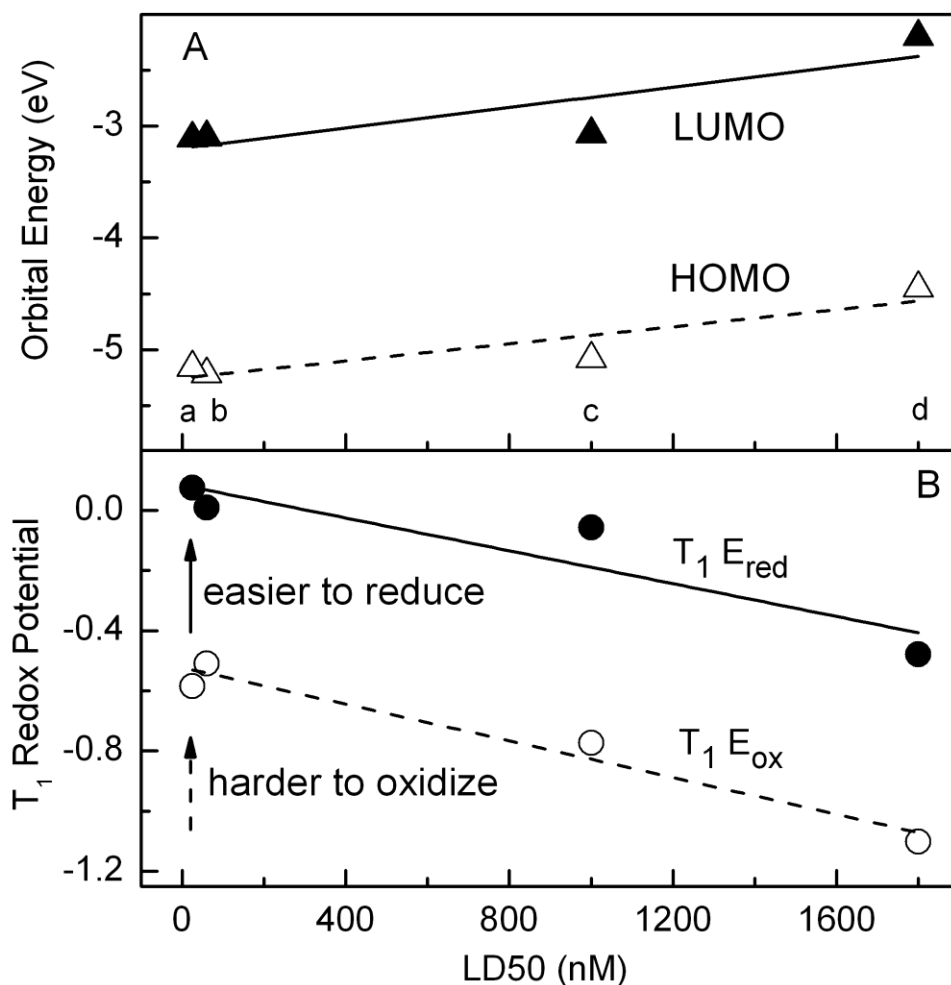


Figure 8. Electronic properties versus cell-killing LD50 value for bacteriochlorins using direct dilution of stock solution into complete culture medium. The data points for increasing LD50 (left to right) reflecting a decrease in photosensitizer activity are $(\text{NC})_2\text{BC-Pd}$ (a) > $(\text{NC})_2\text{BC}$ (b) > $(\text{NC})_2\text{BC-Zn}$ (c) > BC (d). (A) Calculated HOMO energy (open triangles) and LUMO energy (closed triangles). (B) Redox potential of the T₁ excited state (Table 3). The lines in both panels reflect the linear fits to the data.

Electronic tuning of tetrapyrrole photosensitizers for photostability and photoactivity

Ideally, the photoactivity and photostability of a photosensitizer could be independently controlled, at least to some degree. The data in Figure 8 and the reasoning given above suggest that such a situation could in fact contribute to the PDT efficacy of tetrapyrroles. In particular, photoactivity via the Type-1 mechanism could proceed at least in part via transient reduction of

the photosensitizer [Eqn. (2A)] and thus would be enhanced if the photosensitizer is made easier to reduce in the excited state. On the other hand, photobleaching likely proceeds to a significant degree by photooxidation (rather than photoreduction) and photoaggregation (perhaps via the π -cation radical), in addition to photodegradation; thus photostability would be enhanced by making the photosensitizer harder to oxidize. Rendering a tetrapyrrole chromophore harder to oxidize and easier to reduce is, in fact, what generally occurs upon the incorporation of electron-withdrawing substituents or the incorporation of a central metal ion with a high electronegativity (e.g., palladium). Such trends can be seen in the redox properties and the energies of the frontier molecular orbitals (Table 3).^{22,34,35} Furthermore, the strategic choice and placement of substituents allow some control over the relative oxidation and reduction potentials (via HOMO and LUMO energies), as has been shown for synthetic chlorins, bacteriochlorins and related oxophorbines and bacteriooxophorbines that incorporate the keto-bearing five-membered ring of the native photosynthetic chromophores.^{16,19,32,36–38}

The increased photostability engendered by halogenation of the aryl rings of *meso*-tetraaryl bacteriochlorins (e.g., **TDCPBS** in Chart 1) has been noted previously.^{22,25} The more difficult oxidation (and increased photostability) of palladium bacteriochlorophyll *a* derivatives (e.g., **WST9** and **WST11** in Chart 1) than bacteriochlorophyll *a* also has been noted^{20–22,33}, and ascribed in part to the effect of the central palladium ion compared to the native magnesium ion. Additionally the native-like bacteriochlorins bear a 3-acetyl group and the related keto group in the fused five-membered ring spanning the 12- to 15-positions (Chart 1). These groups are basically electron withdrawing in character in that they lower the HOMO and LUMO energies and make the chromophore harder to oxidize and easier to reduce than bacteriochlorins that do not contain such substituents^{16,19,38}, and the same is true of chlorin analogues.^{9,37} Thus, the

photostability of **WST9** and **WST11** is likely provided by effects of both substituents and the electronegative palladium ion to reduce photooxidation.

Again, the effectiveness of these previously studied photosensitizers to produce hydroxyl radicals (or other Type-1 photoproducts) would be diminished compared to compounds that lacked the electron-withdrawing substituents or highly electronegative central metal if the mechanism of that process involves photooxidation [Eqn. (1A)]; however, the activity would be enhanced if there is a contribution from the photoreduction pathway [Eqn. (2A)]. As described above, the same is true of the bacteriochlorins bearing 3,13 substituents that are the focus of the present work and our recent investigation of the PDT efficacy of these photosensitizers.¹¹ On the basis of shifts in MO energy shifts and redox properties obtained upon incorporation of cyano versus acetyl groups at similar positions (Table 3),^{32,36-38} one would expect the combined effects on oxidation potentials [photostability and photoactivity via Eqn. (1A)] and reduction potentials [photoactivity via Eqn. (2A)] to be greater for **(NC)₂BC-Pd** versus the palladium bacteriochlorophyll *a* derivatives **WST9** and **WST11**, all other things being equal. The advantages of **(NC)₂BC-Pd** and related synthetic bacteriochlorins are (1) further enhanced photostability by the use of the geminal dimethyl groups that inhibit formation of chlorin photodegradation products and (2) the availability of macrocycle sites for additional electronic and chemical tuning.

In summary, a combination of favourable electronic effects make the palladium bacteriochlorin **(NC)₂BC-Pd** a photosensitizer with PDT activity (LD50 ~ 25 nM) and photostability that rival or surpass those of synthetic bacteriochlorins that we have studied previously as well as many common PDT agents. The photostability of this compound is enhanced due to diminished photobleaching (via photooxidation, photoaggregation, and

photodegradation), which stem from the effects of the peripheral cyano groups and central palladium ion. The photoactivity of (NC)₂BC-Pd, (NC)₂BC and other tetrapyrrole photosensitizers may derive in part from a contribution of a photoreduction pathway for production of lethal reactive oxygen species such as hydroxyl radicals. Collectively, the fundamental insights gained from the studies described herein may allow the design of bacteriochlorin photosensitizers that have even greater PDT efficacy.

Acknowledgments

This work was supported by grants from the NIH (R01AI050875 to M.R.H.), and the JimmyV NCSU Cancer Therapeutics Training Program. Y.-Y.H. was supported by a grant (R41AI072854) from the National Institute of Allergy and Infectious Diseases to NIRvana Pharmaceuticals, Inc. Characterization of the photophysical, redox and molecular-orbital properties of the bacteriochlorins described herein were initially motivated by solar-energy studies and supported by grants from the Division of Chemical Sciences, Geosciences and Biosciences Division, Office of Basic Energy Sciences of the U.S. Department of Energy to D.F.B. (DE-FG02-05ER15660) and D.H. (DE-FG02-05ER15661).

References

- (A) Yang, E.K.; Ruzié, C.; Krayner, M.; Diers, J.R.; Niedzwiedzki, D.M.; Kirmaier, C.; Lindsey, J.S.; Bocian, D.F.; Holten, D. Photophysical Properties and Electronic Structure of Bacteriochlorin–Chalcones with Extended Near-Infrared Absorption. *Photochem. Photobiol.* 2013. 89. 605-618.
- (1) Agostinis, P., Berg, K., Cengel, K. A., Foster, T. H., Girotti, A. W., Gollnick, S. O., Hahn, S. M., Hamblin, M. R., Juzeniene, A., Kessel, D., Korbelik, M., Moan, J., Mroz, P., Nowis, D., Piette, J., Wilson, B. C. and Golab, J. (2011) Photodynamic therapy of cancer: An update. *CA Cancer J. Clin.* 61, 250–281.
- (2) Kim, H.-J. and Lindsey, J. S. (2005) De novo synthesis of stable tetrahydroporphyrinic macrocycles: Bacteriochlorins and a tetradehydrocorrins. *J. Org. Chem.* 70, 5475–5486.

- (3) Ruzié, C., Krayner, M., Balasubramanian, T. and Lindsey, J. S. (2008) Tailoring a bacteriochlorin building block with cationic, amphipathic, or lipophilic substituents. *J. Org. Chem.* 73, 5806–5820.
- (4) Taniguchi, M., Cramer, D. L., Bhise, A. D., Kee, H. L., Bocian, D. F., Holten, D. and Lindsey, J. S. (2008) Accessing the near-infrared spectral region with stable, synthetic, wavelength-tunable bacteriochlorins. *New J. Chem.* 32, 947–958.
- (5) Mroz, P., Huang, Y.-Y., Szokalska, A., Zhiyentayev, T., Janjua, S., Nifli, A.-P., Sherwood, M. E., Ruzié, C., Borbas, K. E., Fan, D., Krayner, M., Balasubramanian, T., Yang, E., Kee, H. L., Kirmaier, C., Diers, J. R., Bocian, D. F., Holten, D., Lindsey, J. S. and Hamblin, M. R. (2010) Stable synthetic bacteriochlorins overcome the resistance of melanoma to photodynamic therapy. *FASEB J.* 24, 3160–3170.
- (6) Huang, Y.-Y., Mroz, P., Zhiyentayev, T., Sharma, S. K., Balasubramanian, T., Ruzié, C., Krayner, M., Fan, D., Borbas, K. E., Yang, E., Kee, H. L., Kirmaier, C., Diers, J. R., Bocian, D. F., Holten, D., Lindsey, J. S. and Hamblin, M. R. (2010) In vitro photodynamic therapy and quantitative structure-activity relationship studies with stable synthetic near-infrared-absorbing bacteriochlorin photosensitizers. *J. Med. Chem.* 53, 4018–4027.
- (7) Huang, L., Huang, Y.-Y., Mroz, P., Tegos, G. P., Zhiyentayev, T., Sharma, S. K., Lu, Z., Balasubramanian, T., Krayner, M., Ruzié, C., Yang, E., Kee, H. L., Kirmaier, C., Diers, J. R., Bocian, D. F., Holten, D., Lindsey, J. S. and Hamblin, M. R. (2010) Stable synthetic cationic bacteriochlorins as selective antimicrobial photosensitizers. *Antimicrob. Agents Chemother.* 54, 3834–3841.
- (8) Nyman, E. S. and Hynninen, P. H. (2004) Research advances in the use of tetrapyrrolic photosensitizers for photodynamic therapy. *J. Photochem. Photobiol. B: Biol.* 73, 1–28.
- (9) Kee, H. L., Bhaumik, J., Diers, J. R., Mroz, P., Hamblin, M. R., Bocian, D. F., Lindsey, J. S. and Holten, D. (2008) Photophysical characterization of imidazolium-substituted Pd(II), In(III), and Zn(II) porphyrins as photosensitizers for photodynamic therapy. *J. Photochem. Photobiol. A: Chem.* 200, 346–355.
- (10) Mroz, P., Bhaumik, J., Dogutan, D. K., Aly, Z., Kamal, Z., Khalid, L., Kee, H. L., Bocian, D. F., Holten, D., Lindsey, J. S. and Hamblin, M. R. (2009) Imidazole metalloporphyrins as photosensitizers for photodynamic therapy: Role of molecular charge, central metal and hydroxyl radical production. *Cancer Lett.* 282, 63–76.
- (11) Huang, Y.-Y., Balasubramanian, T., Yang, E., Diers, J. R., Bocian, D. F., Lindsey, J. S., Holten, D. and Hamblin, M. R. (2012) Stable synthetic bacteriochlorins for photodynamic therapy: Role of dicyano peripheral groups, central metal substitution (2H, Zn, Pd), and Cremophor EL delivery. *ChemMedChem*, submitted 07/15/2012.
- (12) Mass, O., Taniguchi, M., Ptaszek, M., Springer, J. W., Faries, K. M., Diers, J. R., Bocian, D. F., Holten, D. and Lindsey, J. S. (2011) Structural characteristics that make chlorophylls green: Interplay of hydrocarbon skeleton and substituents. *New J. Chem.* 35, 76–88.
- (13) Weber, G. and Teale, F. W. J. (1957) Determination of the absolute quantum yield of fluorescent solutions. *Trans. Faraday Soc.* 53, 646–655.

- (14) Seybold, P. G. and Gouterman, M. (1969) Porphyrins XIII: Fluorescence spectra and quantum yields. *J. Mol. Spectrosc.* 31, 1–13.
- (15) Gradyushko, A. T., Sevchenko, A. N., Solovyov, K. N. and Tsvirko, M. P. (1970) Energetics of photophysical processes in chlorophyll-like molecules. *Photochem. Photobiol.* 11, 387–400.
- (16) Yang, E., Kirmaier, C., Krayner, M., Taniguchi, M., Kim, H.-J., Diers, J. R., Bocian, D. F., Lindsey, J. S. and Holten, D. (2011) Photophysical properties and electronic structure of stable, tunable synthetic bacteriochlorins: Extending the features of native photosynthetic pigments. *J. Phys. Chem. B* 115, 10801–10816.
- (17) Strachan, J. P., Gentemann, S., Seth, J., Kalsbeck, W. A., Lindsey, J. S., Holten, D. and Bocian, D. F. (1997) Effects of orbital ordering on electronic communication in multiporphyrin arrays. *J. Am. Chem. Soc.* 119, 11191–11201.
- (18) Except for molecular mechanics and semi-empirical models, the calculation methods used in Spartan '08 or '10 have been documented in the following: Shao, Y., Molnar, L. F., Jung, Y., Kussmann, J., Ochsenfeld, C., Brown, S. T., Gilbert, A. T. B., Slipchenko, L. V., Levchenko, S. V., O'Neill, D. P., DiStasio Jr., R. A., Lochan, R. C., Wang, T., Beran, G. J. O., Besley, N. A., Herbert, J. M., Lin, C. Y., Voorhis, T. V., Chien, S. H., Sodt, A., Steele, R. P., Rassolov, V. A., Maslen, P. E., Korambath, P. P., Adamson, R. D., Austin, B., Baker, J., Byrd, E. F. C., Dachsel, H., Doerksen, R. J., Dreuw, A., Dunietz, B. D., Dutoi, A. D., Furlani, T. R., Gwaltney, S. R., Heyden, A., Hirata, S., Hsu, C.-P., Kedziora, G., Khalliulin, R. Z., Klunzinger, P. A., Lee, M., Lee, M. S., Liang, W., Lotan, I., Nair, N., Peters, B., Proynov, E. I., Pieniazek, P. A., Rhee, Y. M., Ritchie, J., Rosta, E., Sherrill, C. D., Simmonett, A. C., Subotnik, J. E., Woodcock III, H. L., Zhang, W., Bell, A. T., Chakraborty, A. K., Chipman, D. M., Keil, F. J., Warshel, A., Hehre, W. J., Schaefer III, H. F., Kong, J., Krylov, A. I., Gill, P. M. W. and Head-Gordon, M. (2006) Advances in methods and algorithms in a modern quantum chemistry program package. *Phys. Chem. Chem. Phys.* 8, 3172–3191.
- (19) Chen, C.-Y., Sun, E., Fan, D., Taniguchi, M., McDowell, B. E., Yang, E., Diers, J. R., Bocian, D. F., Holten, D., and Lindsey J. S. (2012) Synthesis and physicochemical properties of metallo bacteriochlorins. *Inorg. Chem.* 51, *submitted 06/13/2012*.
- (20) Vakrat-Haglili, Y., Weiner, L., Brumfeld, V., Brandis, A., Salomon, Y., Mellroy, B., Wilson, B. C., Pawlak, A., Rozanowska, M., Sarna, T. and Scherz, A. (2005) The microenvironment effect on the generation of reactive oxygen species by Pd-bacteriopheophorbide. *J. Am. Chem. Soc.* 127, 6487–6497.
- (21) Ashur, I., Goldschmidt, R., Pinkas, I., Salomon, Y., Szewczyk, G., Sarna, T. and Scherz, A. (2009) Photocatalytic generation of oxygen radicals by the water-soluble bacteriochlorophyll derivative WST11, noncovalently bound to serum albumin. *J. Phys. Chem. A* 113, 8027–8037.
- (22) Arnault, L. G. (2011) Design of porphyrin-based photosensitizers for photodynamic therapy. *Inorg. Photochem.* 63, 187–233.

- (23) Hartwich, G., Fiedor, L., Simonin, I., Cmiel, E., Schäfer, W., Noy, D., Scherz, A. and Scheer, H. (1988) Metal-substituted bacteriochlorophylls. 1. Preparation and influence of metal and coordination on spectra. *J. Am. Chem. Soc.* 120, 3675–3683.
- (24) Takiff, L. and Boxer, S. G. (1988) Phosphorescence from the primary donor in *Rhodobacter sphaeroides* and *Rhodospseudomonas viridis* reaction centers. *Biochim. Biophys. Acta* 932, 325–334.
- (25) Silva, E. F. F., Serpa, C., Dabrowski, J. M., Monteiro, C. J. P., Formosinho, S. J., Stochel, G., Urbanska, K., Simões, S., Pereira, M. M. and Arnault, L. G. (2010) Mechanisms of singlet-oxygen and superoxide-ion generation by porphyrins and bacteriochlorins and their implications in photodynamic therapy. *Chem. Eur. J.* 16, 9273–9286.
- (26) MacDonald, I. J. and Dougherty, T. J. (2001) Basic principles of photodynamic therapy. *J. Porphyrins Phthalocyanines* 5, 105–129.
- (27) Dabrowski, J. M., Urbanska, K., Arnaut, L. G., Pereira, M. M., Abreu, A. R., Simoes, S. and Stochel, G. (2011) Biodistribution and photodynamic efficacy of a water-soluble, stable, halogenated bacteriochlorin against melanoma. *ChemMedChem* 6, 465–475.
- (28) Dabrowski, J. M., Arnaut, L. G., Pereira, M. M., Monteiro, C. J., Urbanska, K., Simoes, S. and Stochel, G. (2010) New halogenated water-soluble chlorin and bacteriochlorin as photostable PDT sensitizers: synthesis, spectroscopy, photophysics, and in vitro photosensitizing efficacy. *ChemMedChem* 5, 1770–1780.
- (29) Limantara, L., Koehler, P., Wilhelm, B., Porra, R. J. and Scheer, H. (2006) Photostability of bacteriochlorophyll a and derivatives: Potential sensitizers for photodynamic tumor therapy. *Photochem. Photobiol.* 82, 770–780.
- (30) Birks, J. B. (1970) *Photophysics of Aromatic Molecules*. Wiley-Interscience, London, pp 492–517.
- (31) Fajer, J. and Davis, M. S. (1978) Electron spin resonance of porphyrin π cations and anions. In: Dolphin, D. (ed.) *The Porphyrins*. Academic Press, New York, Vol. IV, pp 197–256.
- (32) Kee, H. L., Kirmaier, C., Tang, Q., Diers, J. R., Muthiah, C., Taniguchi, M., Laha, J. K., Ptaszek, M., Lindsey, J. S., Bocian, D. F. and Holten, D. (2007) Effects of substituents on synthetic analogs of chlorophylls. Part 2: Redox properties, optical spectra and electronic structure. *Photochem. Photobiol.* 83, 1125–1143.
- (33) Posen, Y., Kalchenko, V., Seger, R., Brandis, A., Scherz, A. and Salomon, Y. (2005) Manipulation of redox signaling in mammalian cells enabled by controlled photogeneration of reactive oxygen species. *J. Cell Sci.* 118, 1957–1969.
- (34) Gouterman, M. (1978) Optical spectra and electronic structure of porphyrins and related rings. In: Dolphin, D. (ed.) *The Porphyrins*. Academic Press, New York, Vol. III, pp 1–165.
- (35) Felton, R. H. (1978) Primary redox reactions of metalloporphyrins. In: Dolphin, D. (ed.) *The Porphyrins*. Academic Press, New York, Vol. V, pp 53–125.
- (36) Krayner, M., Yang, E., Diers, J. R., Bocian, D. F., Holten, D. and Lindsey, J. S. (2011) *De novo* synthesis and photophysical characterization of annulated bacteriochlorins.

- Mimicking and extending the properties of bacteriochlorophylls. *New J. Chem.* 35, 587–601.
- (37) Springer, J. W., Faries, K. M., Diers, J. R., Muthia, C., Mass, O., Kee, H. L., Kirmaier, C.; Lindsey, J. S.; Bocian, D. F. and Holten, D. (2012) The effects of substituents on synthetic analogs of chlorophylls. Part 3: The distinctive impact of auxochromes at the 7-versus 3-positions. *Photochem. Photobiol.* 88, 651–674.